Amyloid beta: from pre-analytical factors to disease mechanisms

Jamie Toombs

UCL

PhD Neuroscience

I, Jamie Toombs, confirm that the work presented in this thesis is my own. Where information has been derived from other sources, I confirm that this has been indicated in the thesis.

Abstract

Background

Biomarkers are powerful tools for interrogating the basic science of disease processes, in the clinical detection of disease states, and as both targets and endpoints in therapeutic strategy. Amyloid beta (Aβ) is a core biomarker for Alzheimer's disease (AD), but measurement variation between sites and experiments limits its potential. Furthermore, although the role of brain Aβ accumulation early in AD is extremely well attested, the biological mechanisms underlying this remain poorly understood.

Methods

To contribute to the development of treatments for AD patients and those at risk, this thesis set out to identify important pre-analytical confounding factors in Aβ measurement, strategies to mitigate them, and identify disease relevant patterns of Aβ peptide production in human CSF and an induced pluripotent stem cell-derived cortical neuron model of familial AD (fAD).

Results

A series of experiments demonstrated the importance of sample surface exposure to the measurement of Aβ peptides and tau. The volume at which samples are stored and iterative contact with fresh surfaces had profound effect on Aβ, but not tau, with greater surface exposure resulting in depletion of Aβ concentration. The mechanism was demonstrated to be protein surface adsorption. Importantly, the different Aβ peptides did not absorb to polypropylene to the same extent; Aβ42 concentration decreased proportionally more with surface exposure treatment than Aβ40 and Aβ38.

It was observed that the addition of a non-ionic surfactant (Tween 20) to samples significantly mitigated the effect of surface exposure treatments on Aβ peptides and tau. However, the use of this additive did not meaningfully improve variability when sample storage conditions were standardised. Furthermore, variances in clinic to laboratory temperature and time interval did not significantly affect Aβ or tau concentration.

Validation of an *in vitro* model of fAD was conducted. Experiment identified the use of Aβ ratios as a robust method for normalising data variability between and within cell lines over extended time periods. Furthermore, comparison of paired CSF, cell media, cell lysates, and post-mortem cortical

tissue from the same individual demonstrated physiologically consistent patterns of Aβ ratios across sample types.

Finally, comparison of multiple fAD mutation and control cell lines demonstrated quantitative and qualitative differences in secreted Aβ. *APP* V717I neurons increased secretion of Aβ42 and Aβ38 relative to Aβ43 and Aβ40. *PSEN1* mutations increased secretion of longer Aβ peptides relative to shorter Aβ peptides, with mutation specific differences such as greatly increased Aβ43 in *PSEN1* R278I.

Conclusions

This work demonstrated several novel considerations in the use of Aβ peptides as biomarkers for AD. Data principally highlight the importance of Aβ ratios to AD biomarker research, the necessity of controlling pre-analytical sample surface exposure intended for the measurement of 'sticky' protein biomarkers such as Aβ peptides, and the validity of iPSC-derived neuronal models for exploring the production of Aβ in AD and health.

Impact statement

This work formed part of an ongoing movement to improve the quality and reliability of biomarker data in the field of Alzheimer's research. Contribution was to two main areas: the effect of sample surface exposure on the Aβ content of CSF, and the production of Aβ peptides in fAD patient neurons. Concerning the former, experiments identified and characterised a number of previously under-appreciated aspects of CSF and cell media storage and handling (storage volume, consecutive aliquoting, the effect of using a manometer), which inspired investigations by other groups and contributed to proposals for "gold standard" CSF collection protocols. Furthermore, data highlighted the potential of sample additives (Tween 20) to mitigate surface adsorption of vulnerable proteins such as Aβ peptides. This generated a certain amount of interest from ELISA manufacturing companies. Concerning Aβ production in vitro, different fAD genotypes were shown to produce distinct ratios of Aβ peptides, supporting a growing understanding of APP proteolysis mechanisms that will inform understanding of past drug failure and future drug development. Additionally, the notion of Aβ as a biomarker was expanded with presentation of the concept of Aβ peptide ratios as biomarkers for γ-secretase activity. This thesis also represents one of only two studies to compare iPSC-derived neurons with tissues from the same individual, in this case brain tissue homogenate and CSF in an individual with an *APP V717I* mutation. Finally, work culminated in six original publications to Clinical Chemistry and Laboratory Medicine, Alzheimer's & Dementia, Alzheimer's Research & Therapy, and the Journal of Alzheimer's disease, with a seventh under revision at Molecular Psychiatry.

Acknowledgements

I would like to gratefully thank my supervisors Henrik Zetterberg, Selina Wray, Amanda Heslegrave and John Hardy for their expert guidance, zen-like patience, inordinate generosity, and boundless enthusiasm. This has been an amazing experience and privilege.

I would additionally like to thank the many outstanding people I have had the good fortune to work with and beside over the course of this project. Of these, Ross Paterson, Charles Arber, Christopher Lovejoy, Julia Ravey, Lotta Agholme, and Petra Bergtröm deserve especial credit. Their partnership was integral to designing, conducting and reporting the results of the many experiments we conducted together.

Furthermore, I would like to thank the many mentors who imparted their knowledge and skills so generously: Michael Lunn, Viki Worthington, Miles Chapman, Andrew Church, Neghat Lakdawala, Rosmary Monero, Donna Grant, and Michael Chou, Axel Petzold, Jonas Söderblom, Erik Portelius, and Ulf Andreason, Michael Duchen and Gauri Bosale.

Extra-special thanks go to Henrietta Wellington, Martha Foiani, Carolin Heller, and Elena Veleva of the UCL DRI Biomarker Research Laboratory (Formerly the Leonard Wolfson Biomarker Laboratory) for their incredible support and friendship.

Finally, what acknowledgement is complete without a recognition of family? This is for my parents Margaret, Richard, and Mark, and my dearest loves Diana and little Jasper. Thank you so much for your love and support.

Contents

Table of Tables

Table of Figures

Abbreviations

A disintegrin and metalloproteinase (ADAM)

Amyloid precursor protein intracellular domain (AICD)

Alzheimer's disease (AD)

Anterior pharynx defective 1 (APH-1)

Amyloid beta (Aβ)

Amyloid intra-cellular domain (AICD).

Amyloid precursor protein (APP)

Apolipoprotein E (APOE)

Beta-site amyloid precursor protein cleaving enzyme 1/2 (BACE1/2)

Blood brain barrier (BBB)

Calcium signal ([Ca2+]c)

Carboxylic acid terminal fragment (CTF)

Central nervous system (CNS)

Cerebral amyloid angiopathy (CAA)

Cerebrospinal fluid (CSF)

Chinese hamster ovary (CHO)

Computer tomography (CT)

Control (CTRL)

Early onset Alzheimer's disease (EOAD)

Endoplasmic reticulum (ER)

Embryonic pluripotent stem cell (EPSC)

Ethylenediaminetetraacetic acid (EDTA)

Familial Alzheimer's disease (fAD)

Frontal temporal dementia (FTD),

γ-Secretase activating protein (GSAP)

Genome-wide association study (GWAS)

Hank's Balanced Salt Solution (HBSS)

Knock down (KD)

Knock in (KI)

Knock out (KO)

Lactate dehydrogenase (LDH)

Late onset Alzheimer's disease (LOAD)

Long term potentiation (LTP)

Magnetic resonance imaging (MRI)

Mitochondrial associate membranes (MAM)

Mild cognitive impairment (MCI)

Mothers against decapentaplegic (SMAD)

Multivesicular bodies (MVBs)

Neurofibrillary tangle (NFT)

Nicotinic acetylcholine receptor (nAChR)

N-methyl-D-aspartate receptors (NMDAr)

Notch intracellular domain (NICD)

Paired helical filaments (PHF)

Parkinson's disease (PD)

Peripheral nervous system (PNS)

Positron emission tomography (PET)

Presenilin 1/2 (PSEN1/2)

Presenilin enhancer 2 (PEN-2)

Relative centrifugal force (RCF)

Radioimmunoprecipitation assay buffer (RIPA)

Sporadic Alzheimer's disease (sAD)

Transgenic (Tg)

Trans-Golgi network (TGN)

Transmembrane domains (TMDs)

Triggering receptor expressed on myeloid cells 2 gene (*TREM2*)

Vascular cell adhesion molecule 1 (VCAM1)

1 Background

1.1 Project Aims

The aim of this work is to expand understanding of Alzheimer's disease (AD) through improved characterisation of amyloid beta (Aβ) peptide as a biomarker for the disease. Work was conducted in two phases – the first providing data to help guide standardisation strategies in a diagnostic context, and the second exploring production in *in vitro* cell models to better understand what Aβ is a biomarker *of*.

The specific aims of this project are:

I. Identify novel confounding factors in the storage and handling of CSF and cell culture media that may artificially alter detectable Aβ peptides. Factors studied include:
    - Effect of sample storage volume,
    - Effect of sample transfer between tubes,
    - Effect of Tween 20 on sample measurement variation,
    - Effect of using a spinal manometer,
    - Effect of sample transportation time and temperature in clinical context,

II. Investigate the physiological relevance of iPSC-neurons by comparing Aβ peptide profiles in cell culture, CSF, and brain homogenate from a single patient with the *APP* V717I mutation.

III. Investigate the full spectrum of Aβ peptides produced by glutamatergic cortical neurons from six different fAD lines (*APP* V717I, *PSEN1* int4del, *PSEN1* Y115H, *PSEN1* M139V, *PSEN1* M146I, and *PSEN1* R278I) and five non-neurodegenerative controls.

1.2 Alzheimer's disease research in context

On the 3rd of November 1906, Aloysius 'Alois' Alzheimer described a "peculiar severe disease process of the cerebral cortex" to the 37th meeting of the Southwest German Psychiatrists in Tübingen *(Alzheimer, 1907)*. His work highlighted the presence of insoluble extracellular and intracellular proteinaceous deposits in the brain of his patient, Auguste Deter, who displayed symptoms of dementia. The condition was later coined 'Alzheimer's disease' by Alzheimer's distinguished employer, Emil Kraepelin, in the eighth edition of Psychiatrie 1910 *(Hippius and Neundörfer, 2003)*. AD received, at best, modest attention until 1976, when Robert Katzman

catapulted it onto the mainstream medical radar by arguing the equivalence of AD and 'senile dementia' and identified the disease process as a leading cause of death in the USA *(Katzman, 1976)*.

In 1984 Glenner and Wong identified Aβ from cerebro-vascular amyloid fibril deposits using Sephadex G-100 column chromatography and high performance liquid chromatography *(Glenner and Wong, 1984a)*. Work by Masters and colleagues in 1985 confirmed Aβ, in particular Aβ1-42 peptide, as the major constituent of Alzheimer's extracellular plaques, and furthermore that the protein is prone to self-aggregate into oligomer and fibrillary complexes *(Masters et al., 1985)*. The gene encoding the amyloid precursor protein (APP) was first identified by the independent efforts of Kang *et al.* and Tanzi *et al.* in 1987 *(Kang et al., 1987; Tanzi et al., 1987)*, through genetic linkage mapping of Aβ to the *APP* gene located at 21q21.3. Tau had been identified as the primary protein constituting intra-cellular tangles in 1986 *(Wood et al., 1986)*.

A milestone that placed genetics close the pulse of ongoing AD research came in 1991, when Goate *et al.* identified a valine to isoleucine point mutation near the C-terminal of the *APP* gene (*APP* V717I, the London mutation) in families from the UK and USA *(Goate et al., 1991)*. Fitting the pieces of the puzzle together, in 1992 Hardy and Higgins proposed the 'amyloid cascade hypothesis', stipulating that Aβ accumulation is the driving factor of subsequent pathological processes and which remains the dominant theory of AD biology to the current time *(Hardy and Higgins, 1992)*. Sherrington *et al.* quickly followed this up by identifying the link between AD and presenilin mutations in 1995 *(Sherrington et al., 1995)*, a year which also saw the generation of the first transgenic mouse model *(Games et al., 1995)*. Alongside the discovery of high penetrance autosomal dominant mutations, work had also begun highlighting the role of genetic risk factors, such as the APOE-e4 allele *(Corder et al., 1993; Saunders et al., 1993; Strittmatter et al., 1993)*. By the 2010s technological sophistication and international collaborations had enabled sequencing of large cohorts and meta-analysis of genome wide association studies (GWAS) led to the identification of AD-genic TREM2 mutations *(Guerreiro et al., 2013)* and 21 risk factor genes *(Van Cauwenberghe et al., 2016; Naj and Schellenberg, 2017)*

Despite increasing energy for AD research, output from the field in terms of therapeutics has been noticeably low. Memantine was approved for AD treatment in Germany in 1989, and in 1993 tacrine became the first FDA approved drug for AD, although it was discontinued in 2013 due to safety concerns (liver toxicity). Four more drugs, all targeting aspects of the cholinergic system (after the first hypothesis of AD aetiology), were approved over next decade (Table 1). A combination of

donepezil and memantine has been the only 'new' therapy approved since 2003, out of the 188 phase III trials currently listed as suspended, terminated, completed, or withdrawn on clinicaltrials.gov *(National Institute of Health, 2018)*.

Table 1: List of FDA approved AD therapeutics

Drug	Developer	Type	Date Approved	Approved for	Reference
Donepezil hydrochloride (Aricept)	Eisai/Pfizer	Cholinesterase inhibitor	1996	AD	*(Dooley and Lamb, 2000)*
Galantamine (Razadyne)	Jansen	Cholinesterase inhibitor and allosteric potentiator of both nicotinic and muscarinic acetylcholine receptors	2000	Mild to moderate AD	*(Scott and Goa, 2000)*
Mementine (Akatinol)	Forest Laboratories/Merz Pharma	NMDAr antagonist	2003 (1989)	AD	*(Robinson and Keating, 2006)*
Rivastagmine (Exelon)	Novartis	Cholinesterase and butyrylcholinesterase inhibitor	1997	Mild to moderate AD	*(Birks et al., 2015)*
Tacrine (Cognex)	Pfizer, Shionogi Pharma	Cholinesterase inhibitor	1993-2013	Discontinued	*(Giacobini, 1998)*

Table 1: Showing information for the five small molecule drugs that have been approved for the treatment of AD.

The need for better diagnostic accuracy and more detailed understanding of the underlying disease biology have been driving forces behind development of measurement techniques, with an emphasis on probing ever earlier into the disease course. The longstanding tradition of immunohistochemistry still utilises Congo red and thioflavin S to stain amyloid structures, alongside more modern antibody-based techniques. Immunoassay has dominated quantitation of biofluid proteins, yielding increasingly sensitive approaches that presently culminate in the femtolitre detection ranges that hold promise for developing blood-based tests *(Zetterberg et al., 2013)*. Beyond immunological methods, mass spectrometry has become increasingly accessible and utilised for screening large

numbers of proteins without necessarily requiring antibody development. However, techniques aimed at exploring protein conformation (qualitative) rather than concentration (quantitative) remain relatively underdeveloped. Finally, brain imaging has undergone rapid growth with the adoption of computer tomography (CT), magnetic resonance imaging (MRI) and positron emission tomography (PET). The development of Pittsburgh Compound B in 2004 in particular has had considerable impact on this area *(Klunk et al., 2004)*.

In summary, over the last 100 years AD has moved from relative obscurity to a centre-stage world health crisis. Research into the proteomic and genetic biology of the disease snowballed in the latter decades of the 20th century, but translating these gains to clinical therapeutics has proved frustratingly difficult. The field awaits a breakthrough, and the amyloid cascade hypothesis is yet to be conclusively vindicated.

1.3 Alzheimer's disease

AD is a progressive neurodegenerative disease, characterised histologically by extra-cellular plaques (primarily composed of aggregated Aβ peptides) and intra-cellular neurofibrillary tangles (primarily of aggregated, hyper-phosphorylated tau), alongside atrophy of the cortex *(Perl, 2010)*. Clinically, AD presents as insidious loss of cognitive function, progressive impairment of memory encoding and recall, and the attendant inability to maintain an independent lifestyle *(Burns and Iliffe, 2009)*. Diagnosis of AD is dependent on histological identification of Aβ and tau deposition post-mortem, in the context of symptoms having been clinically documented in life *(McKhann et al., 2011)*. Though histopathology is seen as the 'gold standard' in AD diagnosis, and not without dispute *(Scheltens and Rockwood, 2011)*, biological assay and imaging techniques are becoming increasingly powerful tools in clinical diagnostics and predictive diagnosis *(Dubois et al., 2014)*.

Various models of AD aetiology have been proposed (Table 2), though the cause is ultimately unknown. The leading theory, formalised as the 'amyloid cascade hypothesis', posits that Aβ accumulation in the brain following dysregulated production and/or clearance is the trigger for neurodegenerative changes that lead to AD *(Hardy, 2006, 2009; Hardy and Higgins, 1992)*. Alterations in production, clearance and deposition of Aβ, as well as other proteins such as tau, over time become consequential at a cellular and eventually systemic level.

Table 2: Alternative hypotheses for AD genesis

Hypothesis	Description	Key References
Amyloid cascade hypothesis	Aβ dyshomeostasis in the brain leads to the retention of Aβ in the brain and formation of amyloid structures that disrupt many aspects of brain physiology. Cascading effects of this cause neurodegeneration and eventually manifest as AD	***Original:*** *(Hardy and Allsop, 1991)* ***Update:*** *(Selkoe and Hardy, 2016)*
Calcium homeostasis hypothesis	Proposes that there is a bidirectional relationship between Ca2+ signalling and the amyloidogenic pathway. Aβ dyshomeostasis can disrupt Ca2+ signalling, which in turn can promote amyloidogenic APP metabolism.	***Original:*** *(Khachaturian, 1989)* ***Updates:*** *(Berridge, 2010; LaFerla, 2002)*
Cholinergic hypothesis	The clinical manifestations of AD are driven by the downregulation of cholinergic markers, such as acetyltransferase and acetylcholinesterase, and loss of cholinergic neurons in the basal forebrain (nucleus basalis of Meynert, and medial septum), hippocampus, frontal cortex, and amygdala	***Original:*** *(Bartus et al., 1982)* ***Updates:*** *(Craig et al., 2011; Sanabria-Castro et al., 2017)*
GM1 ganglioside hypothesis	Aβ peptides bind to the surface bound GM1 ganglioside. Binding at Lys28 results in conformational changes in the C-terminal region that expose the hydrophobic domain and readily recruit other amyloid beta peptides in a beta sheet. This forms the seed for fibril formation	***Original:*** *(Yanagisawa et al., 1995)* ***Update:*** *(Yanagisawa, 2015)*
Infection hypothesis	The majority of people who reach old age are infected with HSV-1. Compromise of the immune system by aging processes, stress etc. can assist the spread of this virus to the brain. This can occur through the olfactory system, which is among the first to fail in a number of neurodegenerative conditions including AD. Here it triggers neuroinflammation and plaque deposition, and HSV-1 DNA has been found in amyloid plaques. Other microorganisms such as CMV, HIV, measles, spirochaete, and Chlamydia pneumonia have also been implicated, as well as prion-like proteins.	***Original:*** *(Itzhaki et al., 2016)* ***Update:*** *(Fulop et al., 2018)*
Inflammatory hypothesis	Degeneration of the blood–brain barrier and decreased cerebral blood flow disrupt energy metabolism, facilitate protein misfolding, oxidative stress and inflammation, leading to neurodegeneration that eventually manifests as AD. Inflammation is the triggering factor as the limited neurotoxicity of Aβ is exacerbated by the activation of the complement system.	***Original:*** *(Rogers et al., 1992)* ***Update:*** *(McGeer and McGeer, 2013)*
Lipid metabolism hypothesis	Abnormal lipid synthesis, modification, trafficking, and degradation leads to altered Aβ production, synaptic dysfunction, abnormal tau phosphorylation, and inflammation. Cascading effects of this eventually manifest as AD	***Original:*** *(Liu and Zhang, 2014)* ***Update:*** *(Drolle et al., 2017)*
Metal hypothesis	Aβ is central to Alzheimer's disease pathobiology, but neurotoxicity is driven by interaction with Zn2+ and Cu2+ metal ions. Zn and Cu bind to the Aβ 6-14aa domain and catalyse rapid aggregation proximal to synapses, reducing NMDA receptor activity. It is suggested that increased concentrations of Zn2+ and Cu2+ and/or decreased antagonists such as metallothionein-3 are found in the AD and Down's syndrome brain. Cascading effects of this cause neurodegeneration and eventually manifest as AD	***Original:*** *(Armstrong et al., 1995; Bush et al., 1994)* ***Updates:*** *(Bush and Tanzi, 2008; Craddock et al., 2012)*
Oxidative stress hypothesis	AD is caused by free radical damage to neurons, glia and mitochondria from various sources. Damage to tissue creates a cycle of free radical production that eventually overwhelms the body's antioxidant reservoir	***Original:*** *(Markesbery, 1997)* ***Updates:*** *(Nunomura et al., 2001; Zhao and Zhao, 2013)*
Tau hypothesis	Excessive or abnormal phosphorylation of tau results in formation of PHFs and NFTs, destabilising microtubules and disrupting cellular processes. Misfolded tau spreads through neural networks in a prion-like manner. Cascading effects of this cause neurodegeneration and eventually manifest as AD	***Original:*** *(Mudher and Lovestone, 2002)* ***Update:*** *(Kametani and Hasegawa, 2018)*
Traumatic brain injury (TBI) hypothesis	Brain trauma, caused by external force applied to the head in a variety of activities or accidents, can result in acute and potentially chronic death of neurons and glia, elevated protein (Aβ, tau, α-synuclein) concentrations, inflammation, damage to cerebral vasculature, as well as persistent cognitive changes. TBI severity is suggested to associate with dementia risk in late-life, especially in males.	***Original:*** *(Mortimer et al., 1985)* ***Update:*** *(Kokiko-Cochran and Godbout, 2018)*
Vascular hypothesis	Aging and the presence of vascular risk factors create a Critically Attained Threshold of Cerebral Hypoperfusion (CATCH) that disrupt many aspects of brain physiology. Cascading effects of this cause neurodegeneration and eventually manifest as AD	***Original:*** *(De la Torre and Mussivand, 1993)* ***Update:*** *(de la Torre, 2010)*

Table 2: A list of the main hypotheses for the pathogenesis of AD

The key evidence supporting the amyloid cascade hypothesis is the fact that all known genetic mutations that produce heritable forms of AD affect Aβ production *(Selkoe and Hardy, 2016)*. Additionally, many if not most genetic risk factors affect cellular mechanisms for responding to or clearing accumulation of Aβ in the brain *(Van Cauwenberghe et al., 2016)*. Furthermore, changes in Aβ clearance to CSF is the earliest and among the most reliable indicators of AD *(Jack et al., 2013)*. That extensive Aβ plaque pathology is among the most consistent features of AD is also relevant, though arguably weaker evidence given the circular nature of typical AD diagnosis requiring plaque pathology, the fact that a-symptomatic individuals also demonstrate plaque deposition, and that plaque number does not correlate well with symptom severity *(Sperling et al., 2009)*.

The differences between the various hypotheses for AD are yet to be fully reconciled. It may be that the brain is limited in the ways in which it can respond to damage from unrelated causes. It may also be that the common, emergent themes of aberrant protein production / localisation / folding / clearance, excitotoxicity, oxidative stress, energy hypometabolism, lipid dysregulation, vascular pathology, and inflammation are parallel and reciprocal processes. The disruption of one feeding back into others, and under certain conditions reaching a state conducive to AD. The weight of evidence suggests Aβ is likely to be integral to this state.

Epidemiologically, AD is thought to be the most prevalent form of dementia *(Katzman, 1976)*, accounting for 60-80% of all dementia cases *(Alzheimer's Association, 2016)*. Prevalence increases with age, rising from one in 14 at age 65 years to one in six at age 80 years *(Prince et al., 2014)*, with females disproportionately affected over the age of 80 years *(Prince et al., 2014)*. Approximately 850,000 dementia cases have been reported in the UK, 5.3 million in the USA, and 46.8 million worldwide *(Martin Prince et al., 2015)*. In 2016 the UK Office for National Statistics announced AD as among the leading cause of death in England and Wales *(Office for National Statistics, 2016)*, and it was recorded as the fifth leading cause of death (with other dementias) globally *(World Health Organisation, 2016)*. Projections of the number of people affected by mid-century approximate 131.5 million *(Martin Prince et al., 2015)*. Persistent data suggests that incidence of new dementia cases has been falling each decade in Western Europe and the USA since the 1990s *(Matthews et al., 2013; Satizabal et al., 2016; Schrijvers et al., 2012)* attributed cautiously to broad changes in lifestyle. However, prevalence is a balance of incidence and disease duration, the latter of which may increase as lifestyle and care improve *(Prince et al., 2016)*. Additionally, trends in low and middle income areas, thought to contribute more than half of cases *(Martin Prince et al., 2015)*, are yet unclear.

The combination of increased lifespan with an attendant decrease in autonomous capacity already constitutes a heavy social and economic burden in developed countries, and increasingly in low and middle income countries. Without substantial changes to therapeutic effectiveness and organisation of care, AD and dementia will be a limiting factor on global quality of life with mathematical inevitability.

1.3.1 Alzheimer's disease: Subcategories

AD has been an intractable problem in neuroscience for the past century, and a considerable hindrance to its solvation is the heterogeneity of its manifestation. Familial AD (fAD) describes cases where manifestation of pathology can be linked to a heritable genetic mutation, most commonly in the amyloid beta precursor protein gene (*APP*, also known as A4) *(Julia and Goate, 2017)*, presenilin-1 (*PSEN1*) and presenilin-2 (*PSEN2*) genes *(Cai et al., 2015; Kelleher and Shen, 2017)*, and triggering receptor expressed on myeloid cells 2 gene (*TREM2*) *(Guerreiro et al., 2013)*. AD-like pathology also frequently accompanies the chromosomal disorder trisomy 21 (Down's Syndrome) *(Wiseman et al., 2015)*. Sporadic AD (sAD) describes cases where a direct genetic cause cannot be determined, though genetic risk factors, for example apolipoprotein E (APOE) allele, may be present (reviewed in *(Van Cauwenberghe et al., 2016)*).

AD may also be subcategorised into early onset (EOAD) and late onset (LOAD) *(Naj and Schellenberg, 2017)*. These categories are not different forms of AD, but describe whether the clinical symptoms manifest before or after 65 years of age. The distinction is largely a clinical convention, as certain patterns of AD progression have become associated with one or the other. For example, EOAD is more often associated with more aggressive pathology and atypical symptoms whilst LOAD more frequently presents alongside other age-related comorbidities *(Van der Flier, 2016)*. Furthermore, there is considerable overlap with fAD and sAD. Typically, fAD cases have earlier age of onset than sAD cases. For example, no (pathological) *APP* mutation carrier has yet been reported unaffected beyond the age of 67 years *(Holmes, 2002)*. Based on the strong link between fAD and EOAD, which account for 0.3-0.5% of all AD cases *(Rocca et al., 1991)*, it is considered that sAD accounts for ~99% of cases.

fAD and sAD both manifest with considerable heterogeneity in the phenotypic expression of cognitive features *(Lam et al., 2013)*, non-cognitive features *(Masters et al., 2015)*, age at disease onset *(Tellechea et al., 2018)*, disease duration and rate of progression *(Komarova and Thalhauser, 2011)*, as well as distributions and conformations of pathologically misfolded protein and regions of

cortical atrophy *(Lam et al., 2013)*. Grouping AD cases into typical and atypical forms provides some structure to this diversity, though comorbidities *(Cermakova et al., 2015; Clodomiro et al., 2013; Duthie et al., 2011)*, pathological changes beyond the classic amyloid plaque and neurofibrillary tangle formations *(Crutch et al., 2012; Dzamba et al., 2016; Jaunmuktane et al., 2015; Smith and Greenberg, 2009; Winkler et al., 2014)*, and fundamental gaps in our understanding of brain physiology make classification a matter of ongoing discussion.

Typical or 'memory-led' AD begins with amyloid deposition in the basal temporal lobes and associative neocortex *(Grothe et al., 2017; Thal et al., 2002)*. Individuals present with early mild episodic memory (autobiographical) and spatial (navigational) impairment, often with attendant confusion and anxiety. Deficits are subtle and overlap with the prodromal symptoms of other conditions of the central nervous system (CNS). Thus, a diagnosis of mild cognitive impairment (MCI) is commonly made at this stage *(Albert et al., 2011; Petersen et al., 1999)*. As the disease progresses, amyloid deposits in the striatum and sub-cortical regions *(Grothe et al., 2017; Thal et al., 2002)*, and tau accumulates in the neurons of the transentorhinal cortex, later spreading to the hippocampus and basal forebrain *(Braak et al., 2006)*. Progressive impairment to recall, navigation, orientation, timekeeping, numeracy, spelling, linguistic abilities, and problem-solving gradually manifest. In the final stages, Aβ and tau pathology incorporate the hind brain and neocortex, and atrophy of the hippocampus and cortex is typically profound *(Braak et al., 2006; Grothe et al., 2017; Thal et al., 2002)*. The individual's symptoms are often broadly incapacitating, with greatly reduced mobility, coordination, excretion control, and capacity for communication, eventually requiring full-time care. Individuals become increasingly susceptible to secondary infection, with aspirational pneumonia due to swallowing difficulties being the leading cause of death in severe cases, and heart disease and stroke in less severe or vascular associated cases *(Kammoun et al., 2000; Kukull et al., 1994)*.

Atypical AD variants are neurodegenerative conditions that share the same core pathology as typical AD (Aβ and tau accumulation), but differ in lesion distribution, neuron cell type loss, neuronal network disruption, and dominant symptoms (i.e. non-amnestic). Atypical variants are estimated to account for 6-14% of AD cases *(Dubois et al., 2014)*. The most common variants are characterised by visual/biparietal posterior cortical atrophy (PCA) *(Benson et al., 1988; Crutch et al., 2012)*), linguistic logopenic variant primary aphasia (LPA) *(Gorno-Tempini et al., 2011)*, and behavioural/dysexecutive (frontal) features *(Ossenkoppele et al., 2015)*. Although prevalence of atypical cases is low, they are enriched in EOAD *(Koedam et al., 2010; Paterson et al., 2015; Tellechea et al., 2018)* and among

certain risk genotypes (e.g. APOE-ε4/ε4) *(Balasa et al., 2011; Carrasquillo et al., 2014; Van Der Flier et al., 2006; Schott et al., 2006; Tellechea et al., 2018)*.

Finally, it is important to acknowledge the role social environment and interpersonal relationships play in the clinical presentation and experience of affected individuals. Who a clinician sees, what disease stage they are at, what life-history is available, and capacity to engage with examination or respond to treatment will significantly colour diagnosis. There is some evidence to suggest that certain people are able to tolerate more AD-related pathology than others before reaching functional threshold, a concept known as cognitive reserve *(Stern, 2012)*. Education level, occupational attainment, and stimulating leisure activities are associated with increase in this reserve *(Stern, 2012)*. Additionally, a supportive social network may compensate for declining capacities and mask the onset of symptoms that might be more recognisable in its absence. Alternatively, an attentive network may recognise symptoms earlier, or encourage an individual to seek medical attention earlier than one less connected. The size of social networks and quality of relationships are also likely to be meaningful in terms of co-prevalence with certain psychological features and comorbidities. By way of a simplistic example, AD is often associated with depression *(Modrego, 2010)* and cardiovascular disease *(Stampfer, 2006)*. The extent to which such conditions influence, cause, or are caused by AD is unknown, but the role of an individual's environment would seem relevant.

In summary, Alzheimer's disease is a complex neurodegenerative condition, with significant consequence to individual lives and global society. Biomarkers for the protein products of AD associated genes, downstream processes, and biological response to pharmacological and environmental factors represent powerful tools for disentangling this complexity. Better understanding of the role of Aβ in the disease process, and the accurate measurement of differences in Aβ profiles between cases, is crucial to the project of developing effective therapeutics.

1.4 Amyloid beta biology

This thesis concerns the study of Aβ peptides as biomarkers for AD. This section will discuss the current understanding of Aβ biology by introducing the substrate from which it is derived (APP), the enzymes which liberate Aβ from APP, and then detail the properties of various Aβ structures relevant to AD.

First however, a brief overview of Aβ is desirable to set the scene. At the microscopic level, AD is characterised by the proteinaceous accumulations that Alzheimer first described. We now know the

"miliary foci" (amyloid plaques) he observed to consist primarily of aggregated Aβ *(Masters et al., 1985)*. Aβ exists as a series of low molecular weight peptides produced from the sequential cleavage of APP by a form of proteolysis known as secretase activity *(De Strooper et al., 2010)*. Aβ peptides can be truncated both N- and C-terminally depending on the nature of secretase activity involved in their production, as well as by secondary degradation events *(Saido and Leissring, 2012)*. These truncations are expressed as 'Aβx-y', where x is the number of the most N-terminal amino acid present, and y is the number of the most C-terminal amino acid present, relative to the Aβ domain sequence. For example, Aβ1-42 describes a peptide consisting of aspartic acid 1 through to alanine 42 of the Aβ domain. This work will use the convention of only using the C-terminal amino acid when referring to peptides with an N-terminal beginning at aspartic acid 1 (e.g. Aβ1-42 becomes Aβ42). Peptides with N-terminal truncations will be directly specified.

1.4.1 Amyloid Precursor Protein

The genesis of Aβ peptides is a complex biological process involving the sequential cleavage of APP by an assortment of different enzymes. In order to properly engage with this process some discussion of APP is required. This section will introduce what is known of APP genetics, maturation, and function.

1.4.1.1 Amyloid Precursor Protein Genetics

APP is the pro-protein of which Aβ peptides are cleavage products. Mutations in or pertinent to the expression of the *APP* gene are among the most common causes of fAD and have formed the foundation for the present understanding of AD biology. There are currently 52 *APP* mutations that have been investigated in association with AD. Of these, 27 are pathogenic, 15 are not thought to be pathogenic, one is protective, and nine have uncertain pathogenicity *(ALZFORUM, 2019a)*. Additionally, eight *APP* mutations have been linked to cerebral amyloid angiopathy (CAA). Of these six are pathogenic, one is not pathogenic, and one has unclear pathogenicity *(ALZFORUM, 2019a)*. Finally, AD-like pathology with early onset is prevalent in Down's syndrome *(Glenner and Wong, 1984b)*. Down's syndrome is the result of a full or partial triplication in chromosome 21, the chromosome on which *APP* is located *(Wilcock and Griffin, 2013)*. Compellingly, the few known cases where partial triplication of chromosome 21 did not include the *APP* gene did not develop AD for as long as they were observed *(Doran et al., 2017; Wiseman et al., 2018)*.

APP protein is one of a family of type I transmembrane glycoprotein homologues (Table 3) *(Shariati and De Strooper, 2013)*. Only APP contains the Aβ domain. Evolutionarily, the *APP* gene is thought to

have emerged with the earliest functioning synapses *(Shariati and De Strooper, 2013)* and lipoprotein receptors *(Dieckmann et al., 2010)*.

Table 3: Amyloid precursor protein homologues

Protein	Documented Species
APP	*H. sapiens, P. troglodytes, C. lupus familiaris, M. musculus, G. gallus, D. reiro, X. laevis*
APLP-1	*H. sapiens, P. troglodytes, C. lupus familiaris, M. musculus, D. reiro, X. laevis*
APLP-2	*H. sapiens, P. troglodytes, C. lupus familiaris, M. musculus, G. gallus, D. reiro, X. laevis*
APPL	*D. melanogaster*
ALP-1	*C. elegans*

Table 3: Listing the homologue proteins for amyloid precursor protein and the species they have been observed in.

1.4.1.2 Amyloid Precursor Protein Isoforms

Figure 1: APP primary structure

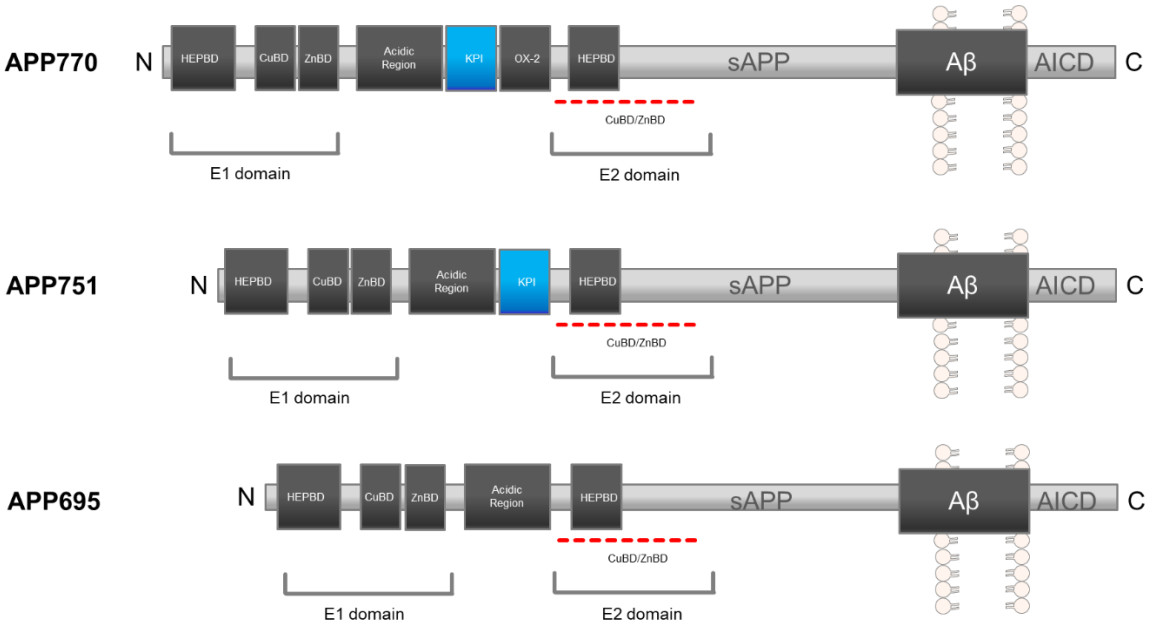

Figure 1: Diagram depicting the structure of the three major isoforms of APP.

APP is located on chromosome 21 (21q21.3) and consists of 19 exons. The Aβ domain is encoded by exons 16 and 17 *(Yoshikai et al., 1990)*. APP mRNA is found expressed in all human tissues, with

protein expression recorded in the cerebral cortex, hippocampus, caudate, cerebellum, appendix, gallbladder, pancreas, duodenum, colon, rectum, testis, prostate, epididymis, seminal vesicle, breast, endometrium, and placenta *(The Human Protein Atlas, 2019)*. Humans produce eight canonical isoforms of APP, with permutations based on the alternative splicing of exons 7, 8, and 15: APP_{770}, L-APP_{752}, APP_{751}, L-APP_{733}, APP_{714}, L-APP_{696}, APP_{695}, L-APP_{677}. APP isoforms lacking exon 15 were first identified in peripheral leukocytes and are designated L-APP *(Sandbrink et al., 1994)*. A number of other APP isoforms have been reported, but are rare and poorly documented: APP_{639} *(Tang et al., 2003)*, APP_{563} *(Perry et al., 1988)*, APP_{365} *(Jacobsen et al., 1991)*, and APP_{305} *(Chen et al., 2013)*).

Of the known isoforms, APP_{770}, APP_{751}, and APP_{695} are most prevalent (Figure 1). APP_{695} is the major isoform expressed by neurons *(Nalivaeva and Turner, 2013; O'Brien and Wong, 2012; Puig and Combs, 2013; Sandbrink et al., 1996a; Tanaka et al., 1988)*, where mRNAs are reported to approximate a ratio of APP_{770}/APP_{751}/APP_{695} = 1:10:20 *(Nalivaeva and Turner, 2013)*. Regional variation exists and APP_{695} is reported highest in the cerebral cortex, hippocampus, and areas proximal to the lateral ventricle *(Golde et al., 1990)*. APP_{770}/APP_{751}/APP_{695} are expressed at a ratio of 4:4:1 in HeLa cells *(Golde et al., 1990)* and APP_{770} and APP_{751} are also the primary forms expressed in glia *(Matsui et al., 2007; De Silva et al., 1997; Simons et al., 1996)*. APP_{770} is sequentially similar to APLP-2, whilst APP_{695} is sequentially similar to APLP-1 as both lack the KPI domain *(Nalivaeva and Turner, 2013)*. It may be that this contributes to the apparent functional redundancy between the protein homologues.

1.4.1.3 Amyloid Precursor Protein translation and transport

Diagrams of APP processing invariably show APP bisecting generic lipid bilayer, which students of neuroscience are guided to assume is the cell plasma membrane. Unfortunately, the dynamics of Aβ biology are nothing so simple. Integral to an understanding of Aβ production is an appreciation of where it is produced. Furthermore one of the most heated areas of discussion centres on the pathophysiological relevance of intracellular verses extra-cellular Aβ and how it gets to the respective location (Figure 2). Therefore, this section will outline the maturation and trafficking of APP and Aβ within a cell.

In both polarised and non-polarised cells, APP is synthesised in the endoplasmic reticulum (ER), where it is folded, N-glycosylated, and may potentially be proteolysed by secretase activity during ER stress *(Plácido et al., 2014)*, with implications for intracellular Aβ accumulation. From there APP can follow a constitutive secretion pathway through the golgi apparatus, where post-translational

modifications such as O- and N-link glycosylation, sialylation, phosphorylation, tyrosine motif sulphonation, and chondroitin sulfate/dermatan sulfate glycosaminoglycanation are applied *(Kins et al., 2006; Plácido et al., 2014)*.

Figure 2: APP transportation and processing

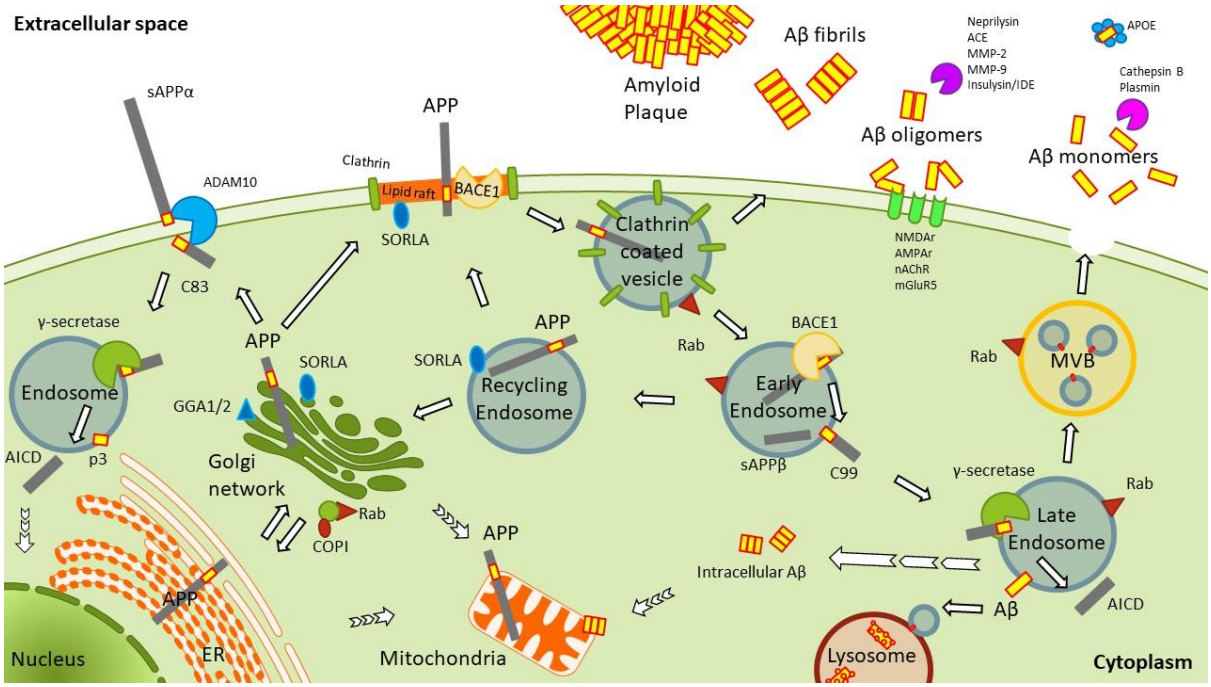

Figure 2: APP is synthesised in the endoplasmic reticulum (ER) and transported to the Golgi network. From there it is rapidly trafficked to the cell plasma membrane. Recycling from the plasma membrane is facilitated by lipid rafts and clathrin mediated endocytosis. At the plasma membrane APP can be cleaved by non-amyloidogenic α-secretase activity (ADAM10). Alternatively, amyloidogenic cleavage can occur by β-secretase activity (BACE1) and then γ-secretase activity, which predominantly occurs in the early endosomes. From the endosome system, APP can be recycled to the Golgi and plasma membrane with the assistance of SORLA, or targeted to the lysosomes for degradation. Aβ peptides may also follow this pathway, or enter multivesicular bodies (MVBs) for exocytosis or degradation. Also depicted is tendency for Aβ to form aggregate structures (oligomers, fibrils, and plaques), and for these to bind to cell surface receptors, or be degraded by interstitial fluid enzymes. Full arrows represent well evidenced pathways, dashed arrows represent pathways for which there is less confidence.

Alternatively, overexpression models suggest some portion of APP may also be localised to mitochondrial associate membranes (MAM) of the ER *(Del Prete et al., 2017)*. MAM are intracellular lipid-raft-like structures involved in mitochondrial lipid metabolism and Ca2+ homeostasis, and which constitute major sites of γ-secretase activity *(Area-Gomez and Schon, 2016)*. Some study has been made of the localisation patterns of different APP isoforms. APP_{695} has been shown to possess different affinities for particular compartments compared to APP_{770} and APP_{751}, such as the ER over the Golgi in circumstances of ER stress *(Plácido et al., 2014)*, and the endosomal system versus the plasma membrane in the secretory pathway *(Ben Khalifa et al., 2012)*. However, these experiments were conducted primarily in non-neuronal cell models, and it will be recalled that isoform expression

patterns differ between cell types (i.e. APP_{695} is the predominant form in neurons) and so this data may have limited neurobiological relevance.

To return to the secretory pathway, after maturation in the *cis*-Golgi APP enters the *trans*-Golgi network (TGN) and is sorted to different cellular destinations in coated vesicles. Work on HeLa cells has suggested adaptor protein complex 4 interacts with the C-terminal YKFFE sequence of APP to facilitate the recruitment of APP into certain of these transport vesicles *(Burgos et al., 2010)*. The complexities of APP distribution are still dimly understood and much debated. Non-polarised and polarised cells (such as neurons) differ in the targeting and transport of APP to destination compartments. In neurons, anterograde axonal transport of APP occurs via kinesin-1-mediated fast transport. These vesicles move mono-directionally at speeds of up to 10μm/s *(Kaether et al., 2000)*, which can be interpreted as high priority trafficking. There is contention over whether APP and its secretases co-localise in transport vesicles *(Brunholz et al., 2012)*. However, recent work suggests co-transportation of APP, ADAM10, and BACE1 can occur in at least some axonal transport vesicles *(Das et al., 2015; Szodorai et al., 2009)*, but quantities may be dependent on certain cellular activity states *(Das et al., 2013)*. Transcytosis of APP towards the dendritic compartment has not been well studied, although anterograde dendritic transport appears to utilise microtubules *(Das et al., 2013)*, and can be stimulated by glycine-induced long-term potentiation *(Tampellini et al., 2009)*. APP is also transported toward the soma. Retrograde axonal transport utilises the relatively slower cytoplasmic dynein transport method *(Brunholz et al., 2012)*. Alternatively, APP can be retro-transported from the Golgi and TGN to the ER in COPI- or Rab6-coated vesicles.

Following post-Golgi transport, APP is recruited to the cell plasma membrane where it has an affinity for cholesterol and sphingolipid enriched domains known as lipid rafts *(Vetrivel and Thinakaran, 2010)*. It is estimated that only ~10% of cellular APP is present at the plasma membrane at any given time, the bulk is retained within the Golgi and TGN *(Haass et al., 2012)*. It should be noted that the precise location of APP delivery along the axon is not known *(Haass et al., 2012)* although the majority of Aβ peptide appears to be pre-synaptic. Whilst within plasma membrane, APP is predominantly processed by the non-amyloidogenic secretase pathway. Amyloidogenic processing is facilitated when APP associates with lipid rafts. The extent to which APP interacts with BACE1 and γ-secretase within lipid rafts at the cell surface is unclear. However, clathrin-mediated endocytosis is essential to the bulk of Aβ production. Aside from the plasma membrane, non-glycosylated APP can localise to mitochondrial membranes, where it can interact with translocases of outer membrane (TOM) and translocases of inner membrane (TIM) import receptor isoforms *(Devi and*

Anandatheerthavarada, 2010). Whether APP gets to the mitochondria from the ER, TGN or multiple pathways is not clear.

Consequent to endocytosis, APP enters the endosome system, where it is processed or recycled to and from the plasma membrane. From the endosomes, APP can be trafficked back to the TGN by SORLA *(Schmidt et al., 2017)*, or be targeted to the lysosomes by N-linked glycosylation (and it is worth noting that this is impeded in the Swedish and London mutations of APP *(Haass et al., 1992, 2012; Lorenzen et al., 2010)*). BACE1 is enriched in endosomes, where the low pH environment is favourable for its enzymatic activity *(Yan et al., 2001a)*, and overexpression of mutant rab5 GTPase has shown that the bulk of amyloidogenic secretase activity occurs in the early endosomes *(Rajendran et al., 2006)*. Studies in HeLa and N2a cells have revealed that Aβ peptides generated in the endosomes become localised to multivesicular bodies, where they become incorporated into intraluminal vesicles that either couple with lysosomes or are secreted as exosomes *(Rajendran et al., 2006)*. Unilateral lesions of the perforant pathway, an axonal route connecting neurons in the entorhinal cortex to the dentate gyrus and other areas of the hippocampus, have demonstrated that axonally transported (thus pre-synaptic) APP likely originates the bulk of Aβ peptides secreted to the extracellular space *(Lazarov, 2005)*. Consistent with this view, synaptic activity has been shown to modulate levels of secreted Aβ *(Cirrito et al., 2008)*, and exosomal markers (Alix and flotillin-1) have been observed associated with plaques *(Rajendran et al., 2006)*. Pre-synaptic components identified in APP transport vesicles included synapsin-I, SNAP25, syntaxin-1B, VAMP2, Munc13-1, and RIM2, but not synaptophysin *(Szodorai et al., 2009)*.

1.4.1.4 Amyloid Precursor Protein Function

The physiological role of APP and its various isoforms remains poorly understood despite considerable study. This is likely due to complex localisation and proteolysis, limited work in human neurons, and lack of a general theory to integrate the findings of disparate experiments. APP is expressed early in development. Isoforms APP770 and APP751 are present throughout each of the three germ layers, whilst APP695 predominates in neuroectoderm *(Dawkins and Small, 2014; Kirazov et al., 2001)*.

Numerous studies have shown APP to be required for correct migration of neural precursor cells *(Rice et al., 2012; Young-Pearse et al., 2008)* and regulation of synaptic architecture along with subsequent activity *(Akaaboune et al., 2000; Jung and Herms, 2012; Kohli et al., 2012; Octave et al., 2013; Tyan et al., 2012)*. This overlaps with apparent functions of Aβ peptides, and it is not

necessarily easy to disentangle the two. Additionally, a role as a cell adhesion molecule is postulated due to the presence of APP at the cell plasma membrane, and significant ectodomain with a sequence structure matches many recognised cell adhesion motifs *(Sosa et al., 2017)*.

Furthermore, recent work has indicated that different APP isoforms have unique interactomes. APP751 proteolysis is mediated by GAP45, which reduces amyloidogenic proteolysis. On the other hand APP695 has been found to have interactions enriched for mitochondrial function, as well as nuclear pore and nuclear transport proteins *(Andrew et al., 2019)*. APP695 is also implicated in cell cycling of neural progenitor cells in conjunction with APP binding protein-1 *(Joo et al., 2010)* and inhibition of Wnt signalling *(Zhou et al., 2012)*.

As with Notch, APP has a cytosolic intracellular domain (NICD and AICD respectively) suggestive of a signalling function. This has variously been reported to include the role of a transcription factor in conjunction with Fe65 and Tip60 *(Pardossi-Piquard and Checler, 2012; Sabo et al., 2001)*, signal transduction in association with Mint1/2/3 *(Swistowski et al., 2009)*, homeostasis of calcium and ATP *(Hamid et al., 2007)*, regulation of filamentous actin structures *(Ward et al., 2010)*, and neuron-specific apoptosis *(Ohkawara et al., 2011)* by promoting activation of p53 *(Pardossi-Piquard and Checler, 2012)* and GSK-3b *(Chang et al., 2006)*. Potentially one of the most interesting suggested functions for AICD is that it regulates the promoter transactivation of neprilysin *(Belyaev et al., 2009; Pardossi-Piquard et al., 2005, 2006)*. Neprilysin is an Aβ-degrading enzyme, depletion of which can be predicted to result in Aβ accumulation or tax other cellular mechanisms of clearance, therefore it may be that part of the function of APP is to act as a pro-protein for which certain products (AICD) regulate the activity of others (Aβ).

In an important study, Heber *et al.* demonstrated that knock out (KO) of APP/APLP-1/APLP-2, APP/APLP-2, and APLP-1/APLP-2 had perinatal lethality in mice *(Heber et al., 2000)*. Individually and in combination APP and APLP-1 KO reduce body weight, grip strength, and locomotor activity of mice *(Heber et al., 2000; Li et al., 1996; Müller et al., 1994; Senechal et al., 2008; Zheng et al., 1995)*, produce age-associated memory deficit *(Senechal et al., 2008)*, and increase vulnerability to epileptic seizures *(Steinbach et al., 1998)*. Conversely, adding soluble human APP to mouse primary cultures protected neurons from glutamate-induced excitotoxicity *(Mattson et al., 1993)*, further linking APP, or its derivatives, with regulation of neuron excitation. Surprisingly, APLP-2 KO alone does not produce a different phenotype from controls *(Heber et al., 2000; Von Koch et al., 1997)*. Thus the picture suggests that considerable functional redundancy exists between the gene homologues, but

certain properties of APLP-2, which APP and APLP-1 may cover in combination, appear essential to early development.

Interestingly, primary culture and stem cell derived neuronal models with permutations of APP/APLP-1/APLP-2 KO do not demonstrate significant death phenotypes compared to controls *(Bergmans et al., 2010; Heber et al., 2000)*, although APP/APLP-2 KO is reported to alter copper homeostasis *(Bellingham et al., 2004)*. If these *in vitro* models reflect *in vivo* physiology, this may suggest that deleterious effects could be systemic, and perhaps involve peripheral organs such as the liver. Indeed, some evidence shows raised pancreatic APP and amyloid deposits in type 2 diabetes, a morbidity commonly associated with AD *(Miklossy et al., 2010)*.

1.4.2 Amyloid precursor protein processing

A key focus of this thesis is improving the understanding of Aβ production in human *in vitro* models of fAD. To generate Aβ, APP undergoes a complex sequence of proteolysis as it is transported between cellular compartments. Sequential cleavage by a series of membrane bound proteases known as secretases liberate the Aβ domain from APP as a peptide. Canonically, there are two relevant cleavage pathways that share a reciprocal (competitive) relationship, although this conceptualisation is becoming outdated as new evidence reveals a much more sophisticated picture of proteolytic activity within and around the Aβ domain (Figure 3) *(Andrew et al., 2016; Chávez-Gutiérrez et al., 2012; Willem et al., 2015)*. APP isoforms appear to be processed by similar mechanisms in neurons, platelets and leukocytes (Li 1999).

Figure 3: Aβ primary structure, proteolytic sites and AD mutations

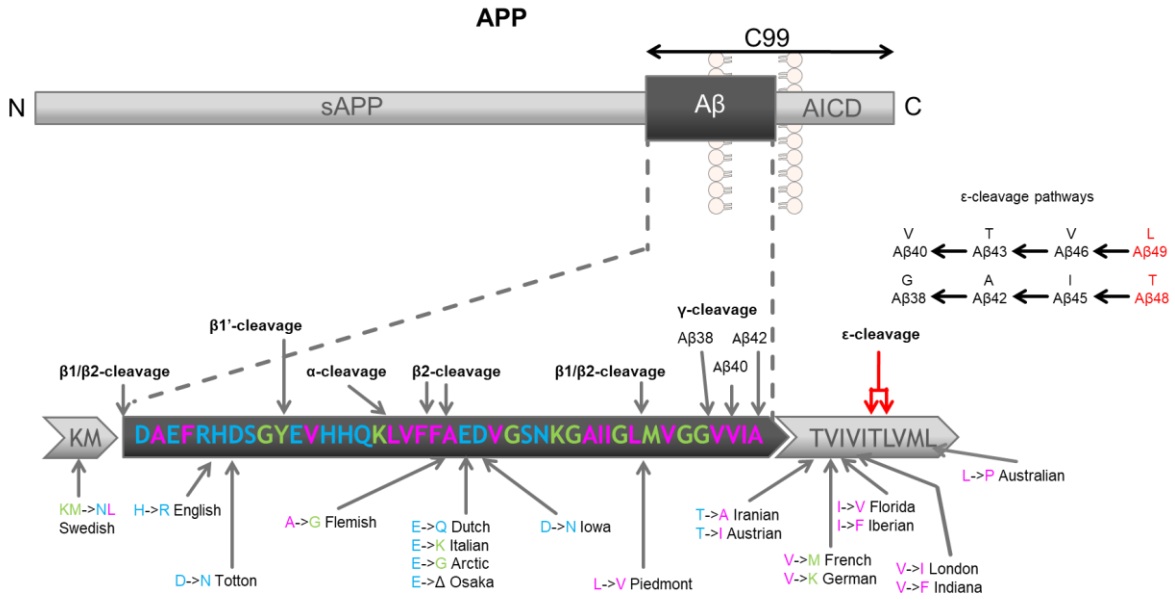

Figure 3: A stylised diagram of the Aβ domain of APP (dark grey). Amino acids are represented by letter and colouring indicates charge state (blue: hydrophilic, green: amphipathic, pink: hydrophobic). Various sites of known secretase activity are depicted above, and AD mutations are indicated below the domain. The alternate cleavage pathways at the ε-cleavage site are highlighted.

1.4.2.1 α-secretase

The non-amyloidogenic pathway consists of cleavage within the Aβ domain of APP (Lys16-Leu17 of Aβ), generating a carboxylic acid terminal fragment (CTF) C83. Further proteolysis of C83 results in N-terminally truncated p3 peptides that do not drive AD pathology (Figure 2). This pathway is thought to be the favoured method of APP processing in non-neuronal cells *(Haass et al., 2012)* and occurs throughout neuron development *(Bergstrom et al., 2016)*. Members of the 'a disintegrin and metalloproteinase' (ADAM) family have been identified as α-secretases. ADAMs are zinc-dependent proteinases that cleave by hydrolysis. The principal α-secretase is ADAM10, and inhibition of this protease reduces sAPPα by up to 90% *(Jorissen et al., 2010; Kuhn et al., 2010)*. ADAM7, ADAM9, ADAM17, and ADAM19 also demonstrate α-secretase activity *(Seals and Courtneidge, 2003)*. ADAM10 is activated by removal of the N-terminal pro-domain in the Golgi, which reveals the catalytic site *(Endres and Deller, 2017; Seegar et al., 2017)*. C-terminal regions of ADAM10 function to guide the proteinase's cellular localization and substrate recognition *(Endres and Deller, 2017; Seegar et al., 2017)*.

Other substrates of the ADAMs besides APP include NOTCH, pro-inflammatory cytokines (TNF-α and IL-6) and receptors (TNFRI, TNFRII, IL-6R and IL15R), cell adhesion molecules (L-selectin, Syndecan-1,

Syndecan-4, VCAM-1, JAM-A , CXCL16), and release of CX3CL1 and VE-cadherin (overviewed in *(Saftig and Reiss, 2011)*). Interactions with PrP^c and tau are particularly interesting given the involvement of these proteins in neurodegeneration including AD. Aβ oligomers have been observed to bind directly to PrP^c at the plasma membrane, resulting in activation of fyn kinase, phosphorylation of tau, NMDAr internalisation and increased reactive oxygen species (ROS). Cleavage of PrP^c by ADAM10 results in its shedding from the membrane and thus limits this potentially toxic interaction *(Jarosz-Griffiths et al., 2019)*. Tau is also an ADAM substrate, generating tau 153-441 fragment *(Quinn et al., 2018)*.

1.4.2.2 β-secretase

The amyloidogenic pathway defines the cleavage of APP by the β-secretase activity of beta-site APP cleaving enzyme 1 (BACE1) at the Aβ domain N-terminus, producing sAPPβ and C99, followed by γ-secretase cleavage of C99 at the domain C-terminus, liberating the Aβ peptide and AICD (Figure 2). BACE1 is a type 1 membrane-anchored aspartate protease, containing two D(T/S) G(T/S) motifs within its extracellular domain *(Ahmed et al., 2010)*. BACE1 has a mostly inactive pro-protein form, concentrated primarily in the ER *(Capell et al., 2000)*, although it may still be able to cleave APP *(Creemers et al., 2001)*. BACE1 is matured in the golgi following glycosylation and cleavage by proprotein convertases (such as furin), phosphorylated by casein kinase-1, and trafficked to the plasma membrane. The bulk of BACE1 is rapidly reinternalized and distributed through the early and late endosomes, where co-localisation and low pH favour β-secretase activity, or returned to the TGN in a phosphorylation dependent manner *(Walter et al., 2001)*. It is estimated that the bulk of Aβ (60-70%) is produced in the endosomes, as this is where mature BACE1 is most concentrated *(Niederst et al., 2015)* (Figure 2).

Other than cleaving prior to Asp-1 of the Aβ domain, BACE1 can also cleave APP between Tyr10 and Glu11, known as β'-secretase activity, which produces an N-terminally truncated peptide (C89) *(Liu et al., 2002; Vassar et al., 1999)* (Figure 3). N-terminal truncations of Aβ have also been identified at amino acid positions 2-x *(Bayer and Wirths, 2014; Vassar et al., 1999)*, which may or may not be BACE1-dependent *(Bayer and Wirths, 2014; Kummer and Heneka, 2014)*. It has been suggested that C-terminal truncation at Leu-34 may also be the work of this enzyme *(Portelius et al., 2014)*. Theoretically, BACE1-BACE1' cleavage could produce an Aβ11 peptide *(Vassar et al., 1999)*. There are conflicting reports regarding the effect of APP post-translational modification on secretase cleavage *(Ando et al., 2001; Lee et al., 2003; Sano et al., 2006)*. There is the suggestion that APP_{695} isoform may be more prone to processing via the β-secretase pathway, whereas KPI-domain containing

isoforms (APP_{751} and APP_{770}) preferentially undergo α-secretase cleavage *(Belyaev et al., 2009)*. However, as APP_{695} is predominantly expressed in neurons whilst APP_{751} and APP_{770} are glial *(Matsui et al., 2007; De Silva et al., 1997; Simons et al., 1996)*, this pattern may therefore be the result of cellular function rather than isoform-specific properties. It has been noted that high levels of BACE1 are found in APP poor, plaque spared brain regions such as the striatum and thalamus. Besides APP, BACE1 has many other substrates which have been overviewed by Vassar *et al. (Vassar et al., 2009)*.

Other enzymes with potential β-secretase-like activity are cathepsin B and meprin β. Cathepsin B has been suggested to increase production of pyroglutamate Aβ3-X and Aβ11-X (where the N-terminal glutamate is cyclised by glutaminyl cyclase), and reduction of cathepsin B has been associated with reduction on amyloid pathology [X]. However, these results are not well replicated [X], and the enzyme does not appear to accumulate in amyloid plaques as is the case with BACE1. Meprin β is a zinc metalloprotease that is implicated in the production of Aβ1-X, Aβ2-X, and Aβ3-X. Unlike BACE1 meprin β activity occurs primarily at the plasma membrane, where it may directly compete with α-secretase activity.

1.4.2.3 BACE2: an alternative β-secretase

Another source of β-secretase activity is BACE2, although it is sometimes considered more akin to an α-secretase given its tendency to cleave APP within the Aβ domain *(Yan et al., 2001b)*, and has also been dubbed a θ-secretase *(Sun et al., 2006)*. This protein shares ~75% homology with BACE1 *(Ahmed et al., 2010)*, and though primarily expressed within the colon, kidney and pancreas *(Bennett et al., 2000)*, where its substrate cleavages influence β cell proliferation and skin pigmentation *(Alcarraz-Vizán et al., 2017; Esterházy et al., 2011; Rochin et al., 2013; Rulifson et al., 2016)*, BACE2 maturation differs from BACE1 in that maturation by removal of the pro-segment occurs by self-cleavage *(Yan et al., 2001b)*.

Within the brain BACE2 is typically expressed in subsets of neurons, oligodendrocytes, astrocytes, and astrocyte-like neural stem cells *(Voytyuk et al., 2018)*, versus the more broadly neuronal BACE1 *(Barão et al., 2016; Irizarry et al., 2001)*. BACE1 KO has been shown to fully ablate Aβ production in mouse models *(Cai et al., 2001; Luo et al., 2003)*, and BACE1 KO does not stimulate compensatory upregulation of BACE2 *(Luo et al., 2003)*. However, *in vitro* experiments have shown that BACE2 can cleave APP at the β-secretase cleavage site *(Farzan et al., 2000)* as well as at Phe19-Phe20, Phe20-Ala21, and Leu34-Met35 *(Abdul-Hay et al., 2012)*, the latter of which is thought to be its principle cleavage site (Figure 3). This endopeptidase-like activity may reflect the role of BACE2 as a powerful

Aβ degrading enzyme rather than involvement in primary production *(Abdul-Hay et al., 2012)*, although the picture is further complicated by the seeming importance of BACE2 for Aβ production in Flemish mutant APP transfected cells *(Farzan et al., 2000)*. Other CNS substrates of BACE2 include plexin domain containing 2 (PLXDC2), fibroblast growth factor receptor 1 (FGFR1), delta and notch-like epidermal growth factor–related receptor (DNER), and vascular cell adhesion molecule 1 (VCAM1). The latter mediates peripheral leukocyte infiltration through the blood brain barrier (BBB), is not a substrate shared by BACE1, and BACE2-dependent VCAM1 shedding is increased in inflammatory conditions both *in vitro* and *in vivo* mouse models *(Voytyuk et al., 2018)*.

Other enzymes with potential β-secretase-like activity are cathepsin B and meprin β. Cathepsin B has been suggested to increase production of pyroglutamate Aβ3-X and Aβ11-X (where the N-terminal glutamate is cyclised by glutaminyl cyclase), and manipulation of cathepsin B has been associated with alterations in Aβ concentration in transgenic mouse brain. However, data are not consistent, and the enzyme does not appear to accumulate in amyloid plaques as is the case with BACE1 *(Andrew et al., 2016)*. Meprin β is a zinc metalloprotease that is implicated in the production of Aβ1-X, Aβ2-X, and Aβ3-X. Unlike BACE1, meprin β activity occurs primarily at the plasma membrane, where it may directly compete with α-secretase activity *(Andrew et al., 2016)*.

1.4.2.4 γ-Secretase

γ-Secretase activity is responsible for the proteolysis of APP within the transmembrane domain, and features in both the amyloidogenic and non-amyloidogenic pathways (Haas and Selkoe 1993) (Figure 2). This activity is performed by a protein complex, called γ-secretase, formed of four subunits: nicastrin, anterior pharynx defective 1a or 1b (APH-1a/b), presenilin enhancer 2 (PEN-2), and presenilin 1 or 2 (PSEN 1/2).

The presenilins are the best studied of all the γ-secretase subunits, and as several *PSEN1* mutations form a subject of interest in this thesis some additional consideration will be given to these proteins. *PSEN1* (14q24.2) and *PSEN2* (1q42.13) encode 50kDa transmembrane pro-proteins that weave through the membrane with nine transmembrane domains (TMDs) *(Laudon et al., 2005; Spasic et al., 2006)*. Either PSEN1 or PSEN2 can be present in the γ-secretase complex and act as aspartic proteases that function as the catalytic site *(Wolfe, 2013)*. Aspartic acid proteases require H_2O molecules to break a substrate's scissile bond, so the ability of PSEN to cleave substrates within the hydrophobic environment of the TMD is interesting. It is suggested that TMDs six and seven, which incorporate the two aspartate residues, form a hydrophilic space within the membrane into which a

substrate is transferred *(Tolia et al., 2006)*. Enzymatic function is activated by PEN-2 assisted auto-endoproteolytic cleavage of the exon 9 loop *(Knappenberger et al., 2004)* into a 30 kDa N-terminal fragment and a 20 KDa C-terminal fragment *(Thinakaran et al., 1996)*, enabling conformations required for aspartic acid proteolysis. It is worth noting that PSEN1 has been ascribed other 'non-proteolytic' functions. PSEN1 mutations have been shown to alter Ca^{2+} concentrations in the ER *(Bezprozvanny and Mattson, 2008)*, and it has been suggested that full-length PSEN1 may form membrane pores that cause calcium 'leak channels' *(Tu et al., 2006)*. However, other evidence indicates this may be the result of its role in the activation of Ryanodine receptor (RyR) *(Chan et al., 2000; Hayrapetyan et al., 2008)*, inositol-3-phosphate (IP3) *(Cheung et al., 2008)*, and sarco(endo)plasmic reticulum Ca^{2+}-ATPase (SERCA) pumps *(Green et al., 2008)*, all of which are involved with calcium homeostasis. Another hypothesised γ-secretase independent function of PSEN1 affects the lysosomal degradation pathway. KO of PSEN1 was shown to reduce the ability of telencephalin-positive vacuoles to fuse with lysosomes in fAD PSEN1-D257A mouse model hippocampal neurons *(Esselens et al., 2004)*. Both calcium homeostasis and lysosome function have potential relevance for AD.

There are currently 246 *PSEN1* mutations that have been investigated in association with AD. Of these, 225 are pathogenic for AD, three are not thought to be pathogenic, one is considered a risk factor, and 17 have uncertain pathogenicity *(ALZFORUM, 2019b)*. Three PSEN1 mutations are pathogenic for CAA *(ALZFORUM, 2019b)*. Of the 45 documented PSEN2 mutations, 16 are pathogenic, 12 are not pathogenic, and 17 have unclear pathogenicity for AD *(ALZFORUM, 2019b)*. No PSEN2 mutations have yet been identified associated with CAA. Furthermore, and interestingly, neither PSEN1 nor PSEN2 are found altered in Down's syndrome, suggesting that the AD-like pathology to which these individuals are vulnerable is a function of increased APP and Aβ *per se*, rather than dysregulated production.

Dissociation of the γ-secretase complex by dodecyl β-D-maltoside (DDM) has revealed two major sub-complexes (and two minor ones) that suggest how γ-secretase may form *(Fraering et al., 2004)*. Nicastrin and APH-1 bind together via multiple transmembrane domain (TMD) interactions *(Chiang et al., 2012; Pardossi-Piquard et al., 2009)*. Physiologically this occurs in the endoplasmic reticulum *(LaVoie et al., 2003)*. This structure recruits full-length PSEN, by the binding of PSEN C-terminal domain to nicastrin *(Capell et al., 2003; Kaether et al., 2004)*, and both N-terminal and C-terminal domains to APH-1 *(Steiner et al., 2008)*. Whether PSEN is recruited alone or as part of a pre-assembled PSEN-PEN-2 complex is not actually demonstrated in the much-cited work of Fraering et

al. *(Fraering et al., 2004)*. Regardless, PEN-2 binds to PSEN1 at the N-terminal domain (fourth TMD) of the latter, forming a structure capable of stable independence from the nicastrin-APH-1 sub-complex *(Fraering et al., 2004; Watanabe et al., 2005)* Due to the existence of two alternate presenilins (PSEN1 and PSEN2) and APH-1 isoforms (APH-1a and APH-b), there are at least four physiologically possible γ-secretase structures *(De Strooper, 2003)*. Once the complete γ-secretase complex has articulated, it is transported through the golgi and trans-golgi network to and from the cell surface. During transition, γ-secretase is matured and activated by proteolysis of presenilin and glycosylation of the various complex sub units *(Takasugi et al., 2003)*. It would be reasonable to hypothesise that cellular mechanisms exist to regulate γ-secretase's activation as it is transported through various cell compartments. Increased γ-secretase activity requires overexpression of all subunits *(Haass et al., 2012)*, or activity enhancing mutation in APH-1 subunits *(Qin et al., 2011)*. Complete KO in mice is embryonically lethal, whilst complete loss of function of PSEN1, Pen-2, and Nicastrin in humans results in acne inversa, but not neurodegeneration or AD *(Wang et al., 2010)*.

γ-secretase cleaves APP toward the C-terminal of its TMD (Figure 3). The area of cleavage activity is broad, spanning from at least 14-43 amino acids *(Kummer and Heneka, 2014; Moore et al., 2012; Portelius et al., 2012)*, and capable of producing peptides of many different lengths, including the often overlooked small fragment products (3-4 amino acids) generated by the sequential nature of γ-secretase cleavage *(Takami et al., 2009)*. Despite some assertions *(Fernandez et al., 2016)*, it is not yet definitively known at which amino acid(s) γ-secretase makes its first cut (and incidentally where the Aβ domain ends is therefore undefined). Cleavage at the epsilon (ε) site (amino acids Thr48 or Leu49 of the Aβ sequence) represents one of the earliest evidenced cleavages of APP by γ-secretase and is considered to define two different peptide cleavage pathways *(Chavez-Gutierrez et al., 2012; Qi-Takahara, 2005; Takami et al., 2009)* However, Takami *et al.* have also suggested cleavage at Met51 or Leu52 could precede Thr48 or Leu49 respectively *(Takami et al., 2009)*. Regardless, point deletion experiments have shown that the number of amino acids between the terminal transmembrane sequence and ε-cleavage site does not alter the point of ε-cleavage, and therefore does not dictate the nature of subsequent cleavages *(Fernandez et al., 2016)*. Rather, it appears to be the arrangement of amino acid side chains along the TMD helix, not the number of amino acids *per se* that guides the initial binding site and subsequent exposure of APP to the catalytic site *(Fernandez et al., 2016)*.

γ-Secretase is a developmentally important enzyme with many substrates beyond APP which include proteins involved in synaptogenesis and dendritic spine maturation (NOTCH, ErbB4, E-cadherin, N-

cadherin, ephrin-B2) *(Barthet et al., 2013)*, regulators of neural and glial process migration and adhesion (ephrin A4, CD44, netrin receptor, neuroligin), and regulators of APP trafficking (LRP1 and SORLA), reviewed by Carroll and Li *(Carroll and Li, 2016)*. A particularly interesting development in this area of study is the identification of regulatory proteins, such as γ-secretase activating protein (gSAP) *(Chu et al., 2015)* and hypoxia-inducible factor 1α (Hif1α) *(Villa et al., 2014)*, which facilitate γ-secretase interaction with certain substrates over others, and may be associated with AD.

1.4.2.5 The tripeptide hypothesis

A feature of γ-secretase proteolysis of APP proteins (whether single or dimerised is a matter of contention *(Fernandez et al., 2016; Itkin et al., 2017)* is that cleavages occur in a sequential manner, approximately every three to four amino acids (Figure 3). This process theoretically, and to a certain extent demonstrably, produces a series of C-terminal tripeptides dependent on the extent of truncation of the Aβ domain at gamma (γ) cleavage sites, and is dubbed the 'tripeptide hypothesis' *(Qi-Takahara, 2005)*. Though the mechanisms of how this occurs remain to be fully elucidated, recent studies are building a working understanding.

It is understood that the substrate binding region proximal to the γ-secretase catalytic site contains three hydrophobic substrate binding 'pockets' which accommodate three substrate residues N-terminal to the scissile amide bond, explaining the propensity for tripeptide cleavage sequence *(Bolduc et al., 2016)*. Despite some initial controversy, a consensus that the APP TMD adopts an alpha-helical arrangement is beginning to emerge. This structure appears to be denatured by γ-secretase into a random coil within the binding pocket region enabling proteolysis. The extent to which the enzyme is successful in making sequential cleavages is determined by the structural stability of the γ-secretase and/or APP *(Chavez-Gutierrez et al., 2012; Fernandez et al., 2016)*. The kinetics of APP transfer through or release from the γ-secretase catalytic site are still mysterious, although the negative charge of the substrate C-terminal has been shown not to assist this transferral *(Fernandez et al., 2016)*.

1.4.2.6 γ-Secretase loss of function

It was proposed that partial loss of function in the γ-secretase catalytic subunit, presenilin (PSEN), may underlie memory impairment and neurodegeneration in the pathogenesis of AD *(Shen and Kelleher, 2007)*. However, recent work has begun to show that γ-secretase carboxypeptidase-like activity, rather than overall activity, is reduced in familial Alzheimer's disease (fAD) with *PSEN* mutation involvement *(Szaruga et al., 2017)*. In other words, 'efficiency' is the major determinant of

Aβ production. Mutant PSEN appears to be less efficient at making successive cleavages of APP, resulting in relative over-production of longer Aβ peptides, whilst proteolysis of other substrates is functionally spared. However, further experimental work is needed to properly substantiate this interpretation.

1.4.2.7 Aβ peptides generated by γ-secretase

Combined with the concept of an initial ε-site cleavage, the tripeptide model predicts two alternative Aβ peptide production pathways: Aβ49 → Aβ46 → Aβ43 → Aβ40 or Aβ48 → Aβ45 → Aβ42 → Aβ38 *(Chavez-Gutierrez et al., 2012)* (Figure 3). Recent experiments have begun to explore and validate the scope of this theory, and γ-secretase-generated peptides currently identified are: Aβ43 *(Almdahl et al., 2017; Lauridsen et al., 2017; Saito et al., 2011; Zoltowska and Maesako, 2016)*, Aβ42, Aβ40, Aβ39, Aβ38, and Aβ37 *(Kukar et al., 2011; Moore et al., 2018)*, possibly Aβ34 and Aβ33 *(Kukar et al., 2011)*, and possibly Aβ17 *(Portelius et al., 2011, 2012)*. Whilst the existence of many of these peptides fit the model, certain peptides (Aβ49-Aβ44) remain to be reliably detected. Additionally, Aβ38 does not neatly fit within either tripeptide pathway and yet is readily detected and associated with the Aβ48 pathway *(Chavez-Gutierrez et al., 2012)*. γ-secretase does not have a fourth substrate binding pocket *(Fernandez et al., 2016)*, and so the mechanism for Aβ38 production within a tripeptide framework remains unclear. How fixed are these pathways? Could there be others (as implicated in *(Matsumura et al., 2014)*? Could the ε-cleavage site extend to Aβ50 or Aβ47? Many questions surround this hypothesis and will require high fidelity human APP processing models as platforms to explore from.

1.4.2.8 η-Secretase

Finally, the most recent addition to the list of APP-secretases was “eta” or η-secretase, identified by the work of two independent groups in variety of models including transgenic mouse CSF and primary culture, Chinese hamster ovary (CHO) cells, human embryonic kidney (HEK) cells, and embryonic pluripotent stem cell (EPSC) -derived human *(Wang et al., 2015; Willem et al., 2015)*. MT5-MMP, a membrane-bound matrix metalloproteinase, is implicated as a potential η-secretase candidate as Aη-α concentrations were partially reduced by KO of this molecule *(Willem et al., 2015)*. Whatever combination of molecules contribute to η-secretase activity, it is thought to result in a cleavage of APP between Asp504 and Met505 (relative to the APP695 sequence) within the flexible extracellular juxtamembrane region, generating CTFη *(Willem et al., 2015)*. Inhibition of lysosomal-cathepsins results in accumulation of CTFη in cell lysates *(Wang et al., 2015; Ward et al., 2017)*, and accumulation of CTFη is found localised to dystrophic neurites and amyloid plaque halos (but not cores) *(Willem et al., 2015)*, suggesting involvement with neurotoxicity. Subsequent cleavage of the

CTFη by α-secretase, β-secretase or β'-secretase activity results in the liberation of an Aη-α, Aη-β or Aη-β' peptide respectively. BACE1 proteolysis of CTFη (generating Aη-β or Aη-β') would also be potentially amyloidogenic and so produce Aβ if interaction with γ-secretase were not altered. Aη-β has been shown to have no effect on synaptic transmission or long term potentiation (LTP) of CA1 pyramidal primary neurons *(Willem et al., 2015)*. Aη-α also had no effect on synaptic transmission, but did demonstrate a lowering effect on LTP. Aη-α has yet to be detected extra-cellularly *(Ward et al., 2017)*. Interestingly, Willem et al. observed that η-secretase processing significantly exceeded amyloidogenic processing by 9.5 ± 1.87 times (p=0.001, Student's t-test) *(Willem et al., 2015)*. β-secretase proteolysis of APP is documented to be a less frequent event than α-secretase proteolysis, neither of which necessarily preclude η-secretase activity, and so this finding may make sense. However, it is somewhat difficult to square this with the proposal that η-secretase products have neurotoxic function and more work is certainly required to interrogate this further, though unfortunately beyond the scope of this thesis.

1.4.3 Amyloid Beta

Having detailed the mechanisms by which Aβ peptides are produced, focus will now shift to the properties they have and the structures they form.

Figure 4: Processes of Aβ aggregation

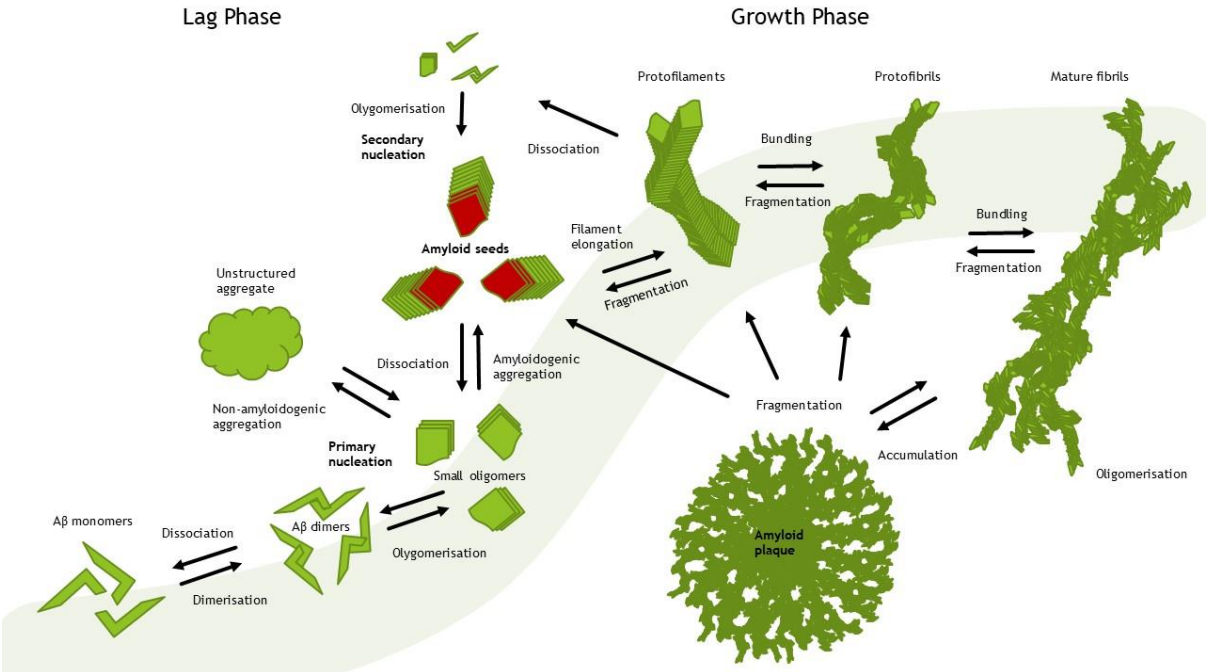

Figure 4: Showing the theorised process of Aβ aggregation from monomers, to oligomers, to protofilaments, to protofibrils, mature fibrils and eventually the distinctive amyloid plaques, characteristic of AD. Multidirectional arrows highlight the dynamic relationship of the various structure as they form and devolve in solution. Phases of lag and growth are recognised in this process, with relative energetic barriers to aggregation usually limiting the formation rates of early oligomers, before certain conformational and environmental changes occur to facilitate the stability of larger fibril structures.

1.4.3.1 Amyloid beta: primary structure and biophysical properties

Aβ peptides are typically polar molecules; the domain C-terminus (amino acids 30-50) is enriched with hydrophobic amino acids, as well as a medial clustering (amino acids 17-21), whilst the extra-membrane projecting N-terminus (amino acids 1-16) has a comparatively higher number of hydrophilic and amphipathic amino acids (Figure 3) *(Enache et al., 2018)*. These domains represent a key feature of Aβ conformation and therefore the extent to which they are present in the sequence of a given peptide determines a significant portion of its biochemistry. Furthermore, in an unfolded state, Aβ (peptide sequences 1-36 to 1-43) are estimated to have a pI of 5.59, and therefore a net negative charge at physiological pH (-2.9 at pH7.4). These intrinsic factors dictate the propensity of molecules to bind to surfaces, and Aβ40 has been shown to adsorb onto hydrophobic as well as positively charged hydrophilic surfaces *(Rocha et al., 2005)*. Given the importance of individual amino acid residues to the conformational and aggregative behaviour of Aβ peptides, it is important to note that rodent APP in the region of Aβ domain differs from human by three N-terminal amino acids (Arg5 is substituted by Gly, Tyr10 by Phe and His13 by Arg) which makes rodent Ab less prone to form amyloid aggregates and less cytotoxic *(Fraser et al., 1992)*.

1.4.3.2 Amyloid beta: secondary and tertiary structures

Substantial investigation of Aβ monomer secondary structures has been conducted, largely focused on Aβ40 and Aβ42, but inclusive of various smaller peptides. Due to a range of, and lack of consistency between, experimental conditions utilized, a definitive understanding has not been reached. However, the general consensus is that in aqueous solution at between 4-25°C and approximately neutral pH (pH 7-7.4), Aβ40 and Aβ42 typically adopt a random coil secondary structure in dynamic equilibrium with heterogeneous collapsed coil structures featuring a hairpin turn toward the C-terminal region *(Ball et al., 2011; Riek et al., 2001; Roche et al., 2016; Vivekanandan et al., 2011)*. Many incongruences in the literature likely arise from variations in pH, temperature, buffer composition, peptide type (e.g. endogenous/recombinant/synthetic etc.), and post-translational modification between experiment conditions *(Hou et al., 2004; Roche et al., 2016)*. Indeed Aβ peptides can be post-translationally modified by oxidation, phosphorylation, nitration, racemization, isomerization, pyroglutamylation, and glycosylation *(Hou et al., 2004; Kummer and Heneka, 2014)*. These factors influence the aggregation dynamics of Aβ and seem to be of relevance to neurotoxicity. Indeed, this may contribute to the documented differences in aggregation propensity observed between recombinant or synthetic Aβ peptides and endogenous forms *(Vandersteen et al., 2012)*. Although an intrinsically disordered structure is energetically favourable for Aβ monomers in neutral buffered solution, under certain conditions Aβ peptides readily adopt

defined β-sheets in aqueous solution *(Nikolic et al., 2011; Schladitz et al., 1999; Serpell, 2000)* and α-helices in organic solvents or the hydrophobic environment of lipid membranes *(Nerelius et al., 2009; Serpell, 2000; Soto et al., 1994; Wei and Shea, 2006)* although each peptide form behaves uniquely *(Wise-Scira et al., 2011)*. The formation of initial non-random secondary structures can be driven by temperature, pH, salt content, and surface interactions that change the Gibbs free energy (ΔG) of the system to make new conformations more favourable. Although there is mounting evidence that Aβ monomers themselves are relatively innocuous physiologically, the properties of aggregated Aβ forms are consistently linked to direct and indirect neurotoxic processes *(Yang et al., 2017)*.

1.4.3.3 Amyloid beta: quaternary structures

Initial nucleation of Aβ appears to be driven predominantly by intermolecular interactions between hydrophobic peptide regions, which differentiate peptides with otherwise similar properties e.g. Aβ40 and Aβ42 *(Meisl et al., 2014; Roche et al., 2016)*. Aβ peptides can engage in dynamic self-aggregation, rapidly forming structures from dimers, trimers, and tetramers, to oligomers of various sizes, which more gradually become fibrils of parallel β-sheets that can measure tens of nanometers *(Serpell, 2000)* (Figure 4). The composition of these aggregates is difficult to dissect, but experiment has shown structures of single type and cross-peptide types can occur, which may have important implications for physiological and pathological roles *(Chakraborty and Das, 2017; Moore et al., 2018)*. Critical aggregation concentration describes the concentration at which ΔG changes abruptly in a manner favourable to increased interaction of a particular molecule. Above a critical aggregation concentration threshold, the number of aggregates of a given size increases. The critical aggregation concentration for Aβ40 and Aβ42 is reported to be within a nanomolar range (approximately 28-120 nM) *(Iljina et al., 2016; Novo et al., 2018)*, at which oligomers formed of approximately 28-88 monomers and with hydrodynamic radii of approximately 7-11 nm are present. Lower level aggregation of smaller structures likely occurs at lower concentration ranges. Physiological concentrations of Aβ in human CSF are in the picomolar range. Measurement of physiological Aβ concentrations in human brain are complicated by different solubility fractions, but also appear (along with mice *(Puzzo et al., 2008; Waters, 2010)*) to be present in picomolar quantities *(Lazarevic et al., 2017)*. However local fluctuations in concentration and other ΔG altering parameters such as temperature, pH, and surface interface properties are very likely an important factor in Aβ aggregation *in vivo*.

In experimental conditions small Aβ oligomer structures form rapidly, within minutes *(Banerjee et al., 2017)*, but with high reversibility, leading to an extended aggregation lag phase *(Arosio et al., 2015)*,

where-after larger structures have greater stability as the number of interactions becomes more significant *(Härd, 2014; Törnquist et al., 2018)* (Figure 4). It was recently shown in two independent studies that the initial dimer structure is formed by the hydrophobically driven interaction of two monomers that form a mirrored S-shaped conformation, which accumulate other dimer subunits in cross-β sheet motifs *(Colvin et al., 2016; Wälti et al., 2016)*. It has been observed that a certain proportion of aggregates, or perhaps certain structural conformations, aggregate irreversibly *(Roche et al., 2016)* forming insoluble 'seeds' that catalyse aggregation when introduced to Aβ monomer containing solutions, and can grow to extended filaments and protofibrils. Increasing evidence suggests that a proportion of Aβ structures that break away from certain aggregate conformations retain seed templating or cross-seeding potential and further facilitate aggregation through prion-like mechanisms *(Marzesco et al., 2016; Olsson et al., 2018; Tran et al., 2017)*. The initial conformations of small Aβ aggregate structures are thought to be important for the morphology of larger fibrils. Different solution and interface environments can lead to formation of different fibril morphologies *(Wood et al., 1996)*, and fAD mutations have been shown to produce distinct Aβ40 fibril morphologies with different aggregation kinetics *(Hatami et al., 2017)*, which likely extends to other Aβ peptides as well. Combined, the properties and behaviours of Aβ make the peptides highly labile and difficult to work with in a manner relevant to preserving disease relevant qualities from *in vivo* to *ex vivo*.

1.4.3.4 Amyloid beta plaques

Aβ protofibrils grow and combine to form diverse fibril structures *(Han et al., 2017)* and insoluble deposits alongside other proteins and lipids, amalgamations which can eventually become the relatively gigantic extracellular structures known as amyloid plaques (Figure 4). Amyloid plaques are a defining feature of AD, and therefore it may come as some surprise that, whilst the composition and distribution of these structures are well described, the process of their formation is understudied and controversial *(D'Andrea and Nagele, 2010)*. Interrogation of the composition of amyloid plaques reveals that they are complex structures inclusive of many different protein types, including whole neurons and glia. Aβ is enormously enriched in these plaques (approximately 80 times that of surrounding tissue *(Liao et al., 2004)*) and constitutes the principle material. Of the Aβ forms present, Aβ42 predominates *(Masters et al., 1985)*. Other proteins that are enriched more than two-fold in plaques compared to surrounding tissue are involved in cell adhesion (collagen I, fibrinogen, actin binding protein, coronin), cytoskeletal (tau), trafficking and sorting (clathrin heavy chain, dynamin, dynein heavy chain), kinases (14-3-3 isoforms), and proteinases (ubiquitin activating enzyme, lysosomal ATPases, cathepsin D, antitrypsin, cystatin B and C) *(Liao et al., 2004)*. These

plaques are found distributed throughout the cortex and sub-cortex in advanced stage AD, with notable sparing of hind brain regions *(Grothe et al., 2017; Thal et al., 2002)*. Different plaque morphologies exist within the brains of the same individual. Two broad categories are commonly described – dense core plaques and diffuse plaques *(Serrano-Pozo et al., 2011)*. Surprisingly, the cataloguing of amyloid plaques is an underdeveloped area of study, but recent indications suggest plaque properties may differ between AD sub-categories *(Rasmussen et al., 2017)*, and potentially brain regions and cell types *(D'Andrea and Nagele, 2010)*.

1.4.3.5 Amyloid beta function

The physiological and pathological functions of Aβ remain poorly understood. Proposed physiological functions of Aβ can be broadly categorised into modulation of synaptic activity and plasticity *(Abramov et al., 2009; Charkhkar et al., 2015; Lauren et al., 2009; Parihar and Brewer, 2011)*, cell signalling and kinase regulation *(Boehm, 2013; Sadigh-Eteghad et al., 2014; Tabaton et al., 2010)*, oxidation regulation *(Baruch-Suchodolsky and Fischer, 2009; Koppaka and Axelsen, 2000; Nelson and Alkon, 2005; Zou et al., 2002)*, cholesterol metabolism *(Beel et al., 2010; Grösgen et al., 2010; Hartmann, 2006; Wood et al., 2003)*, plasma membrane modulation *(Eckert et al., 2005; Kakio et al., 2004; Milanesi et al., 2012; Peters et al., 2009)*, and finally immune response *(Campbell, 2001; Fiala et al., 2007; Halle et al., 2008)*. Dysregulation of these activities largely encompass the pathological capacities of the peptide.

Synaptic loss is the strongest correlate of AD severity *(DeKosky and Scheff, 1990; Scheff et al., 2007; Terry et al., 1991)*, making the role of Aβ in synaptic activity and integrity of great interest. Although plaque burden is not well correlated with symptom severity *(Francis et al., 1999; Sperling et al., 2009)*, Aβ aggregates are frequently found in proximity to dysmorphic neurons, which often contain aggregated P-tau, signs of disrupted cellular transport, and loss of dendritic spine density *(Ferrer and Gullotta, 1990; Moolman et al., 2004; Serrano-Pozo et al., 2011; Spires, 2005; Woodhouse et al., 2005)*. Additionally, Aβ-containing human brain extract has been reported to exert an LTP reducing affect in mouse hippocampal brain slices. This was found to be due to inhibition of pre-synaptic release potential, which was dependent on the presence of APP *(Wang et al., 2017)*. Furthermore, soluble Aβ assemblies have been found co-localised with receptors of the pre- and post-synaptic compartments, of which nicotinic acetylcholine receptor (nAChR) and N-methyl-D-aspartate receptors (NMDAr) are the best studied *(Caspersen et al., 2005; Kay et al., 2013; Koffie et al., 2009; Takahashi et al., 2004)* and to interact with a plethora of receptors and ion channels *(Charkhkar et al., 2015; Dineley et al., 2002; Domingues et al., 2007; Dougherty et al., 2003; De Felice et al., 2007;*

Hsieh et al., 2006; Kamenetz et al., 2003; Pearson and Peers, 2006; Puzzo et al., 2008; Rammes et al., 2017, 2018, 2011; Shankar et al., 2007; Texidó et al., 2011; Wang et al., 2000b, 2000a).

Interestingly, physiological, picomolar concentrations (~200pM) of Aβ monomers are associated with long term potentiation (LTP) and synaptic plasticity *(Domingues et al., 2007; Kelly and Ferreira, 2006)*. However, nanomolar concentrations (~200nM), particularly of oligomers that form readily in such conditions, are associated with long term depression (LTD) *(Snyder et al., 2005)*, and cytoplasmic Ca^{2+} dependent dendritic spine loss *(Demuro et al., 2005; Wu et al., 2010; Zempel et al., 2010)*. Neuronal Aβ production is enhanced and higher concentrations are detected in the interstitial fluid proximal to synapses following stimulation of synaptic activity *(Bero, Adam W; Cirrito, John; Holtzman, David; Lee, Jin-Moo; Raichle, Marvus; Roh, 2011; Cirrito et al., 2005, 2008; Kamenetz et al., 2003)*, raising probability of oligomer/fibril formation. Together, this may point to a negative feedback function for Aβ under normal physiological conditions.

Brain regions with high metabolic activity (e.g. the hippocampus), are vulnerable to accumulation of Aβ in AD brains *(Buckner, 2005; Gouras et al., 1997)*, although others (e.g. the cerebellum) are not greatly affected in AD despite persistent and intense activity *(Grothe et al., 2017; Thal et al., 2002)*. One possibly is that this is due to fundamentally important differences in network connectivity *(Ovsepian and O'Leary, 2015)*, but more work in human appropriate cell models is needed. Cholinergic neurons are a target of the current imperfect AD therapeutics, and may have involvement in earlier stages of the disease than previously thought *(Mufson et al., 2008)*. However, these neuronal types only represent ~5% of basal forebrain neurons *(Deurveilher and Semba, 2011)*. Whilst numbers of GABAergic neurons are estimated to be more significant (~20% *(Sahara et al., 2012)*), evidence for the involvement of GABAergic neurons in AD is less clear. Rossor *et al.* reported these neurons to be relatively spared in a study of post-mortem cortical tissue from AD patients *(Rossor et al., 1982)*, though some studies in transgenic rodents indicate vulnerability of hippocampal GABAergic neurons to Aβ-induced toxicity *(Krantic et al., 2012; Pakaski et al., 1998)*, as well as to tauopathy in APOE4 over expression models *(Andrews-Zwilling et al., 2010)*. Cortical and subcortical glutamatergic neurons are well demonstrated to be severely afflicted by signalling disruption and degeneration in the AD brain *(Butterfield and Pocernich, 2003; Vazin et al., 2014; Viola et al., 2008). In vitro* and *in vivo* studies have shown that Aβ oligomers preferentially bind to glutamatergic neuron membranes and receptors, reducing glutamate signalling and synaptic plasticity *(Vazin et al., 2014)*. The classification 'glutamatergic' describes a heterogeneous group of neurons that share the use of glutamate as an excitatory neurotransmitter, and which are generated

from precursors in the dorsal telencephalon *(Wilson and Rubenstein, 2000)*. Glutamate is the major excitatory neurotransmitter of the CNS and glutamatergic neurons (such as pyramidal and granule cells) constitute the greater part of ~80% of the neocortex *(Wonders and Anderson, 2006)* and subcortical regions, such as the hippocampus *(Strominger et al., 2012)*. Therefore, glutamatergic cortical neurons represent an important target for AD research.

1.5 Biomarkers and Alzheimer's disease

Thus far, this chapter has defined and outlined Alzheimer's disease, and given a background to Aβ biology. This thesis concerns the optimisation and expanded use of Aβ peptides as biomarkers for AD, and the next section will introduce the need for improved AD biomarkers before narrowing focus to a discussion of confounding factors in Aβ measurement and the *in vitro* modelling of AD.

A biomarker is defined as "a characteristic that is objectively measured and evaluated as an indicator of normal biological processes, pathogenic processes, or pharmacologic responses to a therapeutic intervention" *(Atkinson A.J. et al., 2001)*. In other words, a biomarker of X is anything that signals some aspect of the state of X in a biological system. A good biomarker must meaningfully track the state of its dependent process. Ideally this will be in terms of high accuracy (the degree to which measurement matches actual values within the target context i.e. a person's brain). However, even if aspects sample acquisition cause values to diverge from those of the original context, a biomarker may still be useful if relative differences between different states are preserved. A good biomarker must also have high reproducibility. The ability to make the same measurement repeatedly with low error underpins assessment of accuracy and interpretation of results. Finally, in practical terms, a biomarker should be safe and uncomplicated to obtain, as well as cost-effective to measure.

Alongside clinical examination, biomarker research is now a dominant methodology to address AD for case identification, disease mechanism and pathway analysis, assessment of treatment targeting efficacy, and assessment of treatment response endophenotypes. Biomarkers for AD pathology are now incorporated in revised clinical criteria for the disease *(Dubois et al., 2014; McKhann et al., 2011; Ryan et al., 2018)*. Biomarkers can be subdivided into two categories: diagnostic (present at all disease stages, though may not correlate with severity) and progression (correlates with severity, but may not be present at all disease stages) *(Dubois et al., 2014)*. Biomarkers can also be classified by the medium of measurement. Fluid biomarkers are molecules measured within biological fluid and constitute the focus of this thesis.

1.5.1 Biofluids

For biomarker research of CNS disease CSF has the advantage of being semi-continuous with brain interstitial fluid whilst being segregated from blood and other body fluids in contact with peripheral tissues. Low protein concentration has also made CSF an easier matrix to work with in terms of assay development. However, methods of extraction are lumbar puncture or ventricular shunt, which are invasive and high skill requirement procedures that limit ease of sample accessibility. Cerebrospinal fluid (CSF) is an ultrafiltrate of blood plasma. Its consistency is 99% H_2O with low concentrations of electrolytes (Na, K, Ca, Mg, Cl), monosaccharides, and protein. CSF is produced by networks of ependymal cells that form the choroid plexuses lining the lateral, third and fourth ventricles of the brain, at an approximate rate of 500mL per day *(Wright et al., 2012)*. CSF flows through the ventricles, down and back up the subarachnoid space of the spinal column and is resorbed to the venous blood through the arachnoid villi. It is semi-continuous with brain interstitial fluid in the perivascular space, and small quantities are thought to be absorbed into the glymphatic system. Circulation is facilitated by pulsations of the choroid plexus and the motion of ependymal cell cilia. . In an adult human, CSF from the lumbar region contains on average 0.15 to 0.45 mg/mL protein (~0.3% of plasma protein), and 0.50-0.80 mg/dmL glucose (~66% of blood glucose). These values are age and sampling-site dependent. Protein concentration in cisternal and ventricular CSF is lower *(Felgenhauer, 1974; Weisner and Bernhardt, 1978)*. Additionally, CSF from healthy individuals typically contains 0-5 mononuclear cells. CSF pressure, measured at lumbar puncture (LP), is typically 100-180mm of H_2O (8-15mm Hg) with the patient lying on the side and 200-300mm H_2O with the patient sitting up. CSF provides mechanical support to the CNS, but increasing attention is focusing on its role as a filtration system for CNS waste products.

Until recently, blood-based biomarkers of AD have been poor or controversial, though much sought after. The great advantage of using blood derivatives in biomarker research is the ease, low invasiveness, and cost-effective nature of extraction. However, as a peripheral fluid, the blood matrix is complex and contains metabolites from many tissues which may obscure brain-derived biomarker profiles as well as molecules that may bind or degrade brain proteins of interest. Blood plasma is a complex matrix of proteins, fibrinogens, enzymes, glucose, amino acids, fats, cholesterol, phospholipids, vitamins and minerals, electrolytes, hormones and dissolved gases. Serum is plasma from which fibrinogens and coagulant proteins have been removed. Molecules from the brain interstitial fluid pass through the CSF to the blood where they are recycled or filtered as waste through the kidneys. Development of new ultra-sensitive protein measurement techniques (e.g. Single molecular array (Simoa)) have opened this medium up for investigation of brain specific

proteins, such as tau and neurofilament light (NFL) *(Blennow, 2017)*. These developments did not become accessible until after this project had commenced and so, whilst important, do not form part of its scope.

1.5.2 Core biomarkers of AD

A good biomarker of AD must fundamentally be linked to some aspect of the underlying neuropathology and distinguish those with AD from controls and from other disease states. In practice this means validation in neuropathologically confirmed cases of AD *(Group CW, 1998)*, and the sensitivity (ability to detect true positive) and specificity (ability to detect true negative) of detection should be >85% *(Shaw et al., 2007)*. Additionally, accessibility of the biomarker is crucial to utility in a practical clinical context *(Humpel, 2011)*. Finally, to be deployed in a clinical or otherwise professional setting, biomarker measurement must be reliable with recommended intra-assay coefficients of variance (CVs) of <20% *(FDA, 2001; Kadavil, 2013)*, although no official international criteria exists. High structural stability, a long half-life, and low reactivity are advantageous qualities.

Proteins that, on balance, approximate this criteria are known as 'core' biomarkers for AD. At the current time these include Aβ42, total tau (T-tau) and tau phosphorylated at either amino acid 181 or 231 (P-tau181 and P-tau231 respectively). Aβ42 is found decreased in AD CSF versus non-neurodegenerative controls, frontal temporal dementia (FTD), and Parkinson's disease (PD). In contrast, T-tau and P-tau are found raised in AD CSF *(Blennow and Zetterberg, 2009)*. Meta-analysis of CSF Aβ42 has shown a pooled sensitivity of 0.80 (95% CI 0.78–0.82) and a pooled specificity, 0.76 (95% CI 0.74–0.78) for distinguishing AD and non-AD cases, although significant heterogeneity in concentrations were noted *(Mo et al., 2015)*. Another analysis, which compared reports from 9949 AD patients and 6841 controls showed a highly significant average ratio of 0.56 Aβ42 in AD CSF versus control CSF *(Olsson et al., 2016)*. The same study also found an average ratio of 2.56 for AD CSF T-tau and a ratio of 1.88 for a composite of P-tau epitopes for distinguishing AD and non-AD cases, which were also highly significant *(Olsson et al., 2016)*. These effect sizes are depicted in Figure 5. In combination, Aβ42, T-tau and P-tau$_{181/231}$ consistently produce the highest diagnostic sensitivity and specificities, both versus controls and other dementias, particularly in early stages *(Blennow et al., 2010; Ferreira et al., 2014; Hansson et al., 2006)*. Although not yet officially incorporated into the AD diagnostic criteria, a growing literature also supports the utility of ratios of Aβ42:40 *(Anoop et al., 2010; Janelidze et al., 2016; Slemmon et al., 2015)*

There are, as yet, no certified or 'gold standard' reference materials to use as a reference point for any AD biomarker *(Mattsson et al., 2012a)*. The consequence of this is platform-dependent bias across the different assays produced. Furthermore, even when the same assay platform is used, variation in biomarker measurements between laboratories is often high *(Lewczuk et al., 2008; Lucey et al., 2015; Mattsson et al., 2013; Reijn et al., 2007; Verwey et al., 2009)*. Between-site coefficient of variation percentages (%CV) for commercially available T-tau and Aβ42 assays fall on average between 20-30% *(Mattsson et al., 2013)*. FDA guidelines for ligand binding assays, which are among the more looked to bench-marks for an industry without well-defined international regulation, require <20% CV in the linear range (<25% CV at the lower limit of quantification) of the calibration curve for bioanalytical assays to meet validation criteria *(FDA, 2001; Kadavil, 2013)*. In AD, the separation of patient groups by Aβ42 and T-tau is relatively robust, but there exists a considerable 'grey area' where group separation becomes unclear and improved resolution would be highly desirable, especially at early disease stages. By identifying novel confounding factors affecting Aβ measurement this thesis aims to provide evidence to inform sample storage and handling practices, and facilitate standardisation and measurement accuracy within the fluid biomarker field.

Low concentrations of Aβ42 peptide in CSF are taken to indicate a clearance deficit from the brain as a result of sequestration in plaques *(Fagan et al., 2006; Grimmer et al., 2009)*. However, as covered in Section 1.4 the mechanisms of Aβ production, clearance and toxicity are complex. In practical terms, it may be that interpreting Aβ concentration as 'a marker for AD related-neurodegeneration' or 'an indicator of brain amyloid deposition' is not sufficient to support the interpretative needs of experiment. Certainly, one wonders if the many different Aβ peptides have more to give in improving understanding of toxic mechanism, supporting therapeutic strategy and (hopefully) progress.

Several prospective biomarkers for AD are under ongoing investigation. These are beyond the scope of this work, but include NFL *(Olsson et al., 2016)*, Neurogranin *(Kester et al., 2015a; Thorsell et al., 2010; Wellington et al., 2015)*, SorLA *(Caglayan et al., 2014; Fagan and Perrin, 2012; Paterson et al., 2014)*, YKL-40 *(Craig-Schapiro et al., 2010; Janelidze et al., 2015; Kester et al., 2015b; Olsson et al., 2016)*, NSE, VLP-1, GFAP, MCP-1, and HFABP *(Olsson et al., 2016)*, and TREM2 *(Bekris et al., 2018; Liu et al., 2018)*, as well as albumin ratio *(Skillbäck et al., 2017)* and α-synuclein *(Korff et al., 2013; Shi et al., 2018)* for differential diagnosis.

Figure 5: Meta-analysis of AD biomarker effect size

Figure 5: Showing the results of a meta-analysis of Aβ38/40/42, T-tau and P-tau power to identify AD. Effect size is the ratio of mean biomarker concentration of one condition over another e.g. AD vs control (CTRL)). The z-score is a statistic representing how far away the observed ratio is from the null hypothesis of no difference. The size of each circle reflects the total number of subjects used. Data in the public domain, courtesy of ALZBIOMARKER interactive resource and Olsson et al. 2016.

1.5.3 The biomarker challenge

Evidence that AD follows a disease course characterised by protein misfolding, followed by neurodegeneration, followed by clinical symptoms of dementia is extremely well established *(Jack et al., 2013)*, and has withstood testing for decades. However, virtually all therapeutics based on this understanding have failed. Principally, these drugs have targeted aggregated forms of Aβ, or sought to decrease Aβ peptide production in late stage disease with β- or γ-secretase modulators, but other approaches targeting tau *(Medina, 2018)* and inflammation *(Miguel-Avarez et al., 2015)* have also yet to meet with success. It is worth noting that in Phase II trial the anti-Aβ BAN2401 antibody has showed promising signs of Aβ42 reduction and symptom modification (at 18 months, after reporting no cognitive benefit at a 12-month time point *(Logovinsky et al., 2016)*). However, significant questions surrounding the balancing of treatment and control groups persist, and further validation at Phase III is needed. History is not on BAN2401's side.

The challenge, therefore, is to translate knowledge of AD biology into therapeutic success. Reasons attributed to failures in this regard are many and complex but can be organised into at least four categories: issues with trial methodology, differential diagnosis, application of intervention, and disease conceptualisation.

In the case of trial methodology, it is often difficult for large-scale longitudinal trials to recruit and retain sufficient participants to meet power requirements, and design of appropriate statistical methods is not always straightforward.

In terms of differential diagnosis, the fact AD is usually a slow progressive disease of late life means that identifying appropriate controls or individuals without confounding co-morbidities is not easy. The accuracy and precision of CSF biomarkers is crucial in grouping trial participants, diagnosis of patients in clinical, and interpretation of therapeutic effect. As discussed in Section 1.5.2, even the best biomarkers are considerably less than perfect. Initiatives to track immunoassay reliability routinely report that between-site coefficient of variation percentages (%CV) for commercially available T-tau and Aβ42 assays fall on average between 20-30% *(Mattsson et al., 2013)* (Figure 6).

Appropriate application of treatment relies on understanding effective dose regimes in balance with safety, and requires high quality, human valid models. It is possible that drugs may also interfere with measurement of biomarkers such as Aβ, with important consequences for data interpretation. Furthermore, timing of application has been much commented on. Intervention in symptomatic stages of AD may be too late, with cascading pathology too advanced and multifactorial to reverse *(Mehta et al., 2017)*. Accurate biomarkers and detailed understanding of disease biology not only underpin our ability to discern who to treat, but when and how.

Understanding of the pathobiology of AD has grown immensely over the past three decades. Given the level of organisation and time required to complete a clinical trial it is not surprising that many lag behind cutting edge nuances of new research. Candidate drugs are typically screened in model systems. Such systems often over express Aβ in order to mimic late stage human AD brain states, but it may be that aggregates formed in these models have low relevance to the physiological disease process. Along similar lines, some Aβ species may be more relevant than others. Pyroglutamate forms of Aβ (e.g. Aβ3(PE)-42) have been shown to have enhanced cytotoxicity *(Nussbaum et al., 2012)*, whereas low concentrations of monmers, and perhaps certain peptides or greater protportions of C-terminally truncated peptides especially, contribute to normal

physiological function and thus could be considered neuroprotective *(Brothers et al., 2018)*. Aβ targeting therapeutic approaches have so far had poor discrimination for these nuances beyond the extent to which they engage soluble versus insoluble structures. Finally, it is important to concede the possibility that our conceptualisation of AD may not be correct. The weight of evidence falls in favour of the amyloid cascade hypothesis, but it is equally clear that pieces of the puzzle and/or its arrangement are missing. Pursuit of better models and robust replication of results can be the only recourse to these doubts. This thesis will contribute to effort to understand and treat AD by expanding knowledge of confounding factors affecting the measurement of Aβ peptides and their production in an *in vitro* model of fAD.

Figure 6: Results of Aβ1-42 measurement across multiple sites

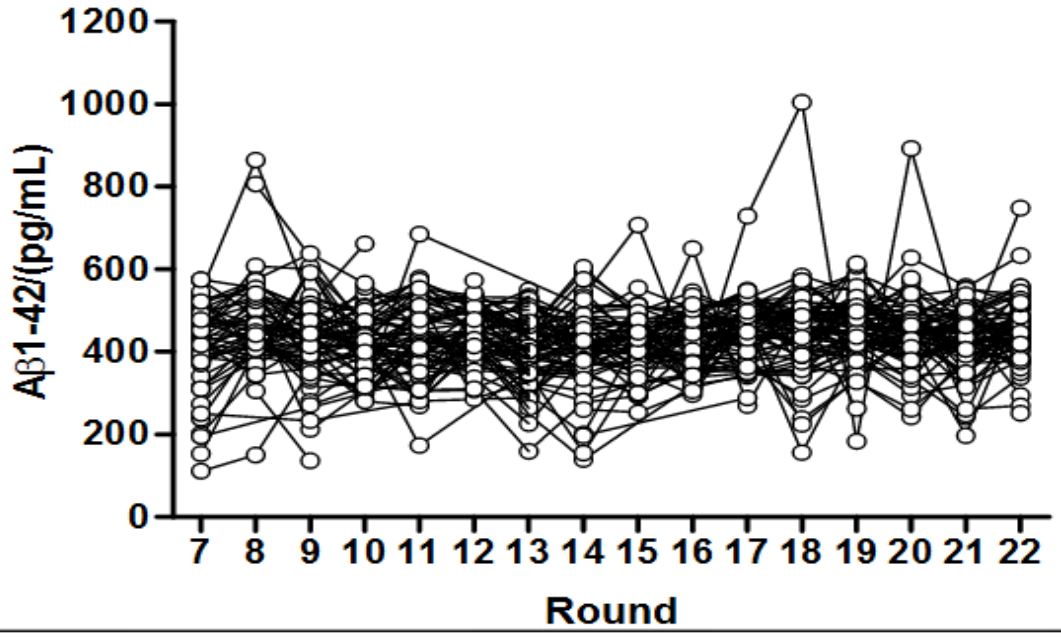

ROUND	7	8	9	10	11	12	13	14	15	16	17	18	19	20	21	22
Mean (pg/mL)	413	466	428	418	430	443	405	406	423	427	458	450	458	448	426	454
SD (pg/mL)	107	108	97	77	99	65	82	98	76	74	75	110	76	90	75	78
CV (%)	26	23	23	19	23	15	20	24	18	17	16	24	17	20	17	17

Figure 6: Summarising the results of the Alzheimer's Association QC program for CSF biomarkers from 2001-2016. Data represents a collaboration of more than 100 sites measuring the same samples for Aβ42 using the INNOTEST ELISA - consistently one of the best performing assays. Image and data provided by the Alzheimer's Association QC program for CSF biomarkers, used with permission.

1.5.4 Confounding factors and amyloid beta

Confounding factors are conditions that artificially influence the measurement of biomarkers from samples. Sample storage and handling practices are an important consideration for biobanking, and large repositories of samples are currently being generated by many international dementia consortiums and independent groups (e.g. Dominantly Inherited Alzheimer's Disease Network (DIAN), Alzheimer's Disease Neuroimaging Initiative (ADNI), European Prevention of Alzheimer's Dementia (EPAD) Longitudinal Cohort Study, The Swedish BIOFINDER Study, UCL Dementia Research Centre clinical cohorts and many more). These initiatives, many of them longitudinal in design, represent the future of appropriately powered research on well characterised disease cohorts.

Table 4: Confounding factors

Pre-analytical	Patient demographics
	Patient medication
	Lumbar vs ventricular CSF
	Patient fasting
	Spinal cord gradient
	Diurnal variation
	Blood contamination
	Sample matrix composition
	Sample pH
	Centrifugation settings
	Post-collection interval
	Sample mixing
	Storage temperature
	Storage vessel material
	Surface exposure
	Freeze/thaw cycles
Analytical	Assay calibration
	Assay reagent batch
	Assay platform
	Operator competence

Table 4: A list summarising the known confounding factors for the measurement of proteins in biological fluid, with a focus on CSF.

Many confounding factors for the measurement of Aβ (primarily Aβ42 and Aβ40) in fluid biomarkers relevant to AD research have been identified. Pre-analytical influences include clinical variables (besides AD and non-AD pathology) such as age, sex, genetic risk factors (e.g. APOE genotype) and medication (e.g. statins *(Chu et al., 2018)*), AD family history *(Liu and Caselli, 2018; Zuo et al., 2006)*, and study design *(Crean et al., 2011)*, CSF collection technique *(Lucey et al., 2015; Rembach et al., 2015)*, diurnal collection time *(Cicognola et al., 2015)*, contamination with blood *(Bjerke et al., 2010)*, interval between collection and freezing *(Le Bastard et al., 2013; Kaiser et al., 2007)*, temperature *(Bibl et al., 2004; Ranganathan et al., 2006; Sancesario et al., 2010)*, pH *(Murphy et al., 2013)*, sample matrix composition *(Slemmon et al., 2012, 2015)*, and assay measurement variation *(Ellis et al., 2012; Fagan et al., 2011; Lewczuk et al., 2008; Mattsson et al., 2010, 2011, 2012b, 2013; Reijn et al., 2007; Vos et al., 2014; Wang et al., 2012)*. Analytical confounding factors are related to the assay itself, for example, differences in technician skills and training, operating procedures, assay manufacturing, or batch-to-batch variations in kits *(Mattsson et al., 2013)*. Several papers have presented studies providing data from assessments of multiple factors *(Le Bastard et al., 2015; Bjerke et al., 2010; del Campo et al., 2012; Fourier et al., 2015; Schoonenboom et al., 2005)*. These confounding factors are summarised in Table 4. Further study of factors influencing the concentration of Aβ in CSF and other biofluids is important to improve understanding of how to preserve disease relevant qualities from *in vivo* to *ex vivo*, and standardising storage and handling practices to ensure reliable interpretation of results.

The experiments of this thesis focused on the interaction of Aβ peptides with polypropylene storage surfaces. Protein adsorption to solid surfaces is a field of study with a long history and an expansive literature. In a recent review, Rabe *et al.* coalesce current understanding of this phenomena with admirable clarity *(Rabe et al., 2011)*. There are four forces responsible for protein adsorption onto solid surfaces: hydrophobic, van der Waals, electrostatic, and hydrogen-bonding interactions *(Haggerty et al., 1991; Haynes and Norde, 1994; Lee and Ruckenstein, 1988)*. Factors that influence these forces, and therefore the nature of protein adsorption to solid surfaces can be thought of in three categories: external parameters, surface properties and protein properties.

External parameters include temperature, pressure pH, ion, salt and dissolved gas concentration *(Faghihnejad and Zeng, 2012)*. Increase in temperature is generally associated with increased adsorption due to a corresponding increase of system entropy and diffusion rate. pH determines the electrostatic state of a protein based on its isoelectric point (pI), and therefore the extent of attraction to the surface and other molecules. Greater ionic strength decreases opposite charge

attraction and increases same charge attraction as a function of the Debye length. Salts can influence protein precipitation as a result of sequestering H2O molecules.

Important surface properties are texture, surface free energy, polarity, charge, and morphology. Proteins with high internal stability do not readily adsorb to hydrophilic surfaces unless there is an electrostatic attraction, in which instance they do not tend to alter conformation. To bind to hydrophobic surfaces, entropy loss must be overcome by gain of energy caused by removing hydrophobic residues from contact with water, accompanied by structural change. Proteins with low internal stability adsorb onto most surfaces irrespective of electrostatic interactions due to favourable conformational entropy gain that binding to the surface provides *(Dill, 1990; Nakanishi et al., 2001; Rabe et al., 2011)*. Polystyrene and polypropylene, among the most common storage materials in medical science, are non-polar and thus hydrophobic *(Faghihnejad and Zeng, 2012; Jang and Kim, 2016; Rocha et al., 2005; Żenkiewicz, 2001)*. Surface texture is highly dependent on manufacture conditions, and co-polymer content.

The primary structure and conformational dynamics of Aβ discussed in Sections 1.4.3.1-4 make the peptide highly labile and difficult to work with. In addition to self-aggregation in solution, Aβ will bind to solid surfaces with some promiscuity. Studies have demonstrated attraction of Aβ to negatively charged phospholipid membranes *(Ji et al., 2002; McLaurin and Chakrabartty, 1997)* and both positive NH_2 and negative COOH coated surfaces *(Moores et al., 2011)*. Aβ40 adsorbs on hydrophobic and positively charged hydrophilic surfaces, where it readily forms parallel β-sheets at surface interfaces *(Rocha et al., 2005)*. Furthermore, other groups have demonstrated different Aβ42 and Aβ40 concentrations measured from CSF stored in polystyrene, polypropylene, copolymers, and glass containers *(Bjerke et al., 2010; Kofanova et al., 2015; Lewczuk et al., 2006a; Murray et al., 2013; Perret-Liaudet et al., 2012a; Vanderstichele et al., 2016)*. Polypropylene was generally found associated with higher peptide measurements. As a result, clinical practice has moved toward standardising the use of polypropylene for CSF storage over other materials such as polystyrene. Despite this, polypropylene is a non-polar material and therefore has hydrophobic properties which are favourable for binding hydrophobic molecules, such as Aβ. An instructive example is given by Murray *et al.*, in which the authors describe how the confounding effect of Aβ adsorption to their polypropylene plate wells led them to misinterpret their data *(Murray et al., 2013)*.

1.5.5 Modelling Alzheimer's disease

In addition to the importance of improving Aβ measurement for clinical diagnostic and trial purposes, a detailed understanding of healthy biology and disease processes is required to guide therapeutic or prophylactic strategy. AD is a disease of the living human brain, a delicate and notoriously difficult organ to access for study. Post-mortem samples of human brain tissue are very valuable, and a great debt is owed to those who have donated their brains for examination. Work on these samples contributed the earliest evidence of AD pathology *(Stelzmann et al., 1995)* and have provided the 'gold standard' confirmation of AD presence *(Scheltens and Rockwood, 2011)*. Due to the degradative processes that occur in dead tissue, other samples are better suited to examination of disease mechanism, particularly at earlier stages of AD. The bulk of our understanding of AD disease mechanisms has been afforded through the use of animal models, in particular the transgenic (Tg) mice, among other species comprehensively reviewed by Woodruff *(Woodruff-Pak, 2008)*. Other methods such as *in silico* computational modelling are also finding increasing use *(Ranjan et al., 2018)*.

1.5.5.1 Animal models: the example of the transgenic mouse

Tg mouse models capture several major aspects observed in human AD. Overexpressing human mutant APP (in models such as Tg2576, PDAPP, TgAPP23) leads to the formation of extracellular amyloid plaques, which are structurally similar to those of the human brain, in an age and Aβ42 dependent manner *(LaFerla and Green, 2012)*. Additionally, just as in human AD, cognitive decline in these mice tends to correlate poorly with plaque load *(Terry et al., 1991)*, but is more strongly associated with concentrations of soluble Aβ oligomers which associate with synaptic loss *(Ashe and Zahs, 2010)*.

However, there are notable differences between the human CNS and that of other species. At a structural level the absence of gyrencephalic cortex in rodents, and the arrangement and connectivity of basal ganglia elements (e.g. the caudate, putamen and subthalamic nuclei), as well as broader differences in neuronal network development, complexity, diversity, density, and white/grey matter ratios, represent profound differences from human anatomy *(Berry et al., 2018; Finlay and Darlington, 1995; Hill and Walsh, 2005; Rakic, 2009)*. In terms of modelling AD, in humans amyloid and tau pathology are well established by the time clinical symptoms manifest, whilst in mice behavioural alterations typically precede insoluble Aβ deposition *(LaFerla and Green, 2012)*. Importantly, whilst single Tg *APP* and *PSEN* mouse models present with increased tau hyperphosphorylation, unlike humans they do not develop NFTs *(Götz et al., 2007)*, or demonstrate

much if any AD-linked neuronal loss *(Ashe and Zahs, 2010)*. Multi-transgenic models (incorporating human mutated *APP*, *MAPT*, and *presenilin 1*), produce mice with NFT pathology downstream of intra- and extracellular Aβ deposition *(Blurton-Jones and LaFerla, 2006; Oddo et al., 2003)*. However, the *MAPT* mutations used are derived from mutations associated with FTD rather than AD, due to the paucity of AD associated *MAPT* genetics, and so questions remain over how translatable pharmacological interventions guided by these models might be to humans *(Berry et al., 2018; LaFerla and Green, 2012)*. Additionally, whilst rodent models do display immune response to aberrant AD-associated proteins, the nature and severity of the inflammation imperfectly mirror that seen in humans *(LaFerla and Green, 2012)*. Indeed, laboratory mouse strains are genetically homogenous and immune-stress privileged in a way that human therapeutic target populations are not *(Berry et al., 2018)*. Finally, there are also important differences in human liver metabolism compared with other species, even other primates, that may impact severity of the disease phenotype and the effectiveness and safety of new drugs in clinical trials *(Passier et al., 2016)*. It has been suggested that putative therapeutics be screened in at least two animal models prior to human trial *(Kieburtz and Olanow, 2007)*. However, this is expensive to achieve, and though in principle this would show that targeted pathways are conserved enough between species to have greater confidence of effect in humans, it does not entirely circumvent the issue.

1.5.5.2 Induced pluripotent stem cell models of Alzheimer's disease

Induced pluripotent stem cells (iPSCs) are stem cells generated by the de-differentiation (reprogramming) of somatic tissues (Figure 7), which have the potential to differentiate to any cell of the three germlines (endoderm, mesoderm, ectoderm), falling short of totipotency only through the inability to derive embryos and certain extra-embryonic tissues. In their Nobel Prize winning work, Takahashi and Yamanaka demonstrated that reprogramming of mouse fibroblasts could be achieved through the expression of only four pluripotency-associated transcription factors: OCT4, Klf4, SOX2, and c-MYC *(Takahashi and Yamanaka, 2006)*. Later work reproduced these results using the same transcription factors in human cells (hiPSCs) through a variety of reprogramming vectors *(Fusaki et al., 2009; Takahashi et al., 2007; Warren et al., 2010; Yu et al., 2007, 2009; Zhou and Freed, 2009)*.

hiPSC-derived neurons hold great promise as neurological disease models. Disease-relevant cell types with a fully human genetic background can be differentiated from reprogrammed cells that are highly comparable to human embryonic stem cells (hESCs) *(Berry et al., 2018; Mallon et al., 2014)*, and often better clinically characterised, although some differences of gene expression between hiPSCs and hESCs have been observed *(Chin et al., 2010)*. Importantly, iPSC-neurons

develop on a physiologically relevant time-frame, and are able to form electrically functional synaptic networks *(Shi et al., 2012a)*. The potential for the study of neural development, physiology, disease mechanisms and pharmacology on functional patient-specific cells opens exciting avenues for personalised, targeted, and regenerative medicine, bypassing the issues of tissue rejection and ethical controversy that limit ESCs.

Figure 7: From adults to stem cells… and back again

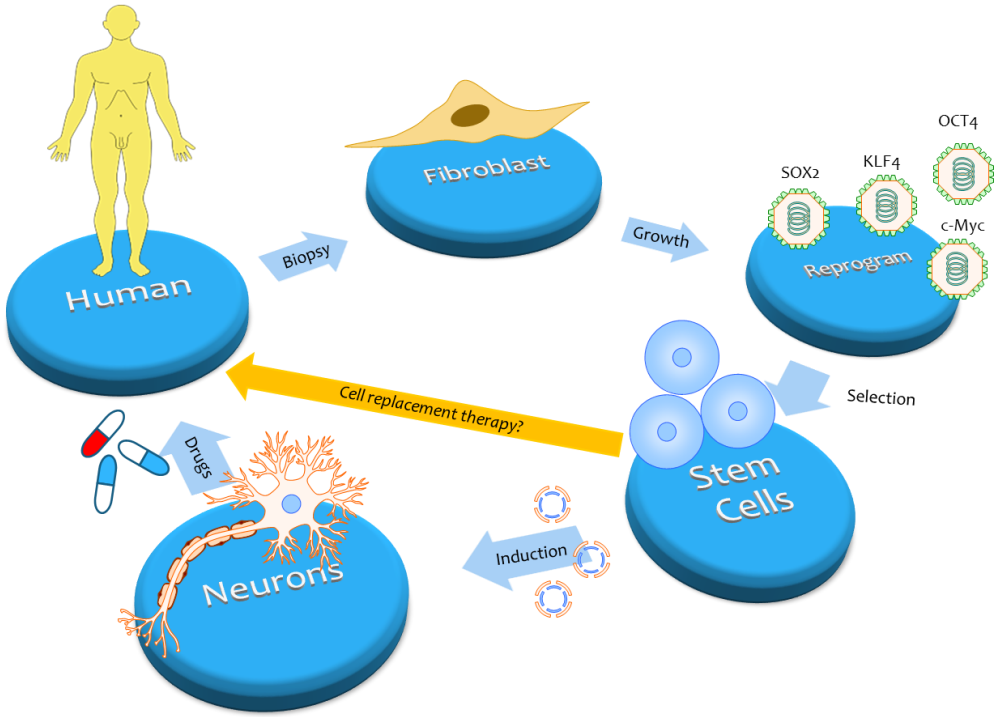

Figure 7: Visualising the process of reprogramming cells from adult humans back to a pluripotent stem cell state and then developmentally forward into any cell type of the three germ lines, such as neurons in this case. Disease specific cells can be used to develop pharmacological interventions for disease by improving our understanding of human biology, or directly screening small molecules in culture. With further development of the technology, stem cells themselves could one day be used in cell replacement therapy.

Induced pluripotent stem cell (iPSC) models are already proving a powerful tool for exploring APP processing in tissue specific cells from individuals with fAD-causing mutations (reviewed in Arber *et al. (Arber et al., 2017)*). Yagi *et al.* found increased levels of secreted Aβ42 in neurons with the *PSEN1* A246E and *PSEN2* N141I mutations *(Yagi et al., 2011)*. Further work on neurons bearing pathogenic *PSEN1* mutations have shown an increased ratio of Aβ42:40 *(Mahairaki et al., 2014; Moore et al., 2015; Ochalek et al., 2017; Sproul et al., 2014; Sun et al., 2017; Woodruff et al., 2013)*. Similarly, iPSC-derived neurons with an *APP* V717I genotype show a raised Aβ42:40 ratio *(Moore et al., 2015)*, as well as increases in Aβ42 and Aβ38 *(Muratore et al., 2014)*. *APP* duplication iPSCs also exhibit high

levels of Aβ40 *(Israel et al., 2012)*. Finally, 3D cerebral organoids provide a potentially valuable system for modelling neurodevelopment in 3D architecture, and possibly CSF due to the presence of choroid plexus tissue *(Lancaster et al., 2013)*. Early reports suggest increased amyloid aggregation in 3D cultures *(Raja et al., 2016)*, as well as an ability to identify candidate proteins involved in AD pathogenesis (Che*n et al*., 2018). However, a comprehensive analysis of the full spectrum of Aβ peptide production across multiple different fAD mutations to explore the mechanisms proposed by Chávez-Gutiérrez *et al.* has yet to be performed in patient-derived neurons *(Chavez-Gutierrez et al., 2012)*.

Work on sAD cell lines has been more limited, although work so far has also tended to show increased production of Aβ, particularly Aβ42, compared to controls *(Israel et al., 2012; Ochalek et al., 2017)*. Kunkle *et al.* recently published findings implicating *APP* in association with late onset AD, which largely overlaps with sAD *(Kunkle et al., 2019)*, although GWAS data over all weight genes linked with amyloid clearance rather than aberrant production in sAD *(Guo et al., 2017; Shen and Jia, 2016)*. It has been noted that increased Aβ in sAD lines is not consistent, particularly compared to fAD cultures, and some lines do not demonstrate this tendency. It is particularly interesting that ochalek *et al.* report that whilst Aβ42 and Aβ40 were significantly raised versus controls in the sAD and fAD lines they studied, (and indeed Aβ40 was higher in sAD than fAD), the Aβ42:40 ratio was not different between sAD and controls *(Ochalek et al., 2017)*.

Despite the energy with which the research community has adopted iPSCs, this is still a young and relatively unrefined field, accompanied by several limitations.

Firstly, although the ability to isolate specific, developmentally representative human cell types for study is a strength of the technology, it cannot replicate the integrated systems and behaviours of a complete organism. Furthermore, it is well established that neural and glia development and death processes are moderated by intricate inter-cellular signalling dynamics. The importance of system interconnection to the manifestation of AD is not currently known, but it is becoming clear that many different types of neuron, activation states of glia, and blood brain barrier factors have fundamentally important roles. However, 3D cultures such as neurospheres *(Choi et al., 2013)* and cerebral organoids *(Lancaster and Knoblich, 2014)*, represent a step toward a more physiologically representative neuronal network architecture and tissue complexity, including the presence of human progenitor cell types and stratified cortical layers.

Secondly, control of genetic integrity has been a focus of initial model optimisation work. The nature of reprogramming exposes cells to persistent genomic integration of the vector if retrovirus or lentivirus are used for this purpose, although non-integrative techniques such as sendai virus and plasmids have been developed. Additionally, retention or loss of epigenetic factors during reprogramming and over passage is an object of continuing concern *(Berry et al., 2018; Kim et al., 2010)*, as is the efficiency of protocols for directed differentiation to produce cells of the desired type *(Berry et al., 2018; Giorgetti et al., 2010)*.

Thirdly, the use of pluripotent cells, and expression of carcinogenically associated transcription factors, represents a risk that currently restricts transplant potential *(Martin, 2017)*. The risk posed by prions has not been explored in detail, but is also relevant to consider in the context of transplanting tissue.

Finally, recognition of biomarker variability between lines from different and even the same donor, as well as between groups, has been low but steadily growing *(Wernig, 2016)*. Alongside the role of genetic integrity in this, it is worth considering the role of culture environment. iPSCs and derivative cells are stably cultured in incubators at 37°C, typically with 5% CO^2 and 95% humidity. However, in most cases cells are removed from this environment for media replenishment exposing them to altered atmospheric and temperature conditions for variable periods of time. Media is typically not stored in these same conditions and thus dissolved gas concentration take additional time to equilibrate after feeding. Furthermore, cells are usually maintained at atmospheric oxygen concentrations (~21%), considerably greater than physiological concentrations (~1-5%) *(Van Der Sanden et al., 2010)*. These 'normoxic' conditions represents a hyperoxic environment for these cells, which has been linked with increased rates of spontaneous differentiation, telomere length alteration (with implications for genomic integrity) *(Chen et al., 2014)*. The process of feeding cells (by pipetting in and out media) exposes cultures to mechanical stress, and sudden molecular and pH change, the effects of which have not been well studied. Finally, surface coating methods vary between use of various materials (mouse embryonic feeder cells, Matrigel, Geltrex, laminin etc.), and differences in iPSC viability have been reported to even alter with surface plastic treatment *(Saha et al., 2011)*.

1.6 Chapter Summary and thesis aims

AD is an emergent global health crisis for which no prophylactic or curative treatments are available. Of the various forms of AD, the proportionally small number of fAD cases manifest pathology

representative of more common sAD forms with causal factors more amenable to study. Decades of experiment shows that Aβ plays a key role, particularly in the early stages of AD. Despite this, the lack of success in the development of effective therapeutics has created a need for better biomarkers and more detailed understanding of basic AD biology. This thesis seeks to address these needs by contributing novel data to guide the storage and handling of samples intended for Aβ measurement, and probe the mechanisms of Aβ production in human glutamatergic cortical neurons.

To reiterate, the specific aims of this project are:

I. Identify novel confounding factors in the storage and handling of CSF and cell culture media that may artificially alter detectable Aβ peptides. Factors studied include:
    - Effect of sample storage volume,
    - Effect of sample transfer between tubes,
    - Effect of Tween 20 on sample measurement variation,
    - Effect of using a spinal manometer,
    - Effect of sample transportation time and temperature in clinical context,

II. Investigate the physiological relevance of hiPSC-neurons by comparing Aβ peptide profiles in cell culture, CSF, and brain homogenate from a single patient with the *APP* V717I mutation.

III. Investigate the full spectrum of Aβ peptides produced by glutamatergic cortical neurons from six different fAD lines (*APP* V717I, *PSEN1* int4del, *PSEN1* Y115H, *PSEN1* M139V, *PSEN1* M146I, and *PSEN1* R278I) and five non-neurodegenerative controls.

2 Methods

2.1 Enzyme Linked Immunosorbent Assay

Figure 8: Common forms of ELISA

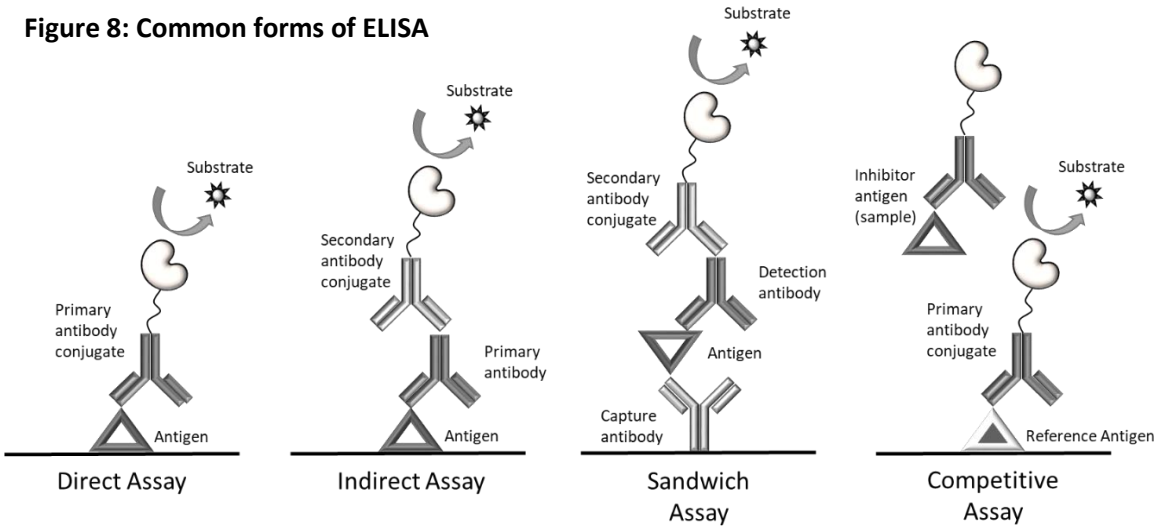

Figure 8: Diagram showing the principles of the most common forms of ELISA.

Enzyme linked immunosorbent assay is an analytical technique to quantify single (singleplex), or multiple (multiplex) molecules in solution. In principle, the antigen of interest is immobilised to a surface and bound to an enzyme which is then stimulated by application of a substrate. The interaction between free biotin (vitamin B7) and streptavidin (a protein purified from *Streptomyces avidinii*) is extremely strong (Kd $\approx 10^{-14}$ mol/L) and even outperforms that between biotin and avidin (Kd $\approx 10^{-15}$ mol/L) when biotin is conjugated to another molecule. For this reason, this protein pair are the predominant means of forming a conjugate antibody-enzyme complex in commercial ELISAs. There are several different formats of ELISA, which can be defined by the approach taken to two concepts: analyte capture (antigen immobilisation and antibody binding) and analyte detection (direct or indirect). These are depicted in Figure 8.

Direct assay involves the immobilisation of antigen to the surface of a 96 well assay plate or silicone bead. Depending on the assay, this can be through streptavidin coating of the plate and biotinylation of the antigen, and direct covalent binding or adsorption of the antigen to the plate surface. The antigen is then bound 'directly' by an antibody-enzyme conjugate and detected through reaction of the enzyme with its substrate. The advantage of direct assay is the comparatively few number of steps in its application, reducing experiment time and risk of measurement error due to reliance on

few reagents and only one antibody (i.e. no potential for cross-reaction). The disadvantages of this format are lower specificity and increased background signal (all proteins in solution will bind to the plate), and lower sensitivity (as no secondary antibody is used for signal amplification).

In indirect assay, the initial method of capture is similar to direct assay and the defining difference comes from the method of linking antigen presence to signal. In this format multiple secondary antibody-enzyme conjugates bind to the primary antibody-antigen complex, and thus 'indirectly' to the antigen. The advantage of this method is increased assay sensitivity, and offers the flexibility to potentially use different primary antibodies with the same secondary antibody. However, the disadvantages of non-specific antigen immobilisation remain, alongside more assay steps and risk of antibody cross-reaction.

Sandwich ELISA involves the initial immobilisation of an antigen-specific antibody to the surface of a 96 well assay plate or silicone bead, rather than the antigen itself. Depending on the assay, this can be through streptavidin coating of the plate and biotinylating of the antibody, and direct covalent binding or adsorption of the antibody to the plate surface. Prior to the addition of sample, the assay plate is blocked with assay buffer (containing blocking agents, common examples of which are albumin, milk, or Tween 20) to minimize non-specific binding of molecules to the plate surface. Upon introduction of sample the antigen is bound and immobilized by the capture antibodies, non-specific proteins are washed out leaving only the analyte of interest. Next, primary antibodies complete the 'sandwich' by binding to a secondary epitope of the antigen, and this complex is then detected by an enzyme conjugated secondary antibody (designated detection antibodies) just as in the indirect assay format. The advantages of sandwich ELISA are high specificity and sensitivity with low background signal, at the cost of a more complicated experiment design and risk of antibody cross-reaction. The advantages provided by this method make it the most popular format for clinical biomarker assay. All ELISAs used in this thesis utilized the sandwich format to measure AD biomarkers.

Finally, direct, indirect, and sandwich ELISAs can all be adapted to a competitive assay format. In this method, a known quantity of antigen is immobilised to the plate, the sample (unknown quantity of antigen) is then introduced alongside enzyme-conjugated antibodies. The antigens of interest in solution bind to the antibodies and 'compete' with antibody binding to the immobilised antigens, and are then washed out. When the enzyme reaction is catalysed, this process results in a signal that is inversely proportional to the antigen concentration of the sample i.e. a large amount of sample

antigen will mean less antibody bound to the plate and generate a low signal. The advantages of this format are the design flexibility it enables for antigens that are not amenable to forming complexes with multiple antibodies. The weaknesses of indirect, direct, or sandwich ELISA are retained as applicable.

The signal produced by the enzyme reaction is measured by a detector. Depending on the assay and enzyme substrates used, signal can be fluorescent, chemiluminescent, or chromogenic. Method of detection is dependent on the nature of the signal. Fluorescent ELISA substrates require a fluorometer, which utilises an electron beam to excite the fluorescent tag bound to the analyte of interest and measures the intensity of emitted light when electrons fall back to ground state energy. In chemiluminescence, light is generated from a chemically exothermic reaction between the enzyme tag and its substrate. A photoreceptor is used to detect this light signal, and is often combined with a photomultiplier that transforms photon energy to a cascading voltage and amplifies the signal, enabling greater sensitivity. For colorimetric-based assays, such as those used in the ELISAs of this thesis, the enzymatic reaction produces a visible spectrum colour change in the assay solution, a laser is passed through the assay solution and strikes a spectrometer. The absorption of energy at maximal absorbance wavelength is proportionate to the intensity of the solution colour, and therefore of the analyte of interest.

The most common enzyme reaction employed by commercial ELISAs, and the one used by ELISAs in this thesis, is that between horseradish peroxidase (HRP) and 3,3',5,5'-tetramethylbenzidine (TMB) *(Josephy et al., 1982)*. HRP is a metalloenzyme found in the roots of horseradish, and is smaller, more stable, and less expensive to produce than alkaline phosphatase. TMB is a chromogenic substrate molecule, which has the advantage of being non-carcinogenic. HRP catalyses the hydrolysis of H_2O_2 into H_2O by oxidation of TMB, a reaction that produces a blue colour with absorbances of 370nm and 652nm. The addition of sulphuric acid stops the ongoing reaction leaving a TMB diamine which produces a yellow colour with a light absorbance of 450nm.

Quantification of sample antigen is achieved by reference to the signal of a series of calibrators (a standard curve) of known concentration ranging from low to high. Calibrator data are typically fitted to a 4-paramater logistic curve, which accounts for maximum and minimum values, and assumes symmetry around the inflection point. When sample signal is plotted, the intercept between the signal and the curve corresponds to the analyte concentration. Two important parameters for assessing ELISA reliability are precision profile and dynamic range (limits of quantification). The

precision profile is a plot of calibrator CV over a range of concentrations. Calculation of the precision profile allows for the estimation of random error across a concentration range and identification of working range of the assay. The dynamic range of the calibration curve are thus defined by the concentrations where the precision profile intersects an acceptable level of variability (typically 20% CV). Samples with concentrations that fall beyond this range cannot be reliably quantified, and measurements become less reliable toward the lower and upper limits of quantification.

2.1.1 Measurement of Aβ1-43

Aβ42 was measured by IBL international ELISA kit (Männedorf, Switzerland), according to manufacturer's instructions. Samples were added undiluted in duplicate to microplate wells coated with a polyclonal capture antibody (#18583) specific for Aβ43 C-terminal (epitope VVIAT, Aβ39-43). The microplate wells were washed with assay wash buffer to remove unbound material. Samples were incubated with a biotinylated detection antibody (#10326) targeting Aβ N-terminus (epitope DAEFRH, Aβ1-5). The microplate wells were washed with assay wash buffer to remove unbound material. The detection complex was completed with the addition of horseradish peroxidase-labelled streptavidin. After an incubation period, tetramethylbenzidine (TMB) substrate was introduced. Peroxidase catalysed hydrolysis produces a colorimetric signal, the absorbance of which was measured using a FLUOstar Omega multi-mode microplate reader (BMG Labtech). Absorbance was measured at 450nm minus a reference signal of 690nm. Sample concentrations were extrapolated from a standard curve, fitted using a four-parameter logistic algorithm. The lower and upper limit of quantification range for this assay is 2.34-150 pg/mL.

2.1.2 Measurement of phospho tau$_{181}$

P-tau$_{181}$ was measured by Fujirebio INNOTEST ® PHOSPHO-TAU(181P) ELISA kit (Innogenetics, Ghent, Belgium), according to manufacturer's instructions. Samples were added undiluted in duplicate to microplate wells coated with an HT7 (IgG1) monoclonal capture antibody specific for human tau (recognising epitope PPGQK, isoform PNS-tau476-480). The microplate wells were washed with assay wash buffer to remove unbound material. Samples were incubated with a biotinylated tau specific AT270 (IgG1) monoclonal detection antibody recognising phosphorylated at Thr$_{181}$ (within the APKTPPS epitope, isoform PNS-tau476-480). The microplate wells were washed with assay wash buffer to remove unbound material. The detection complex was completed with the addition of horseradish peroxidase-labelled streptavidin. After an incubation period, tetramethylbenzidine (TMB) substrate was introduced. Peroxidase catalysed hydrolysis produces a colorimetric signal, the absorbance of which was measured using a FLUOstar Omega multi-mode microplate reader (BMG

Labtech). Absorbance was measured at 450nm minus a reference signal of 690nm. Sample concentrations were extrapolated from a standard curve, fitted using a four-parameter logistic algorithm. The lower and upper limit of quantification range for this assay is 20-199 pg/mL.

2.2 Electrochemiluminescent immunosorbent assay

Figure 9: Principles of MSD electrochemiluminescent assay

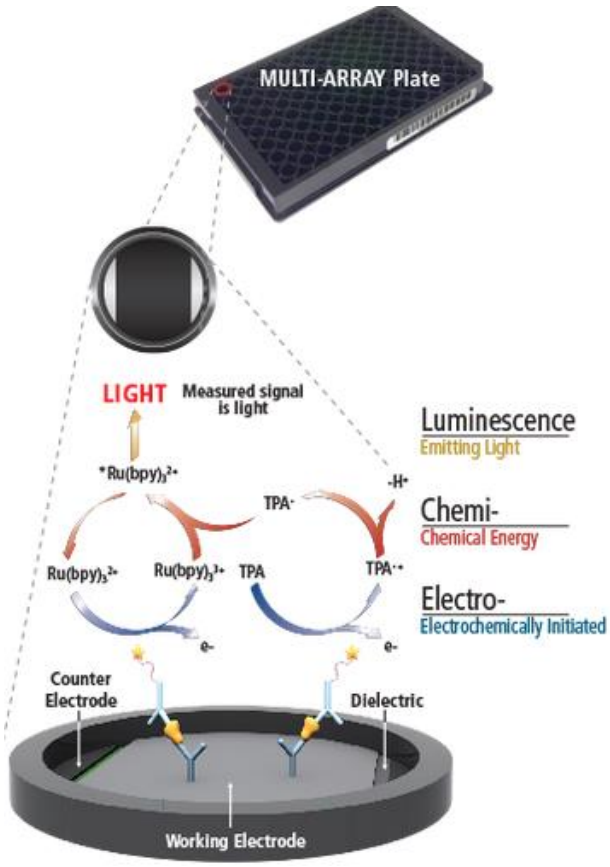

Figure 9: Diagram showing the principles of ECL in the assays produced by Meso Scale Discovery, used with permission (Meso Scale Discovery, 2013).

Electrochemiluminescent immunosorbent assay was conducted using a MSD SPECTRA 6000 (Meso Scale Discovery, Maryland, USA). The assay follows a sandwich assay format (Figure 9). The assay follows a sandwich ELISA format described in Section 2.1, except in the mechanism of producing signal. The MSD assay plate incorporates an electrical circuit that can transmit an electrical current through each well. Detection antibodies are conjugated with ruthenium (Ru^{2+}) otherwise referred to as MSD SULFO-TAG. For the substrate, a buffer solution containing tropopylomine (TPA) is introduced. When an electrical current passed through the assay plate wells Ru^{2+} is oxidised to Ru^{3+}

by the electrical current and reduced to Ru^{2+} by TPA, a reaction which produces light. The emitted light is detected by a photo-multiplier camera and is proportional to the concentration of the target analyte. The photo-multiplier acts as a form of enhanced chemiluminescence enabling a wider and more sensitive dynamic range than for a conventional ELISA. The principles of ECL immunosorbent assay are illustrated in Figure 9.

2.2.1 Measurement of Aβ42 singleplex

Aβ42 was measured by electrochemiluminescence (ECL) using a Meso Scale Discovery V-PLEX Aβ42 (6E10) kit, according to manufacturer's instructions. The microplate wells were washed with assay wash buffer to block the surfaces and remove unbound material. Samples were diluted 1:2 with diluent 35 and added in duplicate to microplate wells coated with proprietary mouse monoclonal peptide specific capture antibodies for human Aβx-42. The microplate wells were washed with assay wash buffer to remove unbound material. Samples were incubated with anti-Aβ (epitope DAEFRHDSGYEVHHQK, Aβ1-16) detection antibody (6E10 clone) conjugated with an electrically excitable SULFO-TAG. The microplate wells were washed with assay wash buffer to remove unbound material. Finally, MSD read buffer was added to each well and samples were measured immediately using an MSD SPECTRA 6000. Concentrations were calculated from ECL signal using a four-parameter logistic curve fitting method with the MSD Workbench software package. The lower and upper limit of detection range for this assay is 3.0-2000pg/mL. The lower and upper limit of quantification range for this assay is 3.0-2000pg/mL.

2.2.2 Measurement of Aβ38/40/42 multiplex

Aβ38/40/42 were measured by electrochemiluminescence (ECL) using a Meso Scale Discovery V-PLEX Aβ peptide panel 1 (6E10) kit, according to manufacturer's instructions. The microplate wells were washed with assay wash buffer to block the surfaces and remove unbound material. Samples were diluted 1:2 with diluent 35 and added in duplicate, alongside an anti-Aβ (epitope DAEFRHDSGYEVHHQK, Aβ1-16) detection antibody (6E10 clone) conjugated with an electrically excitable SULFO-TAG, to microplate wells coated with proprietary mouse monoclonal capture antibodies specific for the C-terminal neo-epitopes for Aβx-38, Aβx-40, and Aβx-42 respectively. The microplate wells were washed with assay wash buffer to remove unbound material. Finally, MSD read buffer was added to each well and samples were measured immediately using an MSD SPECTRA 6000. Concentrations were calculated from ECL signal using a four-parameter logistic curve

fitting method with the MSD Workbench software package. The lower limit of detection and upper limit of detection respectively for each peptide are: Aβ38 = 60-8480pg/mL, Aβ40 = 50-7000pg/mL, Aβ42 = 3.13-1270pg/mL. The lower limit of detection and upper limit of quantification respectively for each peptide are: Aβ38 = 60-8480pg/mL, Aβ40 = 50-7000pg/mL, Aβ42 = 3.13-1270pg/mL.

2.2.3 Measurement of total tau

T-tau was measured by electrochemiluminescence (ECL) using a Meso Scale Discovery V-PLEX Total tau kit, according to manufacturer's instructions. CSF samples were diluted 1:4 (cell media samples were diluted 1:100) with diluent 35 and added in duplicate to microplate wells coated with proprietary mouse monoclonal peptide specific capture antibodies for tau isoforms 352, 381, 383, 410, and 441. The microplate wells were washed with assay wash buffer to remove unbound material. Samples were incubated with proprietary mouse monoclonal anti-tau detection antibody (recognising tau isoforms 352, 381, 383, 410, and 441) conjugated with an electrically excitable SULFO-TAG. The microplate wells were washed with assay wash buffer to remove unbound material. Finally, MSD read buffer was added to each well and samples were measured immediately using an MSD SPECTRA 6000. Concentrations were calculated from ECL signal using a four-parameter logistic curve fitting method with the MSD Workbench software package. The lower and upper limit of detection range for this assay is 3.0-2000pg/mL.

2.3 Cerebrospinal fluid collection

Unless otherwise specified, de-identified human CSF was provided by the Department of Psychiatry and Neurochemistry (University of Gothenburg). Use of CSF met the ethical approval criteria of the regional ethics board at the University of Gothenburg. The CSF samples were collected by lumbar puncture prior to 13:00, from between the L3/L4 or L4/L5 inter-spaces. A volume of 10mL of CSF was collected at ambient room temperature into a 10mL polypropylene tube (Sarstedt, Nümbrecht, Germany cat. 62.9924.284) directly from the needle. In the case of visible blood contamination, the CSF was discarded and the tap continued in a new tube once bleeding had stopped. Samples were centrifuged at 2200 relative centrifugal force (RCF) for ten minutes at 20°C, transferred to another 10mL tube (Sarstedt cat. 62.9924.284) and stored at -80◦C within 1-4 hours of collection. CSF was transported overnight from the University of Gothenburg to University College London frozen on dry ice by international courier. Samples were stored, unthawed, at -80°C upon receipt.

In a number of experiments CSF was divided into AD and non-AD categories. AD CSF was derived from a cohort of individuals with CSF biomarker profiles consistent with AD. These were defined

according to cut-offs that, combined, are 95% sensitive and 87% specific for AD: Aβ1-42 <530 pg/mL, T-tau >350 pg/mL, P-tau >60 pg/mL using Innogenetic's INNOTEST Aβ1-42, hTau and P-tau assays *(Hansson et al., 2006)*. Non-AD CSF (also referred to as CTRL CSF) was defined by a biomarker profile that did not meet these criteria. Hansson *et al.* derived these values by assessment of lumbar CSF taken from 137 patients with MCI and 39 controls followed clinically over a period of 3-6 years, during which time conversion to AD was documented. Association between altered CSF biomarkers and progression to Alzheimer's disease was independent of established risk factors including age, sex, education, APOE genotype, and plasma homocysteine assays *(Hansson et al., 2006)*.

2.4 iPSC culture

iPSCs were grown on geltrex matrix (ThermoFisher, cat. A1413302) in six-well polystyrene culture plates (Nunc, cat. 158007), fed daily with 2mL Essential 8 (Thermo Fisher Scientific, cat. A1517001). Essential 8 was composed of DMEM F-12, L-scorbic acid, Selenium, Transferrin, NaHCO3, Insulin, FGF2, and TGFβ1 (quantities not provide by manufacturer). Cells were routinely passaged with 0.1% EDTA (Invitrogen, cat. 15575-038) approximately every two days, when iPSC colonies were ~300µm in diameter. Cells were cultured in a Heracell 150 incubator (Thermo Fisher Scientific, Cat. 50116047) at 37°C, 5% CO_2. Cell pluripotency was checked for each line by immunocytochemistry, using antibodies to stage-specific embryonic antigen 4 (SSEA4), OCT3/4, and Tra1-82 (Figure 10). SSEA4 and Tra1-82 are proteins expressed on the cell surface of undifferentiated, pluripotent stem cells. OCT3/4 is a transcription factor found in the nuclei of undifferentiated, pluripotent stem cells. Lines were routinely screened (weekly) for the absence of mycoplasma contamination.

Karyotype screens and G-band analysis were performed on newly generated lines by the company of origin or Cell Guidance Systems in the case of CTRL1, SHEF6, *APP* V717I-2, *PSEN1* int4del, and *PSEN1* R278I (Table 5).

Table 5: Cell Lines

Cell line	Mutation	Sex	Age of onset	Age at biopsy	APOE genotype	Origin
Ctrl1	Cognitively normal	M	-	78	3/3	Dr Tilo Kunath
Ctrl2	Cognitively normal ND41886	M	-	64	2/3	Coriel repository
Ctrl3	Cognitively normal RBi001-a	M	-	45-49	3/3	Sigma Aldrich
Ctrl4	Cognitively normal SIGi1001-a-1	F	-	20-24	3/4	Sigma Aldrich
SHEF6	Human embryonic stem cell line – no known mutation	F	-	-	3/3	UK Stem Cell Bank
APP V717I 1	APP London mutation (2 clones)	M	49	58	4/4	StemBancc
APP V717I 2	Unrelated APP London mutation. Pre-symptomatic (1 clone)	F	-	47	3/3	Generated in house
PSEN1 int4del	Intron 4 deletion in PSEN1 (2 clones)	F	47	47	3/3	StemBancc
PSEN1 Y115H	PSEN1 Y115H (1 clone)	M	34	39	3/3	Generated in house
PSEN1 M139V	PSEN1 M139V (1 clone)	F	34	45	2/3	StemBancc
PSEN1 M146I	PSEN1 M146I Pre-symptomatic (1 clone)	M	-	38	3/3	StemBancc
PSEN1 R278I	PSEN1 R278I (1 clone)	M	58	60	2/4	Generated in house

Table 5: Showing the cell lines used in the thesis

2.5 Differentiation of iPSCs to cortical neurons

Differentiation to glutamatergic cortical neurons was performed according to the protocol published by Shi *et al.* (Shi *et al.*, 2012). iPSCs were passaged with 0.1% EDTA (Invitrogen, cat. 25575-038) and

re-plated at a 5:1 well ratio density, sufficient to reach 100% well confluency within 24 hours. When 100% confluence was reached, E8 media was replaced with induction media.

Neural induction was achieved via dual SMAD inhibition (dorsomorphin and SB431542). Induction media consisted of N2B27 media with added 1 µM dorsomorphin (Tocris, cat. 3093) and 10µM SB431542 (Tocris, cat. 1614). N2B27 cell culture media was composed of a 1:1 solution of DMEM/F12 + GlutaMax-I (1X) (Life Technologies, cat. 10565018) and Neurobasal Medium (1X) (Life Technologies, cat. 12348017) with the following supplements: 0.5X N2 supplement (Life Technologies, cat. 17502-048), 0.5X B27 supplement (Life Technologies, cat. 17504-044), 0.5X (100µM) MEM non-essential amino acids (Life Technologies, cat. 11140-050), 10µM 2-mercaptoethanol (Life Technologies, cat. 31350-010), 50U/mL penicillin and 50µg/mL streptomycin (Life Technologies, cat. 15070063), 5µg/mL insulin (Sigma-Aldrich, cat. I9278), and 1mM-glutamine (Life Technologies, cat. 25030-024). Fresh N2B27 was made every seven days and stored at 4°C.

Figure 10: Neuronal differentiation

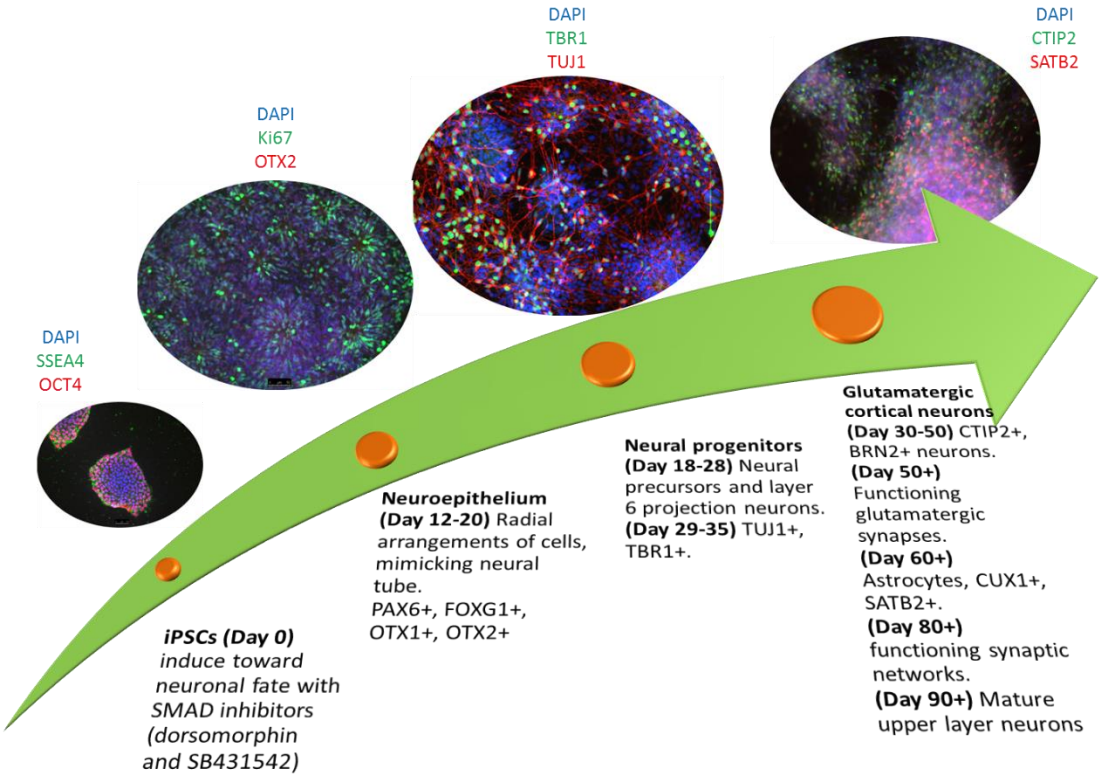

Figure 10: Showing the main stages in the differentiation of iPSCs to glutamatergic cortical neurons, following the Shi protocol (Shi *et al.* 2012).

The switch from E8 to induction media was considered day 0, for the purposes of tracking cell maturation. Induced cells were maintained in induction media for 12 days, with the media replaced daily, during which time they formed a compact neuroepithelial layer. On day 12 the neuroepithelium was passaged with 1mg/mL dispase (Thermo Fisher Scientific, cat. 1715041) and re-plated in 1:50 laminin (Sigma-Alderich cat. L2020-1MG) in Dulbecco's phosphate buffered saline solution (DPBS, Life Technologies, cat. 14190-326) coated plate wells at a ratio of 1:2 wells (6-well plate to 12-well plate (Nunc, cat. 150628). From this point on they were fed with N2B27 media and passaged to 1:100 laminin coated plates.

By day 20 the neuroepithelial cells had formed neural tube-like rosette structures from which neural progenitor cells migrated. At day 20 cultures were passaged with 1mg/mL dispase at a ratio of 1:2 or 1:1 wells. Between days 20-30 cultures continued to differentiate from neuroepithelium to neural precursors and layer VI neurons. Non-neuronal differentiation was looked for by light microscopy and, if detected, additional passage with 1mg/mL dispase was conducted to filter out these cells.

At day 30, cultures were expanded through passage with 500µL accutase (ThermoFisher Scientific, cat. A1110501) at a ratio of between 1:2 and 1:4. At day 35, cells were passaged with 500µL accutase and re-plated at a final density of approximately 50,000 cells per cm^2. At this stage the majority of cells were neural progenitors or deep layer neurons. Over the next 70 days, progenitors continued to differentiate into neurons of the six cortical layers. By day 100, cultures were composed of functional post-mitotic glutamatergic neurons from each of the cortical layers. Neurons used for the experiments in this thesis were grown by Dr. C. Arber and myself.

2.6 Cultivation of 3D organoids

Cerebral organoids were produced by Dr. C. Arber and Mr. C. Lovejoy following the protocol published by Lancaster *et al. (Lancaster and Knoblich, 2014; Lancaster et al., 2013)*. iPSCs were cultured as described in Section 2.4. iPSC cultures were dissociated into single cells with 0.1% EDTA (Invitrogen, cat. 25575-038), followed by 500µL accutase. Cells were re-suspended in 0.5mL embryoid media (40mL DMEM/F12 + GlutaMax-I (1X) (Life Technologies, cat. 10565018), 20% knockout serum replacement (KOSR) (Invitrogen, cat. 10828-028), 3% ESC-Quality FBS (Gibco, cat. 10270-106), 1X MEM non-essential amino acids (Life Technologies, cat. 11140-050), 3.5µM 2-mercaptoethanol (Life Technologies, cat. 31350-010), 4ng/mL FGF2 (Peprotech, cat. 100-18B 1), 50µM ROCK inhibitor (Y27632, Millipore, cat. SCM075)), and aliquoted into ultra-low adherence 96-well ultra-low attachment U-bottom plates (Sigma, cat. CLS7007) at a density of 9000 cells per well.

Cells were then allowed to re-aggregate and form embryoid bodies under gravity in an incubator for five days, replacing the media every two days.

After six days (designated day 0 for the purposes of tracking culture maturity), embryoid bodies were fed with organoid induction media (1:1 solution of DMEM/F12 + GlutaMax-l (1X) (Life Technologies, cat. 10565018), and 1X Neurobasal Medium (Life Technologies, cat. 12348017), 100µM MEM non-essential amino acids (Life Technologies, cat. 11140-050), 50µg of 0.2µm filter sterilised Heparin (Sigma, cat. H3149)), and incubated with daily media changes for four days, during which time neuroectoderm developed. On day 12 embryoid bodies were suspended in Matrigel droplets (BD Biosciences, cat. 356234) to allow neuroepithelial buds and lumen filled voids to form with 3D structures. These embryoid bodies were transferred to a $5cm^2$ culture dish (VWR, cat. 734-2318) and induction media was switched to organoid differentiation media without vitamin A (1:1 solution of DMEM/F12 + GlutaMax-l (1X) (Life Technologies, cat. 10565018) and Neurobasal Medium (1X) (Life Technologies, cat. 12348017) with the following supplements: 1X N2 supplement (Life Technologies, cat. 17502-048), 1X B27 supplement without vitamin A (Life Technologies, cat. 12587010), 100µM MEM non-essential amino acids (Life Technologies, cat. 11140-050), 100µM 2-mercaptoethanol (Life Technologies, cat. 31350-010), 50U/mL penicillin and 50µg/mL streptomycin (Life Technologies, cat. no. 15070063), 5µg/mL insulin (Sigma-Aldrich, cat. I9278)).

From day 18+, embedded embryoid bodies were fed with organoid differentiation media with vitamin A (1:1 solution of DMEM/F12 + GlutaMax-l (1X) (Life Technologies, cat. 10565018) and Neurobasal Medium (1X) (Life Technologies, cat. 12348017) with the following supplements: 1X N2 supplement (Life Technologies, cat. 17502-048), 1X B27 supplement (Life Technologies, cat. 17504-044), 100µM MEM non-essential amino acids (Life Technologies, cat. 11140-050), 100µM 2-mercaptoethanol (Life Technologies, cat. 31350-010), 50U/mL penicillin and 50µg/mL streptomycin (Life Technologies, cat. no. 15070063), 5µg/mL insulin (Sigma-Aldrich, cat. I9278)) and maintained on an orbital shaker under incubator conditions. Media was replaced every three-four days. Orbital agitation facilitates nutrient and gaseous diffusion in support of cells deep within the growing organoid tissue and minimises necrosis.

2.7 Cell Count

Cell counts were conducted by Trypan blue staining. Trypan blue is a diazo dye that can only pass through the membranes of dead cells and does not compromise the viability of live ones. During passage, with cells in suspension immediately prior to re-plating, 10µL of cell solution were mixed

with 10µL of 0.4% Trypan blue (Gibco, cat. 15250061). This mixture was ejected into a haemocytometer (Marenfeld Neubaue-improved, cat. 0640010) and placed on a light microscope with a 10X objective. The average count of unstained cells in each of the four chamber corners was recorded, multiplied by the volume of the haemocytometer (10,000cm^3), and then multiplied by any dilution factors (i.e. 2X from admixture with Trypan blue).

2.8 Cell culture media collection

Cortical neurons and 3D organoids were fed with N2B27 cell culture media, composed of a 1:1 solution of DMEM/F12 + GlutaMax-l (1X) (Life Technologies, cat. 10565018) and Neurobasal Medium (1X) (Life Technologies, cat. 12348017) with the following supplements: 1X N2 supplement (Life Technologies, cat. 17502-048), 1X B27 supplement (Life Technologies, cat. 17504-044), 100µM MEM non-essential amino acids (Life Technologies, cat. 11140-050), 100µM 2-mercaptoethanol (Life Technologies, cat. 31350-010), 50 Units/mL penicillin and 50µg/mL streptomycin (Life Technologies, cat. no. 15070063), 5µg/mL insulin (Sigma-Aldrich, cat. I9278), and 1mM-glutamine (Life Technologies, cat. no. 25030-024). Cells were incubated in N2B27 for 48 hours prior to media collection. Media was collected in Greiner 15mL PP tubes (cat. T1943-1000EA), centrifuged at 2000 RCF for five minutes at 21°C, aliquoted at 1mL into Sarstedt 2mL PP tubes (cat. 72.694.406), and stored at -80°C.

2.9 Cell protein lysate collection

To lyse cells for protein extraction, filter sterilised Radioimmunoprecipitation assay (RIPA) buffer (10mM Tris-HCl (pH 8.0) (Sigma-Aldrich, cat. 07066), 1mM EDTA (Invitrogen, cat. 25575-038), 0.5mM EGTA (Sigma-Aldrich, cat. E3889), 1% Triton X-100 (Sigma-Aldrich cat. X100-500ML), 0.1% sodium deoxycholate (Sigma-Aldrich cat. D6750), 0.1% SDS (Sigma-Aldrich cat. L3771), 140mM NaCl (Sigma-Aldrich cat. S7653) with added 1X EDTA free cOMplete mini (Sigma-Aldrich cat. 4693159001) and 1X PhosStop (Sigma-Aldrich cat. 4906837001) was prepared, cell culture media was removed from the culture plate well and 150uL of RIPA buffer was added. Cells were incubated with RIPA buffer at ambient room temperature for two minutes, then transferred to a 1.5mL Eppendorf (Sigma-Aldrich cat. T9661-1000EA) and homogenized with ten pipette pumps. The Eppendorf was then placed on an orbital mixer at 4°C for one hour, after which it was snap frozen on dry ice for five minutes and stored at -80°C.

2.10 Cell RNA collection

To isolate RNA (alongside DNA and proteins) cell culture media was removed from the culture plate well and 500uL of TRIzol (Life Technologies cat. 15596-026) was added. TRIzol cell lysate was immediately transferred to a 1.5mL Eppendorf (Sigma-Aldrich cat. T9661-1000EA) and homogenized with ten pipette pumps. The TRIzol cell lysate was snap frozen on dry ice for five minutes and stored at -80°C.

2.11 Immunocytochemistry/Immunochistochemistry

Cells for immunocytochemistry analysis were cultured as described in Section 2.5, except that the final passage was made onto laminin-coated glass coverslips (VWR, cat. 631-0149). After removal of media and washing in DPBS (Life Technologies, cat. 14190-326), these cells were fixed in 4% paraformaldehyde (Polysciences inc. cat: 04018-1) in 1X PBS (Thermo Fisher Scientific, cat. 18912014) for 15 minutes. For Aβ immunofluorescence, after fixation, all samples were treated with formic acid for five minutes for antigen retrieval. After three washes in 0.3% triton-X-100 (Sigma-Aldrich cat. X100-500ML) in 1X PBS (PBST), permeabilised cells were blocked in 3% bovine serum albumin (BSA, Sigma-Aldrich cat. A1933) in PBST. Cells were incubated in primary antibodies in blocking solution overnight (Table 6). After three washes in PBST, 400-600nm secondary antibodies (Alexafluor, Thermo Scientific) were added in blocking solution for one hour in the dark. DAPI (Abcam, cat. Ab228549) was added to the cells as a nuclear counterstain at 1µM and the cells were washed three times in PBST. Cells were mounted on ColorFrost slides (Thermo Fisher Scientific, cat. 9951OPLUS) using DAKO mounting media or imaged in PBS. Images were captured on the Opera Phenix (Perkin-Elmer) or a Zeiss LSM microscope (Zeiss).

Immunohistochemistry followed the same process as described for immunocytochemistry except that brain slices were fixed in 4% paraformaldehyde whilst thawing, and then treated with 10% formic acid for ten minutes for antigen retrieval prior to permeabilisation with 0.3% triton-X-100.

Table 6: Antibodies used for immunocytochemistry and western blotting

Antigen	Company	Host	Dilution
DAPI	Abcam (ab228549)		1:10,000
NANOG	Cell Signaling Tech D73G4	Rabbit	1:500
SSEA4	Biolegend MC-813-70	Mouse	1:500
FOXG1	Abcam Ab18259	Rabbit	1:500
pVimentin	MBL International D076-3S	Mouse	1:250
TUJ1	Biolegend 801201 and 802001	Mouse and Rabbit	1:10,000
CTIP2	Abcam ab18465	Rat	1:500
PSD95	Abcam ab2723	Mouse	1:1000
Aβ	Dako M0872	Mouse	1:1000
MAP2	Abcam ab5392	Chick	1:10,000
PSEN1 C-term	Millipore MAB5232	Mouse	1:1000
PSEN1 N-term	Millipore MAB1563	Rat	1:500
β Actin	Sigma	Mouse	1:10,000

Table 6: Showing the antibodies used in immunocytochemistry, immunohistochemistry, and western blot

2.12 Calcium signalling

iPSC-derived cortical neurons were cultured as described in Section 2.5, except that the final passage was made into eight well glass ibidi slides (Ibidi, Munich, Germany, cat. 80827) at a density of 5000 cells per cm^2. Cells were fed with 200µL of N2B27 per well every 3-4 days until the experiment. Cultures were transported to the laboratory of Prof. M.R. Duchen on foot in a polystyrene box. The ibidi chambers were sealed with parafilm (Thermo Fisher Scientific, cat. S37440) and secured to the box with tape alongside 50mL Greiner centrifuge tubes (Sigma-Aldrich, cat. T2318-500EA) filled with warm water (37°C). No atmospheric control was available, and transport took approximately 20 minutes. Cultures were then incubated for 24 hours in a Heracell 150 incubator (Thermo Fisher Scientific) at 37°C, 5% CO_2.

Following the instruction of Dr. G. Bhosale, cells were washed with 300µL Hank's Balanced Salt Solution (HBSS) at 37°C. HBSS was pH adjusted with NaOH to pH 7.4, consisted of $CaCl_2$ (0.1396g/L),

$MgSO_4$ (0.09767g/L), KCl (0.4g/L), KH_2PO_4 (0.06g/L), NaCl (8.0g/L), Na_2HPO_4 (0.04788g/L), $C_6H_{12}O_6$ (1.0g/L), and $NaHCO_3$ (0.35g/L). After washing HBSS was removed and cells were incubated in 200µL of 5µM Fura2 solution at 37°C for 30 minutes. 5µM Fura2 solution consisted of 10uL 1mM Fura2 (Thermo Fisher Scientific, cat. F1201) with 2µL pluronic acid in 1990µL HBSS, and was kept shielded from light. Fura2 is a photosensitive ratiometric fluorescent dye which binds to free intracellular calcium. When bound to calcium, Fura2 emits 340nm light. When not bound to calcium, Fura2 emits 380nm light. Regardless of the presence of calcium, Fura-2 emits 510 nm light. Next, Cells were washed with 300µL HBSS, and then 180µL of HBSS was applied to each well as run buffer.

Calcium signal measurements were obtained using an Olympus IX71 Widefield microscope with a 40X oil immersion objective. Neither atmosphere control nor a heated stage were used. The cells were imaged at 340nm and 380nm with a time interval of 1 second per image. Neuron activity occurs in bursts of action potentials often referred to as electrical spikes, which occur over ~200 milliseconds, with ~5 second intervals between bursts *(Galtieri et al., 2017; Penn et al., 2016)*. Calcium signalling was imaged over a baseline period, then 20µL of either KCl (final concentration 12.5mM) or glutamate (final concentration 100µM) solution were added. KCl solution consisted of NaCl (18.6µM), KCl (125mM), $NaHCO_3$ (4.2mM), NaH_2PO_4 (1.2mM), $MgCl_2$ (1.2mM), $CaCl_2$ (1.2mM), D-Glucose (10mM), HEPES (10mM). Glutamate solution consisted of 1000µM glutamate in 1mL HBSS.

2.13 Quantitative PCR

RNA was harvested using TRIzol (Life Technologies cat. 15596-026) as described in Section 2.10. 2µg of total RNA was reverse transcribed using Superscript IV reverse transcriptase (Thermo Fisher, cat. 18090010) using random hexamers. qPCR was performed using Power Sybr Green (Thermo Fisher, cat. 4402953) and an MX300P real time PCR cycler (Agilent). Primers used for qPCR are shown in Table 7.

Table 7: Oligonucleotide primers used for qPCR

Gene	Forward	Reverse	Amplicon
RPL19	CCCACAACATGTACCGGGAA	TCTTGGAGTCGTGGAACTGC	180bp
TBR1	AGCAGCAAGATCAAAAGTGAGC	ATCCACAGACCCCCTCACTAG	149bp
CTIP2	CTCCGAGCTCAGGAAAGTGTC	TCATCTTTACCTGCAATGTTCTCC	129bp
TUBB3	CATGGACAGTGTCCGCTCAG	CAGGCAGTCGCAGTTTTCAC	175bp

Table 7: Showing the oligonucleotide primers used in the thesis

2.14 Collection of post-mortem brain tissue

Frontal cortex tissue from individual P6/16 (*APP* V717I-1) was obtained from Queen Square Brain Bank. For experiments involving tissue homogenisation and extraction of Aβ fractions, tissue chips of right-side hemisphere frontal cortex were received frozen (-80°C). In experiments involving immunohistochemistry, frozen (-80°C) paraffin-fixed tissue (left-side hemisphere frontal cortex) was cryosectioned using a Leica sledge microtome at 7µm.

2.15 Tissue extraction of amyloid beta

Equipment was cooled to 4°C on ice prior to use. Brain tissue from the frontal cortex was stored at -80°C and thawed on ice at 4°C. 0.25g of tissue were suspended in 10mL protease inhibitor solution (RIPA buffer with added 1X EDTA free cOMplete mini (Sigma-Aldrich cat. 4693159001) and 1X PhosStop (Sigma-Aldrich cat. 4906837001) and then homogenised with 30 strokes of a Dounce glass homogeniser and aliquoted into glass ultracentrifuge tubes. Tissue homogenate was centrifuged at 100,000RCF for 60 minutes at 4°C. The supernatant, representing the soluble protein fraction, was aliquoted into 2mL polypropylene Eppendorf's and stored at -80°C. The pellet, representing the insoluble protein fraction, was re-solubilised in 1mL 70% formic acid solution at 4°C, assisted by 100 strokes of a polypropylene pestle. Insoluble fraction homogenate was centrifuged at 20,000RCF for 15 minutes at 4°C. The supernatant was aliquoted into 2mL polypropylene microcentrifuge tubes (Star Lab, cat. S1620-2700), and 1M Tris at pH 11 was added to neutralise the formic acid. Aliquots were stored at -80°C.

2.16 Western blot

Cells were lysed in RIPA buffer with added 1X EDTA free cOMplete mini (Sigma-Aldrich cat. 4693159001) and 1X PhosStop (Sigma-Aldrich cat. 4906837001). Lysates were loaded with Protein Orange G (Li-Cor, cat. 928-40004) and NuPAGE reducing agent (Invitrogen, cat. NP0009), then denatured at 95°C for five minutes. Following centrifugation at 9300RCF for three minutes at 4°C, electrophoresis was conducted with a NuPage 10% Bis-Tris gel (Invitrogen, cat. 10398622) in 1X NuPage MES SDS running buffer (Invitrogen, cat. NP0002) at 150 volts for one hour. Transfer to nitrocellulose membrane was conducted at 30 volts for one hour at 4°C in transfer buffer (700mL Di-H2O, 100mL 10x Tris, 200mL methanol). The membrane was blocked in 3% BSA (Sigma-Aldrich cat. A1933) and incubated with primary antibody overnight (Table 6). The membrane was washed three times with 0.1% PBS-Tween solution and incubated in secondary antibody (Alexa Fluor 680nm

(Invitrogen, cat. A21058), and 800nm (Rockland, cat. 611-145-112)) for one hour, washed three times in 1X PBS and imaged using an Odyssey Fc (Li-Cor Biosciences).

2.17 Lactase dehydrogenase assay

Cell media samples were thawed at 21°C for one hour and assayed for lactate dehydrogenase (LDH) reaction using a Randox LDH P-L 401 kit (Randox, cat. LD401). LDH is an oxidoreductase that catalyses the conversion of pyruvate to lactic acid, with concomitant conversion of NADH to NAD+, in hypoxic conditions. The assay was performed on a Randox Monza (Randox) according to manufacturer protocol. The reaction mix was created by reconstituting lyophilised NADH (0.18 mmol/L) in 3mL of R1a buffer/substrate (phosphate buffer (50mmol/L, pH 7.5 and pyruvate (0.6 mmol/L)). After running a blank (de-ionised H2O), 10µL sample/quality control was diluted in 500µL reaction mix, vortexed for five seconds and analysed.

2.18 Immunoprecipitation MALDI TOF/TOF mass spectrometry

Mass spectrometry experiments were conducted by Dr. E. Portelius and Dr. E. Gkanatsiou of the University of Gothenburg. Aβ peptides were immunoprecipitated using Aβ-specific antibodies coupled to magnetic beads *(Portelius et al., 2007)*. Briefly, 4 mg of the anti-Aβ antibodies 6E10 and 4G8 (Signet Laboratories, Dedham, MA, USA) were separately added to 50 mL each of magnetic Dynabeads M-280 Sheep Anti-Mouse IgG (Invitrogen, Carlsbad, CA, USA). The 6E10 and 4G8 antibody-coated beads were mixed and added to the samples to which 0.025% Tween 20 in phosphate-buffered saline (pH 7.4) had been added. After washing, using the KingFisher magnetic particle processor, the Aβ peptides were eluted using 100 µL 0.5% formic acid. Mass spectrometry measurements were performed using a Bruker Daltonics UltraFleXtreme matrix-assisted-laser-desorption/ionization time-of-flight/time-of-flight (MALDI TOF/TOF) instrument (Bruker Daltonics, Bremen, Germany). All samples were analyzed in duplicate.

3 Confounding factor: Storage Volume

3.1 Introduction

Aβ has long been recognised as a labile and aggregation-prone peptide with importance to the diagnostic process of AD. As previously discussed in Section 1.5.3, the problem of measurement variability within and particularly between sites is widely recognised. With the advent of large-scale biobanking initiatives, the results from which will shape understanding of disease biology for decades to come, the issue of standardisation and reduction of confounding factors has never been more pressing.

The potential for storage vessels to influence measured concentrations of Aβ and tau was recognised relatively early in the movement to improve biomarker standardisation in the study of neurodegenerative diseases *(Vanderstichele et al., 2000)*. Tests of CSF Aβ42, T-tau and P-tau concentration after exposure to polypropylene, polystyrene and glass surfaces show differences between materials, and the majority of studies focused on biomarker surface exposure have focused on these storage material differences *(Kofanova et al., 2015; Lewczuk et al., 2006a; Perret-Liaudet et al., 2012b, 2012a)*. Compared to samples stored in polypropylene tubes, CSF Aβ42 concentration is significantly decreased by approximately 20% when stored in polystyrene tubes *(Bjerke et al., 2010; Perret-Liaudet et al., 2012b, 2012a)*. Samples stored in glass tubes also have a tendency toward lower Aβ42 concentration than those stored in polypropylene, though typically to a lesser degree than polystyrene *(Bjerke et al., 2010)*. Studying the differences between polypropylene, polystyrene, polycarbonate and polystyrene-acrylonitrile copolymer, Lewczuk *et al.* found that polystyrene significantly decreased Aβ42, Aβ40, and T-tau versus the other materials, whilst only the copolymer significantly altered the Aβ42:40 ratio and T-tau *(Lewczuk et al., 2006a)*. Polypropylene and polycarbonate had similar interactions with the biomarkers tested, with a no-significant tendency for lowered Aβ in the latter. An important realisation was that the polypropylene used to manufacture tubes between different companies, and potentially between tube batches, is not uniform and is formed of different ratios of co-polymers that are often not disclosed. These differences have been shown to be sufficient to alter measured Aβ42 concentrations from the same sample *(Kofanova et al., 2015; Perret-Liaudet et al., 2012b, 2012a)*.

As a result of this work, polypropylene tubes have become widely adopted in AD research and clinical diagnostics. This has been possibly the most successful implementation of international pre-analytical standardisation to date, although the field looks set to shift again toward a new design of 'low protein binding' tubes in the near future *(Vanderstichele et al., 2016)*. However, whilst the interaction of Aβ and tau with common storage tube materials had been relatively well documented, very little had been done to explore other aspects of storage vessels that could potentially confound biomarker measurement. One such understudied aspect was the shape of the storage vessel itself. With the understanding that surface adsorption was a significant factor in protein storage, a key question was to what extent variation in tube dimensions, and therefore size of the surface/sample interface, could affect the quantification of Aβ and tau. Some work suggested the standardisation of storage aliquot volume for the prevention of a freeze-drying effect in the event that lid seal was not airtight *(Teunissen et al., 2009)*, but this had not been experimentally tested and no link to surface adsorption was drawn.

We tested the hypothesis that differences in sample storage volume would affect the measurable concentration of Aβ peptides, T-tau, and P-tau in CSF and cell media as a result of surface area-dependent protein adsorption to the storage tube surface. Additionally, we sought to validate the idea that the mechanism of effect was surface adsorption by including a non-ionic surfactant (0.05% Tween 20) to a duplicate sample series. The use of Tween 20 to increase Aβ42 recovery had been previously reported *(Bjerke et al., 2010; Cullen et al., 2012)*.

3.1.1 Contributions

The author designed and conducted all experiments, conducted the immunoassays, contributed to analysis of Volume Study 1 by graphically plotting data and conducted correlation of sample concentration with tube surface area, conducted statistical analysis of Volume Study 2, cultured iPSC neurons and collected media used in Volume Study 2, and wrote the scientific reports of all data. Volume Study 1 was co-written with RW. Paterson.

Volume Study 1:

Study conception: H. Zetterberg, NC. Fox, MP. Lunn, JM. Schott.

Sample collection: H. Zetterberg.

Experiment design: The author.

Experiment: The author.

Analysis: JM. Nicholas, RW. Paterson, the author.

Scientific report: The author, RW. Paterson, MP. Lunn, JM. Nicholas, NC. Fox, MD. Chapman, JM. Schott, H. Zetterberg.

Volume Study 2:

Study conception: H. Zetterberg, MP. Lunn, JM. Schott.

Sample collection: H. Zetterberg, S. Wray, C. Arber, H. Wellington.

Experiment design: The author.

Experiment: The author.

Analysis: The author.

Scientific report: The author, MS. Foiani, H. Wellington, RW. Paterson, C. Arber, A. Heslegrave, MP. Lunn, JM. Schott, H. Zetterberg.

3.2 Materials and methods

3.2.1 Samples

This study consisted of two experiments. The first tested the effect of storage volume on CSF Aβ42, T-tau, and P-tau$_{181}$, the second looked specifically at the effect of storage volume on the ratios of Aβ38, Aβ40, and Aβ42 in CSF and cell media from iPSC-derived cortical neurons.

In the first study (Volume Study 1) CSF was collected and categorised into AD and Non-AD as described in Section 2.3. Due to large volume requirements, some CSF samples of the same category were pooled (AD n=3, Non-AD n=3) from multiple individuals as illustrated in Figure 11, whilst some individual samples had sufficient volume to be tested without pooling (AD n=1, Non-AD n=1).

In the second study (Volume Study 2) CSF and cell media were collected and categorised as described in Sections 2.3 and 2.8 respectively. CSF (AD: n=3, Non-AD: n=5) was pooled as illustrated in Figure 11. Cell media (n=6) was collected from iPSC-derived cortical neurons from lines categorised as Non-AD (CTRL1, CTRL2, and SHEF6) aged between 80 and 100 days post-induction.

3.2.2 Experimental methods

Figure 11: Volume experiment design

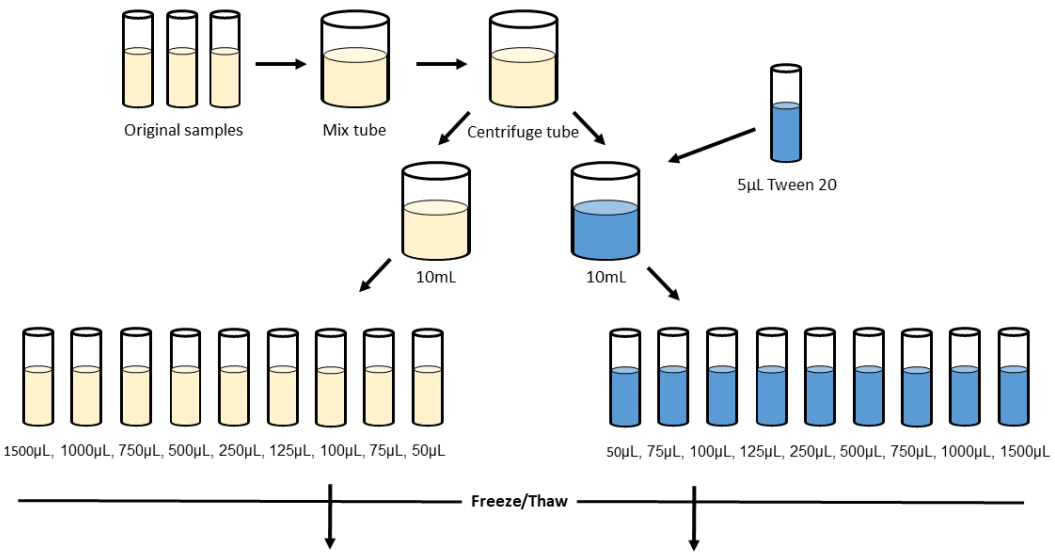

Figure 11: Diagram showing the preparation of samples for the volume experiments.

Volume Study 1 and 2 samples were prepared as illustrated in Figure 11. Patient CSF samples thawed at room temperature for one hour, then pooled together into a 100mL Sarstedt PP beaker (cat. 75.1354.001) and mixed by magnetic stirrer for 30 minutes. The mixed CSF was then transferred into a 50mL Greiner tube and then spun at 2,750 RCF for ten minutes at 4°C. Two 10mL volume aliquots were then created in empty 50mL Greiner tubes. A limitation of this design was the fact that Aβ concentration was not measured from tubes precursory to the final aliquot. This would have given a fuller picture of how well the concentrations measured reflect physiological concentration.

In Volume Study 1, 5µL of Tween 20 (final concentration 0.05%) was added to one of the 10mL tubes as a control for protein adsorption/aggregation. The 10mL aliquots were each divided into 1mL aliquots (Sarstedt 2mL PP cat. 72.694.406) and CSF was divided into a series of volumes, ranging 50µL to 1500µL in Sarstedt 2mL PP storage tubes (Sarstedt, Nümbrecht, Germany, cat. 72.694.406), and stored at -80°C. Prior to assay, aliquots were thawed at 21°C for one hour.

In Volume Study 2, CSF and cell media were treated by the No Tween pathway only Figure 11. Additionally, a more limited volume series (100µL, 125µL, 250µL, 500µL, 1000µL in Sarstedt, cat. 72.694.406 tubes) was chosen to enable more samples to be run in each assay plate and exclude the high and low extreme aliquots, which the results of Volume Study 1 showed to be vulnerable to

experimental artefacts, such as lack of dead volume. Sample aliquots were frozen at -80°C. Prior to assay, aliquots were thawed for one hour at 21°C.

In Volume Study 1, samples were analysed for Aβ42 and T-tau by singleplex MSD ECL immunoassay (Section 2.2.1 and 2.2.3 respectively), and for P-tau$_{181}$ by INNOTEST ELISA (Section 2.1.3). In Volume Study 2 Aβ38, Aβ40, and Aβ42 were measured by triplex MSD ECL immunoassay (Section 2.2.2).

3.2.3 Statistical analysis

The relationship between analyte measurement and sample treatment (volume) was assessed by mixed model regression analysis. Data normality was assessed by histogram, qq-plot and Shapiro-Wilk test, linearity was assessed by scatterplot of the residual variance. All analyses set alpha at 0.05, and confidence intervals at 95%. The formula used for the mixed model was:

lme(sample concentration ~ treatment + X, random = ~1|sample) + ε

lme is the command for a linear mixed model function in R programming software. The dependent variable, 'sample concentration', was the average of duplicate concentration or ratio values of a given Aβ peptide in pg/mL. The fixed effect variable, 'treatment', was sample volume, and 'X' represents other fixed effects (such as disease status, cell type, assay plate, sample pooling status). The random effect variable, 'sample', represents variation due to unaccounted for differences between samples, and '~1|' specifies an independent intercept for each sample. ε represents residual variation not accounted for by the stated parameters of the model.

In Volume Study 1, analysis was conducted by Dr R.W. Paterson and Dr J. Nicholas in STATA. Graphs were created by myself using SPSS version 21. In Volume Study 2, analysis was conducted by myself in R, and graphs were composed using the ggplot2 package.

3.2.4 Assay variation

For Volume Study 1, percent CV of intra- and inter-assay variability respectively was Aβ42 (5.9%, 6.4%), T-tau (1.7%, 21.2%), and P-tau (5.8%, 5.8%), based on comparison of calibrator 2 in each assay. For Volume Study 2, intra- and inter-assay variation respectively was Aβ42 (4.3%C, 9.9%), Aβ40 (4.5%, 9.5%), and Aβ38 (1.6%, 5.3%), calculated from the concentrations of an internal control CSF sample included in assay plates. Intra- and inter-assay CV was calculated according to ISO 5725-2 standards *(British Standards Institution, 1994)*.

3.3 Results

3.3.1 Aβ concentration is altered by storage volume

In both AD and Non-AD CSF (no Tween 20), an approximately two-fold change Aβ42 concentration was observed between the largest and smallest aliquot volumes (Figure 12A). For Non-AD samples, regression analysis predicted a significant increase in Aβ42 concentration (0.95pg/mL [95% confidence interval (CI) 0.36 – 1.50, p = 0.02]) per increase of 10µL aliquot volume. A similar effect was seen in AD CSF: 0.60pg/mL (CI 0.23– 0.98pg/mL, p = 0.003) per 10µL aliquot volume. In CSF with added 0.05% Tween 20 there was no significant relationship between aliquot volume and Aβ42 concentration in either the AD or Non-AD CSF (Figure 12B). No differences were observed between pooled and individual CSF.

Figure 12: The effect of storage volume on CSF Aβ42 concentration

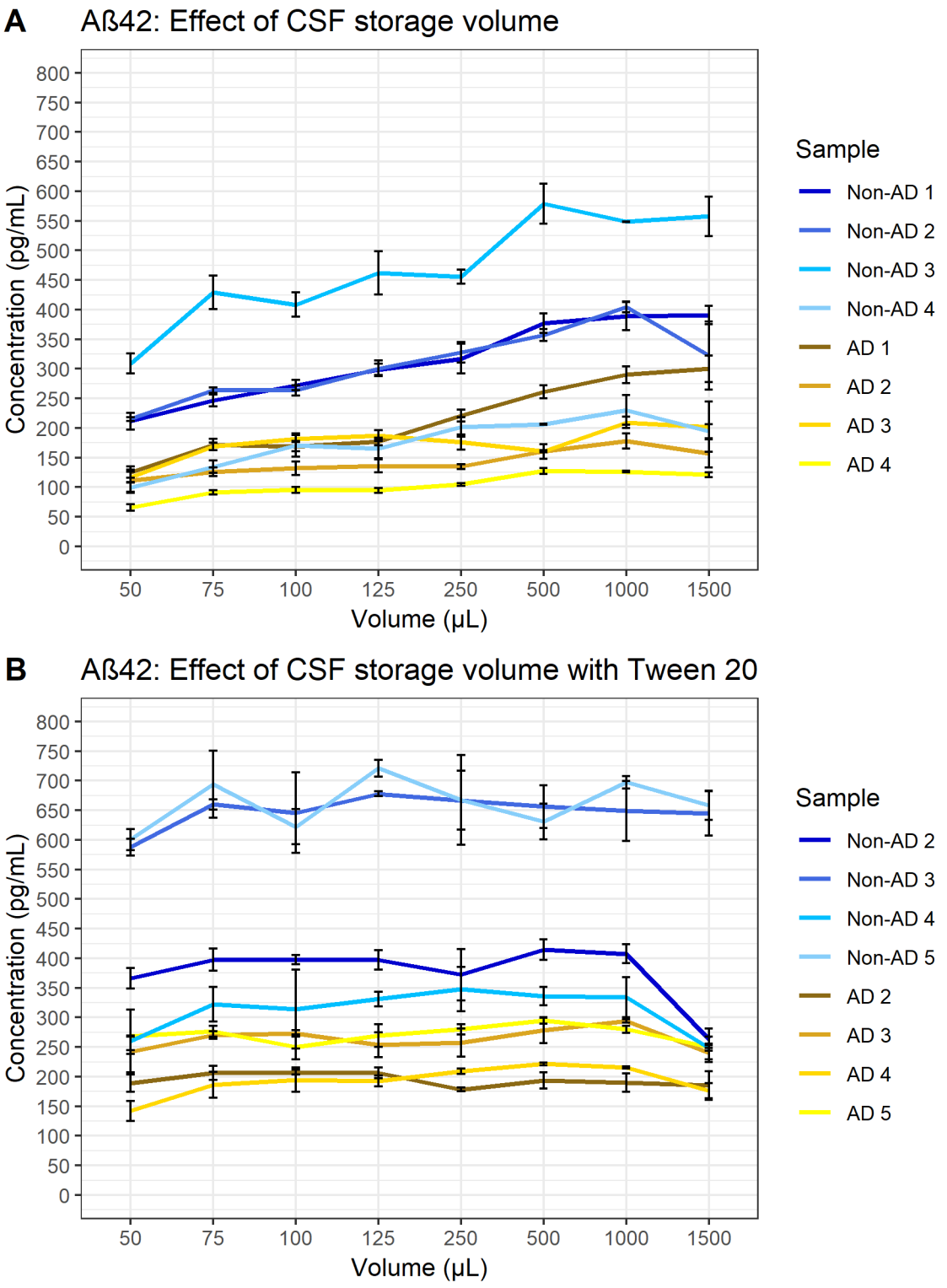

Figure 12: Showing the effect of storage volume on Aβ1-42 concentration in **A)** untreated CSF, and in **B)** CSF treated with 0.05% Tween 20. Samples S1-7 are of pooled CSF, S8 and S9 are CSF from unique individuals. Data are mean of replicates. Error bars represent standard deviation.

3.3.2 Tau concentration is not altered by storage volume

In AD and Non-AD Tween CSF, there was no overall significant association between measured T-tau concentration and aliquot volume (Figure 13). Non-AD T-tau concentration increased by 0.17pg/mL per 10µL volume increase (CI − 0.53 – 0.87pg/mL, p = 0.06). AD T-tau increased by 0.05pg/mL per 10µL volume increase (CI −1 .78– 1 .88pg/mL, p = 0.96). One sample (Non-AD 1) did demonstrate a significant concentration change with volume, but this was not replicated by any other samples tested. No differences were observed between pooled and individual CSF. The addition of Tween 20 (Figure 13B) made no difference to the relationship between T-tau and volume.

Similarly, there was no significant association between No Tween sample P-tau concentration and aliquot volume in AD CSF (0.03pg/mL (CI − 0.01– 0 .06pg/mL, p = 0.10) (Figure 14A). In Non-AD CSF samples the relationship between volume and P-tau concentration was statistically, but not clinically, significant (0.03pg/mL (CI 0.00 – 0.05pg/mL, p = 0.03), driven by variability at the extreme high and low volume measurements. Measurements at 75µL were an artefact of insufficient dead volume, as the assay required 75µL of sample. The cause of measurement variability at 1500µL was not determined. With the addition of Tween 20 (Figure 14B) any association between P-tau and volume disappeared. No differences were observed between pooled and individual CSF.

Figure 13: The effect of storage volume on CSF T-tau concentration

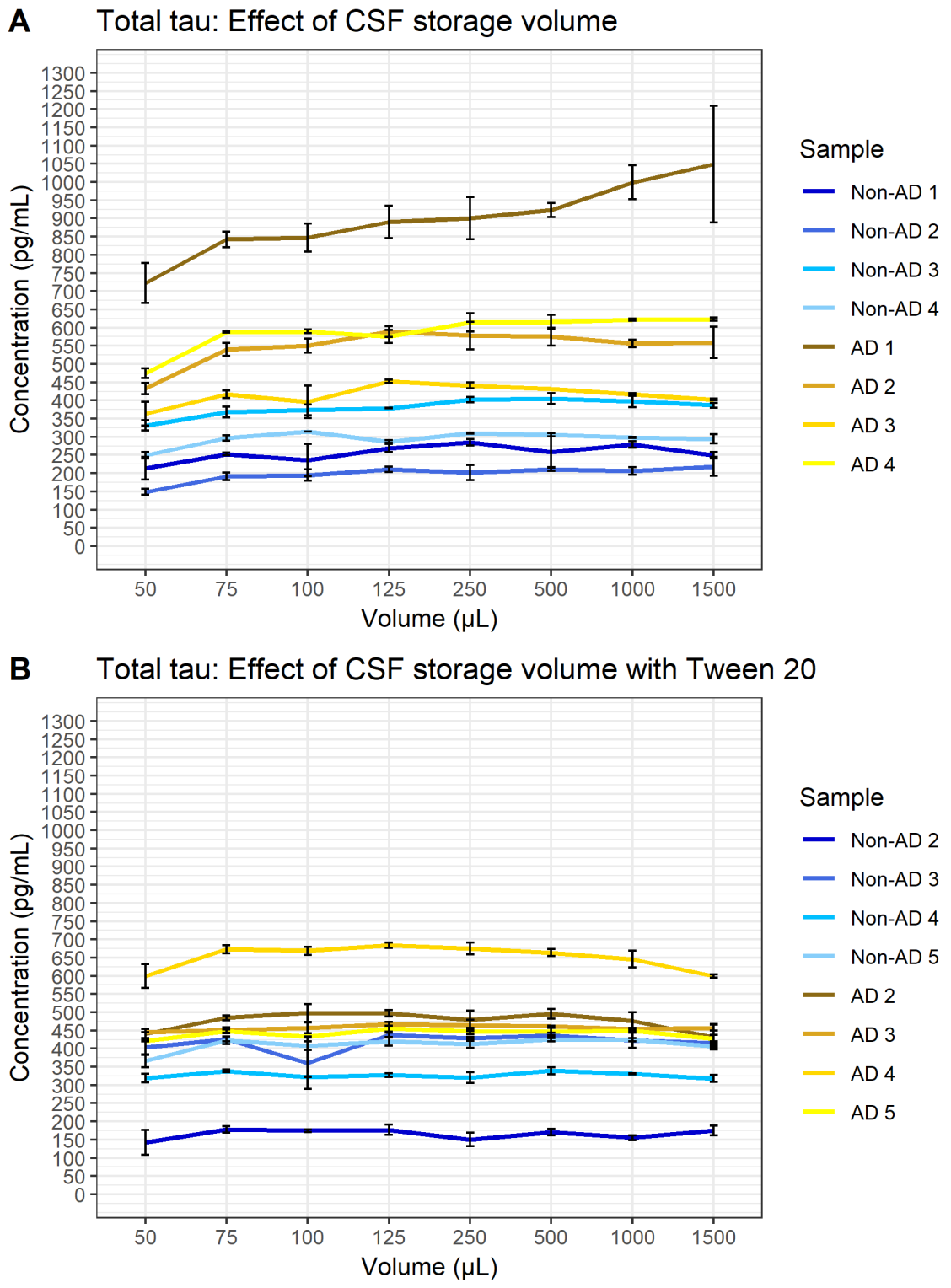

Figure 13: Showing the effect of storage volume on T-tau concentration in **A)** untreated CSF, and in **B)** CSF treated with 0.05% Tween 20. Samples S1-7 are of pooled CSF, S8 and S9 are CSF from unique individuals. Data are mean of replicates. Error bars represent standard deviation.

Figure 14: The effect of storage volume on CSF P-tau concentration

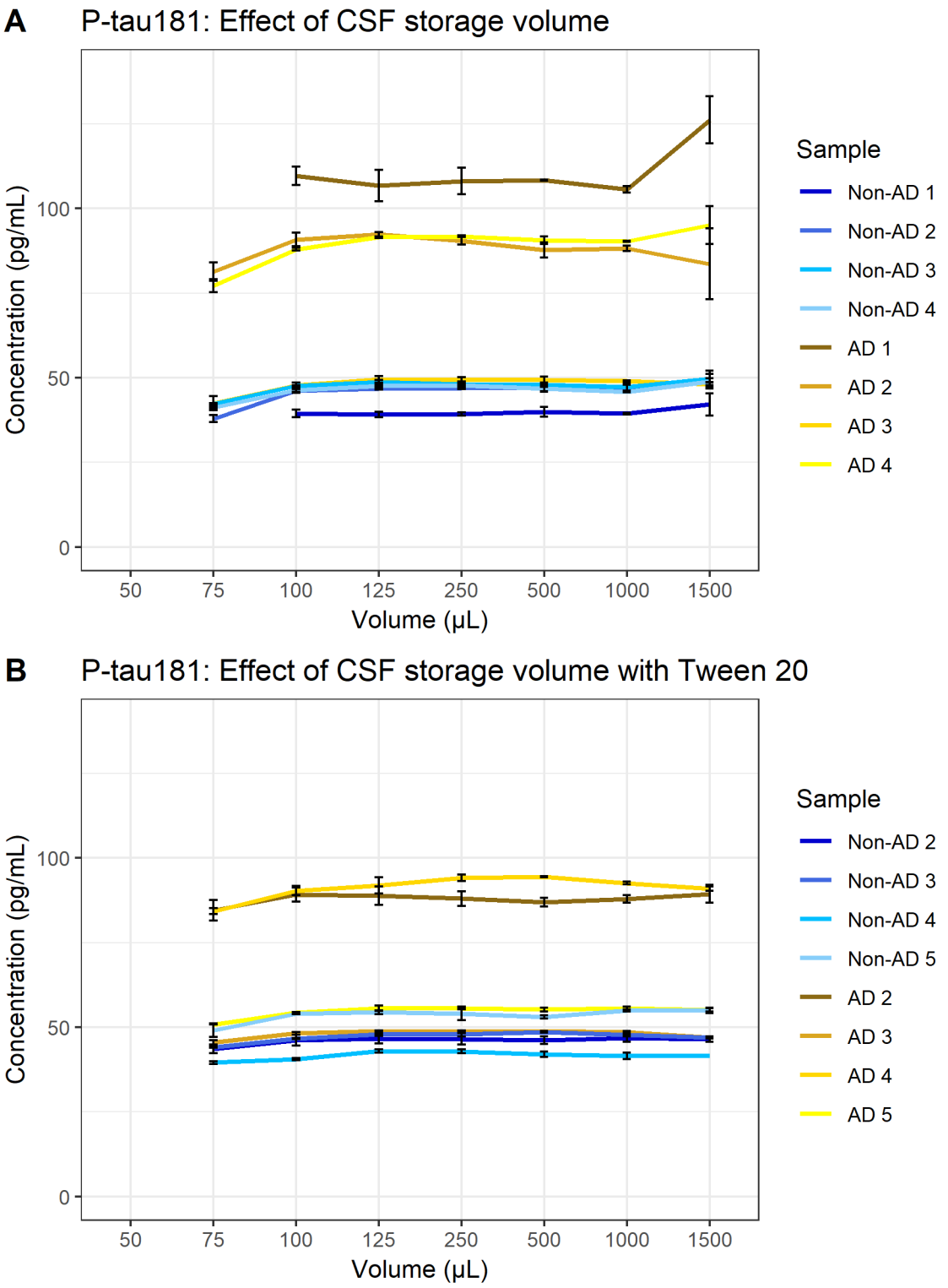

Figure 14: Showing the effect of storage volume on T-tau concentration in **A)** untreated CSF, and in **B)** CSF treated with 0.05% Tween 20. Samples S1-7 are of pooled CSF, S8 and S9 are CSF from unique individuals. Data are mean of replicates. Error bars represent standard deviation.

3.3.3 Mechanism: surface adsorption

Figure 15: Comparison of concentration by volume and surface area

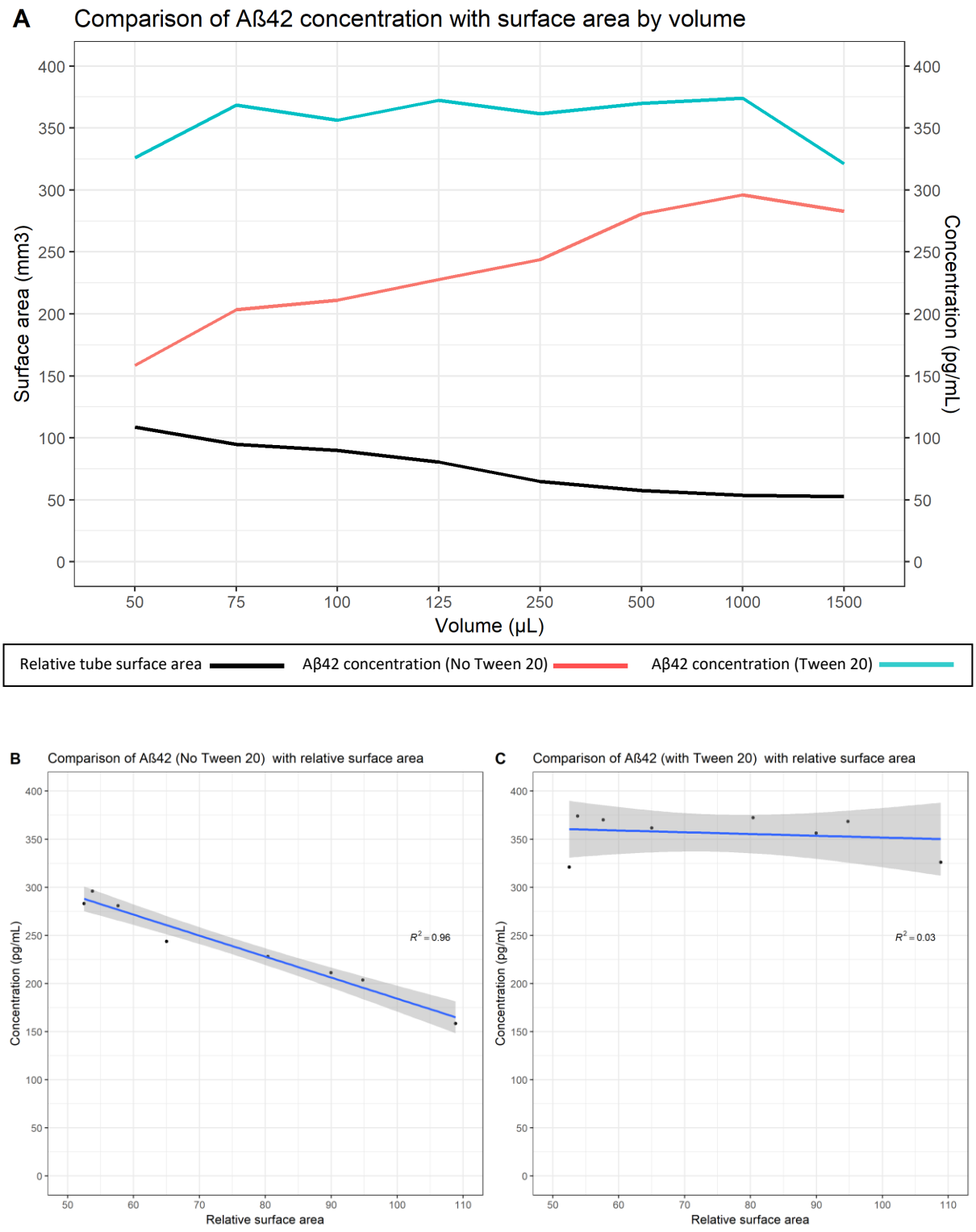

Figure 15: A) Shown against the left Y-axis (surface area) is the surface area relative to volume, to which sample is exposed at different storage volumes in the tubes used. Shown against the right y-axis (concentration) are average Aβ42 concentrations for all samples with and without 0.05% Tween 20. **B)** Correlation analysis of averaged Aβ42 concertation with relative tube surface area exposure at each volume in samples without Tween 20. **C)** Correlation analysis of averaged Aβ42 concertation with relative tube surface area exposure at each volume in samples with Tween 20. The blue lines represent linear regression of the data. The shaded areas represent a 95% confidence interval.

To assist interpretation of these data, we asked 'what proportion of Aβ42 would we expect to lose if it were binding to the tube surface'? To answer this, we calculated the relative internal surface area of the experiment tube exposed at each given volume (Figure 15) (tube dimensions were provided by the manufacturer). Calculations were made by adding the lateral internal surface area of a hollow cylinder to that of a cone, using the relevant formulas from www.aqua-calc.com. Experimental results from No Tween CSF closely matched the pattern that would be predicted if Aβ42 was being adsorbed to the tube in a surface area dependent manner ($R^2 = 0.912$). In solution, Tween 20 molecules concentrate at surface interfaces and increase the solubility of hydrophobic molecules, and therefore either out-competes Aβ for surface binding sites or interacts with Aβ in a manner to disrupt its binding to surfaces or forming conformations capable of masking its epitopes. These results weight interpretation toward disruption of surface binding.

3.3.4 Effect of storage volume on Aβ ratios

The ratios of Aβ42:40 and Aβ42:38 have been proposed as more accurate biomarkers of AD than Aβ42 considered alone *(Anoop et al., 2010; Janelidze et al., 2016; Slemmon et al., 2015)*. We considered that use of Aβ ratios might be less vulnerable to the effect of storage volume, as it had previously been reported that Aβ42:40 was not significantly altered during experiments in which CSF was exposed to different tube materials *(Lewczuk et al., 2006a)*. We conducted Volume Study 2 to investigate whether this might be a viable analytical technique for mitigating the confounding effect of different storage volumes.

3.3.5 Aβ ratios are altered by storage volume

Detectable Aβ42/40/38 concentration was observed to be significantly lower (all $p < 0.001$) in samples of smaller storage volumes in both CSF (Figure 16) and CM (Figure 17). Results from these data predict for every 10µL change in CSF storage volume a concentration change of Aβ42: 1.1pg/mL (0.6%), Aβ40: 9.2pg/mL (0.3%) and Aβ38: 3.1pg/mL (0.2%), and for every 10µL change in CM storage volume a concentration change of Aβ42: 0.5pg/mL (0.3%), Aβ40: 2.5pg/mL (0.2%) and Aβ38: 0.4pg/mL (0.1%) (Table 8). Results for CSF Aβ42 are highly consistent with those previously reported for CTRL CSF (a change of 0.95pg/mL per 10µL) *(Toombs et al., 2013)*. Concordantly, ratios of Aβ42:40 and Aβ42:38 changed significantly with storage volume. In CSF Aβ42:40 change was 0.2% of an initial ratio value per 10µL ($p < 0.001$), and in CSF Aβ42:38 change was 0.3% per 10µL ($p < 0.001$) (Table 8). In CM, change in the Aβ42:40 and Aβ42:38 ratios were 0.1% and 0.2% of the ratio per 10µL ($p < 0.001$) respectively (Table 8). The magnitude of change per unit volume was reduced in both CSF

and CM ratios versus Aβ42 alone. The ratio of Aβ40:38 showed a trend toward decreased Aβ40, which bordered on significance in CSF (p = 0.054), and CM (p = 0.028) (Table 1).

The pattern of effect in CM Aβ42:40 and Aβ42:38 was similar to that observed in CSF, although the absolute values were not directly comparable (Table 8). Furthermore, CM Aβ40:38 was significantly reduced whereas in CSF had bordered on not significant (Table 8). This was due to a relatively smaller effect size of volume on CM Aβ38.

Figure 16: The effect of storage volume on CSF Aβ ratios

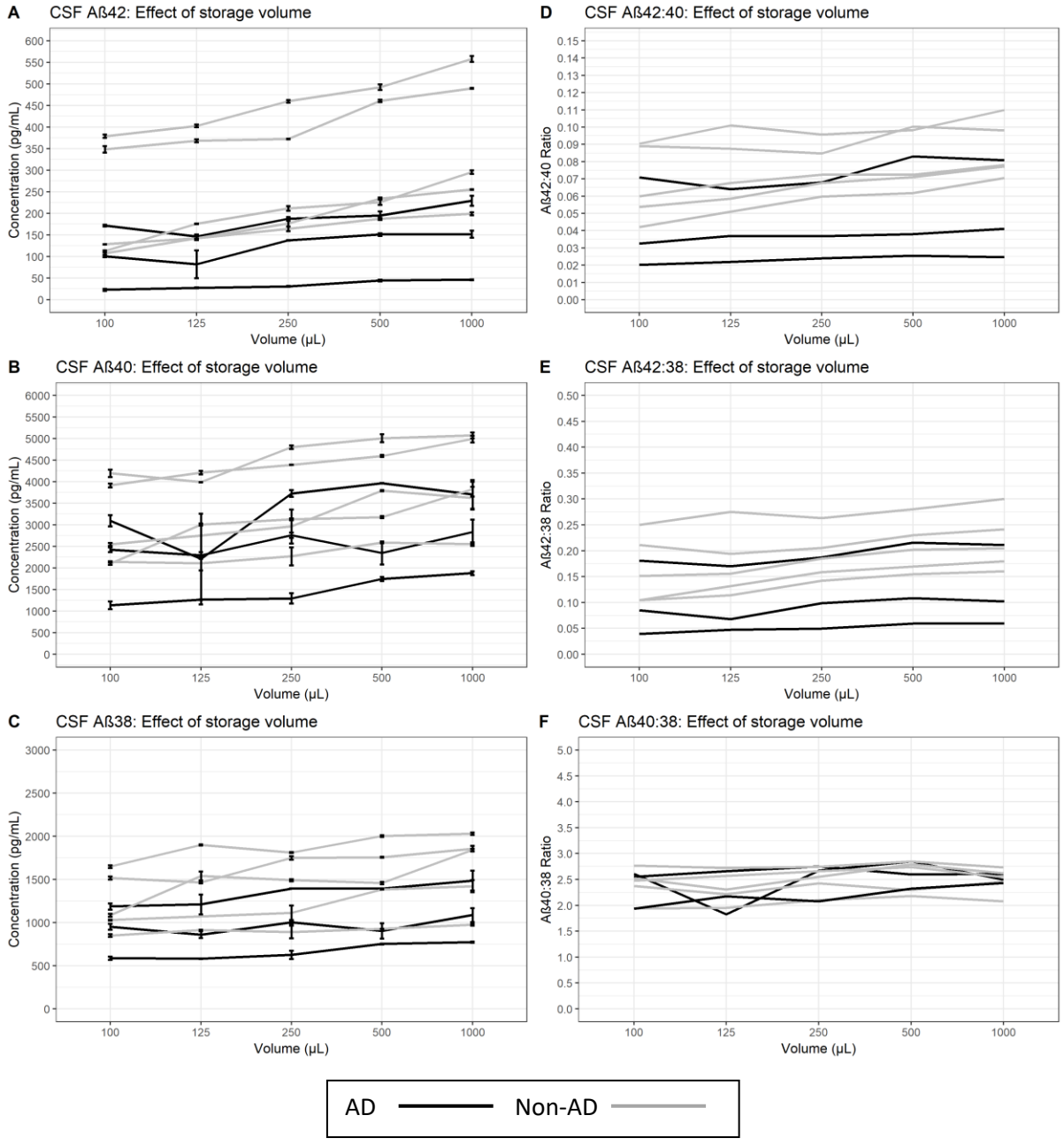

Figure 16: Showing the effect of storage volume on CSF **A)** Aβ42, **B)** Aβ40, **C)** Aβ38, **D)** Aβ42:40, **E)** Aβ42:38, **F)** Aβ40:38.

Figure 17: The effect of storage volume on cell media Aβ ratios

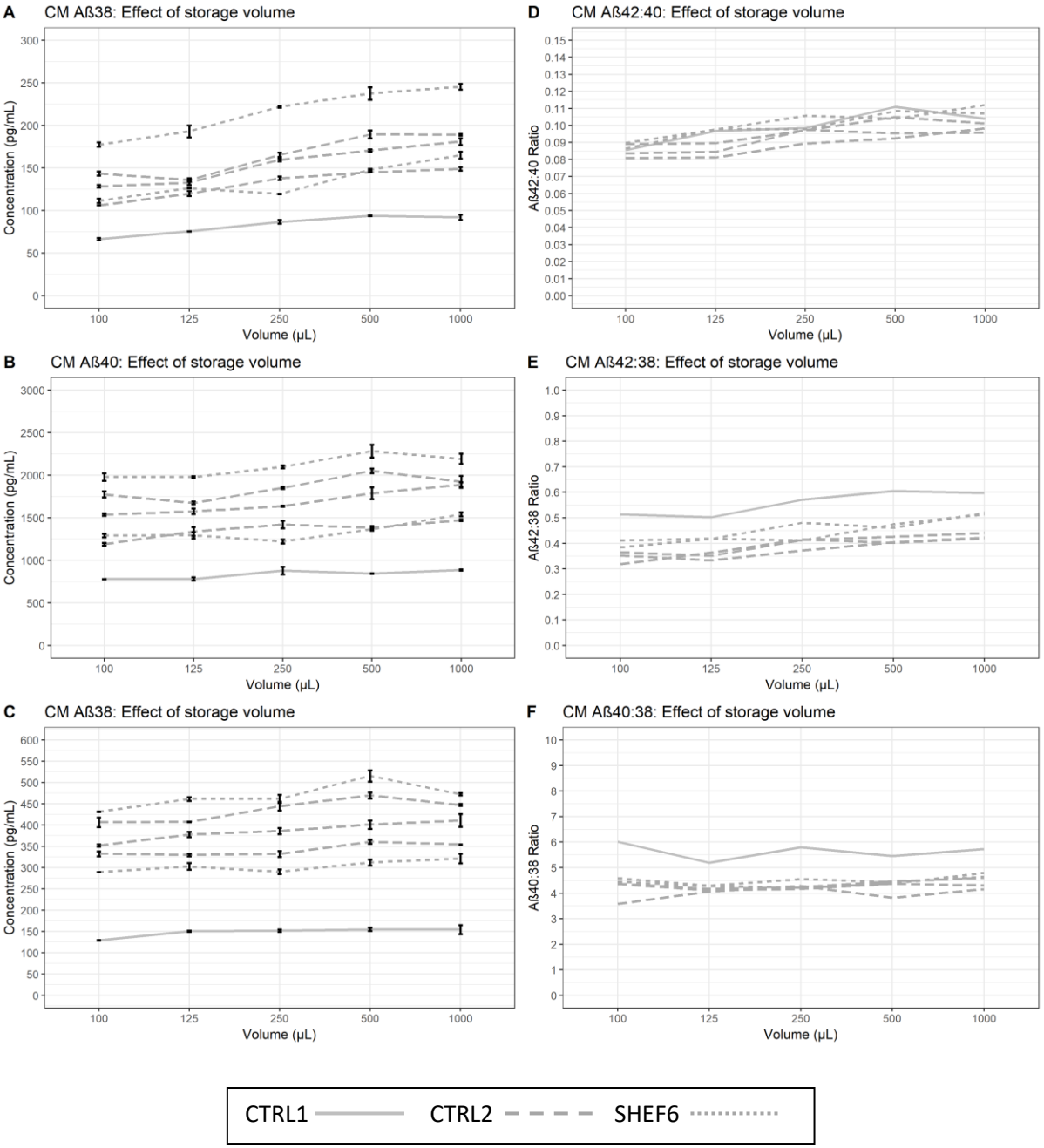

Figure 17: Showing the effect of storage volume on cell media **A)** Aβ42, **B)** Aβ40, **C)** Aβ38, **D)** Aβ42:40, **E)** Aβ42:38, **F)** Aβ40:38.

Table 8: Summary of volume experiment results

Biofluid	Peptide	% Change per unit	p	95% confidence interval	
CSF	Aβ42	0.6%	<0.001	0.403	0.707
CSF	Aβ40	0.3%	<0.001	0.202	0.435
CSF	Aβ38	0.2%	<0.001	0.168	0.322
CSF	Aβ42:40	0.2%	<0.001	0.160	0.313
CSF	Aβ42:38	0.3%	<0.001	0.205	0.415
CSF	Aβ38:40	0.1%	0.54	-0.001	0.148
CM	Aβ42	0.3%	<0.001	0.235	0.427
CM	Aβ40	0.2%	<0.001	0.106	0.217
CM	Aβ38	0.1%	<0.001	0.053	0.156
CM	Aβ42:40	0.2%	<0.001	0.104	0.234
CM	Aβ42:38	0.2%	<0.001	0.160	0.293
CM	Aβ38:40	0.1%	<0.001	0.007	0.108

Table 8: Summarising the results of Volume Study 2 and the effect of storage volume on Aβ concentration and ratios in CSF and cell media (CM). Data from AD and non-AD samples were combined. Change per unit is the exponentiated coefficient of the mixed model linear regression analysis. A unit is 10µL.

3.4 Discussion

The results of these experiments show that the storage volume of a CSF sample is potentially sufficient to influence whether or not its Aβ42 concentration meets a clinical AD criteria, as a change of 10µL volume was observed to result in a change of ~1pg/mL in concentration (or 0.6% of initial concentration). However, it is difficult to give a hard estimate for the amount of concentration loss necessary to mislead interpretation of the ratio, as this will depend on how close the individual peptide values are to a chosen diagnostic threshold. For example, a sample with an Aβ42 concentration a little above an AD diagnostic cut-point could give a result below the cut-point if stored in small volumes. In contrast, T-tau and P-tau$_{181}$ were generally unaffected by storage volume. Therefore, ratios of Aβ42:T-tau and Aβ42:P-tau, which have been proposed as diagnostically useful values *(Counts et al., 2017; De Jong et al., 2006)*, also have the potential to mislead diagnosis if sample volume is not standardised. The experiment design cannot exclude other mechanisms of Aβ concentration change (such as aggregation in solution and adoption of epitope masking conformations), but the correlation of tube surface area Aβ42 concentration showed that surface adsorption is sufficient to explain virtually all of the observed effect.

Contrary to our initial hypothesis, Aβ peptides were not affected to the same extent when CSF samples were stored at different volumes in the polypropylene tubes used. Of the three peptides studied, Aβ42 was most prone to adsorption and thus ratios of Aβ42:40, Aβ42:38 were shown to decrease with lower volumes, although the size of the effect was reduced versus Aβ42 alone (estimated to be half that of Aβ42). Therefore, whilst Aβ ratios may mitigate the risk of misdiagnosis, they cannot be counted on to fully prevent it if sample handling is not standardised.

The effect of storage volume on Aβ peptides in cell media was found to be very similar to CSF, with a differential effect on Aβ42, compared to Aβ40 and Aβ38. This is relevant to cell models in AD research, where Aβ measurement variability within and between cell lines presents a hindrance to building a convergent literature of cell biology, which use of ratios may help reduce (see Section 8.3.4).

Following on from this work, Vanderstichele *et al.* observed significant decreases in Aβ1-42 (–13.6%), Aβ1-40 (–15.5%), and Aβ1-38 (–10.6%) between CSF stored at 1500µL (Sarstedt cat. 72.706) and 500µL (Sarstedt cat. 72.730.006) in PP tubes, but not in Eppendorf LoBind tubes *(Vanderstichele et al., 2016)*. They found that the Aβ42:40 ratio was not significantly altered by the difference in volume, whilst Aβ42:38 was altered by 3.4%, although they did observe differences between peptides when exposed to surfaces of new tubes (see Section 4.4). This is in contrast to our model which predicts larger, significant, changes in Aβ42:40 (23.7%) and Aβ42:38 (30.9%). It is worth noting that the volume effect is closely related to tube dimension *(Toombs et al., 2013; Willemse et al., 2017)*, and our results represent the difference between 1000µL and 100µL rather than 1500µL and 500µL, which have different relative surface area exposure to the tube. Additionally, the tubes used by Vanderstichele *et al.* for each volume were not the same *(Vanderstichele et al., 2016)*., and neither matched the tube we tested (Sarstedt cat. 72.694.007), which may reduce the direct comparability of results. Lewczuk *et al.* found a slight reduction in Aβ42:40 ratio in polystyrene-acrylonitrile copolymer tubes compared to polycarbonate, but no difference among other tubes, despite an apparent tendency for decreased Aβ42:40 in polystyrene-based tubes relative to polypropylene *(Lewczuk et al., 2006a)*. Therefore, the effect of storage volume on Aβ peptide ratios, if it is real, appears to be subtle.

Subsequent reports have confirmed no, or limited, effect of tube volume on CSF T-tau concentration *(Willemse et al., 2017)*, although data is not unanimous. Vanderstichele et al. reported that T-tau concentration could be marginally influenced by storage volume, with a 4.5% concentration decrease

when stored at 500µL compared to a 1.6% decrease when stored at 1500µL *(Vanderstichele et al., 2017)*. Although, our original results support the idea that T-tau is not vulnerable to surface exposure, one high concentration sample in Volume Study 1 did demonstrate a decrease in concentration with decreased volume, and it may be that tau proteins can be prone to surface exposure in particular forms or at high concentrations. Interestingly, Willemse *et al.* noted that CSF Aβ42 concentration loss was a greater (more than two-fold) when the initial concentration was higher *(Willemse et al., 2017)*, and potentially this could apply to more than just Aβ.

The addition of Tween 20 to CSF strongly mitigated the effect of storage volume in Aβ42. Subsequent experiments also demonstrated this effect on Aβ38 and Aβ40 concentration when treated to another method of surface exposure (discussed in Chapter 4). Tween 20 also appeared to nullify the anomalously variable concentration results observed at 1500µL volume in P-tau, although the ultimate cause of this was never determined. The storage concentration of Tween 20 used in this study was 0.05%, the generally accepted critical micelle concentration (CMC) for Tween 20 is 0.007%, although micelle formation has been shown to initiate at 0.002% *(Deechongkit et al., 2009)*. Therefore the Tween 20 molecules in our samples would be expected to be in micelle arrangement during storage and in the initial stages of the assay as well as being in competition for tube surface and liquid/air interface distribution with other hydrophobic molecules. The mechanism of effect is thus proposed to be less favourable conditions for Aβ peptide surface binding or aggregation in solution in the presence of Tween 20. This work supported the findings of Pica-Mendez *et al. (Pica-Mendez et al., 2010)* and was subsequently verified by other groups in the context of storage volume *(Vanderstichele et al., 2017)*. Given the apparent effectiveness of adding a final concentration of 0.05% Tween 20 to CSF to the mitigation of AD biomarker surface adsorption we proposed that the concept of CSF sample additives should be further explored.

Despite the limitation of relatively small sample size, the broad findings in CSF have been well replicated by subsequent independent investigations, although some conflicts in detail remain to be resolved. Additionally, data in cell media continue to represent the only example in the literature at the present date. Additionally, this experiment could have been improved by measurement of CSF and cell media in all storage tubes used during processing, prior to the final aliquot. This would give an indication of how Aβ concentration is affected when stored at larger volumes in larger vessels as well as how representative values obtained are of physiological concentrations. This is particularly relevant in light of the effect of transferring sample between surfaces discussed in Chapter 4A further limitation is the fact that the experiment method followed a 'top down' model that has been

criticised by Kastantin *et al.* and future work would benefit from validation of the adsorption mechanism with high resolution imaging techniques *(Kastantin et al., 2014)*.

3.5 Chapter summary

The findings reported in this chapter have potentially important ramifications for the diagnostic process of AD, and the goal of developing standardised AD biomarker cut-points. Aβ42 considered on its own, or in ratio with other AD biomarkers such as T-tau, P-tau$_{181}$ is vulnerable to giving false negative and positive results in polypropylene tubes if surface exposure is not standardised. This effect can be mitigated by the addition of 0.05% Tween 20 early in the sample aliquoting process, and standardisation of sample storage practices. The use of Aβ ratios may also mitigate storage volume as a confounding factor in comparison to using Aβ42 measurements alone, although these too may be partially vulnerable to subtle differences between peptide adsorption propensities.

3.5.1 Publications arising from this work

Toombs J, Paterson RW, Lunn MP, Nicholas JM, Fox NC, Chapman MD, Schott JM, Zetterberg H. Identification of an important potential confound in CSF AD studies: aliquot volume. Clin Chem Lab Med. 2013 Dec;51(12):2311-7. doi: 10.1515/cclm-2013-0293.

Toombs J, Foiani MS, Wellington H, Paterson RW, Arber C, Heslegrave A, Lunn MP, Schott JM, Wray S, Zetterberg H.Amyloid β peptides are differentially vulnerable to preanalytical surface exposure, an effect incompletely mitigated by the use of ratios. Alzheimers Dement (Amst). 2018 Mar 22;10:311-321

4 Confounding factor: Serial tube transfer

4.1 Introduction

The results of the volume experiments had shown that the propensity of Aβ to adsorb to surfaces is in part dependent on surface area exposure and can be diminished in the presence of 0.05% Tween 20. We next considered whether exposure of CSF to a new surface could affect sample Aβ concentration.

Making aliquots of a stock sample in new tubes is a common practice when making dilutions or when sharing samples among collaborators, and important to the facilitation of AD research. As previously discussed in Section 3.1, the study of protein adsorption has a large literature in physical chemistry journals and across the wider biomedical field. A few studies have tested the effect of serial surface exposure on various proteins *(Bratcher and Gaggar, 2014)*, and a number of analytical techniques actively incorporate surface depletion in their methods *(Desrumaux et al., 2001; Hlady et al., 1999)*. Prior to our investigation, very little work had directly addressed the potential of this issue to confound biomarker measurement in the AD field. The extent of research was the description that iterative contact with storage tubes reduced Aβ42 concentration, though no supporting data was shown *(Perret-Liaudet et al., 2012b, 2012a)*, and a brief report by Pica Mendez *et al* showing that samples incubated for 30 minutes with 0.05% Tween 20 increased measurable Aβ42 concentration in CSF samples stored in polypropylene tubes *(Pica-Mendez et al., 2010)*.

Based on our previous results and the implications of the literature we hypothesised that CSF and cell media Aβ concentration would be depleted by serial transfer between storage tubes. We were also interested in the effect such treatment would have on the ratios of Aβ peptides. As this study was conducted alongside our investigation into the effect of storage volume on Aβ ratios our initial hypothesis was that different Aβ peptides would be affected to a similar extent.

4.1.1 Contributions

The author conceived of, designed, and conducted all experiments described in this chapter, cultured iPSC neurons and collected media used in Transfer Study 2 (alongside C. Arber and H. Wellington), conducted the statistical analyses, and wrote the scientific reports.

Transfer Study 1:

Study conception: The author.

Sample collection: H. Zetterberg.

Experiment design: The author.

Experiment: The author.

Analysis: The author.

Scientific report: The author, RW. Paterson, JM. Schott, H. Zetterberg.

Transfer Study 2:

Study conception: The author, H. Zetterberg, MP. Lunn, JM. Schott.

Sample collection: The author, H. Zetterberg, C. Arber, H. Wellington.

Experiment design: The author.

Experiment: The author.

Analysis: The author.

Scientific report: The author, MS. Foiani, H. Wellington, RW. Paterson, C. Arber, A. Heslegrave, MP. Lunn, JM. Schott, S. Wray, H. Zetterberg.

4.2 Materials and methods

4.2.1 Samples

This study consisted of three experiments. The first tested the effect of serial tube transfer on CSF Aβ42, T-tau, and P-tau$_{181}$, the second looked specifically at the effect of serial tube transfer on the ratios of Aβ38, Aβ40, and Aβ42 in CSF and cell media from iPSC-derived cortical neurons. The third experiment tested the contribution of the pipette tip to any effect on Aβ peptide concentration.

In the first study, Transfer Study 1, CSF was collected and categorised into AD and Non-AD as described in Section 2.3. CSF samples of the same category were pooled (AD n = 2, Non-AD n = 2) from multiple individuals as illustrated in Figure 18.

In the second experiment, Transfer Study 2, CSF and cell media were collected and categorised as described in Sections 2.3 and 2.8 respectively. CSF (AD: n = 5, Non-AD: n = 4) was pooled as illustrated in Figure 18. Cell media (n = 5) was collected from iPSC-derived cortical neurons (APP V717I-1, PSEN int4del-4, CTRL1, CTRL2, and SHEF6) aged between 80-100 days post-induction.

In the third experiment, a separate group of samples (CSF n = 2 and CM n = 2) were aliquoted into four different volumes (100, 250, 500, and 1000 mL). These samples were collected and categorised as described in Sections 2.3 and 2.8 respectively. The CSF samples used were both pooled from individuals with CSF with a profile consistent with AD. Cell media was collected from CTRL1 and CTRL2.

4.2.2 Experimental method

In Transfer Study 1 and 2 samples were prepared as illustrated in Figure 18. Patient CSF samples were thawed at room temperature for one hour, then pooled together into a 100mL Sarstedt PP beaker (cat. 75.1354.001) and mixed by magnetic stirrer for 30 minutes. The mixed CSF was then transferred into a 50mL Greiner tube (cat. T2068-450EA) and then spun at 1750 RCF for ten minutes at 4°C. Two equal volume aliquots were then created in empty 50mL Greiner tubes (cat. T2068-450EA). An oversight of this design was the fact that concentrations of Aβ and tau in tubes precursory to the final aliquot were not measured.

Transfer Study 1 consisted of a pilot experiment and a replication experiment. In the pilot, centrifuged samples were split into two 25mL aliquots. 12.5µL of Tween 20 (final concentration 0.05%) was introduced to one aliquot, creating paired Tween and No Tween sample pools. From these pools 1mL aliquots (in Sarstedt PP 2mL storage tubes cat. 72.694.406) were derived and stored at -80°C. Aliquots were thawed at 21°C for one hour, and used for another experiment, the remaining 950µL was re-stored at -80°C. Aliquots were thawed at 21°C for one hour, and sample was aliquoted sequentially between tubes (Sarstedt 2mL PP cat. 72.694.406) leaving the following volumes in each tube: Tube 0 = 215µL, Tube 1 = 200µL, Tube 2 = 200µL, Tube 3 = 200µL, and Tube 5 = 110µL. Only four transfers were conducted in this experiment.

Figure 18: Transfer experiment design

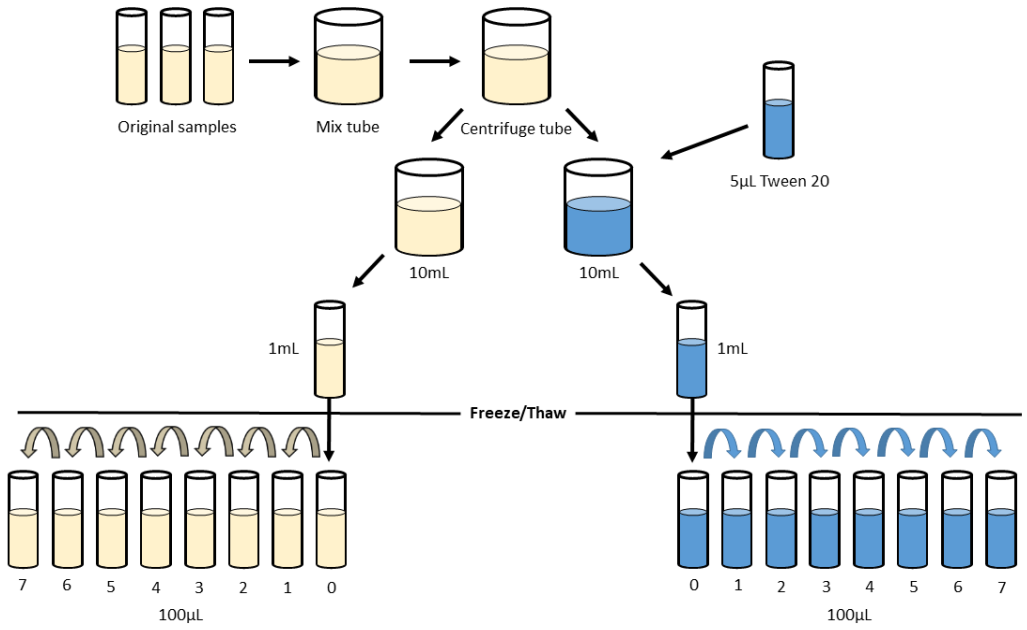

Figure 18: Diagram showing preparation of samples for serial tube transfer experiments.

It was recognised that the different aliquot volumes and extra freeze/thaw cycle were a flaw in the experiment design. Therefore, a replication experiment was conducted. Centrifuged samples were split into two 10mL aliquots. 5µL of Tween 20 (final concentration 0.05%) was added to one of the 10mL tubes. The 10mL aliquots were each divided into 1mL aliquots (Sarstedt 2mL PP cat. 72.694.406) and stored at -80°C. Aliquots were thawed at 21°C for one hour, and sample was aliquoted sequentially between tubes leaving 100µL in each tube (Sarstedt 2mL PP cat. 72.694.406) as shown in Figure 18. The number of transfers was increased to seven in order to observe if the effect on concentration would be maintained or change over a greater treatment range.

In Transfer Study 2, CSF and cell media were prepared by the No Tween pathway illustrated in Figure 18. 1mL sample aliquots were frozen at -80°C and were thawed for one hour at 21°C prior to assay. A seven transfer series of 100µL aliquots (Sarstedt 2mL PP cat. 72.694.406) was created. In both Transfer Study 1 and 2 samples were assayed immediately after the transfer series had been completed.

The third experiment tested the effect of pipetting and aspirating CSF and cell media on Aβ peptide concentration. Aliquots of different volumes were prepared as described in Section 3.2.2 and Figure

11. Immediately prior to sample dilution during assay, each volume for each sample was mixed with a varying number of pumps (0, 5, 10, and 20) with a pipette tip (TipOne; Starlab, Milton Keynes; cat. S1113-1700). Tips used for samples given the 0 pump treatment were therefore not pre-wetted.

In Transfer Study 1 and the pipette experiment, samples were analysed for Aβ42 (Section 2.2.1) and T-tau by singleplex (Section 2.2.3) as well as Aβ38/40/42 triplex MSD ECL immunoassay (Section 2.2.2). P-tau measurement was not included as, following the results of Volume Study 1, we did not anticipate it would add additional information over T-tau. In Transfer Study 2, Aβ38/40/42 were measured by triplex MSD ECL immunoassay (Section 2.2.2).

4.2.3 Statistical analysis

The relationship between analyte measurement and sample treatment (volume) was assessed by mixed model regression analysis in R. Data normality was assessed by histogram, qq-plot and Shapiro-Wilk test, linearity was assessed by scatterplot of the residual variance. Data did not meet the regression model's assumption of linearity. To meet this requirement, average concentration was transformed by the natural logarithm (ln). To calculate the proportional change per treatment unit, e was exponentiated to the power of the model's output coefficient. All analyses set alpha at 0.05, and confidence intervals at 95%. The formula used for the mixed model was:

lme(ln sample concentration ~ treatment + X, random = ~1|sample) + ε

lme is the command for a linear mixed model function in R programming software. The dependent variable, 'ln sample concentration', was the average of duplicate concentration or ratio values of a given Aβ peptide transformed by ln. The fixed effect variable, 'treatment', was the number of tube transfers, and 'X' represents other fixed effects (such as disease status, cell type, assay plate, sample pooling status). The random effect variable, 'sample', represents variation due to unaccounted for differences between samples, and '~1|' specifies an independent intercept for each sample. ε represents residual variation not accounted for by the stated parameters of the model. Graphs were created using the R package ggplot2.

4.2.4 Assay variation

For Transfer Study 1, percent CV of intra- and inter-assay variability respectively were Aβ42 singleplex (5.0%, 9.9%), Aβ38 (5.5%, 5.5%), Aβ40 (8.5%, 8.8%), Aβ42 triplex (12.2%, 12.2%), T-tau (5.6%, 15.6%), calculated from concentrations of an internal control CSF sample. For Transfer Study 2, intra- and

inter-assay variation respectively was Aβ42 (4.3%C, 9.9%), Aβ40 (4.5%, 9.5%), and Aβ38 (1.6%, 5.3%), calculated from the concentrations of an internal control CSF sample. Intra- and inter-assay CV) was calculated according to ISO 5725-2 standards *(British Standards Institution, 1994)*.

4.3 Results

4.3.1 Aβ concentration decreases with tube transfer

The results of Transfer Study 1 demonstrated that Aβ42 decreased significantly with successive tube transfers in both AD and non-AD CSF (Figure 19A). Over seven and four transfers, mixed model analysis of Aβ42 triplex assays estimated an average 21% concentration decrease per transfer for AD and non-AD CSF relative to initial concentration. Values for Aβ42 singleplex assays were highly comparable to those of the triplex results (Pilot = 28%, Replication = 23% concentration decrease per transfer) (Figure 19A-B). This effect was strongly mitigated, but not entirely prevented by Tween 20, which reduced the effect to approximately 5% concentration decrease per transfer in all assays (Figure 19A-B).

Aβ peptides Aβ38 and Aβ40 were also affected by iterative sample transfer between tubes (Figure 19C-D). Over seven transfers AD and non-AD Aβ38 decreased by 16.3% per transfer respectively, whilst Aβ40 decreased by 16.5% per transfer. For comparison with the Pilot experiment data, when limited to four transfers the model predicted decreases of 12% and 13% for Aβ38 and Aβ40 respectively. The presence of Tween 20 strongly mitigated the treatment effect to approximately 1% per transfer (Figure 19C-D), which was not significant after four transfers, but became so after seven.

Figure 19: Effect of serial tube transfer on Aβ peptide concentration

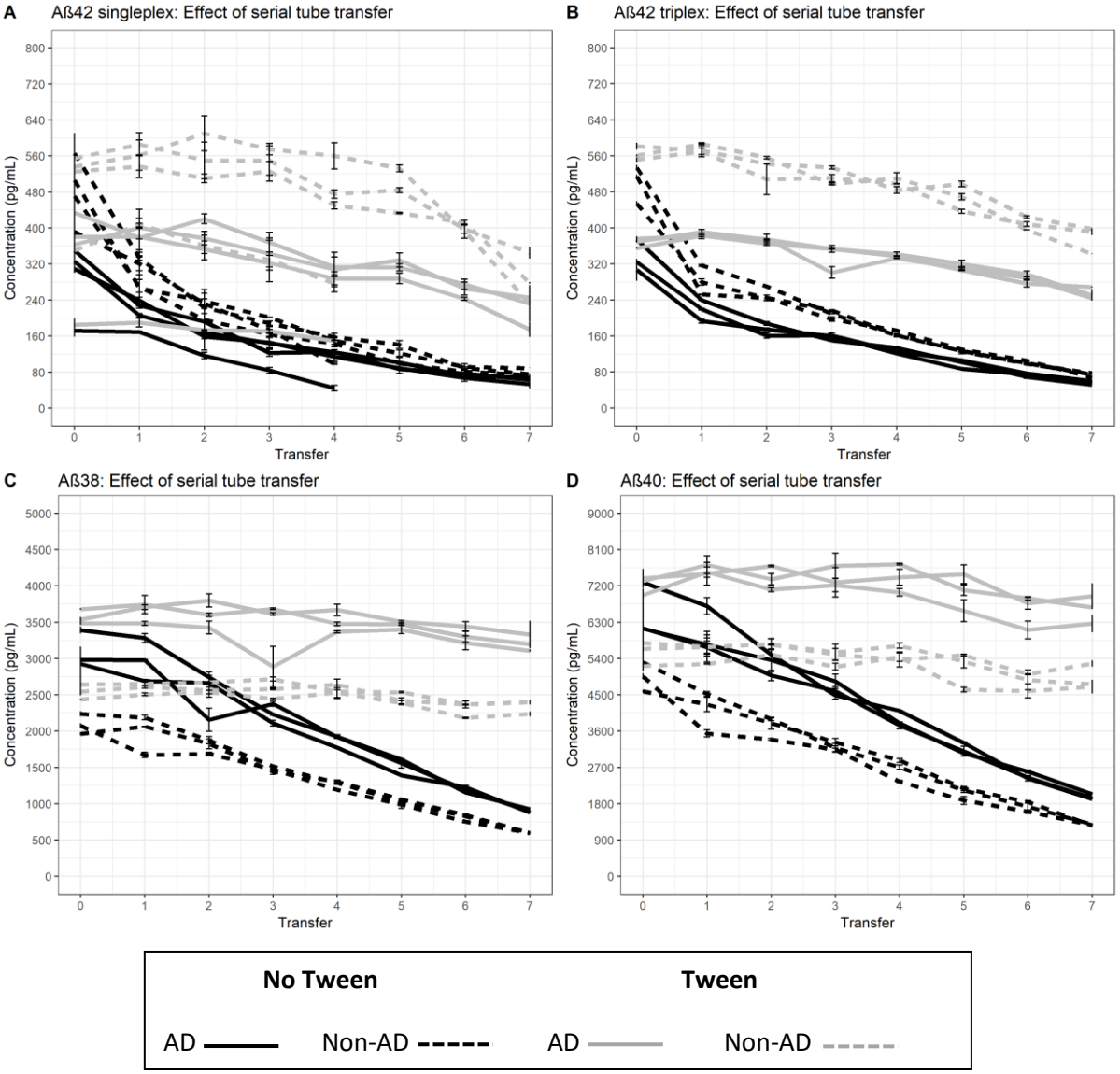

Figure 19: A) CSF Aβ42 concentration change over serial tube transfers with and without Tween 20 as measured by the MSD singleplex assay. Data shown include the results of a pilot study (only four transfers) and a replication experiment (seven transfers). **B)** CSF Aβ42 **C)** CSF Aβ38 and **D)** CSF Aβ40 concentration change over serial tube transfers with and without Tween 20 as measured by the MSD triplex assay. Samples used were the same as those used in the replication experiment in panel A. Error bars represent standard deviation.

4.3.2 T-tau concentration decreases slightly with tube transfer

Figure 20: Ttau: Effect of serial tube transfer

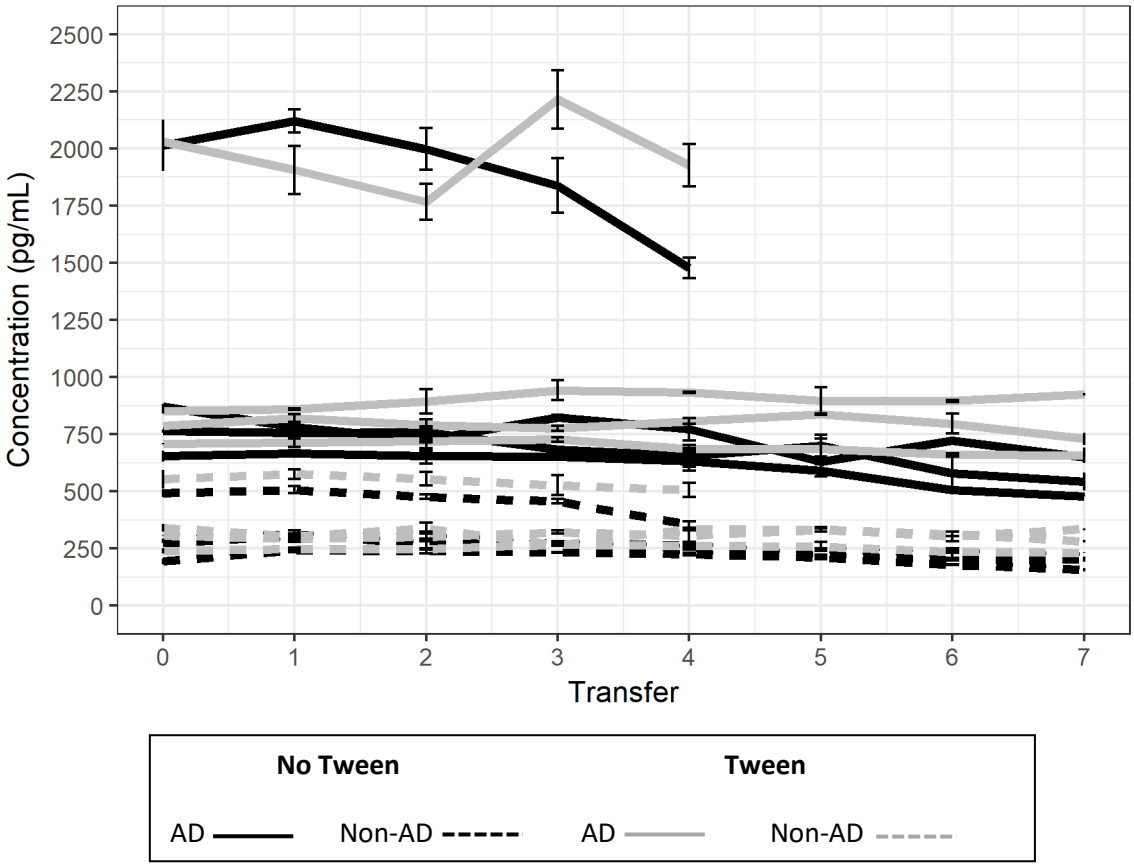

Figure 20: CSF T-tau concentration change over serial tube transfers with and without Tween 20. Data shown include the results of a pilot study (only four transfers) and a replication experiment (seven transfers). Error bars represent standard deviation.

When T-tau was measured in the same samples, serial transfer was found to not to cause a significant change in concentration over four transfers in the samples of the replicate experiment. However, a small but significant decrease in concentration (4% per transfer) was observed in these samples over seven transfers (Figure 20, Table 9). In the pilot study samples (which were only treated with four transfers) the AD sample appeared to be more strongly affected than the other samples measured, but overall the model only predicted a 7% decrease per transfer, which was the same as for the Non-AD sample. In samples treated with Tween 20, no significant effect was observed on T-tau concentration.

Table 9: Summary of Transfer Study 1 results

		Four Transfers								Seven Transfers							
		No Tween				Tween 20				No Tween				Tween 20			
Experiment	**Peptide**	**% Change per unit**	**p**	**95% confidence interval**		**% Change per unit**	**p**	**95% confidence interval**		**% Change per unit**	**p**	**95% confidence interval**		**% Change per unit**	**p**	**95% confidence interval**	
Pilot	Aβ42 Singleplex	28.8%	<0.001			5.9%	0.009										
Pilot	Ttau	7.3%	0.004	-0.120	-0.033	1.0%	0.511										
Replication	Aβ42 Singleplex	23.6%	<0.001			4.0%	<0.001	-0.060	-0.022	21.4%	<0.001	-0.256	-0.226	7.8%	<0.001	-0.097	-0.066
Replication	Aβ42	21.2%	<0.001	-0.271	-0.207	3.3%	<0.001			21.5%	<0.001	-0.255	-0.229	5.5%	<0.001	-0.064	-0.049
Replication	Aβ38	12.1%	<0.001	-0.148	-0.110	0.5%	0.365	-0.015	0.006	16.3%	<0.001	-0.191	-0.166	1.5%	<0.001	-0.020	-0.011
Replication	Aβ40	13.1%	<0.001	-0.156	-0.124	0.1%	0.822	-0.008	0.006	16.5%	<0.001	-0.191	-0.170	1.9%	<0.001	-0.025	-0.014
Replication	Aβ42:40	9.4%	<0.001			3.3%	<0.001	-0.046	-0.020	6.0%	<0.001	-0.075	-0.049	3.6%	<0.001	-0.043	-0.031
Replication	Aβ42:38	10.4%	<0.001	-0.146	-0.073	2.9%	<0.001	-0.037	-0.021	6.2%	<0.001			4.0%	<0.001	-0.047	-0.036
Replication	Aβ38:40	1%	0.167			0.4%	0.503	-0.016	0.008	0.2%	0.537	-0.005	0.009	0.4%	0.129	-0.001	0.009
Replication	T-tau	1.6%	0.068	-0.034	0.001	0.6%	0.388	-0.008	0.021	4.5%	<0.001	-0.056	-0.036	0.2%	0.492	-0.009	0.004

Table 9: Summarising the results of Transfer Study 1 and the effect of serial tube transfer on Aβ concentration and ratios in No Tween and Tween CSF. Data from AD and non-AD samples were combined. The model's predictions based on four and seven transfers are shown. Change per transfer is the exponentiated coefficient of the mixed model linear regression analysis.

4.3.3 Amyloid beta ratios are affected by tube transfer

Although the Aβ peptides tested all decreased with iterative exposure to new tube surfaces, Aβ42 appeared to behave differently from Aβ40 and Aβ38 and it was decided to examine this further.

Transfer Study 2 tested the tube transfer effect in additional CSF and cell media samples. The additional CSF data supported the findings of Transfer Study 1 for the effect on Aβ peptide concentrations (Figure 21, Table 10). Furthermore, the data highlighted the distinct effect on Aβ42 relative to the shorter peptides. Aβ42:40 and Aβ42:38 were observed to decrease significantly over the transfer series, whilst Aβ40:38 was not significantly affected (Figure 21, Table 10). Although AD and Non-AD CSF was affected similarly by the treatment, it is noteworthy that the use of Aβ42:40 and Aβ42:38 separated the two diagnostic categories better than the peptides considered individually.

The first transfer had a notably large effect on Aβ42 in this experiment, equivalent to 39% of the total Aβ42 lost overall (as compared to Aβ40 = 24.1% and Aβ38 = 8.8%). When transfer 0 was removed from the data series, the effect of transfer on Aβ42 and Aβ40 was diminished (18.8% and 16.3% respectively) whilst Aβ38 remained essentially the same (16.0%) but remained significant in all cases ($p = <0.001$). The effect on Aβ42:40 and Aβ42:38 was greatly diminished (2.9% and 3.4% respectively) but remained significant in all cases ($p = <0.001$). Data from samples measured in Transfer Study 1 (Figure 19) showed that adding Tween 20 to samples normalised the initial loss of Aβ42, and so similarly mitigated the transfer effect on the Aβ42:40 and Aβ42:38 ratios (3.6% and 4.0%) even with the data for transfer 0 included, although overall the effect remained significant ($p = <0.001$).

Figure 21: Effect of serial transfer on CSF Aβ ratios

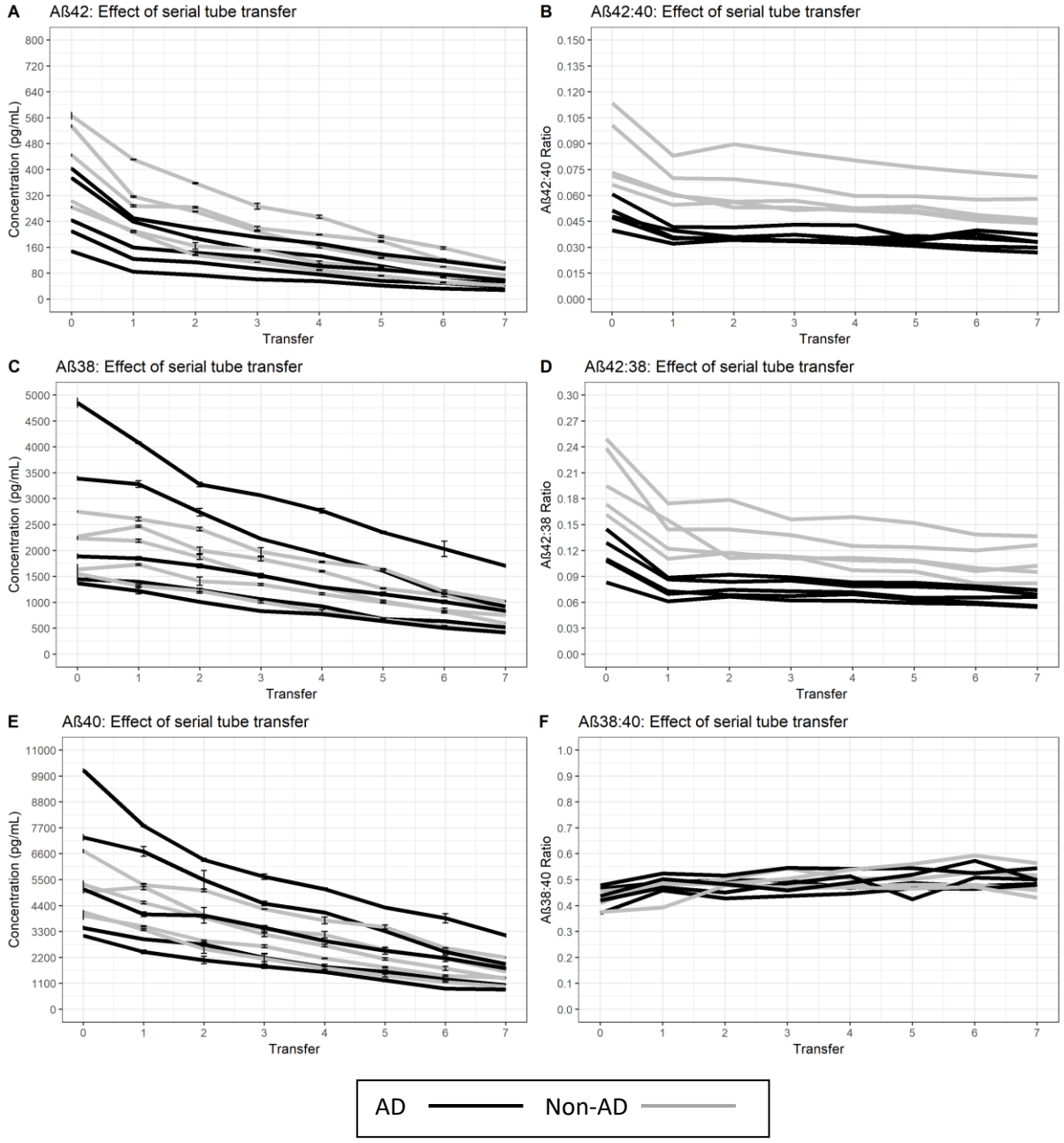

Figure 21: Effect of serial tube transfer on CSF Aβ. Results in CSF show the concentration of **A)** Aβ42, **C)** Aβ40, and **E)** Aβ38 decreased with consecutive transfer of sample to new storage tubes. **B)** Aβ42:40 and **D)** Aβ42:38 ratios were decreased, particularly at the first transfer. **F)** Aβ38:40 showed a significant tendency to increase with each transfer. Error bars represent standard deviation.

4.3.4 Aβ concentration decreases with tube transfer in culture media

To assess the effect of transfer on Aβ in cell media we assayed samples collected from mature cortical neurons from fAD and Non-AD cell lines. Aβ peptide concentrations in cell media were significantly affected by transfer of sample between tubes (Figure 22, Table 10). Concentrations of Aβ

were noticeably lower in tested cell media than in CSF, and the effect size observed reflects this. The effect of tube transfer on the ratio of Aβ peptides was comparable to that seen in CSF with a decrease of Aβ42 relative to shorter peptides (Figure 22, Table 10).

Figure 22: Effect of serial transfer on cell media Aβ ratios

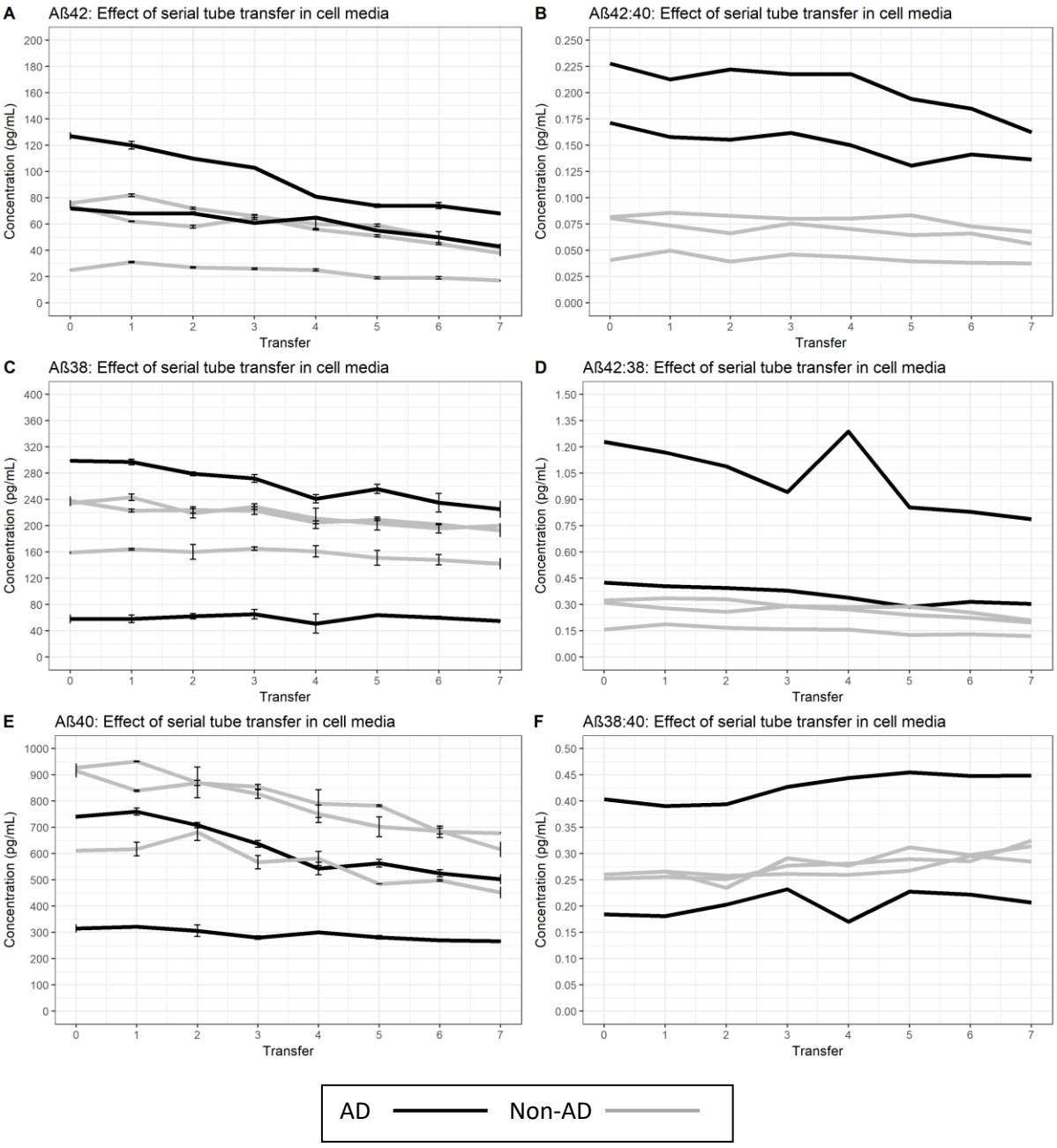

Figure 22: Effect of serial tube transfer on cell media Aβ. Results in CSF show the concentration of **A)** Aβ42, **C)** Aβ40, and **E)** Aβ38 decreased with consecutive transfer of sample to new storage tubes. **B)** Aβ42:40 and **D)** Aβ42:38 ratios were decreased, particularly at the first transfer. **F)** Aβ38:40 showed a significant tendency to increase with each transfer. Error bars represent standard deviation.

Table 10: Summary of Transfer Study 2 results

Biofluid	Peptide	% Change per unit	p	95% confidence interval	
CSF	Aβ42	20.0%	<0.001	-0.234	-0.212
CSF	Aβ40	16.0%	<0.001	-0.181	-0.167
CSF	Aβ38	14.5%	<0.001	-0.166	-0.148
CSF	Aβ42:40	4.8%	<0.001	-0.057	-0.041
CSF	Aβ42:38	6.4%	<0.001	-0.077	-0.055
CSF	Aβ38:40	1.7%	<0.001	0.011	0.023
CM	Aβ42	7.8%	<0.001	6.993	9.219
CM	Aβ40	4.8%	<0.001	4.103	5.711
CM	Aβ38	2.4%	<0.001	1.676	3.205
CM	Aβ42:40	3.1%	<0.001	2.315	4.082
CM	Aβ42:38	5.5%	<0.001	4.532	6.799
CM	Aβ38:40	2.4%	<0.001	1.599	3.334

Table 10: Summarising the results of Transfer Study 2 and the effect of serial tube transfer on Aβ concentration and ratios in CSF and cell media (CM). Data from AD and non-AD samples were combined. Change per unit is the exponentiated coefficient of the mixed model linear regression analysis. A unit is one transfer.

4.3.5 Aβ concentration decreases with tube transfer in culture media

To test whether exaggerated Aβ peptide loss at first transfer may have been due to adsorption to the pipette tip, we conducted a pilot experiment to measure Aβ42/40/38 peptide concentration change in response to a varying number of aspirations using the same tip. The number of fluid pumps had no effect on Aβ peptide concentration in either CSF or CM, with the exception of small volume (<250uL) CSF samples treated with 15 pumps or more, in which Aβ42 concentration showed a tendency for decrease (Figure 23). Relevant to the experiments conducted for this thesis, paired, two-tailed t-test showed no significant difference between 0 pumps and 5 pumps, although it was observed that measurement variability was greater in the 0 pump group (Figure 23). The initial exaggerated decrease in Aβ42 observed in CSF cannot therefore be attributed to adsorption to the pipette tip.

Figure 23: Effect of pipette mixing on CSF and cell media Aβ concentrations

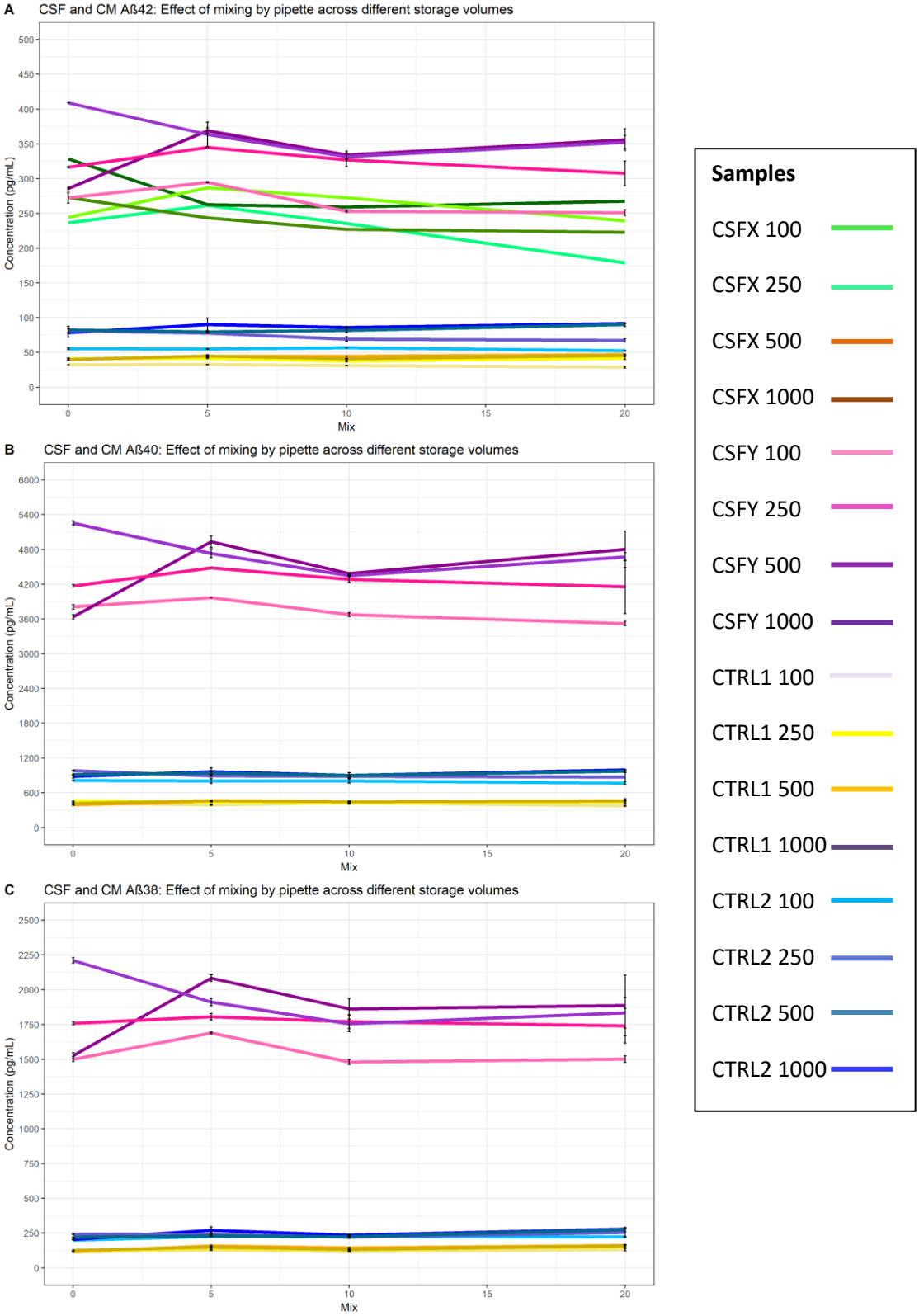

Figure 23: Effect of mixing by pipette in CSF and cell media across different storage volumes. Results show the concentration of **A)** Aβ42, **B)** Aβ40, **C)** Aβ38 were not significantly affected by different levels of exposure to the pipette tip. Sample CSFX Aβ42 was measured by MSD singleplex assay. Error bars represent standard deviation.

4.4 Discussion

In summary, we demonstrated that the concentration of Aβ peptides could be profoundly affected simply by transferring sample to a new storage aliquot, whilst T-tau concentration was more stable. Inclusion of 0.05% Tween 20 greatly mitigated, but did not entirely prevent, this effect in CSF. A survey of four academic AD diagnostic reference centres found that 0–2 transfers are typical in the course of CSF collection and processing, although more can occur depending on intended use *(Willemse et al., 2017)*. As such, the effect on Aβ42 after one transfer is of particular concern.

The dramatic decrease in Aβ42 observed following the first transfer of CSF in some of the samples testing raises the question of whether sub-populations of Aβ42, for example with different N-terminal truncations or post-translational modifications, could adsorb at different rates. The more linear loss of Aβ42 following initial transfers might suggest that certain isoforms could be rapidly depleted upon exposure to new surfaces of different material compositions. This is speculation, but it is interesting that Vanderstichele et al. also found a large decrease in Aβ42 (42.5%) after transfer of sample from a low bind tube to a PP tube *(Vanderstichele et al., 2016)*. If this were to be the case, it would mean that potentially important, disease-relevant Aβ species may be underrepresented in clinical or research samples, and be additionally vulnerable to pre-analytical protocol variation.

Interestingly, Aβ42 concentration decreased more relative to Aβ40 and Aβ38, supporting the findings of the volume study. This meant that the ratios of Aβ42:40 and Aβ42:38 were also altered by serial transfer of sample between fresh polypropylene surfaces, although the effect size was noticeably smaller compared to Aβ42 concentration considered alone. The use of Aβ ratios may also therefore be a strategy for mitigating measurement vulnerability to pre-analytical confounding factors.

In follow up to these data, relative to initial concentration Vanderstichele *et al.* observed significantly lower concentrations of Aβ42 (11.0%), Aβ40 (7.3%), and Aβ38 (2.7%) in CSF collected into PP tubes compared to low binding tubes *(Vanderstichele et al., 2016)*. Additionally, they report a concentration decrease of Aβ42 (42.5%), Aβ40 (27.8%), and Aβ38 (16.7%) after one transfer between PP tubes (Sarstedt 62.554.502, and either 72.706 or 72.730.006). In comparison, at the first transfer our results showed a similar decrease of Aβ42 (39.0%) and Aβ40 (24.1%), but smaller decrease of Aβ38 (8.8%). It is worth noting that low bind tubes were found to negate the effect of transfer between tubes *(Vanderstichele et al., 2016)*. Pica-Mendez *et al.* also noted a significant decrease in Aβ42 concentration relative to control when CSF was transferred to a number of different polypropylene tubes, notably 37.9% in the tube likely to be closest in material and dimensions to the

one we used (Sarstedt 1.25mL Cat. 72.609.001) *(Pica-Mendez et al., 2010)*. They also described the fact that 0.05% Tween 20 nullified this effect, but did not present data *(Pica-Mendez et al., 2010)*. However, a subsequent report by Willemse et al. reported a 5% decrease (up to 10% in small volume samples) in Aβ42 and Aβ40 per transfer over four transfers between tubes, and that Aβ42:40 therefore remained constant over transfer treatment *(Willemse et al., 2017)*. An effect size of 5-10% is at odds with the Aβ42 (20%) and Aβ40 (16%) decrease per transfer that we observed over equivalent transfers. The tubes used by Willemse et al. (Sarstedt cat. 72.694.007) *(Willemse et al., 2017)* are identical to the tubes we studied (Sarstedt cat. 72.694.406), except that cat. 72.694.406 is certified DNA and RNase free. Other differences in protocol or laboratory environment may also be involved, and a degree of inter-laboratory variation should be taken into consideration until these factors are identified.

Repeated aspirations and ejections from the same tip did not significantly alter Aβ concentration in either CSF or CM. Indeed even when the tip was not pre-wetted no effect was seen, contrary to what others have described *(Willemse et al., 2017)*. Therefore, this cannot account for the initial exaggerated decrease we observed at the first transfer step. Given this, we hypothesise the existence of a sub-population of Aβ42 that is more readily adsorbed to PP and rapidly depleted from solution. This interpretation would be consistent with the data reported by Vanderstichele et al. *(Vanderstichele et al., 2016)*, but not Willemse et al. *(Willemse et al., 2017)*. A similar, adsorption attributed, initial effect on fluorescein-labelled bovine serum albumin (BSA), also found in the B27 fraction of the CM used in our study, has been reported *(Natascha Weiß, 2010)*. It is possible that competition for surface binding sites by this and other proteins of the CM matrix might explain why the first transfer step effect was not observed in these samples, although we did not examine fluid protein content as a variable.

In regard to effect of tube transfer on T-tau, the experiments reported in this chapter show that this biomarker is generally unaffected by this form of treatment. This is in line with other studies that have shown T-tau to be unaffected by transfer between different tube materials *(Perret-Liaudet et al., 2012a; Willemse et al., 2017)*. However, one high concentration sample showed a tendency toward meaningful decrease, and a similar finding in the volume study (Section 3.3.3) may be recalled. Vanderstichele et al. recently reported a significant decrease in T-tau following transfer to PP storage tubes *(Vanderstichele et al., 2016)*, and it could be that there are sample specific differences in T-tau isoform composition that are more or less vulnerable to surface adsorption.

One limitation of this study was the low number of samples used (two CSF pools), and although other groups have replicated the broad findings, nuances of differential Aβ adsorption remain to be fully validated. A major limitation to this study was the fact that Aβ and tau concentrations were not measured in all storage tubes used during processing, prior to the final aliquot. If, as we speculate, certain Aβ forms are lost to the tube surface preferentially then they may have begun to be depleted prior to the point of measurement in this experiment format.

The findings reported in this chapter have potentially important ramifications for the diagnostic process of AD where low concentrations of Aβ42 and high tau are a key positive marker, and for research practices of sharing samples between groups. Aβ42 considered on its own, or in ratio with other AD biomarkers, is vulnerable to giving false negative and positive results in polypropylene tubes if surface exposure is not standardised. This effect can be mitigated by the addition of a final concentration of 0.05% Tween 20 early in the sample aliquoting process.

4.5 Chapter summary

The findings reported in this chapter further demonstrate the importance of surface exposure as a confounding factor for biomarker research. Aβ42 considered on its own, or in ratio with other AD biomarkers such as T-tau and Aβ40 is increasingly vulnerable to giving false positive results for AD with each iteration of contact with a new storage vessel, even if that vessel is made of polypropylene. The effect on ratios of Aβ peptides was particularly interesting. On the one hand the effect of transferring sample between tubes was lessened when ratios were used, and so treatment of data in this way may be more reliable than measurements of individual peptides. However, the effect was not completely mitigated and data indicate that Aβ42 is a peptide particularly vulnerable to surface adsorption, which could potentially mislead results if surface exposure is not standardised. Adding 0.05% Tween 20 to the sample early in the sample aliquoting process, proved effective for mitigating the effect of serial sample transfers.

4.5.1 Publications arising from this work

Toombs J, Paterson RW, Schott JM, Zetterberg H. Amyloid-beta 42 adsorption following serial tube transfer. Alzheimers Res Ther. 2014 Jan 28;6(1):5. doi: 10.1186/alzrt236. eCollection 2014.

Toombs J, Foiani MS, Wellington H, Paterson RW, Arber C, Heslegrave A, Lunn MP, Schott JM, Wray S, Zetterberg H.Amyloid β peptides are differentially vulnerable to preanalytical surface exposure, an

effect incompletely mitigated by the use of ratios. Alzheimers Dement (Amst). 2018 Mar 22;10:311-321

5 Tween 20 and measurement variance

5.1 Introduction

Measurement variability within and between sites is a significant issue in the AD field and scientific disciplines more broadly. Over the past decade increasing attention has been devoted to understanding the extent and source of measurement variation in assays for AD biomarkers. The Alzheimer's Association QC program for AD CSF biomarkers is the largest ongoing international project, tracking inter- and intra-site variation in a number of the most popular biomarker assays for clinical diagnostics and research at more than 80 sites *(Mattsson et al., 2011, 2013)*. Results showed modest and gradual improvements between 2011 and 2013 (despite doubling the number of participating sites in this period) with coefficients of variance between sites shifting from 13%-36% *(Mattsson et al., 2011)* to 20%-30% *(Mattsson et al., 2013)*, and intra-site variability ranging from 9-19% *(Mattsson et al., 2013)*. Aβ42, T-tau and P-tau have been the most rigorously tested biomarkers, and results tend to fall within a roughly similar range albeit with a tendency for slightly lower variation in tau *(Carrillo et al., 2013)*. Reports from other groups, which include a mix of different centres and assay platforms, show broadly similar findings with inter-site variability falling mostly within the 20%-40% range *(del Campo et al., 2012; Carrillo et al., 2013; Lewczuk et al., 2006b; Mattsson et al., 2012b; Verwey et al., 2009)*, and although some claim much more impressive capabilities *(Bittner et al., 2016)* these are not common or well replicated. Intra-assay variability is typically much lower (in the range of 3%-15%) *(Bittner et al., 2016; Lewczuk et al., 2006b; Mattsson et al., 2010)*, although it is not always clear whether presented data represent assays conducted by multiple or the same operators. It is likely that the latter accounts for the lower end of the variance estimate.

Simplistically, lowering inter-site variation is important for the establishment of standard diagnostic AD biomarker concentration reference ranges (cut-offs) and the development of 'gold standard' reference materials, which would enable better translation of results between sites, trials, and increase research power by pooling compatible data. Lowering intra-assay variation is important for improving diagnostic confidence in clinics linked to specific centres. Overall, between laboratory concordance for sample diagnosis is respectable, approximating 90% in the Alzheimer's Association

QC program for the majority of the samples assessed *(Mattsson et al., 2013)*, but can still lead to patient misclassification and influence clinical decision-making or clinical trial *(Garciá Barrado et al., 2015; Mo et al., 2017)*. The current situation is insufficient to allow global biomarker cut-offs for AD and other diseases to be assigned. Issues with laboratory procedure standardisation and assay performance have been the most frequently suggested sources of this variation.

The experiments reported in Chapters 3 and 4 showed that the addition of 0.05% Tween 20 could be a potential strategy to mitigate pre-analytical confounding factors in CSF. Next we questioned whether measurement variability of CSF Aβ and tau treated in a standardised manner could be improved by the addition of Tween 20. We hypothesised that the addition of 0.05% Tween 20 to CSF would decrease ambient measurement variance in samples stored and handled in the same standardised conditions.

5.1.1 Contributions

The author designed, and conducted the experiment described in this chapter, conducted the assays, conducted the statistical analyses with advice from JM. Nicholas and A. Petzold, and wrote the scientific reports.

Study conception: H. Zetterberg, JM. Schott.
Sample collection: H. Zetterberg.
Experiment design: The author.
Experiment: The author.
Analysis: The author, JM. Nicholas, A. Petzold.
Scientific report: The author, RW. Paterson, JM. Nicholas, A. Petzold, JM. Schott, H. Zetterberg.

5.2 Materials and methods

5.2.1 Samples

CSF was collected as described in Methods Section 2.3. CSF samples were categorised as either pooled from multiple individuals (n=3) or from single subjects (n=3).

5.2.2 Experimental methods

Figure 24: Sample variation experiment design

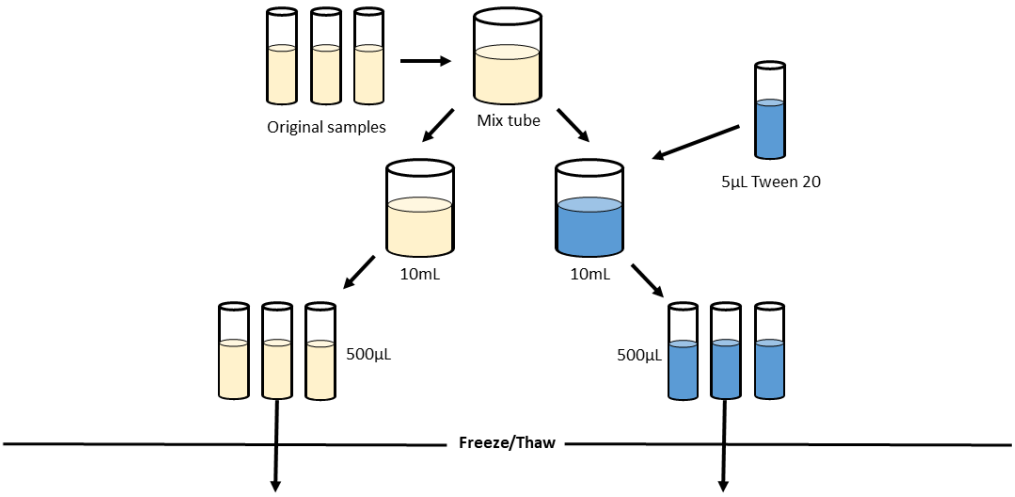

Figure 24: Diagram showing preparation of samples for Tween variation experiments.

As shown in Figure 24, centrifuged CSF samples were transferred at a volume of 11mL into a 100mL Sarstedt PP beaker (cat. 75.1354.001) and mixed by magnetic stirrer for 30 minutes, forming the pooled group. CSF from individual subjects was treated in the same way except that it was not pooled with other samples. Each sample was then divided in two equal volumes (50mL Greiner tubes cat. T2068-450EA), and Tween 20 (final concentration 0.05%) was added to one. Tween and No Tween samples were then aliquoted into storage tubes (Sarstedt 2mL PP storage tubes cat. 72.694.406) at 500µL. Sample aliquots were frozen at -80°C. Prior to assay, aliquots were thawed for one hour at room temperature (21°C).

Samples were assayed for Aβ38/40/42 (Section 2.2.2), and T-tau by MSD by ECL immunoassay (Section 2.2.3), P-tau$_{181}$ was measured by INNOTEST ELISA (Section 2.1.3). All assays were conducted by the same operator. To assess intra-plate variability, each sample were assayed in three duplicates. To assess inter-plate variability, the assay was repeated four times. Assays were conducted under double blind conditions.

5.2.3 Statistical analysis

Intra- and inter-assay CV) was calculated according to ISO 5725-2 standards *(British Standards Institution, 1994)*. Results are shown in Table 11. Differences between Tween and No Tween groups

were assessed by paired two-way t-test. Differences between pooled and individual CSF were assessed by unpaired two-way t-test. To investigate the contribution of covariates, mixed model analysis of data was conducted in R. To control for increasing variance as concentration increased, sample concentration was transformed by ln.

5.3 Results

5.3.1 Tween 20 decreases variability in Aβ42 measurement

For measurements of Aβ42 in the same sample across different assays, %CVs of 'Tween' samples were significantly lower than in 'No Tween' samples ($p = 0.04$) (Table 11). Further exploration with the use of linear mixed model analysis revealed that this result was driven by individual subject samples, whilst variance in pooled samples also decreased but did not reach significance (Table 12). No significant differences between Tween and No Tween samples were found in Aβ40, Aβ38, T-tau or P-tau. However, the average degree of variability between measurements for all samples and for all biomarkers, whether intra- or inter-assay, was $< 10\%$, meaning that concentration measurements can be considered highly repeatable regardless of Tween 20 status.

Table 11: AD biomarker variation: t-test analysis

Sample	Aβ38		Aβ40		Aβ42		T-tau		P-tau	
	Intra (%CV)	Inter (%CV)	Inter (%CV)	Intra (%CV)	Intra (%CV)	Inter (%CV)	Intra (%CV)	Inter (%CV)	Intra (%CV)	Inter (%CV)
733	2.0	7.3	3.5	4.7	2.2	**6.2**	6.4	8.8	4.4	9.7
Tween 733	2.5	5.7	3.7	5.4	2.1	**2.7**	4.0	7.8	1.9	7.7
724	3.0	5.4	3.5	3.5	1.9	**3.5**	5.4	8.2	1.7	5.5
Tween 724	2.4	5.6	3.8	4.3	2.4	**2.9**	5.1	7.9	2.6	7.9
806	2.0	5.9	2.8	5.8	2.5	**8.2**	6.1	6.8	2.0	5.4
Tween 806	2.7	5.3	3.5	3.8	2.5	**3.5**	2.5	9.2	1.4	4.0
Pool1	3.6	5.6	3.6	4.3	2.9	**4.4**	3.1	6.3	1.2	6.4
Tween Pool1	2.0	5.3	4.1	4.6	2.2	**3.8**	2.7	5.3	2.2	5.4
Pool 2	3.2	5.5	2.1	4.7	2.1	**6.4**	3.9	8.9	2.4	5.1
Tween Pool 2	2.6	4.9	3.7	4.8	2.5	**3.3**	12.7	12.7	2.2	5.5
Pool 3	1.9	5.3	2.8	3.9	2.0	**4.7**	2.9	6.5	1.6	4.3
Tween Pool 3	1.9	6.4	2.4	4.6	1.7	**4.6**	4.0	8.4	1.8	5.0
Average No Tween	2.62	5.83	3.05	4.48	2.27	**5.57**	4.63	7.58	2.22	6.07
Average Tween	2.35	5.53	3.53	4.58	2.23	**4.47**	5.17	8.55	2.02	5.92
t-test	0.476	0.453	0.134	0.827	0.862	**0.043**	0.778	0.293	0.719	0.830

Table 11: The T-test analysis shows the mean intra- and inter-assay %CV by sample for each biomarker. This mean was calculated from 12 %CVs derived from each sample duplicate pair (n = 3 within each plate) across all plates (n = 4). A two-tailed, paired t-test compared Tween and No Tween sample versions for each biomarker. Inter-plate measurements of Aβ42 showed significant difference dependent on Tween status (p=0.04) with Tween samples having lower %CVs.

Table 12: AD biomarker variation: mixed model analysis

Sample	Aβ38		Aβ40		Aβ42		T-tau		P-tau	
	Individual	Pool	Individual	Pool	Individual	Pool	Individual	Pool	Individual	Pool
Residual variance of Tween samples relative to No Tween	-7%	+4%	0.3%	+19%	**-45%**	-15%	+14%	+11%	-6%	-10%
p	0.698	0.820	0.986	0.318	**0.001**	0.364	0.461	0.591	0.700	0.558

Table 12: Results of a linear mixed model analysis showing the effect of Tween 20 on measurement variation relative to samples without Tween for individual or pooled subject CSF for each biomarker. Results were calculated using a linear mixed effects model on data transformed by ln. Addition of Tween 20 to samples tended to lower the residual variance of Aβ42. However, this was only significant in individual subject CSF.

5.4 Discussion

Tween 20 treatment lowered the variability and detectable quantities of Aβ42, but did not have a significant impact on Aβ40, Aβ38, T-tau or P-tau$_{181}$. Analysis also highlighted that Tween 20 in individual CSF samples had a stronger stabilising effect on Aβ42 concentration than did pooled CSF. The reason for this is unclear, and experiments previously discussed in Chapters 3 and 4 did not find differences between pooled and individual samples. However, the result suggests the use of Tween 20 as an additive is relevant for clinically relevant samples. Despite this, measurement variation was low in all assays conducted and any beneficial effect of adding Tween 20 is unlikely to be meaningful over standardising storage and handling practice. Ultimately, there may not be sufficient incentive to treat CSF with Tween 20.

Detergents, such as Tween 20, are known to affect protein solubility and interaction with potential implications for matrix composition, biomarker ratios, or antibody activity. Subsequent work from other groups has shown that 0.05% Triton-X 100 or Tween-20 does not affect sensitivity, specificity, diagnostic accuracy *(Berge et al., 2015)* or intra-assay variability for CSF Aβ42 concentration *(Vanderstichele et al., 2016)*. Furthermore it was found that prewashing tubes with detergent-containing buffers was also effective in reducing Aβ42 adsorption *(Vanderstichele et al., 2016)*. However, the use of detergent even at low concentrations is a significant issue in mass spectrometry analysis, where detergent molecules coat columns and tubing and contaminate sample signal. Similar artefacts have been noted when using other sample additives, such as protease inhibitors *(Simonsen et al., 2013)*. Therefore samples treated with Tween 20 early in the pre-aliquoting stages of sample processing, where it is likely to be most effective, would not be appropriate for such a platform. This, on top of the added cost in resources and procedural steps during CSF collection, as well as the equivalent benefits provided by low protein binding tubes *(Vanderstichele et al., 2017)*, weigh against the implementation of Tween 20 as a standardised additive.

This study was limited by the low number of samples assessed, and the fact that results represent a single-site and single-operator. Whether Tween 20 would have greater effect on the stabilisation of biomarker measurement between sites remains unresolved. However, due to suitably low variability being achieved through standardised treatment of samples alone, concerns over implementation, and the fact that low bind tubes have been shown to have equivalent adsorption mitigating properties *(Vanderstichele et al., 2016)*, standardised use of Tween 20 as an additive would not seem worthwhile.

5.5 Chapter summary

In summary, it was found that although adding 0.05% Tween 20 to CSF samples did decrease variability in Aβ42 measurements, the effect was not impressive enough to recommend its use over general standardisation of sample handling protocol.

5.5.1 Publications arising from this work

Toombs J, Paterson RW, Nicholas JM, Petzold A, Schott JM, Zetterberg H. The impact of Tween 20 on repeatability of amyloid beta and tau measurements in cerebrospinal fluid. Clinical chemistry and laboratory medicine. 2015;53(12):e329-32. Epub 2015/06/24

6 Confounding Factor: Manometer

6.1 Introduction

Having identified two relevant confounding aspects to Aβ measurement in CSF and cell media, and determined that the use of Tween 20 as an additive was unlikely to be practical solution, we moved to looking at Aβ adsorption at an earlier stage in the pre-analytical process and one more directly related to clinical practice.

CSF is most commonly obtained by lumbar puncture (LP). This involves inserting a spinal needle between the spinous processes of the lumbar vertebrae (typically L3/L4 or L4/L5) *(Hansson et al., 2018)*, puncturing the dura mater, and entering the subarachnoid space. CSF then flows passively into a collection tube due to gravity and pressure difference. During the collection of CSF, a manometer may be used to measure CSF opening pressure (the initial pressure of the CSF in the subarachnoid space), when the patient is in the lateral decubitus position. High (>25 cm H_2O) and low CSF opening pressures (<6cm H_2O) *(Lee and Lueck, 2014)* are seen in a range of different non-neurodegenerative conditions, and thus may inform differential diagnosis in the correct clinical context.

Though less common in dementia clinic, CSF from non-neurodegenerative individuals is valuable and increasingly sample cohorts from these individuals are shared in dementia research collaborations (e.g.*(Cunningham et al., 2018)*). Additionally, it would not be unreasonable to employ manometers in a clinical trial setting where any confounding effect could potentially bias results to great consequence. Prior to our investigation, the effect of manometers on CSF biomarker concentrations had not been rigorously examined. Bjerke et al. had mentioned that two different catheters had no significant effect on Aβ42 adsorption, but did not present any data or details on the experiment *(Bjerke et al., 2010)*. Another study had noticed a significant increase in Aβ42 concentration over 36 hours with an indwelling catheter, listing the catheter as a potential, though unlikely, cause *(Bateman et al., 2007)*.

To test the hypothesis that contact with a manometer would decrease Aβ concentration we conducted a laboratory simulation in which quantities of pooled CSF were pipetted through a manometer or straight into a collection tube.

6.1.1 Contributions

The author designed, and conducted the experiment described in this chapter, conducted the assays, conducted the statistical analyses, and wrote the scientific reports. MS. Foiani assisted with the conduct of the experiment.

Study conception: H. Zetterberg, K. Blennow, MP. Lunn, NC. Fox, JM. Schott.
Sample collection: H. Zetterberg.
Experiment design: The author.
Experiment: The author, MS. Foiani.
Analysis: The author, JM. Nicholas, A. Petzold.
Scientific report: The author, MS. Foiani, RW. Paterson, A. Heslegrave, S. Wray, JM. Schott, NC. Fox, MP. Lunn, K. Blennow, H. Zetterberg.

6.2 Materials and methods

6.2.1 Samples

CSF was collected as described in Section 2.3. Pooled CSF samples (n=20) were divided into two 2mL aliquots in 25mL polypropylene (PP) collection tubes (Sarstedt, Nümbrecht, Germany, cat. 63.9922.254), designated 'Manometer CSF' and 'No Manometer CSF' depending on whether or not CSF was passed through a manometer.

6.2.2 Experiment method

To conduct the experiment in controlled conditions, a lumbar puncture was simulated in the laboratory (Figure 25). Centrifuged CSF samples were thawed at room temperature for one hour, then pooled together into a 50mL Greiner tube (cat. T2068-450EA) and mixed on a roller for five minutes. Two equal volume aliquots were then created in empty Sarstedt PP 2mL storage tubes (cat. 72.694.406). A volume of 1.5mL CSF (Manometer CSF) was manually ejected into a manometer made of styrene-butadiene copolymer (K-resin®) (Rocket Spinal manometer, Rocket Medical PLC, Washington, UK, order code:R55990, NHS SC Code: FTP002), using a 5mL pipette (Eppendorf PP 1-5mL graduated pipette tips; (Starlab, Milton Keynes, UK, cat. I1053-000). Styrene-butadiene copolymer (K-resin®) has a computed formal charge of 0 and a molecular weight of 158.23956 g/mol. This brand of manometer is stock listed by the British National Health Service and used by specialist clinics that perform lumbar puncture in the UK. After 60 seconds of CSF injection, the

manometer valve was released and the CSF allowed to drain into a 25mL collection tube (Sarstedt cat. 63.9922.254). The approximate inflow rate of CSF through the manometer during the experiment was ~0.04 cm^3/s (diameter = 4mm, velocity = 21cm/minute), similar to what would be expected during LP with an opening pressure of 21cm H_2O. Alternatively, 1.5mL CSF from the No Manometer CSF tube was ejected by pipette directly into a 25mL over the course of 60 seconds. Aliquots of 0.5mL Manometer and No Manometer CSF were created in 2mL tubes (Sarstedt cat. 72.694.406) and stored at -80°C. Prior to assay, samples were thawed for one hour at room temperature (21°C). The samples were assayed for Aβ38/40/42 by MSD triplex ECL immunoassay (Section 2.2.2).

Figure 25: Manometer study experiment design

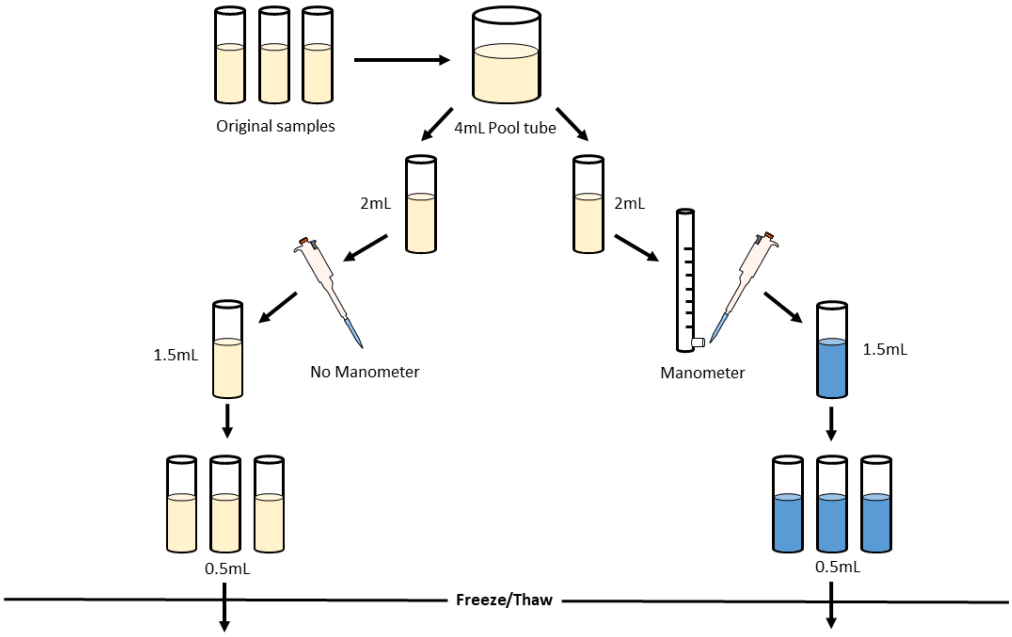

Figure 25: Diagram showing the manometer experiment process.

6.2.3 Statistical analysis

Data for each Aβ peptide was found to be normally distributed (D'Agostino-Pearson test, Shapiro-Wilk test). Manometer and No Manometer results were compared by two tailed, paired t-test in Microsoft Excel 2010.

6.2.4 Assay variation

Coefficient of intra-assay variability was <3% for all peptides. Inter-assay variability was Aβx-42 = 6.7%, Aβx-40 = 9.5%, Aβx-38 = 3.8%), calculated from the concentrations of an internal control CSF sample. Intra- and inter-assay CV was calculated according to ISO 5725-2 standards *(British Standards Institution, 1994)*.

6.3 Results

6.3.1 Use of a manometer reduces measurable Aβ concentration

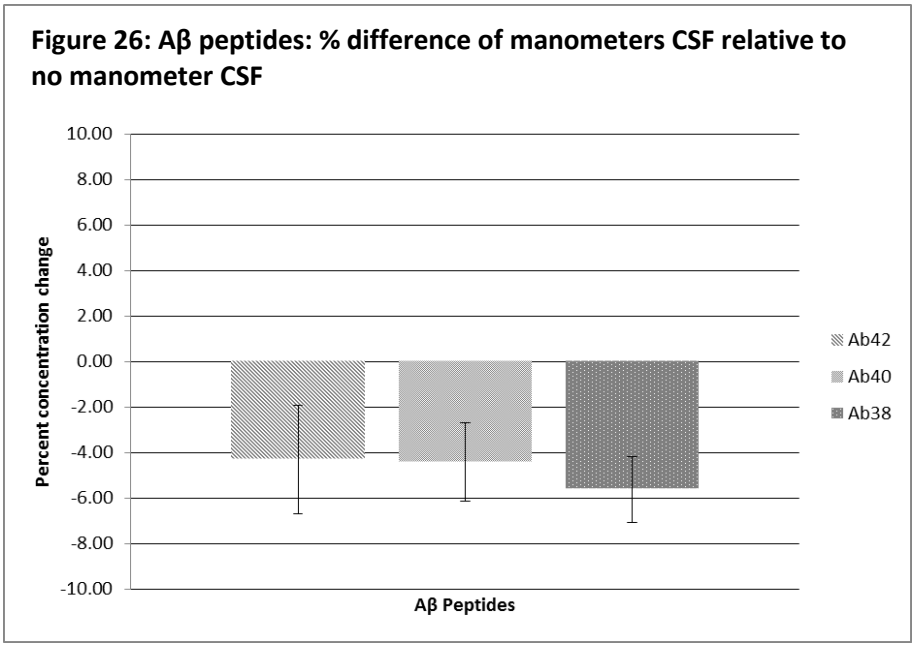

Figure 26: Showing the percent difference of Aβ peptide concentration in CSF pipetted through a manometer relative to the same CSF merely pipetted into a collection tube . All Aβ peptide concentrations tested decreased with manometer use. Error bars represent standard error of the mean.

Relative to No Manometer CSF, Manometer CSF Aβ concentration was decreased by Aβ42: 4.3% (± 2.4 standard error of the mean (SE)), Aβ40: 4.4% (± 1.7 SE), and Aβ38: 5.6% (± 1.5 SE) (Figure 26). A paired t-test showed that this was statistically significant in all peptides - Aβ42: p = 0.047, Aβ40: p = 0.026, Aβ38: p = 0.002. Comparison of the ratios Aβ42:40, Aβ42:38, and Aβ40:38 revealed no significant differences between Manometer CSF and No Manometer CSF samples (Aβ42:40: p = 0.626, Aβ42:38: p = 0.896, and Aβ40:38: p = 0.158.

6.4 Discussion

During a routine LP procedure, a manometer may be employed to measure the opening pressure of CSF. Our findings suggest a decrease of 4–6% for A38/40/42 after CSF passes through a Rocket Spinal Manometer, made of styrene-butadiene copolymer (K-resin®). To our knowledge this material has not previously been studied in terms of its interaction with Aβ peptides. This small concentration change would seem unlikely, by itself, to greatly influence diagnosis of AD in individuals attending clinic. However, the effect may be more relevant to clinical trials for AD therapeutics, where altered Aβ concentration is often a secondary endpoint, as use of large datasets does not compensate for such forms of systematic error *(Bohm and Zech, 2010)*. Sampling procedures in cross-sectional studies where the use of manometers has not been standardized may result in biased biomarker profiles between cohorts. For example, cognitively normal control samples continue to be challenging to acquire in large numbers, and AD focused collaborations may share sample cohorts without shared collection protocols. Furthermore, inconsistent use of manometers in longitudinal studies could raise levels of residual variation (statistical 'noise') in intra-individual biomarker data, which may obscure a real change, e.g., in a clinical trial; or create a bias if baseline CSF were to be taken without a manometer, but subsequent follow-ups used one. In either scenario, lack of standardization in manometer use could mislead, or obscure, therapeutic effect in the region of 5–10% difference between comparators. These results are likely to be relevant to catheters, which are used in time-course studies of CSF Aβ concentration in trials assessing physiological variability or target engagement *(Bateman et al., 2007; Den Daas et al., 2013; Lucey et al., 2015; Ooms et al., 2014; Slats et al., 2012)*, though material and dimensions may alter the degree of Aβ concentration change. Finally, we found that the ratio of Aβ peptides was unaffected by manometer treatment, due to similar degree of treatment-dependent protein loss between each peptide measured. This provides a further reason to consider the use of Aβ ratios as diagnostic biomarkers for AD *(Blennow et al., 2012; Janelidze et al., 2016; Struyfs et al., 2015; Terrill-Usery et al., 2016; Vanderstichele et al., 2016)*. Our data supports the implication that an Aβ ratio may be useful in routine clinical diagnosis from the perspective of controlling for pre-analytical variation. The results of Chapters 3 and 4 also bear this out, albeit with the caveat that different materials, such as polypropylene, may have subtle effects on Aβ ratios.

The experiment was a simulation of LP procedure conducted in the laboratory. An advantage of this was the ability to closely control the conditions of the experiment, for example removing the potential bias in CSF gradients from sequential tapping CSF with and without a manometer, as well as standardising timing and volume. However, this approach also had limitations in fully capturing

the circumstances of a real LP procedure. The dimensions and material of a pipette tip (polypropylene) differ from those of a lumbar needle (often stainless steel with a hub that can be made of metal or polypropylene). Additionally, CSF was stored at 21°C prior to contact with the manometer, while CSF collected during LP would be at approximately 37°C, pH 7.33, decreasing and increasing rapidly respectively, once outside the body *(Muizelaar et al., 1991)*. Finally, the sample size of the study was small (n = 20), and conclusions drawn from it would benefit from independent replication.

6.5 Chapter summary

In summary, this study revealed a small, significant, decrease in Aβ38/40/42 when CSF was exposed to a spinal manometer. Ratios of Aβ peptides were unaffected. Ongoing and future trials measuring CSF opening pressure would be well served to consider the implications of this in study design.

6.5.1 Publications arising from this work

Toombs J, Foiani M, Paterson RW, Lunn M, Heslegrave A, Wray S, Schott JM, Fox NC, Lunn MP, Blennow K, Zetterberg H. Effect of Spinal Manometers on Cerebrospinal Fluid Amyloid-β concentration J Alzheimers Dis. 2017;56(3):885-891. doi: 10.3233/JAD-161126.

7 iPSC-neurons as a model to understand amyloid beta production in fAD

7.1 Introduction

The first phase of work concerned improvement of the reliability of Aβ as a biomarker for AD by identification of pre-analytical confounding factors in CSF and cell culture media, and adapting strategies to mitigate them. From there, the scope of work evolved into the examination of Aβ peptide production as part of a validation of an *in vitro* model of human fAD. Better understanding of Aβ biology will improve interpretation of it as a biomarker for AD.

The relative merits of AD model technologies have been discussed in Section 1.5.5. A robust protocol for *in vitro* culture of functional glutamatergic cortical neurons has been developed by Shi *et al. (Shi et al., 2012b, 2012a)*. There are four steps to the process: 1) the directed differentiation of human iPSCs to cortical stem and progenitor cells, including neuroepithelial ventricular zone cells, basal progenitor cells and outer radial glial. 2) a period of cortical neurogenesis and synaptogenesis consistent with a human *in-utero* time-frame. 3) neuronal terminal differentiation representing the six cortical layers, and astrocyte genesis. 4) Establishment of electrophysiological networks.

The Shi protocol is one of the most widely used methods for generating glutamatergic cortical neurons in adherent culture *(Begum et al., 2015)*, and makes use of SMAD inhibition. SMAD describes a family of signal transducing proteins for transforming growth factor beta (TGF-B) receptors, and is a portmanteau of mothers against decapentaplegic (MAD), a protein of the SMAD family originally identified in *Drosophila*, and small body size (SMA), a protein of the SMAD family originally identified in *C. elegans*. Neurons derived from this protocol accurately recapitulate the single-cell transcriptomic signature of primary human fetal cortical neurons, and express many genes unambiguously associated with neuronal and synaptic function *(Handel et al., 2016; Patani et al., 2012)*. Neuro-differentiation and development occur within a time frame analogous to *in vivo*, this has been demonstrated in both 2D and 3D culture, though with the implication that 3D cultures may mature slightly faster than 2D *(Odawara et al., 2016; Paşca et al., 2015)*. Cortical neurons

differentiated according to this protocol eventually express the six tau isoforms present in human adult brain (after 365 days in culture) following an *in vivo*-relevant timescale *(Sposito et al., 2015)*, with accelerated maturation in MAPT mutation lines *(Iovino et al., 2015)*. One particularly interesting study compared transcribed protein-coding genes, long intergenic non-coding RNAs, and CpG methylation between iPSC-derived cortical neurons and donor-matched post mortem brain tissue (a cognitively normal individual with a Braak stage of 1 and a CERAD Neuritic Plaque score of 0). Results showed similarity between the two increased with extended time in *in vitro* culture *(Hjelm et al., 2013)*.

The electrophysiological properties of cortical neurons in adherent culture derived from this method have been well described. Whole cell current-clamp *(Gunhanlar et al., 2018; Shi et al., 2012a)* voltage clamp *(Bergstrom et al., 2016)*, and single cell patch clamp *(Wu et al., 2016)* have demonstrated robust electrical activity. Populations of deep layer neurons have been shown to fire single action potential bursts in response to current injection at day 28 *(Shi et al., 2012a)*, as well as spontaneous non-synchronous activity *(Haenseler et al., 2017)*. More complex synchronous activity has been observed from approximately day 65 onwards *(Bergstrom et al., 2016; Gunhanlar et al., 2018; Shi et al., 2012a)*. Communicative functionality has also been established in 3D culture, with RT-PCR experiments demonstrating that many of the major subunits of the NMDA and AMPA receptors are present between weeks 4 and 15 post-induction *(Kirwan et al., 2015)*. These results have been supported by calcium signalling experiments showing calcium flux and spontaneous electrophysiological activity in co-cultures of cortical neurons with microglia *(Kirwan et al., 2015; Nadadhur et al., 2017)*. Study of neuronal network data suggest that *in vitro* human 3D cortical networks have similar connectivity patterns to cortical neurons *in vivo* (large numbers of neurons with few connections, and a small number of highly connected cells that act as hubs) *(Kirwan et al., 2015)*.

As a model of AD, glutamatergic cortical neurons derived from this protocol have shown different APP processing dynamics between different fAD mutation lines and versus controls *(Moore et al., 2015)*. Furthermore, neurons with a mutant *APP* genotype, but not *PSEN1*, have increased total tau and tau phosphorylation *(Moore et al., 2015)*, a link between Aβ and tau that has also noted in overexpression models *(Choi et al., 2014; Muratore et al., 2014)*. It has also been shown that cortical neurons generated by this protocol internalise tau from conditioned media, where it can stimulate the generation of more aberrant tau in a prion-like manner *(Wu et al., 2016)*. These cells have also been used for exploratory drug screening experiments. Brownjohn *et al.* conducted a phenotypic,

small-molecule screen in Down's syndrome and fAD neurons and identified avermectins as γ-secretase independent molecules possessing γ-secretase-like properties in the proteolysis of APP *(Brownjohn et al., 2017)*. Additionally, the Shi protocol has been used as a platform for the study of several other diseases of the CNS, including Down's syndrome *(Shi et al., 2012c)*, MAPT mutations *(Iovino et al., 2015; Sposito et al., 2015)*, and Huntington's disease *(Mehta et al., 2018)*, investigation of neuronal estrogen biology *(Shum et al., 2015)*, and neuropsychological conditions such as schizophrenia and autism *(Boissart et al., 2013; Roessler et al., 2018)*.

Given enormous potential for a mature science of iPSC technology to interrogate AD biology, and facilitate therapeutic development in complement to animal models, it is important to examine Aβ biology and pathology in human neurons directly impacted by AD. This chapter will describe the characterisation of the cell lines used and contribute data to the ongoing endeavour to improve measurement variability in their use as AD models.

7.1.1 Contributions

The author designed the media collection protocol, cultured 2D iPSC neurons and collected media and lysates alongside C. Arber. Brain tissue was sectioned by T. Lashley, and homogenised by the author and C. Arber. Immunocytochemistry was conducted by the author and Dr Arber. Immunohistochemistry and Western blotting were conducted by C. Arber. Live cell calcium imaging was conducted by the author under the supervision of M. Duchen and G. Bosale. The author conducted all immunoassays, conducted the statistical analyses, and co-wrote the scientific report alongside C. Arber.

Study conception: S. Wray, H. Zetterberg, JM. Schott, N. Fox. NS. Ryan.
Sample collection: The author, C. Arber, C. Lovejoy, N. Willumsen, T. Lashley.
Karyotyping: Cell Guidance Systems.
Genotyping: C. Kun-Rodriguez, L. Darwent, and C. Arber.
Immunocytochemistry: The author, C. Arber.
Immunohistochemistry: C. Arber.
Western Blots: C. Arber.
Calcium imaging: The author, G. Bosale, M. Duchen.
Immunoassays/LDH assay: The author.
Analysis: The author.

Scientific report: C. Arber, The author, C. Lovejoy, NS. Ryan, RW. Paterson, N. Willumsen, E. Gkanatsiou, E. Portelius, K. Blennow, A. Heslegrave, JM. Schott, J. Hardy, T. Lashley, H. Zetterberg, S. Wray.

7.2 Materials and methods

7.2.1 Samples

All cortical neurons used in experiments were cultured, and media collected, as described in Sections 2.4-8.

For calcium signalling experiments, iPSC-derived cortical neurons used were from the APP V717I-1.1 (n=2), CTRL1 (n=2), and CTRL2 (n=1) lines, aged at 100 days post-induction.

The cell lines used in time course experiments consisted of two iPSC-derived control lines (CTRL1 (n = 1), and CTRL2 (n = 1)), one ESC-derived control line (SHEF6 (n = 2)), two clones of one *APP* mutation line (*APP* V717I-1.1 (n = 3), and *APP* V717I-1.3 (n = 2)), two clones of one *PSEN1* mutation line (*PSEN1* int4del.4 (n = 1), and *PSEN1* int4del.6 (n = 2)). Cells were cultured by Dr C. Arber and myself.

For paired sample comparison experiments, iPSC-derived cortical neuron lines used consisted of two clones from one *APP* mutation line (*APP* V717I-1.1 (n = 3), and *APP* V717I-1.3 (n = 2). Cells were cultured by Dr C. Arber and myself. In addition to media, cell lysates were collected as described in Section 2.9. Post-mortem brain tissue from the frontal cortex was collected as described in Section 2.14 by the Queen Square Brain Bank. For immunoassay analysis of AD biomarkers tissue was homogenised and processed to extract different Aβ solubility fractions as described in Section 2.15 by Dr C. Arber and myself. Samples used consisted of technical-replicates of one *APP* mutation brain (*APP* V717I-1). CSF was collected from the *APP* V717I-1 patient at the specialist cognitive disorders clinic (National Hospital for Neurology and Neurosurgery, in association with the Dementia Research Centre, UCL), referred for diagnostic LP for investigation of a suspected neurodegenerative condition. Ethical permission was obtained from the National Hospital for Neurology and Neurosurgery and the Institute of Neurology joint research ethics committee (09/H0716/64) and informed consent was obtained. CSF was collected by LP between 09:00 and 10:30. A volume of up to 20mL of CSF was collected at ambient room temperature into two 10mL polypropylene tubes (Sarstedt, Nümbrecht, Germany cat. 63.9922.254) directly from a 22-gauge Quincke needle, without manometer. In the case of visible blood contamination, the CSF was discarded and the tap continued

in a new tube once bleeding had stopped. Samples were centrifuged at 1750 RCF for five minutes at 21°C, and aliquoted at 1mL into 2mL PP tubes (Sarstedt cat. 72.694.406) and frozen at -80°C within 1-4 hours of collection.

7.2.2 Experimental methods

Cell karyotyping was conducted as described in Section 2.4. Genotyping was conducted using Sanger Sequencing by Drs. C. Kun-Rodriguez, L. Darwent, and C. Arber. Immunocytochemistry was conducted as described in Section 2.11 by Dr C. Arber and myself.

Calcium signalling experiments were conducted as described in Section 2.12. Microscope image fields were selected on the basis of the most structurally intact network of neurons that could be resolved within the shortest time frame after microscope mounting.

For time course experiments, cell media (N2B27) was collected from each well at three time-points separated by 48 hours of incubation (days 100, 102, and 104). This process of media collection was then repeated on the same cells at days 200, 202, and 204 post-induction.

Extracellular amyloid plaques are relatively common in aged brain tissue, but also constitute a defining pathological feature of AD. To assess whether our *in vitro* 2D and 3D models capture this aspect of AD immunohistochemistry and immunocytochemistry were used to compare extracellular Aβ accumulation in brain and iPSC-derived cortical neuron tissue from the same individual respectively (Section 2.11). The antibodies used were Aβ (Dako, M0872), MAP2 (Abcam, ab5392), and DAPI (Abcam, ab228549). This work was conducted by Dr. C. Arber.

Cell media and cell lysate samples, post-mortem brain tissue homogenate, as well as CSF from the individual *APP* V717I-1 were analysed for Aβ38, Aβ40, and Aβ42 by triplex MSD ECL immunoassay (Section 2.2.2). Ttau was measured by MSD ECL immunoassay (Section 2.2.3), and LDH by Randox Monza biochemistry analysis (Section 2.17).

7.2.3 Statistical analysis

For calcium signalling experiments, data was compiled using a Metafluor software package. Images were analysed in Image J where the pixel greyscale signal intensity of 340nm and 380nm images were recorded in selected regions of interest (neuronal soma, identified by gross morphology) minus the signal of a blank region of interest. The quantified signal ratio of 340:380nm was used to

determine the neuronal calcium signal response to KCl or glutamate. Graphs were created in Microsoft Excel.

For time course experiments, mean concentrations for each biomarker were calculated from duplicate measurements, and variation between inductions was calculated by coefficient of variance. Data normality was assessed by histogram, qq-plot, and Shapiro-Wilk test. Given data non-normality, Spearman's rank correlation coefficient was conducted to assess the relationship between cell media concentrations of Aβ or tau and LDH. For time course experiment data, variation between different inductions of the same line was calculated by coefficient of variance. Analysis was conducted in R, and graphs were composed using the ggplot2 package.

For analysis of paired sample data, different sample types were generated from tissues of the same patient and so the sample size was limited to n=1. Statistical comparisons between different sample types were conducted from technical replicate measurements, and data distribution therefore reflects procedural variation. Statistical comparisons were conducted using Mann-Whitney U analysis in R, where data of each sample type was compared to that of cell media individually. In cases where no technical replicates were available (e.g. *APP* V717I-1 CSF) it was not possible to obtain a significance value. Analysis was conducted in R, and graphs were composed using the ggplot2 package.

7.2.4 Assay variation

For paired sample and time course measurements, intra- and inter-assay variation was Aβ38 (3.6%, 6.8%), Aβ40 (5.6%, 7.4%), Aβ42 (3.8%, 10.5%), Aβ43 (7.4%, 13.2%), and Ttau (7.9%, 12.6%) calculated from the concentrations of an internal control CSF sample included in assay plates. Intra- and inter-assay CV) was calculated according to ISO 5725-2 standards *(British Standards Institution, 1994)*.

7.3 Results

7.3.1 Karyotype and genotype screen

The process of cellular reprogramming involves the use of a vector (viral or plasmid) to alter genetic expression through either integrative (retrovirus, lentivirus) or non-integrative (Sendai virus, plasmid, synthetic mRNA) means. Use of integrative methods risk off target insertions or deletions, as well as unintended persistence of sequence in the nuclear DNA, and it is important to determine

that transformed cells do not retain these unwanted artefacts before carrying the lines forward. Non-invasive protocols, such as the one used in this thesis do not have these vulnerabilities, the trade-off being generally lower reprogramming efficiency.

Never-the-less, in the artificial environment of cell culture there are many factors that can affect faithful cell division, not least the enzymes used in passage. It has been observed that successive passages increase the chance of chromosomal level anomalies *(Berry et al., 2018)*, and so karyotyping of each line was performed prior to engaging in the differentiation of iPSCs to cortical neurons. Normal karyotype was demonstrated for each line examined (Figure 28A). Furthermore, a number of cell lines were from individuals with specific fAD mutations, and it was important to confirm that these cells retained their fAD-relevant genotype after reprogramming. Genotyping confirmed retention of the appropriate fAD mutations (Figure 28B).

Figure 27: Results of fAD line karyotyping and genotyping

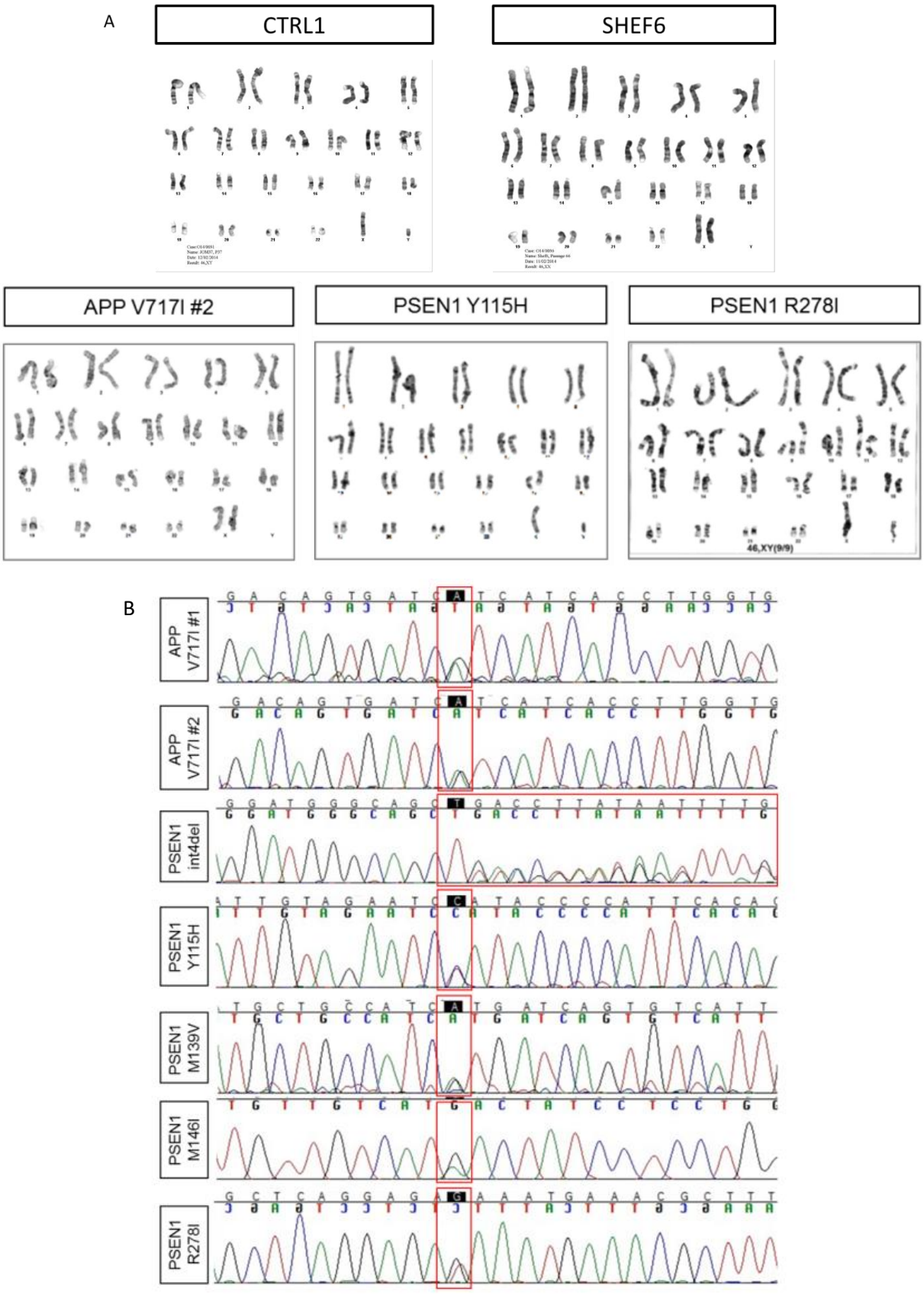

Figure 28: A) human cell lines show normal karyotypes. B) fAD mutation lines show expected genotypes. Images generated by Dr. C. Arber and used with permission.

7.3.2 Immunocytochemistry

iPSC-derived glutamatergic cortical neurons were cultured and differentiated as described in Sections 2.4-8. A portion of the cells from each line examined in this thesis were plated onto glass coverslips at each of the major differentiation milestones, and fixed in 4% paraformaldehyde. Immunocytochemistry was conducted following the method described in Section 2.11, to identify proteins expressed by cells at each major developmental stage.

Results (Figures 29-31) showed expression of pluripotency markers SSEA4, OCT3/4, and Tra1-81 in iPSC cultures. Following neural induction by dual SMAD inhibition neuroepithelium formed with characteristic rosette morphology and the expression of Ki67, PAX6, and OTX2. Neural progenitors and deep layer neurons (TBR1+) were present after 30 days post-induction complete with projecting axons (TUJ1+). Over a subsequent 70 days, mid layer (CTIP2+) and superficial layer (SATB2+ and BRN2+) neurons differentiated. A sub-population of astroglia (GFAP+) were also present.

Figure 28: Immunocytochemistry of Non-AD control iPSC lines

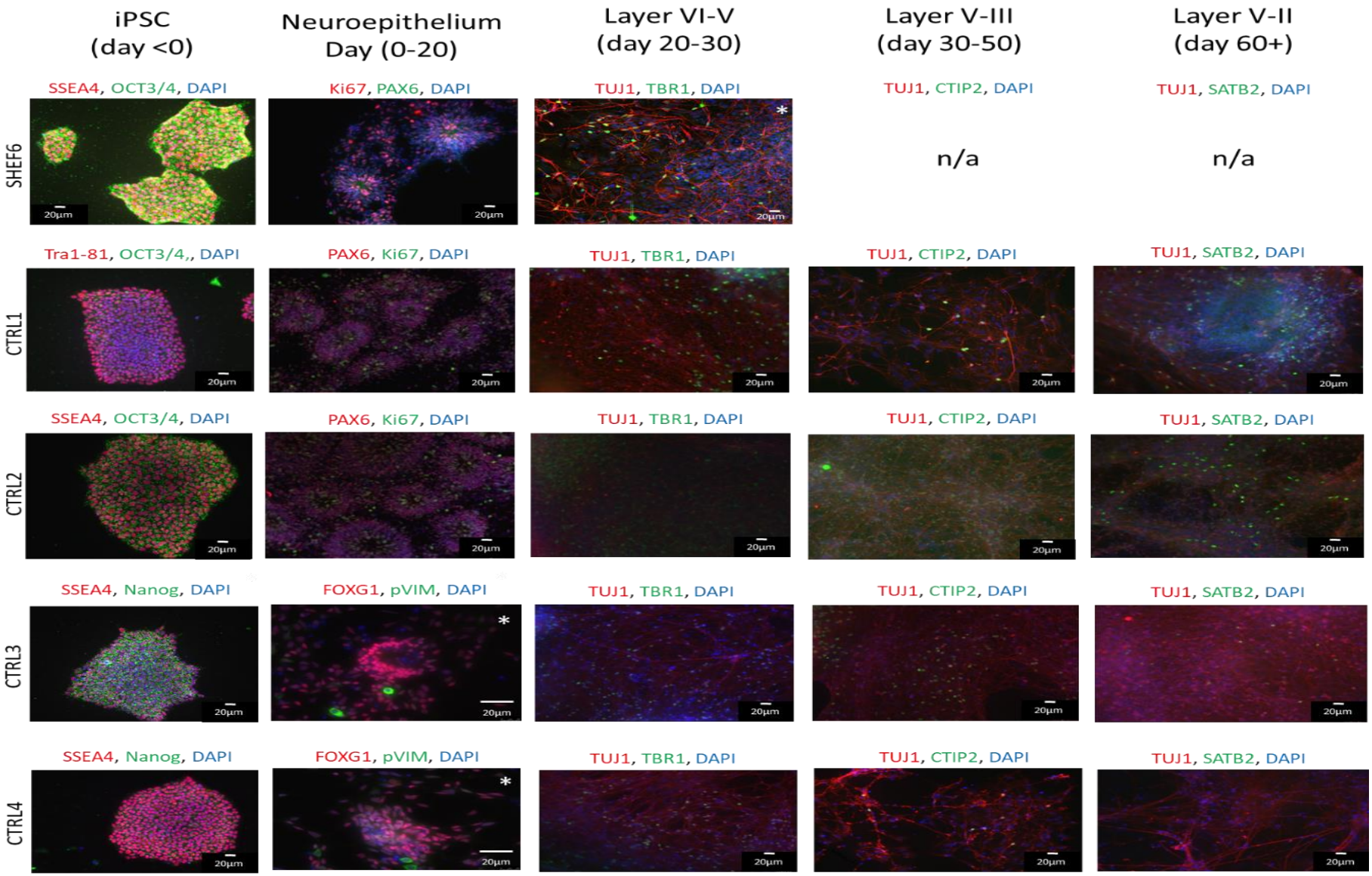

Figure 29: Showing immunocytochemistry for each of the Non-AD control lines for markers of pluripotency (SSEA4, TRA1-81, OCT3/4, and Nanog), markers associated with neuroepithelial radial glia (PAX6 and phosphor vimentin (pVIM)), proliferating cells (Ki67 and FOXG1), and markers of the various neuronal cortical layers (TBR1, CTIP2, SATB2, and BRN2), as well as the axonal marker TUJ1. DAPI is a marker of nuclear protein. White asterisks indicate images provided by Dr. C. Arber, and used with permission.

Figure 29: Immunocytochemistry of fAD *PSEN1* iPSC lines

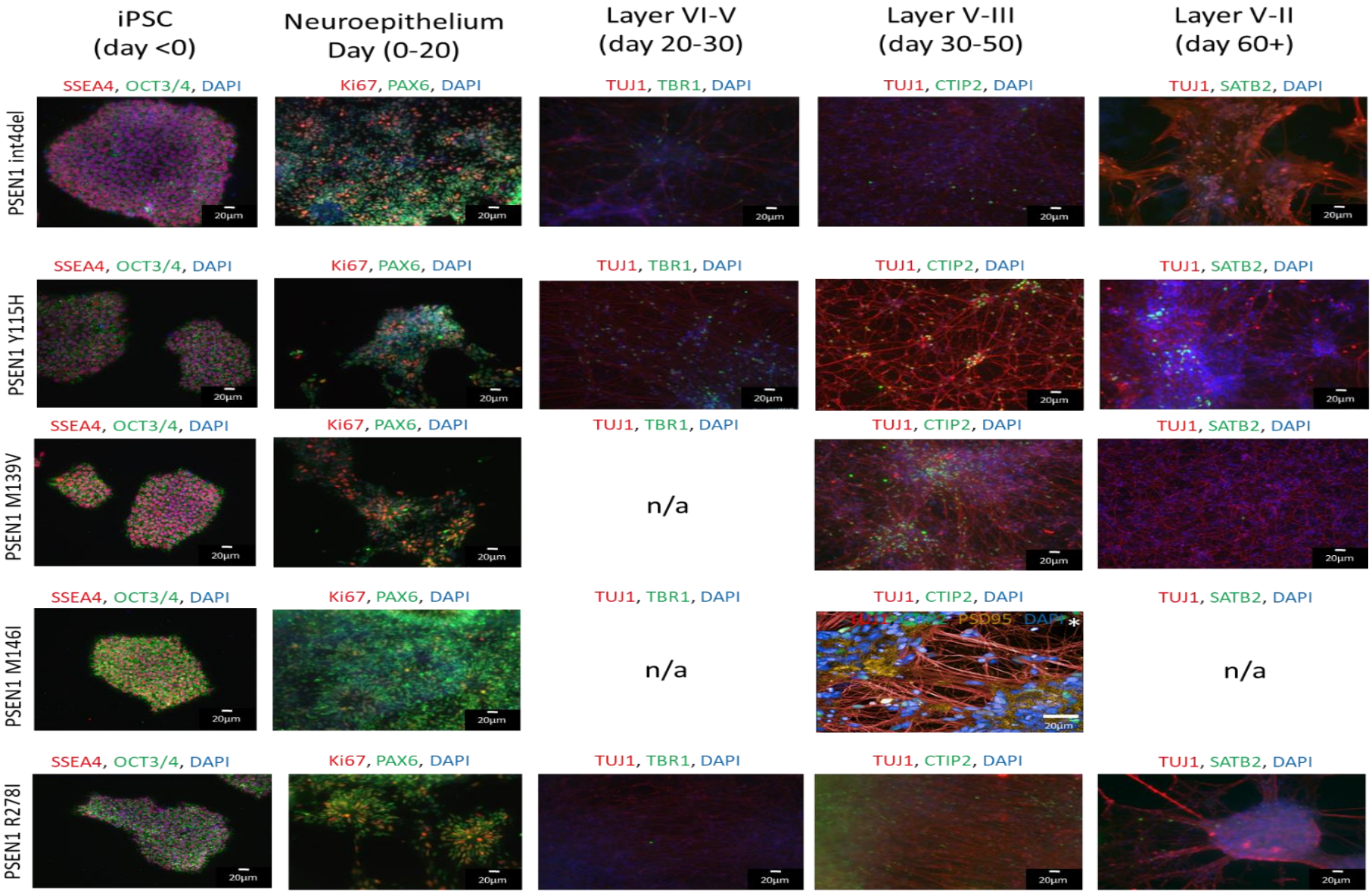

Figure 30: Showing immunocytochemistry for each of the *APP* V717I mutation lines for markers of pluripotency (SSEA4, TRA1-81, and OCT3/4), markers associated with neuroepithelium (Ki67 and PAX6), and markers of the various neuronal cortical layers (TBR1, CTIP2, SATB2, and BRN2), as well as the axonal marker TUJ1. A marker of glutamatergic synapses (PSD95) is shown in panel PSEN1 M146I Layer V-III, this image was taken using an Agilent Seahorse XF analyser. DAPI is a marker of nuclear protein. White asterisks indicate images provided by Dr. C. Arber, and used with permission.

Figure 30: Immunocytochemistry of fAD *APP* V717I iPSC lines

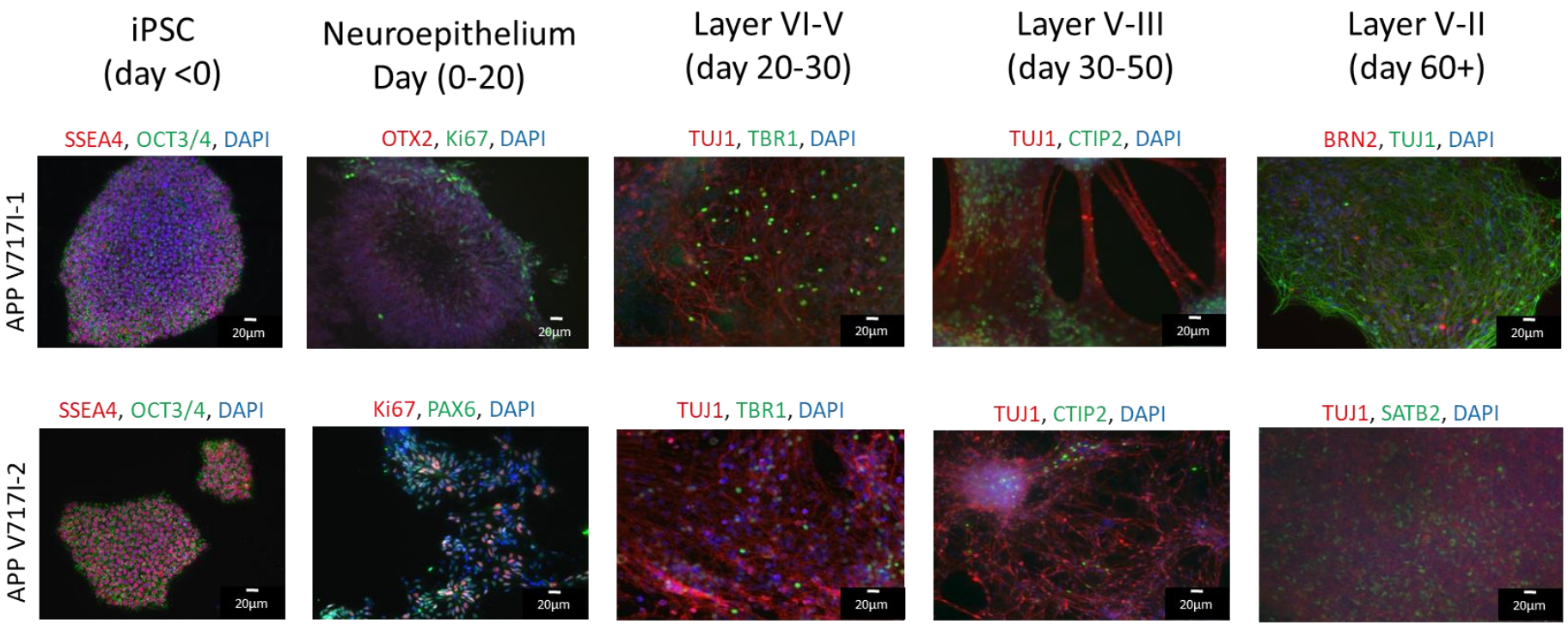

Figure 31: Showing immunocytochemistry for each of the *APP* V717I mutation lines for markers of pluripotency (SSEA4, TRA1-81, and OCT3/4), markers associated with neuroepithelium (Ki67 and PAX6), and markers of the various neuronal cortical layers (TBR1, CTIP2, SATB2, and BRN2), as well as the axonal marker TUJ1. DAPI is a marker of nuclear protein.

7.3.3 Calcium signalling

Neurons are specialised cells for fast and intricate communication processes. Compelling evidence for the function of Aβ peptides in the regulation and disruption of neuronal activity has been gradually building, and data point particularly to the importance of synaptic transmission to Aβ exocytosis *(Cirrito et al., 2005, 2008)* and disrupted calcium homeostasis to neurotoxicity *(Abramov et al., 2004; Arispe et al., 1993; Berridge, 2011; Camandola and Mattson, 2011; Eckert et al., 2010)*. It is therefore important that an *in vitro* neuronal model of Aβ biology should demonstrate electrically functional properties.

Neurons maintain free cytosolic Ca^{2+} at a concentration of ~100nM, and store excess in the ER and mitochondria, or export it to the extracellular space against the massive 20000-fold concentration gradient *(Clapham, 2007)*. During membrane depolarisation, voltage-gated calcium channels (such as nAChRs and NMDArs) open allowing Ca^{2+} (and Na^{+} with much lower affinity) ions to enter the cell *(Simons, 1988)*. The increase of Ca^{2+} above resting level within the cytosol is known as a calcium signal. Cytosolic Ca^{2+} acts as a crucial secondary messenger which binds to various proteins (e.g. calmodulin) causing conformational changes that expose hydrophobic regions and facilitate inter-molecular interactions, including pre-synaptic vesicular-membrane fusion that enables neurotransmitter release *(Jahn and Fasshauer, 2012)*. Therefore, demonstration of functional calcium signalling in response to ionic and neurotransmitter stimulation provides validation of neuronal functional maturity.

The majority of neurons observed responded with a single calcium signal immediately following stimulation with 12.5mM KCl and with 100µM glutamate (Figure 32). Out of a total 127 cells observed, a single neuron from the CTRL1 displayed continuous, regular calcium signalling approximately every 30 seconds for as long as it was recorded (six minutes) (Figure 32E). In the initial moments of recording, the 340nm:380nm ratio signal from this cell was falling to baseline, potentially indicating spontaneous activity prior to stimulation. A number of other neurons demonstrated tiny fluctuations (340:380nm = 0.05-0.1 above baseline) in the 340nm:380nm ratio post-stimulation (neuron 20 (Figure 32A) and neuron 13 (Figure 32C)). It is unclear whether these fluctuations reflect true calcium signals, rather the fact that these neurons all eventually demonstrated indications of calcium toxicity (a prolonged high 340nm:380nm that either plateaued or continued to increase) suggests these may denote stress.

Figure 31: Live cell calcium imaging

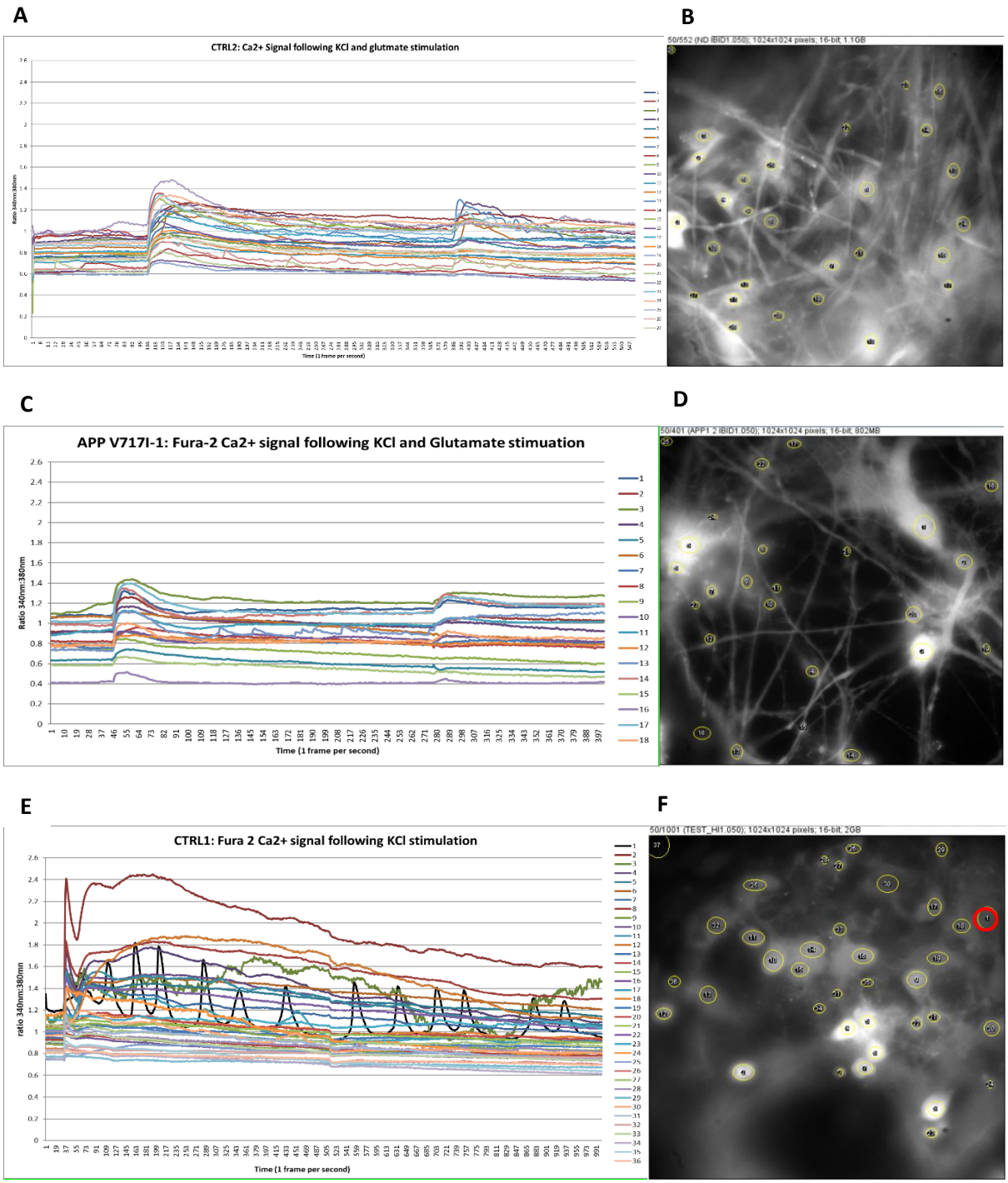

Figure 32: A) CTRL2 cortical neuron calcium signals in response to 12.5mM KCl administered at 106 seconds, and 100µM glutamate at 186 seconds. B) Image of CTRL2 neurons at 50 seconds in the 340nm channel. C) fAD genotype (*APP1* V717I) cortical neuron calcium signals in response to 12.5mM KCl administered at 46 seconds, and 100µM glutamate at 280 seconds. D) Image of (*APP* V717I) neurons at 50 seconds in the 340nm channel. E) CTRL1 cortical neuron calcium signals in response to 12.5mM KCl administered at 34 seconds and followed over an extended time frame. Neuron 1 (E: black line, F: circled red) is noteworthy for regular calcium signals following KCl stimulation, and potential spontaneous activity prior to stimulation. The disturbance at 500 seconds reflects the microscope stage being accidentally jolted. F) Image of CTRL1 neurons at 50 seconds in the 340nm channel.

7.3.4 Variability of Aβ peptide concentrations over time and between independent inductions

The issue of cell culture variability is often discussed in terms of controlling reprogramming efficiency and maintaining genotypic homogeneity between culture batches *(Berry et al., 2018)*. A relatively neglected aspect is the variability in protein biomarker measurements between and within differentiated cell lines.

Environmental factors known to alter *in vitro* neuronal protein expression include: temperature, oxidation, infection, culture purity, as well as cell density, viability, maturity and electrical functionality. Whilst certain of these factors (e.g. temperature, oxidation, and infection) are relatively easy to standardise with good laboratory practice, and others (purity and electrical maturity) demonstrably robust, long term neuronal culture following the Shi protocol *(Shi et al., 2012a)* is vulnerable to differences in culture density.

The different neuronal progenitors that represent a strength of this approach differentiate at different rates. When the final passage is made at ~day 35 post-induction, a population of cells are still mitotic and continue to differentiate. Furthermore the extended time course required for the culture to reach a mature, terminally differentiated state provides scope for unique levels of cell death. We considered that the concentration of secreted Aβ peptides would broadly relate to the number of viable neurons within each culture. Given emerging evidence that production of different Aβ peptides may follow predictable and dependent patterns *(Chavez-Gutierrez et al., 2012; Takami et al., 2009)*, we hypothesised that ratios of Aβ peptides might normalise for variations in cell density between cultures.

7.3.4.1 Tau, but not Amyloid beta, correlates with cell death

Concentrations of secreted Aβ42, Aβ40, Aβ38, Aβ43, T-tau, and LDH were quantified in 2D iPSC-derived neuronal conditioned media from three non-AD and two fAD iPSC lines. LDH is a cytosolic enzyme, and its presence in the extracellular space is a marker of cytotoxic membrane disruption that accompanies cell death. Secreted Aβ43, Aβ42, Aβ40 and Aβ38 did not correlate with LDH (Figure 33A-D). In contrast, secreted tau displayed a strong positive correlation with LDH, and therefore to level of cell death (Figure 33E).

Figure 32: Lactate dehydrogenase correlation with Aβ and total tau

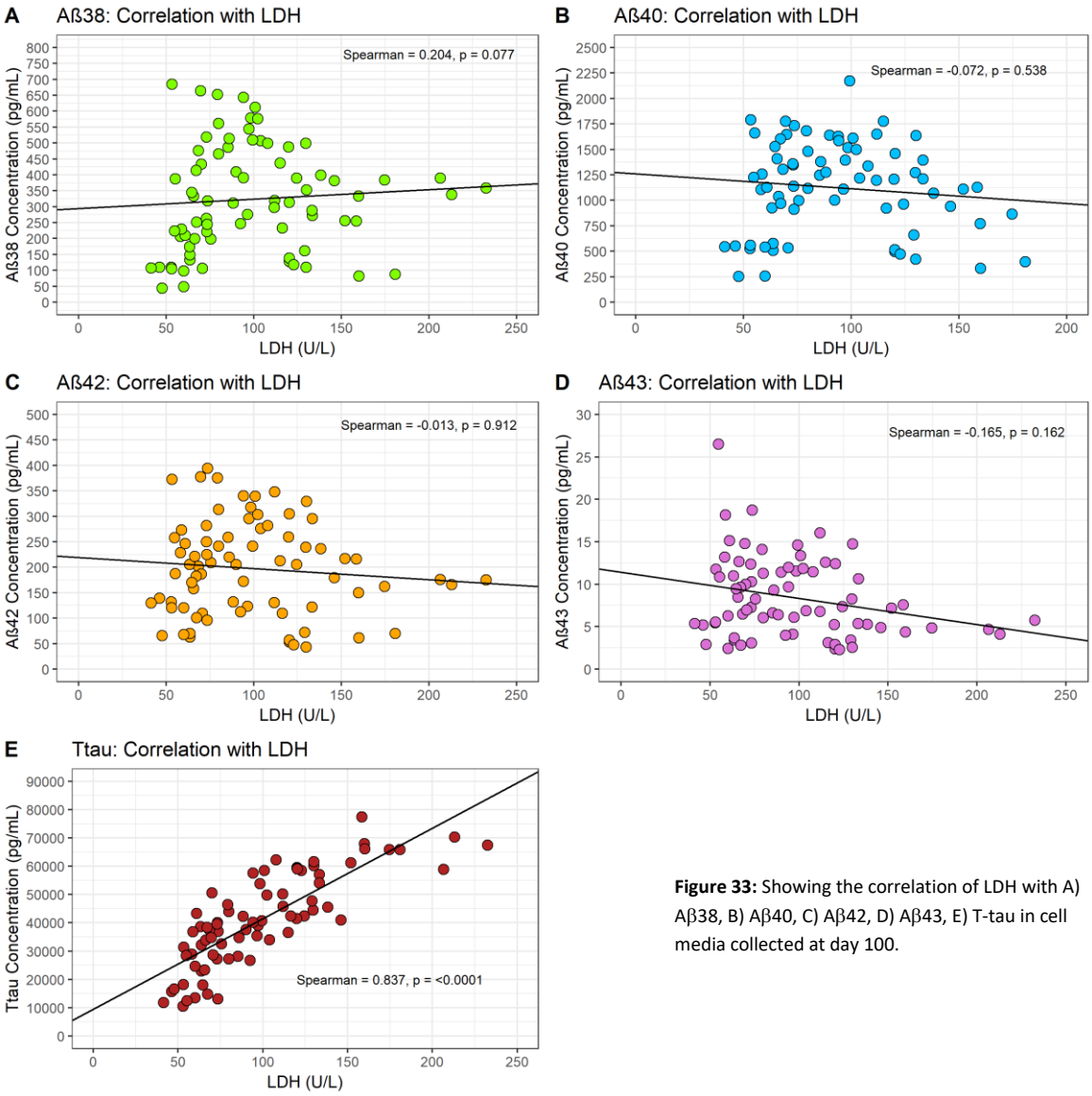

Figure 33: Showing the correlation of LDH with A) Aβ38, B) Aβ40, C) Aβ42, D) Aβ43, E) T-tau in cell media collected at day 100.

7.3.4.2 High variability of Amyloid beta peptide concentrations over time and between inductions

When cell culture media concentrations of Aβ peptides were examined longitudinally, acceptable measurement consistency (average CV = 8.3% ± 1.4 95% confidence interval (CI), inclusive of all peptides) was observed within each induction over the course of six days (Figure 34). However, a large degree of variability (average CV = 30.1% ± 5.7 CI) was observed over the longer time period of 100 days (Figure 34). Furthermore, different iPSC clones of the same reprogrammed fibroblast line and independent inductions of the same iPSC line were highly variable, in some cases even over the

course of six days, with differences between inductions and clones being comparable to that between different cell lines (Figure 34).

Figure 33: Cell media Aβ concentration over time

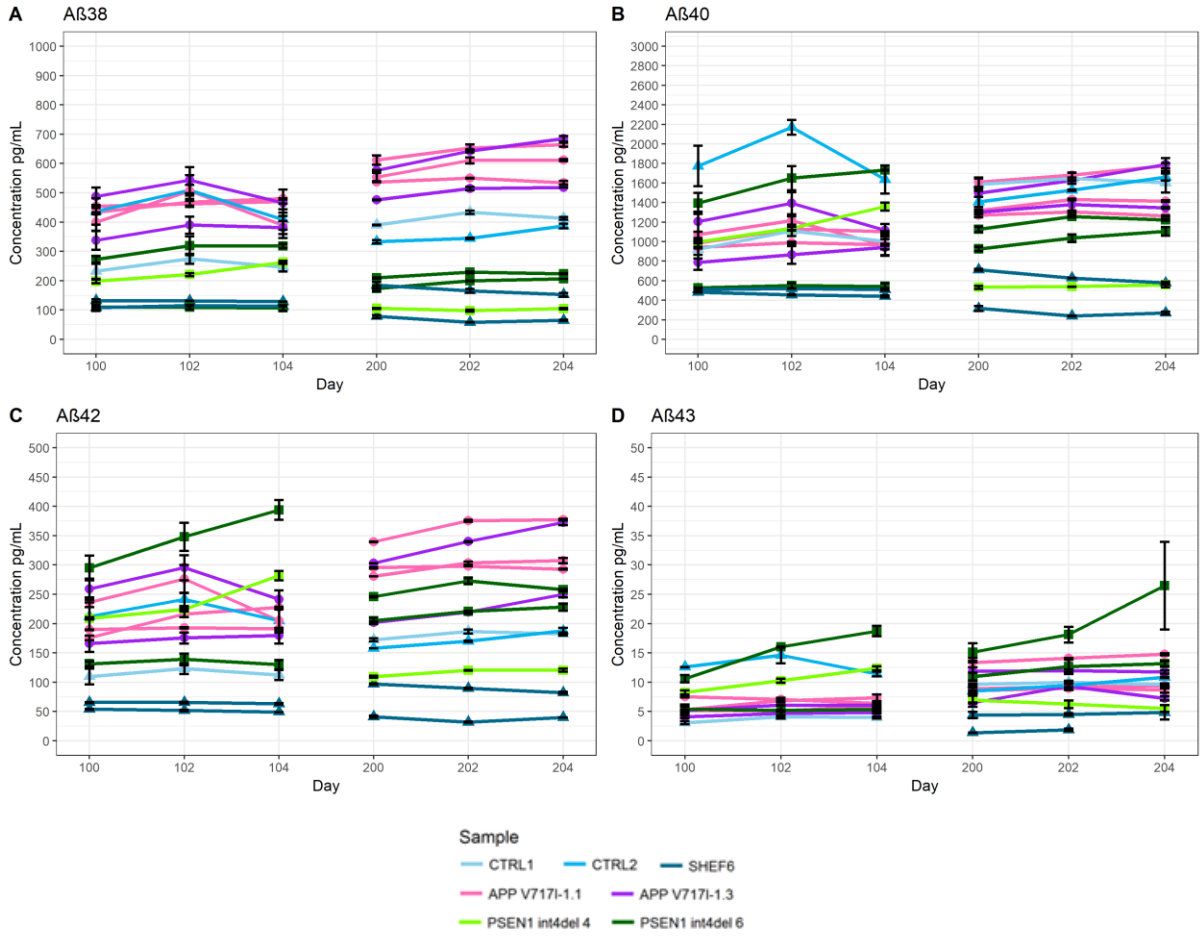

Figure 34: Longitudinal concentrations of A) Aβ38, B) Aβ40, C) Aβ42, and D) Aβ43 in cell media collected from different inductions of non-AD and fAD cell lines, including from different clones of APP V717I and PSEN1 int4del mutation lines.

7.3.4.3 Amyloid beta ratios are consistent over time and between independent inductions

To examine whether data normalisation might reveal more meaningful patterns, derived Aβ peptides were analysed as ratios to the most abundant product, Aβ40. Additionally, the Aβ42:38 ratio was investigated, as this ratio is a potential biomarker of APP processivity. When ratios of Aβ peptides were used, variability over time collapsed. Over six days variation for all ratios was low (average CV = 5.1% ± 1.6 CI) (Figure 35). Over the longer time frame of 100 days ratios of Aβ42:40, Aβ42:38, and Aβ38:40 demonstrated similarly low variation (average CV = 5.9% ± 1.4 CI), whilst Aβ43:40 retained a relatively large degree of variation (average CV = 20.5% ± 4.3 CI), although this

was half that of Aβ43 alone (average CV = 40.7% ± 11.5 CI) (Figure 35). Furthermore, greater consistency was observed between different inductions and clones of the same line when ratios of Aβ were employed. Importantly, the reduced variability over time and between inductions/clones highlighted distinct patterns of separation between fAD mutations and CTRL1, CTR2 and SHEF6 lines. Despite, representing cells from three different individuals and from both iPSC- and ESC-derived sources, ratios of all Aβ peptides were all but indistinguishable between the non-AD lines. A phenotype of increased Aβ42:40 relative to these controls was demonstrated in both fAD mutation cells (Figure 35A). Furthermore, both clones of cells bearing an intron 4 deletion in *PSEN1* demonstrated raised Aβ42:38 and Aβ43:40 relative to control lines (Figure 35B-D). The ratio Aβ38:40 appeared to distingush *APP* and *PSEN1* mutation lines from each other as well as controls, as this ratio was raised versus controls in *APP* V717I, and slightly decreased versus controls in *PSEN1* int4del.

Figure 34: Cell media Aβ ratios over time

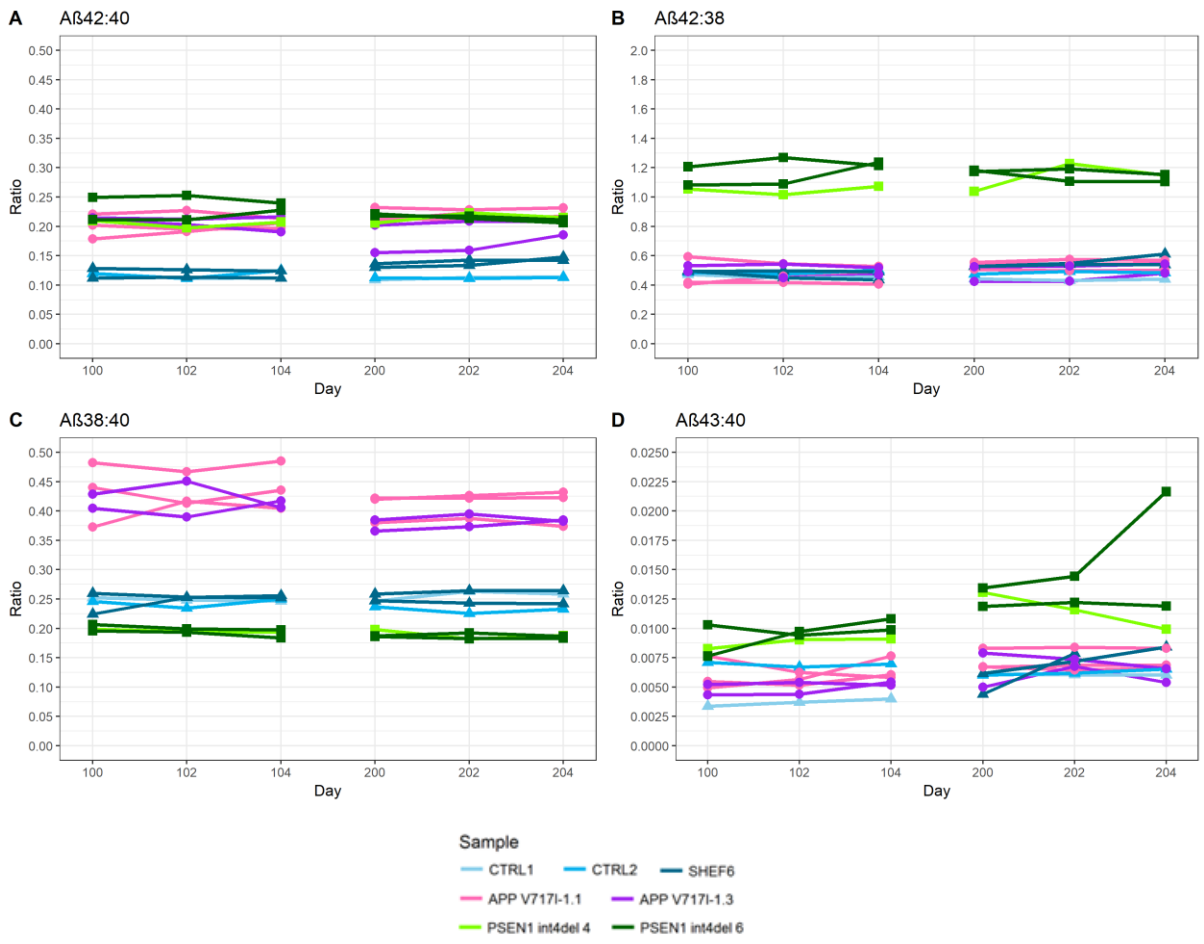

Figure 35: Longitudinal ratios of A) Aβ42:40, B) Aβ42:38, C) Aβ38:40, and D) Aβ43:40 in cell media collected from different inductions of non-AD and fAD cell lines, including from different clones of APP V717I and PSEN1 int4del mutation lines.

7.3.4.4 Ttau concentrations are high and variable over time and between independent inductions

Concentrations of T-tau were extremely high in cell culture media, and samples had to be diluted 1:100 (compared to 1:4 for CSF) in order to fit within the linear range of the assay standard curve. Measurements from the same induction showed considerable variability over both six-day (average CV = 19.4% ± 1.5 CI) and 100-day time frames (average CV = 29.2% ± 10.3 CI), and differences between different inductions and clones of the same line were comparable to those between different cell lines (Figure 36A). Additionally, a trend for T-tau concentrations to decrease after successive 48-hour time points was observed during both week 100 and week 200 collections.

Figure 35: Cell media Ttau ratios over time

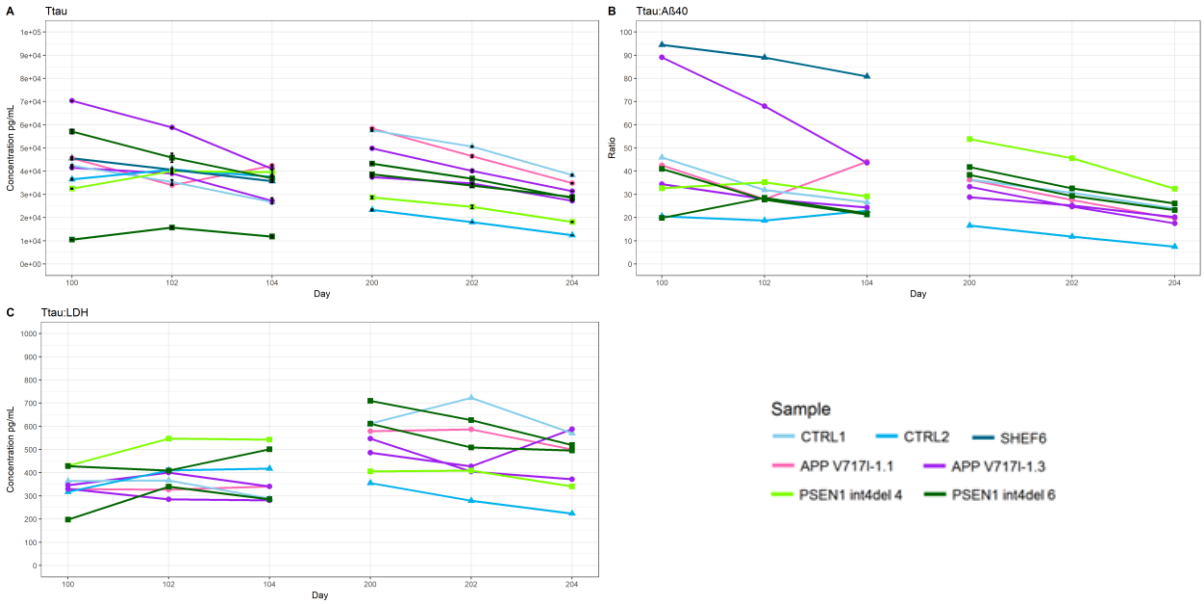

Figure 36: Longitudinal concentrations of A) T-tau, B) Ttau:Aβ40, and C) Ttau:LDH in cell media collected from different inductions of non-AD and fAD cell lines, including from different clones of APP V717I and PSEN1 int4del mutation lines.

Different iPSC clones of the same reprogrammed fibroblast line and independent inductions of the same iPSC line were highly variable, even over the course of six days, with differences between inductions and clones being comparable to that between different cell lines (Figure 36). Normalisation of Ttau values in ratio to Aβ40 did not improve interpretability of the data between days 100-104, although between days 200-204 the distinctions between Non-AD, *APP* V717I, and *PSEN1* int4del became more defined (Figure 36B). Finally, the use of a Ttau:LDH ratio appeared to stabilize the successive decrease in Ttau concentration, especially between days 100-104, although no genotype specific pattern emerged (Figure 36C).

7.3.5 Comparison of amyloid beta profiles in paired biosamples

Having characterised relevant protein expression and excitatory function in our cortical neuron model, as well as identifying the utility of using Aβ ratios to investigate Aβ production biology, we asked the question: how well does Aβ production *in vitro* reflect patterns observed within adult human biofluids and tissues? One highly interesting study compared RNA transcription in iPSC-derived neurons and glia culture with temporal tissue from the same non-neurodegenerative individual and observed similar CpG methylation after neuronal differentiation *(Hjelm et al., 2013)*. Additionally, whilst a number of genes were up- or down-regulated *in vitro*, differences in down-regulation decreased with time in culture *(Hjelm et al., 2013)*. To contribute to this slowly emerging area of study, we compared relative Aβ levels in iPSC conditioned media, iPSC-neuronal lysates, *ex vivo* lumbar CSF, and post-mortem brain tissue homogenate from the same fAD patient donor (*APP* V717I-1).

7.3.5.1 iPSC-cortical neuron cultures do not generate extracellular amyloid plaques

Experiment by immunocytochemistry and western blot demonstrated that APP was expressed in 2D, 3D, and post-mortem tissue (Figure 37). APP expression was greater in 3D than 2D culture systems, due to the relative differences in cell density, which was higher in the cell dense environment of the organoid. However, deposition of amyloid into dense-core and diffuse plaques was only observed in post-mortem brain of this individual, but not in either 2D or 3D *in vitro* models (Figure 37).

Figure 36: APP expression in Post mortem, 2D, and 3D cortical neurons

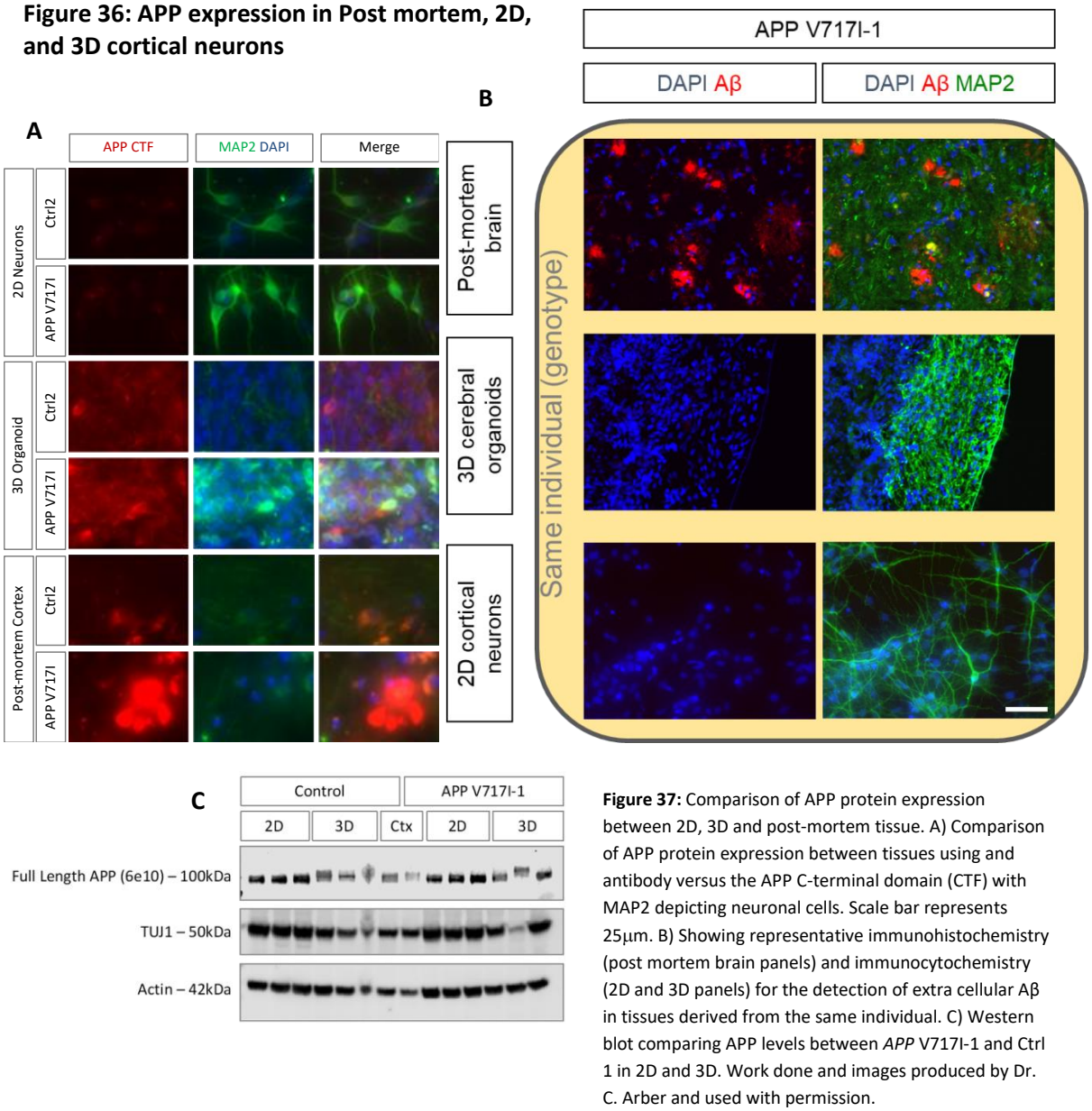

Figure 37: Comparison of APP protein expression between 2D, 3D and post-mortem tissue. A) Comparison of APP protein expression between tissues using and antibody versus the APP C-terminal domain (CTF) with MAP2 depicting neuronal cells. Scale bar represents 25μm. B) Showing representative immunohistochemistry (post mortem brain panels) and immunocytochemistry (2D and 3D panels) for the detection of extra cellular Aβ in tissues derived from the same individual. C) Western blot comparing APP levels between *APP* V717I-1 and Ctrl 1 in 2D and 3D. Work done and images produced by Dr. C. Arber and used with permission.

7.3.5.1.1 Amyloid beta ratios in paired biosamples

When absolute concentrations of Aβ38/40/42 were compared in cell media, cell lysates (soluble and insoluble fractions), frontal cortex (soluble and insoluble fractions), and lumbar CSF from the same individual results showed gross differences in the quantities of Aβ peptides present between sample types (Figure 38). Concentrations were universally highest in CSF (although the experiment was not appropriately powered to estimate significance in this case), whilst cell media Aβ42 (Figure 38A) and Aβ40 (Figure 38B) were lower, and cell lysate and brain fraction concentrations lower again. Aβ38 concentration also differed significantly between cell media and other sample types (Figure 38C).

Additionally, there was a tendency for insoluble lysate and brain fractions to have more Aβ38 than the soluble fractions (Figure 38C).

Use of Aβ ratios highlighted some interesting patterns. No significant difference in Aβ42:40 was found between cell media with the soluble brain fraction, although variability between brain tissue extraction replicates was high (Figure 38D). However, Aβ42:38 and Aβ38:40 ratios were clearly divergent between cell media and soluble brain fraction (Figure 38E-F). Aβ38 was very difficult to detect in soluble brain fraction, with only one replicate generating a signal, comparable to that obtained more reliably in the insoluble fraction. Aβ42:40 and Aβ42:38 were decreased in CSF relative to cell media, but the Aβ38:40 ratio was highly comparable. This was also the case for the soluble cell lysate fraction. The insoluble fractions of cell lysates and brain homogenate demonstrated similar Aβ ratios to each other, but in all cases distinct from cell media. This reflected proportionally lower Aβ42 and/or increased Aβ40 and Aβ38 content.

Figure 37: Comparison of Aβ peptide concentration and ratios between paired samples

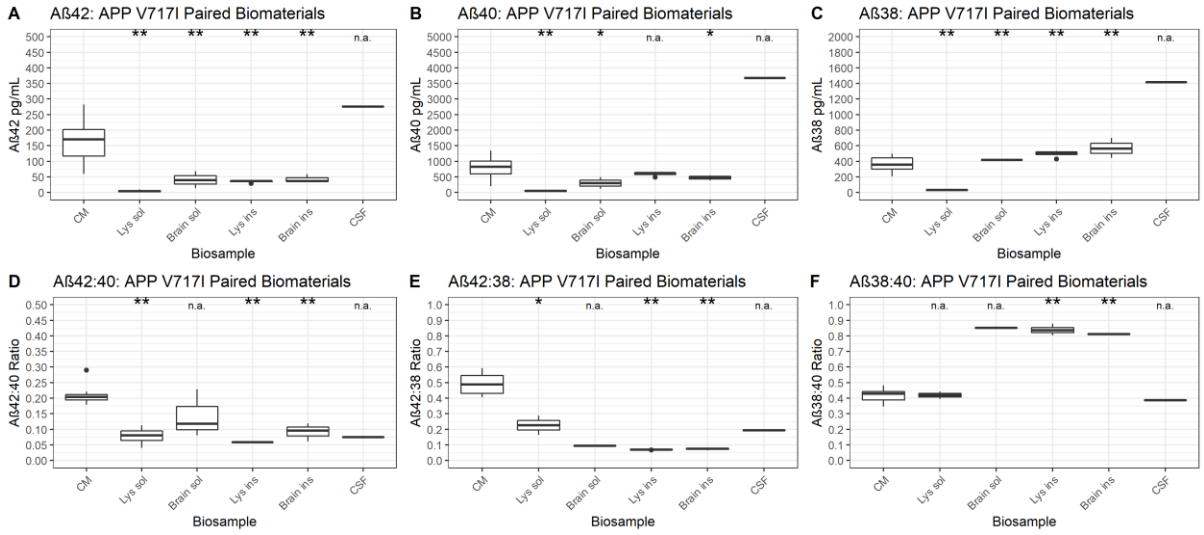

Figure 38: showing comparative A) Aβ42, B) Aβ40, C) Aβ38, D) Aβ42:40, E) Aβ42:38, and F) Aβ3840 in cell media, cell lysates, homogenised frontal cortex (brain), and lumbar CSF from the same individual with an *APP* V717I genotype. Cell lysates and brain tissue were partitioned into soluble (sol) and insoluble (ins) fractions by ultracentrifugation and solubilisation in SDS and formic acid respectively.

7.4 Discussion

The protocol for cortical neuronal differentiation devised by Shi *et al.* has been widely validated for cortical development and electrophysiology *(Gunhanlar et al., 2018; Haenseler et al., 2017; Kirwan et al., 2015; Nadadhur et al., 2017; Shi et al., 2012a)*. The neurons produced in our hands showed normal karyotype, retained fAD mutation genotype, and followed expected development into glutamatergic cortical neurons and glia of the six cortical layers, as demonstrated by expression of neuron and cortical layer specific markers. Live calcium imaging of iPSC-derived neurons demonstrated that most cortical neurons examined exhibited a single transient calcium signal in response to KCl stimulation. This is indicative of the presence of functional ion channels in the cell plasma membranes, which is further attested by PSD95-positive staining demonstrated in Figure 39. The neurons also exhibited a transient calcium signal in response to glutamate stimulation, though relatively fewer than had responded to KCl. This implies that a subpopulation of neurons had functional glutamate receptors. Additionally, very few neurons demonstrated continuous or spontaneous activity suggesting that either the cells observed did not represent a fully mature population or that the conditions of the experiment were not optimal.

There were some substantial limitations to this experiment. First was the lack of temperature and atmospheric control whilst the cultures were mounted on the microscope, and the time of exposure to these conditions during mounting and focusing the microscope on an appropriate area of interest. This also applies to the conditions of transportation between laboratories that, despite a 24 hour rehabilitation period in an incubator, were likely not ideal for culture integrity. Thus conditions did not faithfully reflect the physiological environment, nor the limited time exposed to ambient laboratory conditions during media replenishment. Secondly, glutamate response was measured after KCl treatment. Although this had the advantage of demonstrating response to both treatments in the same neurons, it is possible that conditions following KCl introduction interfered with the glutamate response. Finally, although a strength of this technique is the simultaneous examination of multiple neurons with relative efficiency, sample sizes used were small (only *APP* V717I, CTRL1 and CTRL2 were observed, and replicate n = 1-2 per line). Data is too preliminary to draw any conclusions regarding differences between fAD and control lines in this regard. However, Aβ (and particularly oligomeric structures) are thought to bind to glutamatergic neuron membranes and synaptic receptors resulting in decreased LTP, and it would be worthwhile to investigate this further.

Thus, cortical neurons produced by this protocol express proteins from each of the cortical layers, and manifest calcium signals in response to KCl and glutamate, complementing work by other

groups *(Begum et al., 2015; Gunhanlar et al., 2018; Haenseler et al., 2017; Handel et al., 2016; Kirwan et al., 2015; Nadadhur et al., 2017; Shi et al., 2012a)*, with the caveats that the population of mature glutamatergic neurons may be small even between day 80-100, and the method of calcium imaging used requires further optimising.

Turning to the production of Aβ in the cell lines cultivated, the experiments that followed Aβ and T-tau secretion longitudinally demonstrated three important points regarding study of Aβ and tau in neuronal culture media. First, the strong correlation of T-tau with LDH suggests that a significant proportion of the quantities of T-tau present is due to cell death rather than physiological secretion. In contrast there was no correlation of LDH with any of the Aβ peptides examined, potentially due to rapid and constitutive secretion of Aβ into the extracellular space by healthy cells. This suggests that acute levels of cell death are not likely to greatly confound interpretation of peptide concentration.

The second point addresses the use of ratios to overcome inherent variability in biomarker concentrations between different lines and inductions. Culture density, linked with but distinct from cell death, is a challenging variable to control when comparing samples by quantitative characteristics. We observed that, although Aβ peptide concentrations were relatively consistent over short periods of time within a given induction, over a longer time course and between different inductions variability was such that differences between lines were difficult to confidently resolve. As cells were free to differentiate and die for 65-165 days prior to media collection, whilst collection methods were otherwise well standardised, we suspected differences in culture density to be a major source of this variability. As the nature of APP proteolysis means that concentrations of Aβ peptides are derived from the same source and are to some extent dependent, normalising Aβ peptide measurements in ratio to other peptides greatly reduced variability in temporal and replicate parameters and revealed genotype-specific patterns. In contrast, ratios of Aβ with tau were less useful. Although ratios of Aβ38/40/42 produced very consistent results, measurements involving Aβ43 were more variable. This could be due to differences in assay performance as Aβ43 was analysed by ELISA rather than as part of the ECL triplex. Alternatively, it has been shown that neurons derived from the protocol used produce increasing quantities of longer Aβ peptides as they mature over 100 days post-induction *(Bergstrom et al., 2016)*. It is possible that whilst production of peptides up to Aβ42 may stabilise within this period, Aβ43 and longer fragments could take more time resulting in the generally increased Aβ43:40 ratio observed at 200 days relative to 100 days.

The third point concerns the nature of genotype-specific patterns. Both *APP* V717I and *PSEN1* int4del cell lines expressed greater Aβ42:40 than non-AD control lines, a finding which complements a fast solidifying body of evidence in the literature in regard to the effect of fAD mutations on APP processing *(Mahairaki et al., 2014; Moore et al., 2015; Ochalek et al., 2017; Sproul et al., 2014; Sun et al., 2017; Woodruff et al., 2013)*. The Aβ42:38 ratio is a potential readout of γ-secretase carboxypeptidase-like cleavage efficiency *(Szaruga et al., 2015)* and the Aβ38:40 has been used to compare the theorised Aβ49 versus Aβ48 dependent pathways *(Takami et al., 2009)*. The ratios Aβ42:38, Aβ38:40 and Aβ43:40 showed qualitative differences between *APP* V717I and *PSEN1* int4del cell lines, hinting at potentially disease and therapeutically relevant mechanisms underlying production of different Aβ peptides. For example, *PSEN1* int4del cells appeared to favour the production of longer Aβ peptides over shorter fragments. This was not the case for *APP* V717I, where difference from non-AD control lines was only observed in the between Aβ42 and Aβ38 in relation to Aβ40. These data fit conceptually with two emerging hypothesis of Aβ production: the tripeptide hypothesis of APP proteolysis by γ-secretase *(Takami et al., 2009)*, and the partial loss of function hypothesis of γ-secretase mutation *(Szaruga et al., 2017)*. These are concepts that are explored further in Chapter 9.

Thus, in cultured cortical neurons Aβ production ratios appear tightly regulated within a narrow physiological range. This remains stable over substantial periods of time once cells have reached maturity around 100 days post-induction. The use of ratios in analysis overcomes experimental variability, allowing meaningful comparisons between fAD lines.

It is important to note that neither 2D nor 3D organoid culture systems developed Aβ plaques. High Aβ production (nM range concentration) and\or low Aβ clearance are prerequisite for the formation of these structures *in vitro*. Others have successfully generated cultures with Aβ plaques using methods of Aβ overexpression, such as co-expression of *APP* and *PSEN1* mutations *(Choi et al., 2014)*. The neurons produced by our model do not produce excessive quantities of Aβ overall, but alter the quality of production. Additionally, the nature of media replacement precludes Aβ accumulation sufficient to form large deposits *(Choi et al., 2015)*. However, whilst the presence of plaque structures are a defining AD phenotype, the cells of our model are advantaged in that they represent a real human fAD genotype enabling the collection of highly relevant data regarding the biological effect of these mutations on the quantitative and qualitative production of different Aβ peptides.

Comparisons of iPSC-derived neurons with paired tissues and clinically relevant fluids are extremely rare. Analysis of Aβ peptide ratios in cell media, cell lysates, frontal cortex brain homogenate, lumbar CSF revealed that cell media and soluble fraction brain homogenate contained similar ratios of Aβ42:40, whilst the ratio in CSF was noticeably lower. Additionally, Aβ42:38 was also lower in CSF than cell media, whilst Aβ38:40 was highly comparable. Reduced CSF Aβ42 is considered to reflect preferential deposition of Aβ42 in amyloid plaques and/or peptide specific clearance disruption *(Blennow, 2017)*, whilst Aβ38 and Aβ40 are not typically found altered in AD CSF. Indeed, dense-core and diffuse plaques were observed by immunohistochemistry in post-mortem brain of this individual, and together these preliminary results are consistent with Aβ production and clearance in fAD. Aβ38 was difficult to detect in the soluble brain homogenate fraction, with only one sample producing detectible signal. In this case soluble fraction ratios of Aβ42:38 and Aβ38:40 mirrored those of the insoluble fraction, but not cell media, conflicting with the hypothesis that cell media models the soluble brain environment. More work is needed to characterise the solubility of Aβ peptides in this context.

Finally, results from cultured neuron lysates, representing intracellular and membrane bound Aβ, show depletion of Aβ42 relative to Aβ38 and Aβ40, suggesting an intracellular bias against Aβ42 retention. The two fractions differ primarily in that relative proportions of Aβ38 were higher in the insoluble fraction. Study of intracellular Aβ has been problematic due to antibody cross-reactivity with full length APP and dependence on non-human or non-neuronal model systems *(LaFerla et al., 2007)*. Despite this, it has been proposed that accumulation of Aβ in neurons forms the seeding templates that precipitate the formation of amyloid plaques when the cell dies and releases its Aβ into the extracellular space *(D'Andrea and Nagele, 2010; LaFerla et al., 2007)*. This has been described in human post-mortem entorhinal cortex and hippocampus *(D'Andrea et al., 2001)*, and a dynamic relationship between intra-cellular and extracellular Aβ has been noted *(Oddo et al., 2004, 2006)*. The results presented here do not support the accumulation of intracellular Aβ42 in developmentally early iPSC-derived neurons, but may direct attention toward intracellular Aβ38. Further work is required to verify these results and understand the dynamics of Aβ, particularly Aβ38, in these sample types.

7.5 Chapter summary

Characterisation experiments demonstrated the genetic integrity, appropriate cortex-genesis, and mature functionality of the cortical neurons generated for study. Furthermore, a method of using Aβ

peptide ratios was established which normalised for differences between different inductions enabling reliable interpretation of Aβ secretion patterns from various fAD mutation lines. Finally, comparison of paired cell media, cell lysates, and lumbar CSF from the same individual revealed intriguing Aβ profiles that support notions of Aβ production and clearance in fAD.

7.5.1 Publications arising from this work

Charles Arber[1§], Jamie Toombs[1,2§], Christopher C. Lovejoy[1], Natalie Ryan[3], Ross W. Paterson[3], Nanet Willumsen[1,4], Eleni Gkanatsiou[5], Erik Portelius[5,6], Kaj Blennow[5,6], Amanda Heslegrave[1,2], Jonathan M. Schott[3], John Hardy[1,2], Tammaryn Lashley[4], Nick C. Fox[3], Henrik Zetterberg[1,2,5,6±] and Selina Wray[1±] Familial Alzheimer's disease patient-derived neurons reveal distinct mutation-specific effects on amyloid-beta. Mol Psychiatry. 2019

8 Aβ production in fAD mutations

8.1 Introduction

Having characterised genotypic, phenotypic and functional aspects of the cell model, and identified interesting mutation-specific patterns in Aβ peptide production ratios, the next step was to examine a wider array of Aβ peptides in a larger number of fAD mutations. We expanded our investigation to include additional *PSEN1* fAD iPSC lines and a sample set that included paired neurons generated by 2D adherent culture and 3D cerebral organoids. Given the variability in concentrations between inductions and the corresponding difficulty of interpreting data, measurement of T-tau was not pursued. Very few studies have explored Aβ dynamics in both human neuronal models and at endogenous expression levels.

The fAD mutations available for study were: *APP* V717I, *PSEN1* int4del, Y115H, M139V, M146I, and R278I. This section will give a brief overview of the epidemiology, neuropathology, and known effects on Aβ production.

The *APP* V717I point mutation was first identified in two kindreds (English and American) with early onset AD (57 ± 5 years) *(Crawford et al., 1991; Goate et al., 1991)*. There are now approximately 30 known kindreds with this mutation worldwide, making it one of the most prevalent *APP* mutations. The neuropathology associated with this mutation is of extensive amyloid plaque and NFL positive lesions Crawford et al., 1991; Goate et al., 1991), although variability in non-typical features was noted as one individual from the English family also had mild amyloid angiopathy and cortical and brainstem Lewy bodies. This mutation has been observed to increase Aβ42 production with little effect on Aβ40 *(Eckman et al., 1997; Herl et al., 2009; De Jonghe et al., 2001; Theuns et al., 2006)*. Additionally, in iPSC models, *APP* V717I has been reported to alter neuronal APP subcellular localization, Aβ38 and sAPPβ generation, and tau expression and phosphorylation *(Muratore et al., 2014)*. The cell lines used in this thesis were derived from two patients not previously described in the literature.

The *PSEN1* L113_I114insT (int4del) mutation was first identified in two English individuals in 1998 (Tysoe 1998). Subsequently, at least nine kindreds with the mutation have been identified, all from the British isles *(Janssen et al., 2003; De Jonghe et al., 1999; Rogaeva et al., 2001; Sassi et al., 2014)*. The mutation is associated with a very young onset ranging between 34-41 years. *PSEN1* int4del is

the result of the deletion of a single nucleotide (guanine) from the intron 4 splice donor site. This results in altered splicing and the production of two deletion transcripts and one insertion transcript. The deletion transcripts produce C-terminally truncated PSEN1 proteins, whilst the insertion transcript produces a full-length PSEN1 with one extra amino acid (threonine) inserted between codons 113 and 114. De Jonghe et al. have shown that only the product of the insertion transcript alters Aβ production *in vitro (De Jonghe et al., 1999),* where overall amyloidogenic processing of APP is increased (~2.5 fold) *(Szaruga et al., 2015)* and the ratio of Aβ42:40 is increased *(De Jonghe et al., 1999; Szaruga et al., 2015)*. Neuropathologically, *PSEN1* int4del presents with typical amyloid plaques and NFTs, with considerable neuronal loss in the hippocampus. The cell line used in this thesis was derived from a patient not previously described in the literature.

The *PSEN1* Y115H point mutation was first identified in a French kindred *(Campion et al., 1995)*, and subsequently a few more kindreds have been found from France *(Campion et al., 1999)*, Germany *(Finckh et al., 2005)* and Great Britain. Age of onset occurs approximately between 35-47 years if age *(Campion et al., 1995, 1999; Finckh et al., 2005)*, with a very aggressive disease course. Neuropathological presentation is of typical AD *(Finckh et al., 2005)*. This mutation is associated with an increased Aβ42:40 ratio in both extracellular and intracellular compartments *(Murayama et al., 1999; Shioi et al., 2007)*, but an overall decrease in Aβ production as well as Notch cleavage *(Sannerud et al., 2016)*, suggestive of broad γ-secretase loss of function. The cell line used in this thesis was derived from a patient not previously described in the literature.

The *PSEN1* M139V point mutation has been reported in at least nine families from the USA and Europe *(Boteva et al., 1996; Clark et al., 1995; Finckh et al., 2000; Gómez-Isla et al., 1999; Hanisch and Kolmel, 2004; Hüll et al., 1998; Hutton et al., 1996; Larner and Du Plessis, 2003; Palmer et al., 1999; Rippon et al., 2003; Sandbrink et al., 1996b; Żekanowski et al., 2003)*. Age of symptom onset occurs approximately between 32-60 years of age. Affected individuals present with atypical AD symptoms. Most cases have featured myoclonus and seizures often early in the disease course *(Finckh et al., 2000; Fox et al., 1997; Hanisch and Kolmel, 2004; Hüll et al., 1998; Kennedy et al., 1995; Sandbrink et al., 1996b)*, whilst speech disruption is also common, with a link to chromosome 14 *(Boteva et al., 1996; Kennedy et al., 1995)*. Neuropathology is consistent with AD, and formation of NFTs and neuronal loss are observed to occur relatively rapidly *(Gómez-Isla et al., 1999)*. However, atypical plaque deposition has been described in at least one case, where plaques were prevalent in the occipital cortex and cerebellum in addition to the more typical temporal, parietal, frontal cortices *(Larner and Du Plessis, 2003)*. Surprisingly, symptoms did not include myoclonus spastic

paraparesis, cerebellar signs, or gait disturbance in this case *(Larner and Du Plessis, 2003)*. Biochemically, the mutation alters the carboxypeptidase-like activity of γ-secretase *(Chávez-Gutiérrez et al., 2012)*. The consequence of this is reported to be lowered production of Aβ40 and Aβ38 and increased Aβ42 in several different cell models, *(Chávez-Gutiérrez et al., 2012; Houlden et al., 2000; Murayama et al., 1999; Shioi et al., 2007)*. The cell line used in this thesis was derived from a patient not previously described in the literature.

The *PSEN1* M146I point mutations have been identified in a small number of British and Danish kindreds *(Janssen et al., 2003; Jørgensen et al., 2008; Li et al., 2016; Lindquist et al., 2009)*. Two codon variants have been reported for the *PSEN1* M146I missense point mutation (G>C *(Lindquist et al., 2009)*, and G>A *(Janssen et al., 2003)*. The average age of symptom onset range is given as 38-57 years of age *(Jørgensen et al., 2008; Lindquist et al., 2009)*. Neuropathology information is limited, but the mutation appears to manifest a typical EOAD phenotype *(Goate et al., 1991; Lindquist et al., 2009)*. *In vitro* cortical neurons of this genotype exhibit increased Aβ42/Aβ40 ratios *(Moore et al., 2015)*, as well as size, number and clustering of lysosomes, associated with increased concentrations of LAMP1 and a decrease in bidirectional lysosome motility *(Hung and Livesey, 2018)*. The cell line used in this thesis was derived from a patient not previously described in the literature.

The *PSEN1* R278I point mutation was first identified in two members of a kindred with the onset of atypical AD symptoms occurring between 48-51 years of age *(Godbolt et al., 2004)*. Symptoms were characterized by early language impairment, and relative preservation of episodic memory, MRI showed white matter lesions, but minimal atrophy, and clinical criteria for AD was not met. This mutation has been observed to impair the maturation of PSEN1, with decreased concentrations of the N-terminal fragment (NTF) and C-terminal fragment (CTF) *(Saito et al., 2011)*. *In vitro* studies have shown that the carboxypeptidase-like activity of γ-secretase is uniquely impaired, resulting in favoured production of longer Aβ peptides *(Szaruga et al., 2015)*, especially Aβ43 *(Nakaya et al., 2005; Saito et al., 2011)* Some evidence suggests that AICD production may also be slightly impaired *(Szaruga et al., 2015)*. The cell line used in this thesis was derived from a patient not previously described in the literature.

This selection of fAD mutations represents a relatively large number in comparison with other studies that have investigated AD biomarkers in fAD patient cell lines, and reflects a mix of AD causing genotypes, with a weighting toward *PSEN1* mutations.

8.1.1 Contributions

The author designed the media collection protocol, cultured 2D iPSC neurons, collected cell media, cell lysates, conducted all immunoassays, conducted all statistical analyses and co-wrote the scientific report alongside C. Arber. Culture of 3D organoids and collection of media and lysates of these was conducted by C. Arber and C. Lovejoy. C. Arber conducted Western blotting, qPCR, and immunocytochemistry. E. Portelius and E. Gkanatsiou conducted IP MALDI TOF/TOF.

Study conception: S. Wray, H. Zetterberg, JM. Schott, N. Fox. NS. Ryan.
Sample collection: The author, C. Arber, C. Lovejoy, N. Willumsen.
Experiment design: The author, C. Arber, S. Wray.
Experiment: The author, C. Arber, E. Gkanatsiou, E. Portelius.
Analysis: The author, C. Arber.
Scientific report: C. Arber, The author, C. Lovejoy, NS. Ryan, RW. Paterson, N. Willumsen, E. Gkanatsiou, E. Portelius, K. Blennow, A. Heslegrave, JM. Schott, J. Hardy, T. Lashley, H. Zetterberg, S. Wray.

8.2 Materials and methods

8.2.1 Samples

iPSC-derived cortical neurons used in these experiments were cultured for 100 days post-induction as described in Section 2.5. The cell lines used consisted of five control lines (CTRL1-4 and SHEF6), two APP V717I patient lines (*APP* V717I-1 and V717I-2), and five *PSEN1* mutations with one patient line each (*PSEN1* int4del, Y115H, M139V, M146I, R278I). *APP* V717I-1 and *PSEN1* int4del each had two clones (*APP* V717I-1.1 and *APP* V717I-1.3, and *PSEN1* int4del.4, *PSEN1* int4del.6). Information for each cell line can be found in Table 5. 2D cell cultures were by myself and Dr C. Arber, and as 3D cerebral organoids by Dr C. Arber and Mr C. Lovejoy.

8.2.2 Experimental methods

Cell lines were characterised for neuronal markers by immunocytochemistry as described in Section 2.11 and qPCR as described in Section 2.13. Primers used for qPCR are shown in Table 7.

Cell media (N2B27) was collected from each well after 48 hours of incubation, centrifuged and aliquoted as described in Section 2.8. Immediately after the aspiration of media, cell lysates and RNA were collected from representative wells as described in Sections 2.9 and 2.10 respectively. At least

three inductions, representing biological replicates, were generated for each cell line. Cell media samples were analysed for Aβ38, Aβ40, and Aβ42 were measured by triplex MSD ECL immunoassay (Section 2.2.2). Analysis for the full spectrum of Aβ peptides was conducted by immunoprecipitation MADLI TOF/TOF by Dr E. Gkanatsiou and Dr E. Portelius (Section 2.18).

APP expression, generation of APP proteolysis products, and PSEN1 protein expression in the cell lines were investigated by western blot (Section 2.16).

8.2.3 Statistical analysis

The use of seven fAD lines, together with five controls, represents sufficient statistical power for a false discovery rate of 0.2 *(Germain and Testa, 2017)*. Data normality was assessed by histogram, qq-plot and Shapiro-Wilk test. Spearman's rank correlation coefficient was conducted to assess the relationship between Aβ ratios and age of onset, and Non-AD and fAD line Aβ peptide spectra. Tests for significance were conducted by Mann Whitney U. Analysis was conducted in R, and graphs were composed using the ggplot2 package.

8.2.4 Assay Variation

Percent CV of intra- and inter-assay variability respectively were Aβ38 (4.7%, 13.3%), Aβ40 (5.9%, 9.4%), Aβ42 (4.7%, 12.6%), Aβ43 (7.4%, 13.2%), T-tau (7.9%, 12.6%), calculated from concentrations of an internal control CSF sample. Intra- and inter-assay CV was calculated according to ISO 5725-2 standards *(British Standards Institution, 1994)*.

8.3 Results

8.3.1 Comparison of 2D and 3D model neurons

Characterisation of iPSCs from both 2D and 3D cell lines confirmed expression of pluripotency markers (NANOG and SSEA4) in stem cell cultures (Figure 39A). 2D cultures expressed forebrain regional marker FOXG1 and radial glial marker pVIM at day 25 post-induction and expression of synaptic marker PSD95, cortical layer V marker CTIP2 and pan-neuronal marker TUJ1 at day 100 post-induction (Figure 39A). Cerebral organoids were also confirmed to display forebrain specification via FOXG1 and neuronal commitment via TUJ1 at day 40 post induction (Figure 39A). It was not possible to maintain *PSEN1* M139V to day 100 in 3D culture, and so 3D cell media is not represented in this analysis. Furthermore, Expression levels of cortical layer markers *TBR1* and *CTIP2* and neuronal marker *TUBB3* were quantified by qPCR for 2D lines (Figure 39B). Comparison of APP

protein expression between 2D, 3D and post-mortem tissue by western blotting, showed comparable expression of APP, with 3D organoids showing increased variability likely due to the increased cellular diversity and heterogeneity of this system. (Figure 39C).

Figure 38: Immunocytochemistry and protein expression in 2D and 3D cell lines

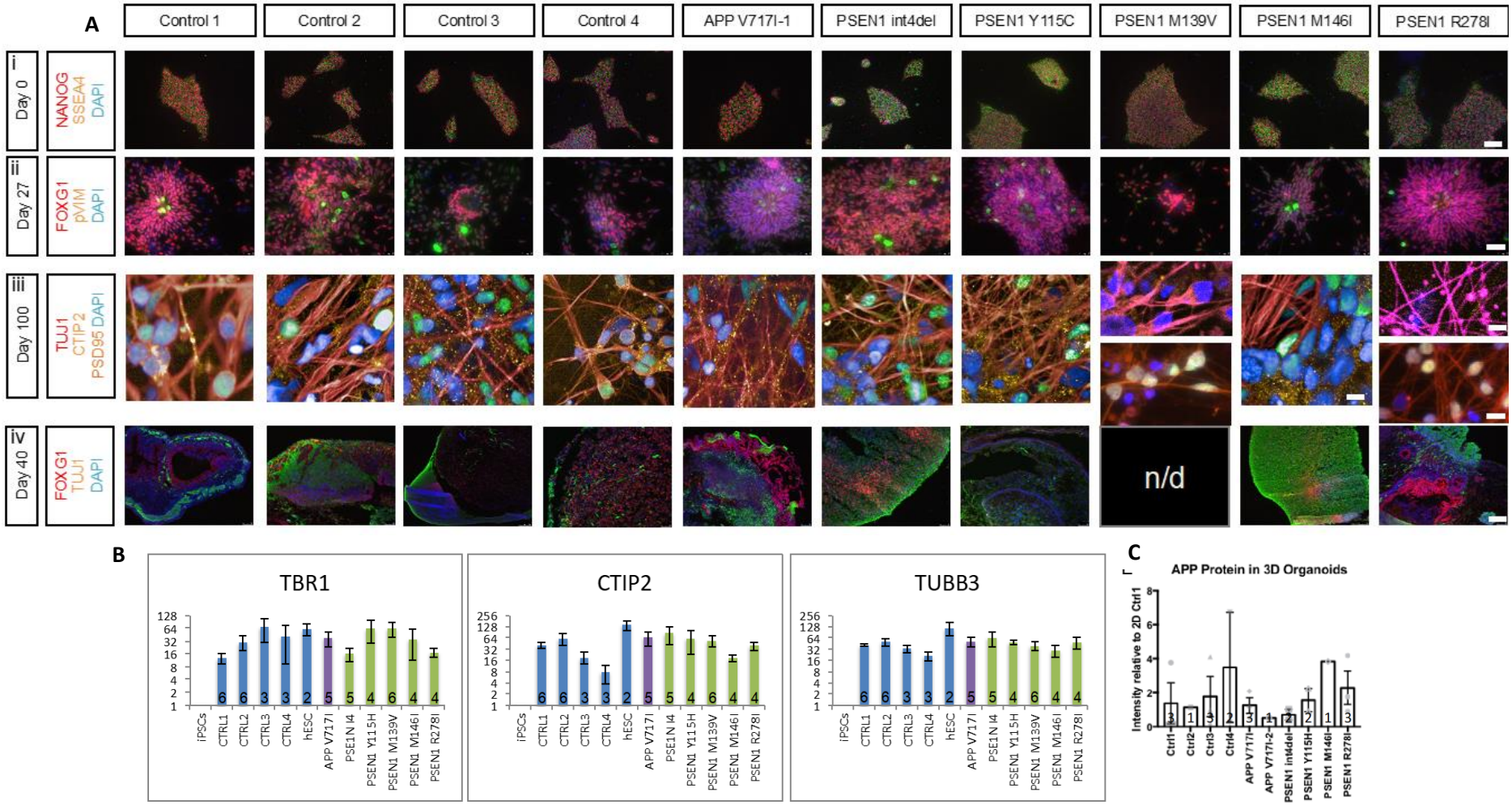

Figure 39: A) Showing immunocytochemistry for each line used in comparison of an expanded set of Aβ peptide ratios between fAD genotypes and controls. NANOG and SSEA4 are markers of pluripotency, and denote undifferentiated stem cells. FOXG1 is a transcription factors that promote proliferation of the neuroectoderm and phosphor vimentin (pVIM) is a marker of mitotic m-phase radial glia. PSD95 is a synaptic protein of glutamatergic neurons. CTIP2 is a marker of layer V-III cortical neurons, and TUJ1 is an axonal marker. DAPI is a marker of nuclear protein. B) Expression levels of cortical layer markers TBR1 and CTIP2 and neuronal marker TUBB3 quantified by qPCR. Number of independent neural inductions for each line is displayed in the histogram. C) Relative quantities of APP in 3D versus 2D cultures for each line. Numbers within histogram bars represent sample n. Work in 2D conducted by Dr C. Arber. Work in 3D conducted by Mr. C. Lovejoy. Images produced by Dr. C. Arber and used with permission.

8.3.2 Mutation-specific effects on APP cleavage, highlighting relative increments in Aβ42 and Aβ43

When cell media was analysed for Aβ peptides by ECL and ELISA, 3D cultures closely followed the results of their 2D counterparts in the fAD lines, although greater variability between 3D and 2D control lines was observed. In both 2D and 3D cultures, Aβ42:40 was increased in all fAD mutations, to approximately twice that of controls for most fAD lines (Figure 41A). The *PSEN1* R278I mutation displayed the smallest increase in Aβ42:40.

Aβ42:38, a putative biomarker for γ-secretase cleavage efficiency, was significantly increased in all *PSEN1* mutation lines versus non-AD (Figure 41B). Specifically, *PSEN1* int4del and *PSEN1* Y115H demonstrated similar Aβ42:38, whereas *PSEN1* M139V, *PSEN1* M146I and *PSEN1* R278I exhibited decreasing changes versus non-AD. *APP* V717I mutant neurons also showed a small, yet significant, increase in Aβ42:38.

Aβ38:40 is a proposed marker of γ-secretase cleavage pathway. Interestingly, this ratio was able to distinguish neuronal lines based on mutation status (Figures 41C and 35C). Compared to non-AD cells Aβ38:40 was significantly increased in *APP* V717I, whilst in *PSEN1* mutations the ratio was unchanged versus non-AD in *PSEN1* Y115H, *PSEN1* M146I and *PSEN1* R278I, and decreased in *PSEN1* int4del, *PSEN1* M139V. Once more results from 3D cultures closely aligned with those of 2D.

Ratios of Aβ43 to other Aβ peptides have rarely been described in the literature. Results showed that in comparison to non-AD, all *PSEN1* mutations, except *PSEN1* M146I, demonstrated increased Aβ43:40 (Figure 41D). The magnitude of increase in *PSEN1* R278I is particularly noteworthy given the comparatively small degree of change in the Aβ42:40 ratio we observed in this line, and the previous reports of elevated Aβ43 in this mutation *(Saito et al., 2011; Veugelen et al., 2016)*. *APP* V717I was not observed to differ from non-AD. Results for Aβ42:43 and Aβ38:43 generally mirror results for Aβ38:40. These ratios compare products on the two cleavage product pathways (Figure 41C, E and F, see also Figure 3) where ratios were raised in *APP* V717I versus non-AD. This was not the case for *PSEN1* mutations, where changes in Aβ production pathway shift are not supported (Figure 41C, E and F).

When Aβ peptide ratios were compared with age of onset for each genotype, the Aβ42:40 ratio showed negative correlation (Figure 40), depicting younger at of onset with higher Aβ42:40 ratios. Aβ43:40 showed a weak positive correlation (Figure 40), suggesting that Aβ43 is less well correlated

to age of onset. Combining Aβ42 and Aβ43 relative to Aβ40 and Aβ38 did not enhance correlation, suggesting Aβ42 shows the strongest link with age of onset.

In summary, our panel of fAD iPSC-derived neurons display a series of mutation-specific alterations in the relative production of different Aβ peptides, highlighting varied size and scale of changes in γ-secretase endopeptidase and carboxypeptidase-like cleavage of APP. The *APP* V717I mutation specifically alters the endopeptidase cleavage pathway, with Aβ38:40 and Aβ42:43 results reinforcing the proposed shift in product lineages *(Chávez-Gutiérrez et al., 2012)*. *PSEN1* mutations lead to higher relative proportions of either Aβ42 or Aβ43 via reduced carboxypeptidase-like activity, and may implicate a role for Aβ43 in AD pathogenesis.

Figure 39: Correlation between age of onset and Aβ ratios in fAD neurons

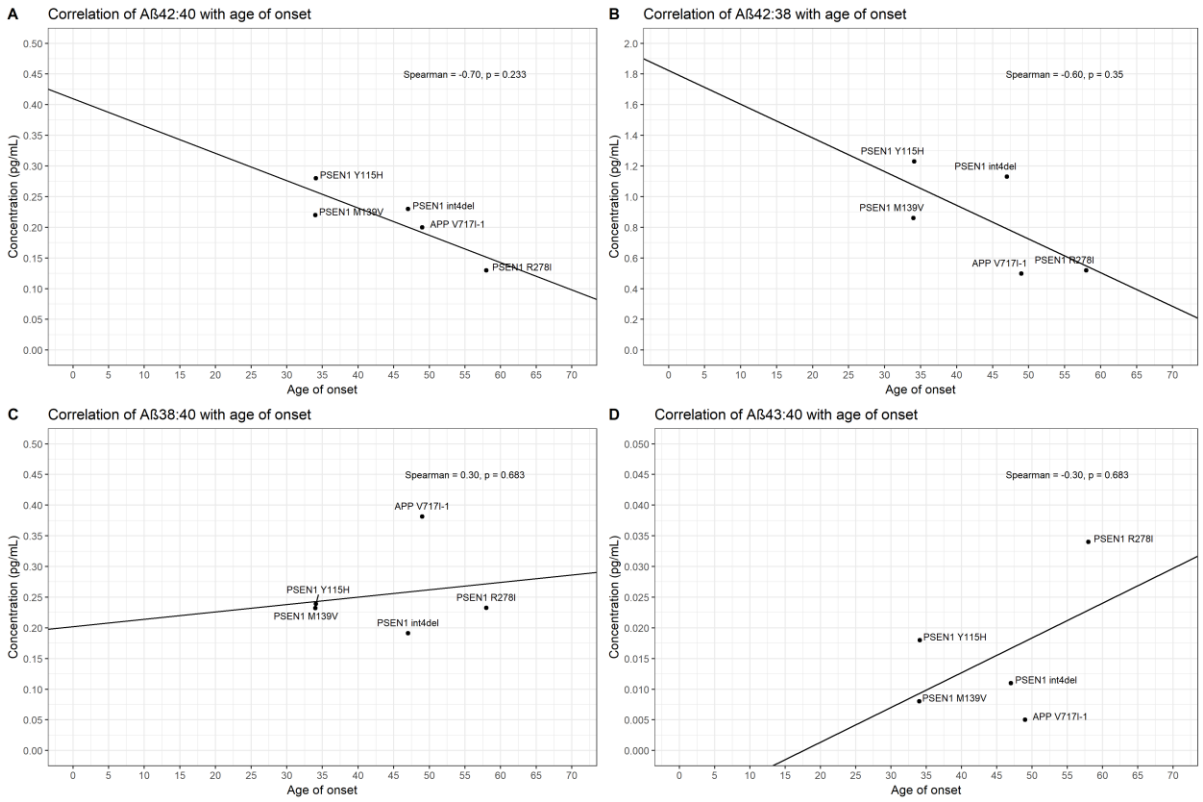

Figure 40: Analysis of age of onset correlation to Aβ ratios and Aβ secretome analysis by mass spectrometry infers mutation-specific differences of β/α/γ-secretase relative contribution. A-D) Mean ratio data for Aβ42:40 and Aβ43:40 were correlated with age of onset for each genotype. No statistical correlation is achieved with this sample size.

Figure 40: fAD neurons display mutation-specific Aβ profile differences

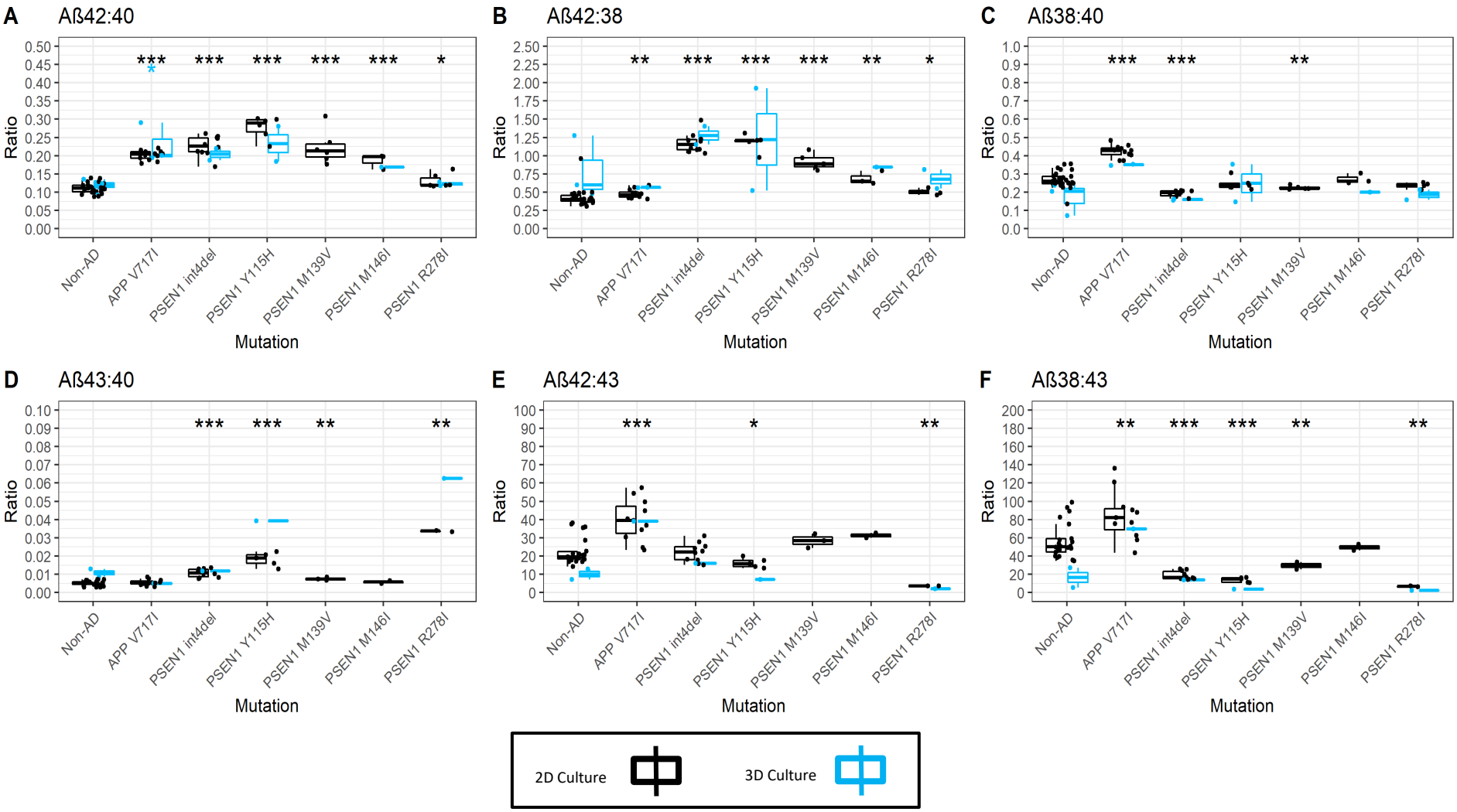

Figure 41: Conditioned media was collected at 100 days post-neuronal induction for analysis. Results from the ratios A) Aβ42:40, B) Aβ42:38, C) Aβ38:40, D) Aβ43:40, E) Aβ42:43, F) Aβ38:43 are displayed. 2D data was generated from multiple inductions per line, specifically APP V717I-1 clone 1 (n=7), APP V717I-1 clone 3 (n=3), APP V717I-2 (n=2), PSEN1 Int4del clone 4 (n=5), PSEN1 Int4del clone 6 (n=5), PSEN1 Y115H (n=6), PSEN1 M139V (n=6), PSEN1 M146I (n=3), PSEN1 R278I (n=6). Control data was generated from the following inductions: Ctrl 1 (n=5), Ctrl2 (n=6), Ctrl3 (n=7), Ctrl4 (n=6), and SHEF6 (n=4). 3D data consisted of two inductions of each line, except APP V717I-1 clone 3, SHEF6, and M139V for which no data is available. Significance levels: * = <0.05, ** = <0.01, *** = <0.001.

8.3.3 Mass spectrometry highlights varied reduction in γ-secretase activity relative to other secretases as a result of fAD mutations

To investigate the secretome of Aβ peptides and to infer different activities of the α-, β- and γ-secretases, MALDI TOF/TOF mass spectrometry was performed on Aβ peptides immunoprecipitated from 2D iPSC-neuronal supernatants. Given that Aβ profiles were consistent in 2D and 3D cultures, only media from 2D cultures were analysed. As demonstrated in Figure 35, using ratios of Aβ peptides to Aβ40 acts as an internal normalisation to represent the data, and therefore was utilised to probe the mass spectrometry data.

Mass spectrometry confirmed the broad findings for relative amounts of Aβ38/40/42 generated using the MSD immunoassay previously described, although Aβ43 was not detectable with this method of analysis. Aβ42:40 was significantly raised in all fAD mutations except *PSEN1* R278I (Figure 42A), which had been the mutation where this ratio was least altered in the immunoassay. Aβ42:38 was significantly increased versus non-AD in all *PSEN1* mutations except *PSEN1* Y115H (although a clear tendency for increase, proportional to the immunoassay results, was observed) and R278I where the level of significance in the immunoassay had once again been weak (Figure 42B). Aβ38:40 was significantly increased in the *APP* V717I line versus non-AD, unchanged versus non-AD in *PSEN1* Y115H, *PSEN1* M146I and *PSEN1* R278I, and decreased in *PSEN1* int4del and M139V (Figure 42C), mirroring the immunoassay results.

Moving beyond Aβ38/40/42, mass spectrometry highlighted several interesting patterns among less well studied peptides. Aβ39 ratios displayed a similar, though not identical, pattern to Aβ38 whereby specifically *APP* V717I showed increased Aβ39:40 relative to non-AD and *PSEN1* mutant neurons (Figure 42D). Aβ38 is often used as the final fragment in the Aβ48>45>42>38 pathway, although Aβ39 is reported as an alternative fragment generated from Aβ42 *(Matsumura et al., 2014)*. Aβ42:39 was found to be raised significantly in a subset of *PSEN1* mutant neurons as well as *APP* V717I versus non-AD (Figure 42E), complementing findings of Aβ42:38 by MSD.

No differences in Aβ37:40 were observed between non-AD and any fAD mutation (Figure 42F), indicating that the disease mechanism that results in impaired γ-secretase carboxypeptidase-like efficiency mainly affects the processing of longer Aβ peptides, which is in line with the proposed mechanistic model for fAD (Szaruga *et al*., 2017).

Relative to the γ-secretase-dependent peptide Aβ40, *PSEN1* int4del neurons exhibited significantly raised levels of BACE1-BACE2 products (Aβ19/20) and BACE1-BACE1/BACE2 products (Aβ34) (Figure 42G-I) (Yan *et al*., 2001; Shi *et al*., 2003; Bergstrom *et al*., 2016), as well as a non-significant skew toward increased α- secretase products (Aβ15/16) (Figure 42K-L), and Aβ17, attributed to either γ-secretase cleavage *(Portelius et al., 2011)* or endothelin-converting enzyme cleavage *(Eckman et al., 2001)* (Figure 42J). Similarly, *PSEN1* Y115H significantly increased BACE1-α-secretase products and displayed a tendency for increased BACE1-BACE2 products (Figure 42G-L). These effects were not evident in other fAD neurons, which displayed grossly similar secretomes to non-AD samples (Figure 41).

Figure 41: Mutation specific differences of Aβ secretomes from multiple proteolytic pathways

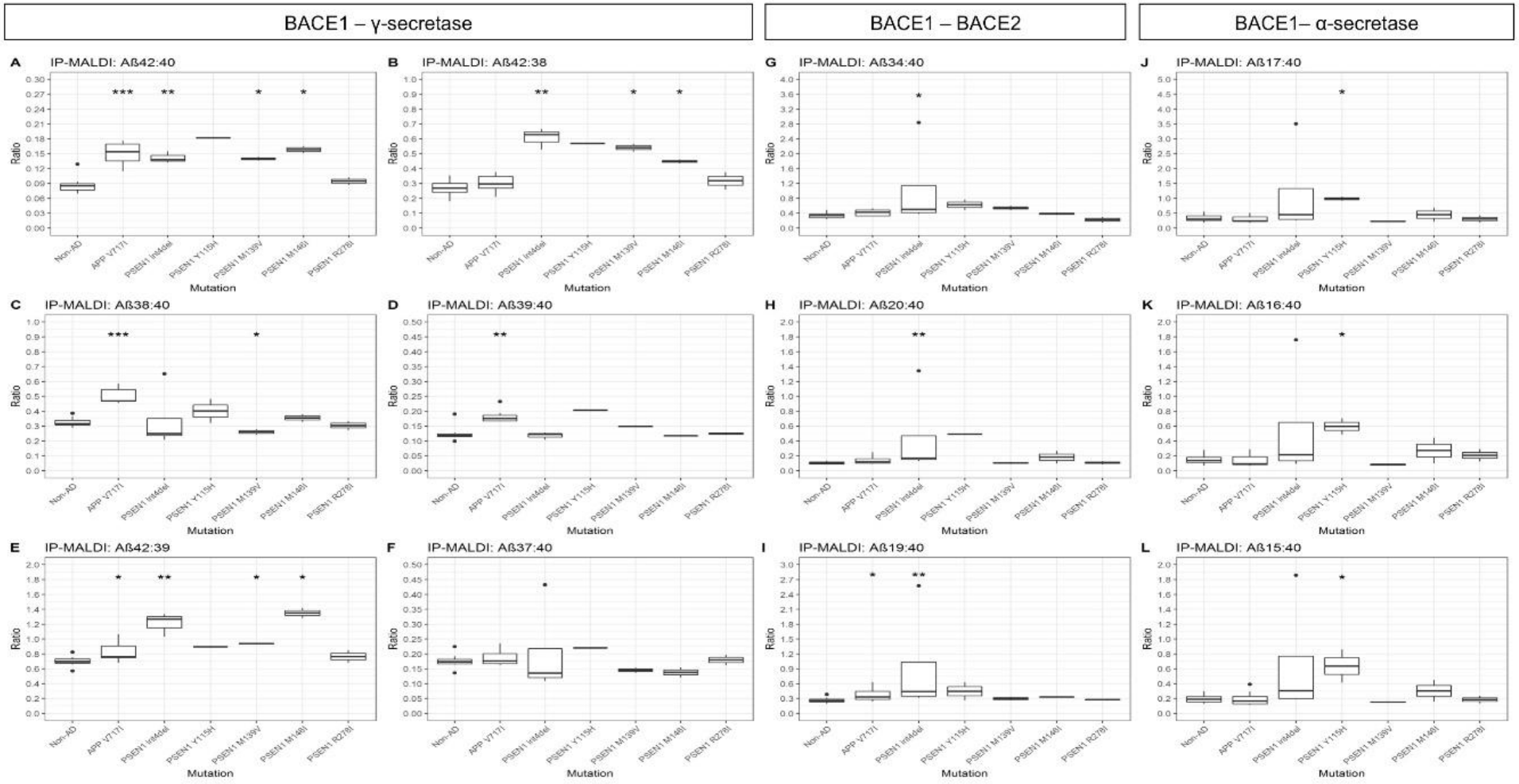

Figure 42: Results from mass spectrometric analysis of cell media for Aβ peptides generated by A-F) BACE1 and γ-secretase activity G-I), BACE1 and BACE2 activity, and J-L) BACE1 and α-secretase activity normalised as ratios. Mean data was generated at day 100 from multiple independent inductions per line, specifically non-AD (n=10) consisting of pooled data of Ctrl1 (n=2), Ctrl2 (n=2), Ctrl3 (n=2), Ctrl4 (n=2) and Shef6 (n=2). fAD data was generated from the following, APP V717I-1 clone 1 (n=5), APP V717I-1 clone 3 (n=2), PSEN1 int4del clone 4 (n=2), PSEN1 int4del clone 6 (n=2), PSEN1 Y115H (n=2), PSEN1 M139V (n=2), PSEN1 M146I (n=2) and PSEN1 R278I (n=2). Significance levels: * = <0.05, ** = <0.01, *** = <0.001.

Figure 42: Mass spectrometry analysis of N-terminally truncated Aβ peptides

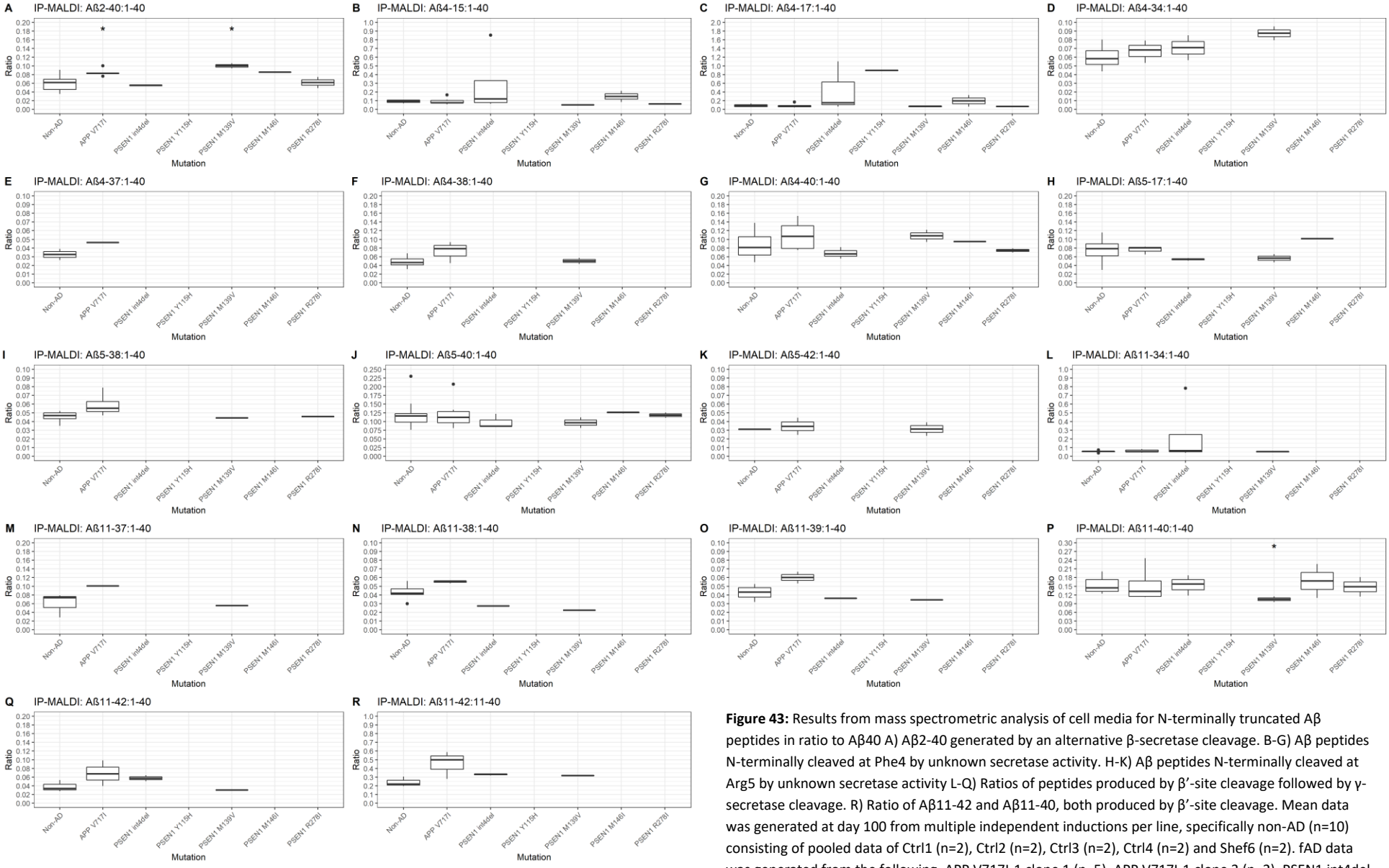

Figure 43: Results from mass spectrometric analysis of cell media for N-terminally truncated Aβ peptides in ratio to Aβ40 A) Aβ2-40 generated by an alternative β-secretase cleavage. B-G) Aβ peptides N-terminally cleaved at Phe4 by unknown secretase activity. H-K) Aβ peptides N-terminally cleaved at Arg5 by unknown secretase activity L-Q) Ratios of peptides produced by β'-site cleavage followed by γ-secretase cleavage. R) Ratio of Aβ11-42 and Aβ11-40, both produced by β'-site cleavage. Mean data was generated at day 100 from multiple independent inductions per line, specifically non-AD (n=10) consisting of pooled data of Ctrl1 (n=2), Ctrl2 (n=2), Ctrl3 (n=2), Ctrl4 (n=2) and Shef6 (n=2). fAD data was generated from the following, APP V717I-1 clone 1 (n=5), APP V717I-1 clone 3 (n=2), PSEN1 int4del clone 4 (n=2), PSEN1 int4del clone 6 (n=2), PSEN1 Y115H (n=2), PSEN1 M139V (n=2), PSEN1 M146I (n=2) and PSEN1 R278I (n=2). Significance levels: * = <0.05, ** = <0.01, *** = <0.001.

Finally, few results for N-terminally truncated Aβ peptides ratios in fAD cell lines showed significant differences from non-AD. The exceptions to this were the *APP* V717I and *PSEN1* M139V lines, which displayed increased Aβ2-40:40 (p=0.01 and p=0.04 respectively), as well as decrease in Aβ11-40:40 (p=0.03) in *PSEN1* M139V alone (Figure 43). In general, similar mutation-specific effects were seen for Aβ11-x (generated by cleavage of APP at the Aβ' site) as for the Aβ1-x peptides that have so far been described e.g. a tendency for increased Aβ11-42:11-40 in the fAD lines were measurements were available (Figure 43R). This ratio has been previously reported to be increased in fAD, and it is speculated that such N-terminally truncated forms may be potently cytotoxic *(Siegel et al., 2017)*. Why mutations directly affecting γ-secretase activity should influence β-secretase activity is unclear and further investigation of N-terminal truncations at the Aβ' site with larger sample numbers would be desirable.

Together these data show fAD mutation-dependent effects on APP proteolysis. Mass spectrometry data reinforce the findings that *APP* mutations alter endopeptidase cleavage and that *PSEN1* mutations reduce γ-secretase carboxypeptidase-like activity and. Additionally *PSEN1* int4del and Y115H mutations appear to display a greater deficiency in γ-secretase activity than other *PSEN1*-mutation bearing neurons, shown by an increase in α- and β-secretase-dependent products relative to γ-secretase-dependent peptides.

8.3.4 γ-Secretase protein levels are altered in a subset of PSEN1 mutant lines

PSEN1 mutations have been shown to alter γ-secretase stability *(Szaruga et al., 2017; Wanngren et al., 2014)*, and so investigation of total PSEN1 protein levels was conducted using western blotting (Figure 44). Neurons harbouring the *PSEN1* mutation R278I displayed a band at 40 kDa; relating to full length PSEN1 that has not undergone autocatalysis and maturation *(Saito et al., 2011; Szaruga et al., 2015; Veugelen et al., 2016)*. As a result, this line exhibited reduced mature PSEN1 levels (Figure 44B). Despite proper maturation, the *PSEN1* mutations M139V and M146I showed a high degree of variability in PSEN1 protein levels. In a subset of neural inductions, PSEN1 levels were considerably lower than control neurons, however, this was inconsistent (Figure 44). *PSEN1* int4del and Y115H lines showed consistent PSEN1 protein levels that were similar to *APP* V717I mutant neurons and non-AD lines (Figure 44A).

Figure 43: PSEN1 protein levels are variably altered in a subset of PSEN1 mutant neurons

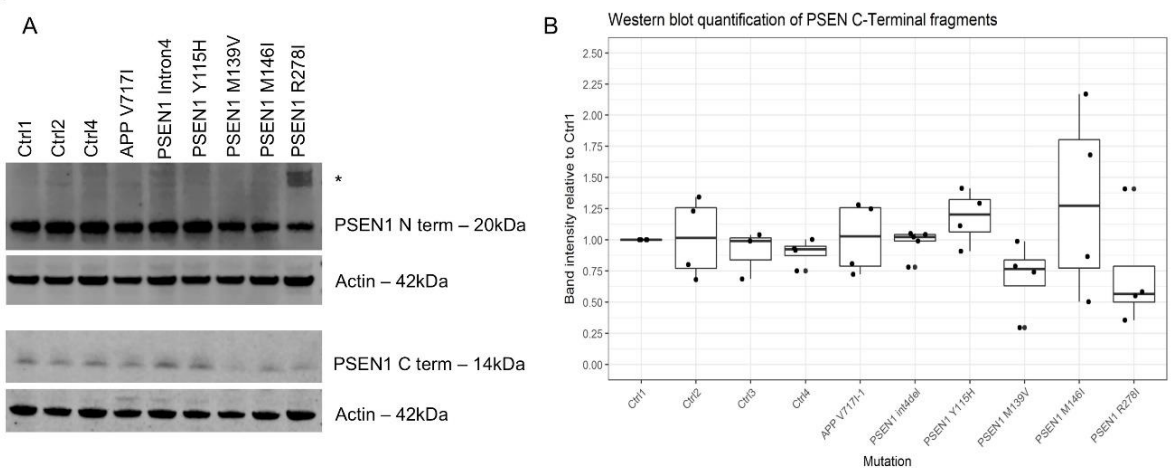

Figure 44: A) Representative western blot of 3 control neuron lysates and 6 fAD lysates. The asterisk depicts immature, full length PSEN1 protein at 40 kDa. Image produced by Dr C. Arber. B) Quantification of independent neuronal lysates, replicates are depicted by numbers within histogram.

These data suggest that mature PSEN1 protein levels are variably altered when harbouring M139V, M146I or R278I amino acid substitutions. These lines showed Aβ profiles that were most similar to control secretomes (Figure 42 and 43). The *PSEN1* mutant lines that showed greatest reduction in γ-secretase-dependent Aβ peptides, int4del and Y115H, displayed PSEN1 protein levels similar to controls. These data suggest three alternative mechanisms behind PSEN1 partial loss of function, lack of PSEN1 protein maturation, lack of PSEN1 stability and reduced catalytic activity of γ-secretase.

8.4 Discussion

In this study, we systematically investigated the production of Aβ species using *in vitro*, patient-derived stem cell models of fAD. The main finding was that different fAD mutations have qualitatively distinct effects on APP processing and Aβ production by γ-secretase; affecting APP ε-cleavage pathway and carboxypeptidase-like activity in different ways. Additionally, these results represent the first investigations into Aβ43 and smaller Aβ peptides in hiPSC neuronal models without overexpression. Finally, fAD mutation effects were shown to be consistent between 2D cortical neurons and 3D cerebral organoids.

The data presented offer a human neuronal validation of two hypotheses advocated by Chavez-Gutierrez *et al. (Chávez-Gutiérrez et al., 2012)*. Firstly, that pathogenic *APP* mutations favour increased γ-secretase Aβ48>45>42>38 ε-cleavage. The concomitant increases in Aβ38:40, Aβ42:40, and Aβ42:43 observed in *APP* V717I cells are consistent with this idea. Interestingly, this pattern extended to Aβ39:40, Aβ39 being the true tripeptide postcedent of Aβ42 *(Matsumura et al., 2014)*. Study of Aβ39 has been largely limited to models of oligomerisation *(Anand et al., 2008; Cloe et al., 2011)* and further investigation is called for.

The second tenet substantiated by our data is that mutations in *PSEN1* lead to inefficient γ-secretase carboxypeptidase activity. This predisposes neurons to the accumulation of longer Aβ fragments, demonstrated by consistently increased Aβ42:40 alongside increased Aβ42:38 in *PSEN1* mutation cell lines. The observed increase in Aβ43:40 reinforces the idea of reduced carboxypeptidase efficiency on the Aβ49>46>43>40 pathway, and it is interesting that different mutations seem to specifically effect one pathway or both. Reduced carboxypeptidase activity can be further explained by three distinct mechanisms. Firstly, reduced γ-secretase activity is suggested for *PSEN1* int4del and Y115H lines, potentially due to their location near the substrate docking domain *(Somavarapu and Kepp, 2016; Takagi-Niidome et al., 2015)*. Secondly, incomplete maturation of PSEN1 protein with R278I mutations leads to reduced levels of mature protein *(Saito et al., 2011; Veugelen et al., 2016)*. Finally, *PSEN1* M139V and M146I mutations lead to variably altered PSEN1 levels, consistent with altered protein stability *(Szaruga et al., 2017; Wanngren et al., 2014)* and supported by studies of PSEN1 abundance in brain tissue of early onset AD patients *(Mathews et al., 2000; Verdile et al., 2004)*. This variability in PSEN1 protein levels is likely to reduce the pool of functional γ-secretase enzyme. This finding demonstrates the advantage of using a more physiological model, such as iPSC-derived neurons, as protein instability could explain why the pathogenic M139V protein shows close to wild-type biochemical enzyme kinetics *(Chávez-Gutiérrez et al., 2012)*. Reduced carboxypeptidase activity is especially relevant given the recent suggestion that shorter Aβ peptides may be protective, meaning reductions in Aβ38 and Aβ40 could lie behind certain *PSEN1*-associated pathology *(Moore et al., 2018)*. It remains unclear why *PSEN1* mutations affect the carboxypeptidase-like activity of γ-secretase without an apparent change to endopeptidase activity, but can be explained due to enzyme-substrate interaction destabilisation as proposed by Szaruga et. al. (2017).

Three findings described by the data add to the complexities of the tripeptide hypothesis. Firstly, *PSEN1* int4del and M139V mutations reduce Aβ38:40, potentially suggesting alterations to the ε-

cleavage pathway. It is important to note that altered γ-secretase efficiency between the two tripeptide pathways can also explain these findings. Secondly, *APP* V717I mutations may lead to small yet significant increases in Aβ42:38 and Aβ42:39, suggesting reduced carboxypeptidase activity in these neurons. Thirdly, Aβ37:40 ratios were not significantly altered where this might have been expected in the PSEN1 lines, suggesting either that the effect of reduced γ-secretase carboxypeptidase-like efficiency may diminish beyond a focal point in the APP C-terminal sequence or that Aβ37 is γ-secretase independent.

Given the divergence of different phenotypes in different lines, the use of additional *PSEN1* and *APP* lines in future work will provide added validation and potentially highlight further details. Larger studies may make it possible to correlate the functional outcome of the different APP processing defects to clinical symptoms. For example, whether mutations pre- and post-codon 200 of *PSEN1* could predict age of onset *(Ryan et al., 2016)*. Despite limitations on patient numbers, our study represents one of the largest series of fAD lines, allowing a unique comparison of the effects of different mutations on the Aβ secretome.

8.5 Chapter summary

Five control iPSC lines and seven iPSC lines generated from fAD patients were used to investigate the effects of mutation on the Aβ secretome of human neurons generated in 2D and 3D. All fAD mutation lines demonstrated an increased Aβ42:40 ratio relative to controls, yet displayed varied signatures for ratios of Aβ43, Aβ38 and short Aβ fragments. Four qualitatively distinct mechanisms behind raised Aβ42:40 are proposed. 1) *APP* V717I mutation alters γ-secretase ε-cleavage site preference. Whereas, distinct *PSEN1* mutations lead to either 2) reduced γ-secretase activity, 3) altered protein stability or 4) reduced PSEN1 maturation, all culminating in reduced γ-secretase carboxypeptidase-like activity. These data support Aβ mechanistic tenets in a human physiological model and substantiate iPSC-neurons for modelling fAD.

8.5.1 Publications arising from this work

Charles Arber[1§], Jamie Toombs[1,2§], Christopher C. Lovejoy[1], Natalie Ryan[3], Ross W. Paterson[3], Nanet Willumsen[1,4], Eleni Gkanatsiou[5], Erik Portelius[5,6], Kaj Blennow[5,6], Amanda Heslegrave[1,2], Jonathan M. Schott[3], John Hardy[1,2], Tammaryn Lashley[4], Nick C. Fox[3], Henrik Zetterberg[1,2,5,6±] and Selina Wray[1±] Familial Alzheimer's disease patient-derived neurons reveal distinct mutation-specific effects on amyloid-beta. Mol Psychiatry. 2019.

9 Discussion

9.1 General overview

The first chapter introduced the pathology of AD with focus on the molecular biology of Aβ. Aβ, alongside tau, has served as an important biomarker for the clinical diagnosis of AD, and the tenets of the amyloid cascade hypothesis have played a major role in guiding therapeutic development over the last two decades. Ultimately, drug trial successes have been few, and whilst progress has been made in biomarker-based identification of early AD pathology, issues in pre-analytical standardisation hold this methodology back from its potential. The overarching aim of this thesis was to improve the utility of Aβ as a biomarker of AD by identifying pre-analytical confounding factors affecting its measurement and investigating the production of different Aβ peptides in an *in vitro* fAD model.

Taken together, work identified Aβ peptide surface absorption as a major pre-analytical confounding factor, specifically in terms of sample storage volume and the transfer of sample between different vessels. Aβ42 was particularly vulnerable to these variables, and the different propensities for different Aβ peptides to bind to certain surface materials was a key finding with important implications for clinical adoption of Aβ ratios. Strategies to mitigate these confounding factors identified the addition of 0.05% Tween 20 to samples and the standardisation of surface exposure as likely to be effective, with the latter being recommended. In the second phase of work, well-established iPSC-derived glutamatergic cortical neuron models of fAD were used to investigate Aβ peptide production. Results identified the use of Aβ ratios as a strategy for overcoming between-batch variability and assisting data interpretation. In a cohort of one of the largest range of fAD mutations to date, different fAD genotypes were shown to produce distinct ratios of Aβ peptides, supporting a growing understanding of APP proteolysis mechanisms that will inform dissection of past drug failure and future drug development.

This chapter will summarise and discuss the data for each of the thesis aims.

9.2 Aim 1: Identify novel confounding factors in the storage and handling of CSF and cell culture media that may artificially alter detectable Aβ peptides

In this thesis the following pre-analytical confounding factors were investigated in human lumbar CSF and cell culture media: sample storage volume, sample transfer between storage tubes, sample transfer through a manometer and pipette tips, sample pre-storage temperature, and sample transport method.

The greatest effects, and therefore those most likely to bias Aβ biomarker measurement, were observed in factors where surface exposure was a common element. Prior to these experiments the effect of surface exposure on measurable Aβ concentration had received little attention beyond the impact of storage vessel material differences *(Bjerke et al., 2010; Kofanova et al., 2015; Lewczuk et al., 2006a; Perret-Liaudet et al., 2012b, 2012a)*. Results showed that Aβ42 concentration decreased by approximately 1pg/mL for every 10µL decrease in sample storage volume in polypropylene tubes, potentially sufficient to mislead clinical diagnosis if Aβ42 concentrations border AD diagnostic cut-points or if low volume samples were to be used. Furthermore, transfer of sample between sequential polypropylene storage tubes, in simulation of sample processing for storage or aliquoting for collaborative sharing, decreased Aβ42 concentration by approximately 20% of the initial concentration per iteration. This was also true of CSF Aβ passed through a K-resin manometer, although the effect size was considerably smaller (~5%). T-tau and P-tau concentrations were generally not affected by these conditions, and in polypropylene the effect on Aβ38 and Aβ40 was proportionally less than on Aβ42. These findings are of particular importance as ratios of Aβ42 to these other biomarkers are becoming increasingly relied on in diagnostic and research settings. Subsequent replication of these experiments by other groups verified the principle findings, although with a certain degree of variation in the details such as the effect size on different Aβ peptide ratios *(Pica-Mendez et al., 2010; Vanderstichele et al., 2017; Willemse et al., 2017)*.

One of the most interesting implications raised by these results is the possible effect different ratios/conformational seeds of Aβ may have on Aβ surface adsorption dynamics in fluid matrix. Combining data presented in this thesis showing different adsorption propensities of certain Aβ peptides, fAD genotype-dependent Aβ ratio profiles, and work from others presenting potential formation of genotype-biased fibril structures *(Törnquist et al., 2018; Vandersteen et al., 2012)*, there may be important disease relevant Aβ peptide profiles or structures within samples that we

could be, but are not, detecting. Although still not well understood, Aβ monomers, oligomers, and fibrils adopt a range of conformations in solution, and indeed current models highlight the importance of C-terminal sequence for multimer stability and predict the presence of a laterally exposed hydrophobic 'patch' unique to certain Aβ42 fibrils *(Colvin et al., 2016; Wälti et al., 2016)*. These properties may contribute to differences observed in Aβ42 versus Aβ40 nucleation rate constants *(Esbjörner et al., 2014; Meisl et al., 2014)* and the range of adsorption dynamics at different polymer surfaces *(Moores et al., 2011; Rocha et al., 2005)*. Assays capable of identifying concentrations of a wider range of Aβ peptides and aggregate structures could be valuable for identifying the nature of underlying disruption to APP proteolysis and so inform personalised treatment strategies for future patients.

Strategies tested to mitigate the confounding effects of surface exposure were the addition of 0.05% Tween 20 to samples and protocol standardisation. Both approaches were found to be effective at reducing the impact of surface exposure on biomarker measurement in pre-analytical storage and handling. However, inclusion of non-ionic surfactant in samples in the early stages of collection and processing is undesirable in terms of potential interference with certain analytical techniques (e.g. mass spectrometry), and also for increasing the complexity to routine collection logistics. Use of Tween 20 as a sample additive was not found to provide additional benefit over careful standardisation of sample treatment. Furthermore, recent studies make a compelling case for the use of low bind storage tubes, which rely on surface texturing and hydrophilic polymer mixes to reduce protein binding to comparable effect without the same limitations.

The effect of temperature and collection-storage interval on measurable concentrations of Aβ and tau in CSF have received considerable attention as part of the movement to improve sample handling practices in AD research temperature *(Bibl et al., 2004; Bjerke et al., 2010; Ranganathan et al., 2006; Sancesario et al., 2010)*. In a 'live' clinical setting data presented in this thesis showed no significant difference between transporting samples at 4°C and ambient temperature in terms of Aβ42, T-tau, and P-tau concentration. Although the literature remains conflicted on this issue, these results converge with the work of *(Le Bastard et al., 2015; Bjerke et al., 2010; Simonsen et al., 2013)* and support the appropriateness of current practices in a clinical biomarker setting. Furthermore, collection of cell media for the measurement of Aβ peptides does not appear to require any more stringent temperature control, though standardisation remains highly desirable.

Over the last 20 years, the investigation of pre-analytical confounding factors has developed into a credible subfield in AD biomarker research. Many aspects of the pre-analytical process have been identified as having the potential to influence biomarker measurement, and Aβ has been among the most vulnerable and best studied proteins. Hansson *et al.* recently published a proposal for the "gold standard" of CSF collection to be fresh CSF collected straight from the LP needle into a low binding tube, and analysed within 4 hours (stored at 20–25°C) without any further handling *(Hansson et al., 2018)*. This procedure limits the number of processing steps, while the use of low binding tubes mitigates binding of proteins to the tube walls in accordance with, and citing, the work presented here. It should be noted that a potential weakness of this is the lack of a centrifugation step to remove contaminating cell debris. Greater emphasis on mid-flow, low cell count CSF might be desirable, but this ultimately serves to highlight the difficulty in balancing known factors and the challenge of implementing best practice methods that still lies ahead. Finally, as new technologies develop to improve biomarker detection it is inevitable that new variables will arise to confound measurements and the need for data to guide standardisation seems unlikely to diminish.

9.3 Aim 2: Investigate the physiological relevance of iPSC-neurons by comparing Aβ peptide profiles in cell culture, CSF, and brain homogenate from a single patient with the APP V717I mutation.

iPSC-derived cell types are an exciting technology for the understanding and therapeutics of disease. At the time of writing, and despite an explosion of work developing, characterising, and interrogating various cell types, the field is still in its infancy with only the merest scratch being made to the depth of its potential. However, the cash-value of this technology is the degree to which cells produced accurately model relevant *in vivo* systems and processes. To this end, much effort has been devoted to the molecular genetic and epigenetic control of the reprogramming and differentiation process, but hard comparisons between the model and the aspect of the living system it attempts to reflect have been extremely rare, especially in regard to the human brain. To date only one study has reported on the comparability of paired human neuronal culture and brain tissue, and concluded that differences in gene expression decreased as cultured neurons were matured in a non-neurodegenerative individual *(Hjelm et al., 2013)*. This thesis presented a case study comparing Aβ peptide profiles in cortical neuron-, CSF-, and frontal cortex tissue-derived samples from the same individual with an *APP* V717I mutation.

Results showed that soluble fraction ratios of Aβ42:40 secreted into culture media by iPSC-derived cortical neurons were similar to those found in the post-mortem brain homogenate of the same

individual. This is a promising suggestion that *in vitro* Aβ production usefully reflects that which occurs *in vivo* in a diseased state. That such a phenotype occurs in both developmentally young cultured neurons and aged neurons from an elderly individual is interesting, and further evidence that the symptomatic pathology of AD likely requires additional factors beyond the dysregulation of Aβ production. Aβ42:40 and Aβ42:38 were lower in the CSF than in the cell media, whilst Aβ38:40 ratios were comparable. This data fit with the hypothesis that cultured neurons produce *in vivo* relevant ratios of Aβ peptides, but that Aβ42 in particular is sequestered in the brain parenchyma (attested by immunocytochemistry in this individual) and not efficiently cleared to the CSF. The available measurement of Aβ38:40 in soluble fraction brain homogenate did not match cell culture media and does not fit the interpretation presented above. There were limitations to the measurement of Aβ38 in this fraction that will require further work to address. Additionally, the insoluble brain fraction did not yield an expected high Aβ42:40 ratio, and it is possible that Aβ solubilisation was incomplete in these fractions. Thus results, though initially promising, should be treated as preliminary until Aβ extraction and solubilisation technique can be optimised.

9.4 Aim 3: Investigate the full spectrum of Aβ peptides produced by glutamatergic cortical neurons from six different fAD lines and five non-neurodegenerative controls

Sporadic and familial forms of AD share great pathological similarity, and better understanding of Aβ production, its modulation and impact on cell physiology in fAD is a promising route toward finding methods to control the disease. To this end, Aβ peptide production was compared between iPSC-derived cortical neurons from individuals with *APP V717I*, five *PSEN1* mutations, and non-neurodegenerative controls. An important finding was the ability of Aβ ratios to normalise variability over time and between different inductions of the same line. This enabled more robust interpretation of Aβ production in the different genotypes studied. Results were highly consistent with those reported for the same mutations by other groups *(Chávez-Gutiérrez et al., 2012; Houlden et al., 2000; Moore et al., 2015; Muratore et al., 2014; Murayama et al., 1999; Nakaya et al., 2005; Saito et al., 2011; Shioi et al., 2007; Szaruga et al., 2015)*. Furthermore, investigation of a large panel of Aβ peptides by immunoassay and mass spectrometry identified production patterns that shed more light on the mechanisms behind AD-related APP proteolysis. Both *APP* V717I cell lines demonstrated a bias toward Aβ42 and Aβ38 relative to Aβ43 and Aβ40, consistent with a proposed dual pathway model of γ-secretase proteolysis termed the tripeptide hypothesis *(Bolduc et al., 2016; Chávez-Gutiérrez et al., 2012; Matsumura et al., 2014; Takami et al., 2009)*. Study of additional

peptides suggested that Aβ39 may be on the Aβ48 pathway, but C-terminal cleavage pathway distinctions broke down at Aβ37. *PSEN1* mutations shared some Aβ peptide profile similarities but differed in certain other aspects (e.g. degree of Aβ43 over-production in *PSEN1* R278I). These mutations all decreased γ-secretase activity, resulting in over-production of C-terminally longer peptides relative to more C-terminally truncated peptides, and consistent with a partial loss of function paradigm for γ-secretase in fAD *(Chávez-Gutiérrez et al., 2012; Szaruga et al., 2015; Woodruff et al., 2013)*. Together these results offer evidence to support a burgeoning model of APP proteolysis mechanisms and suggest new understanding of Aβ peptide ratio profiles as biomarkers for γ-secretase activity, which could have utility if γ-secretase modulator therapy is pharmaceutically revisited. Finally, these data provide a platform to support exciting new work testing the hypothesis that nuances in the relationship between the presence of different Aβ peptides combinations may be more or less toxic and guide more effective therapeutics for AD *(Moore et al., 2018)*.

9.5 Future directions

Over the course of work, it became clear that certain lines of enquiry would benefit from further exploration beyond the limits of the project, and a number of tangential questions were also raised. One question that emerged from the method standardisation phase of the project was: can surface adsorption be used to identify toxic Aβ structures and kinetics? Work demonstrated differential propensity for certain Aβ peptides to bind to storage vessel surfaces, and an extensive literature documents the variety and disease relevance of certain oligomeric and fibrillar Aβ forms. Despite the improvements to Aβ measurement lo-bind tubes provide, it might prove interesting to examine surface adsorbed Aβ from CSF and blood in the context of distinguishing AD patient categories.

Regarding Aβ biomarker development *in* vitro, although the number of fAD mutations studied *in vitro* was comparatively large in the context of the current literature, to validate findings further it would be desirable to include others, particularly more *APP* mutations and sAD lines, and increase the number of individuals of each genotype. A comprehensive catalogue of Aβ production profiles by genotype could help identify common patterns between mutations that could guide therapeutic strategy, and delineate how Aβ production and clearance mechanisms differ between fAD lines and sAD lines.

A further step in this line of enquiry is to explore the relationship between Aβ production ratios and the physiological function, and dysfunction, in human neuronal culture. Building on groundwork laid in this thesis, a key experiment to conduct in this vein is the comparison of electrophysiology and

calcium signalling between fAD, sAD, and control neurons. Furthermore, testing the effect of Aβ profile 'correction' by γ-secretase modulators or peptide specific antibodies on these functional readouts would be of great interest.

Along similar lines, adding to the number of individuals with paired biomaterials would be extremely valuable for assessing the wider validity of our case study's results. Optimisation of the Aβ solubilisation procedure is also needed. A major limitation was the lack of a positive control for insoluble Aβ recovery. Future experiments will require this to ensure complete Aβ solubility is achieved.

9.6 Conclusion

The principle conclusion of this work is that Aβ peptides have great potential as biomarkers in the basic science and diagnostic settings of neurodegenerative disease research, particularly that of AD. This thesis contributed to the improved use of Aβ as a diagnostic biomarker for AD. Aβ peptides, more so than tau, are vulnerable to a number of pre-analytical variables which can influence its use and quality as a biomarker for AD. Innate biophysical properties predispose Aβ peptides to adsorption to various surfaces at unequal rates, which is likely to be a highly pertinent consideration for biobanking and trial initiatives, and can be mitigated by specific treatment and standardisation of storage surfaces. Additionally, this thesis contributed to knowledge of Aβ peptide production in different fAD mutations and proposed the expanded understanding of Aβ as a biomarker for γ-secretase activity. The use of Aβ peptide ratios were identified as a practical method for overcoming issues of variability in an in vitro culture model of fAD. Furthermore, Aβ production in this model was found to have interesting comparability with Aβ from other anatomical compartments of the same subject.

10 References

Abdul-Hay, S.O., Sahara, T., McBride, M., Kang, D., and Leissring, M.A. (2012). Identification of BACE2 as an avid β-amyloid-degrading protease. Mol. Neurodegener. *7*, 46.

Abramov, A.Y., Canevari, L., and Duchen, M.R. (2004). β-Amyloid Peptides Induce Mitochondrial Dysfunction and Oxidative Stress in Astrocytes and Death of Neurons through Activation of NADPH Oxidase. J. Neurosci. *24*, 565–575.

Abramov, E., Dolev, I., Fogel, H., Ciccotosto, G.D., Ruff, E., and Slutsky, I. (2009). Amyloid-beta as a positive endogenous regulator of release probability at hippocampal synapses. Nat. Neurosci. *12*, 1567–1576.

Ahmed, R.R., Holler, C.J., Webb, R.L., Li, F., Beckett, T.L., and Murphy, M.P. (2010). BACE1 and BACE2 enzymatic activities in Alzheimer's disease. J. Neurochem. 1045–1053.

Akaaboune, M., Allinquant, B., Farza, H., Roy, K., Magoul, R., Fiszman, M., et al. (2000). Developmental regulation of amyloid precursor protein at the neuromuscular junction in mouse skeletal. Mol. Cell. Neurosci. 355–367.

Albert, M.S., DeKoskyb, S.T., Dicksond, D., Duboise, B., Feldmanf, H.H., Foxg, N.C., et al. (2011). The diagnosis of mild cognitive impairment due to Alzheimer's disease: Recommendations from the National Institute on Aging-Alzheimer's Association workgroups on diagnostic guidelines for Alzheimer's disease. Alzheimer's Dement. *7*, 270–279.

Alcarraz-Vizán, G., Castaño, C., Visa, M., Montane, J., Servitja, J.M., and Novials, A. (2017). BACE2 suppression promotes β-cell survival and function in a model of type 2 diabetes induced by human islet amyloid polypeptide overexpression. Cell. Mol. Life Sci. 2827–2838.

Almdahl, I.S., Lauridsen, C., Selnes, P., Kalheim, L.F., Coello, C., Gajdzik, B., et al. (2017). Cerebrospinal fluid levels of amyloid beta 1-43 mirror 1-42 in relation to imaging biomarkers of Alzheimer's disease. Front. Aging Neurosci. 9.

ALZFORUM (2019a). https://www.alzforum.org/mutations/app.

ALZFORUM (2019b). https://www.alzforum.org/mutations/psen-1.

Alzheimer's Association (2016). 2016 Alzheimer's disease facts and figures. Alzheimers. Dement. *12*, 459–509.

Alzheimer, A. (1907). Uber eine eigenartige Erkrankung der Hirnrinde. Allg Zeits Psychiatry Psych. Y Gerichtl. Med *64*, 146–148.

Anand, P., Nandel, F.S., and Hansmann, U.H.E. (2008). The Alzheimer beta-amyloid (Abeta(1-39)) dimer in an implicit solvent. J. Chem. Phys. *129*, 195102.

Ando, K., Iijima, K.I., Elliott, J.I., Kirino, Y., and Suzuki, T. (2001). Phosphorylation-dependent Regulation of the Interaction of Amyloid Precursor Protein with Fe65 Affects the Production of beta-Amyloid. J. Biol. Chem. *276*, 40353–40361.

Andrew, R.J., Kellett, K.A.B., Thinakaran, G., and Hooper, N.M. (2016). A Greek Tragedy: The Growing Complexity of Alzheimer Amyloid Precursor Protein Proteolysis * The Canonical-,-, and-Secretases and APP Fragments. J Biol Chem *291*, 19235–19244.

Andrew, R.J., Fisher, K., Heesom, K.J., Kellett, K.A.B., and Hooper, N.M. (2019). Quantitative interaction proteomics reveals differences in the interactomes of amyloid precursor protein isoforms. J. Neurochem. *149*, 399–412.

Andrews-Zwilling, Y., Bien-Ly, N., Xu, Q., Li, G., Bernardo, A., Yoon, S.Y., et al. (2010). Apolipoprotein E4 Causes Age- and Tau-Dependent Impairment of GABAergic Interneurons, Leading to Learning and Memory Deficits in Mice. J. Neurosci. 13707–13717.

Anoop, A., Singh, P.K., Jacob, R.S., and Maji, S.K. (2010). CSF Biomarkers for Alzheimer's Disease Diagnosis. Int. J. Alzheimers. Dis. *2010*, 1–12.

Arber, C., Lovejoy, C., and Wray, S. (2017). Stem cell models of Alzheimer's disease: progress and challenges. Alzheimers. Res. Ther. *9*, 42.

Area-Gomez, E., and Schon, E.A. (2016). Mitochondria-associated ER membranes and Alzheimer disease. Curr. Opin. Genet. Dev. *38*, 90–96.

Arispe, N., Rojas, E., and Pollard, H.B. (1993). Alzheimer disease amyloid beta protein forms calcium channels in bilayer membranes: blockade by tromethamine and aluminum. Proc. Natl. Acad. Sci. U. S. A. *90*, 567–571.

Armstrong, R.A., Winsper, S.J., and Blair, J.A. (1995). Hypothesis: is Alzheimer's Disease a Metal-induced Immune Disorder? Neurodegeneration 107–111.

Arosio, P., Knowles, T.P.J., and Linse, S. (2015). On the lag phase in amyloid fibril formation. Phys. Chem. Chem. Phys. 7606–7618.

Ashe, K.H., and Zahs, K.R. (2010). Probing the Biology of Alzheimer's Disease in Mice. Neuron 631–645.

Atkinson A.J., J., Colburn, W.A., DeGruttola, V.G., DeMets, D.L., Downing, G.J., Hoth, D.F., et al. (2001). Biomarkers and surrogate endpoints: Preferred definitions and conceptual framework. Clin. Pharmacol. Ther. *69*, 89–95.

Balasa, M., Gelpi, E., Antonell, A., Rey, M.J., Sánchez-Valle, R., Molinuevo, J.L., et al. (2011). Clinical features and APOE genotype of pathologically proven early-onset Alzheimer disease. Neurology *76*, 1720–1725.

Ball, K.A., Phillips, A.H., Nerenberg, P.S., Fawzi, N.L., Wemmer, D.E., and Head-Gordon, T. (2011).

Homogeneous and heterogeneous tertiary structure ensembles of amyloid-β peptides. Biochemistry 7612–7628.

Banerjee, S., Hashemi, M., Lv, Z., Maity, S., Rochet, J.C., and Lyubchenko, Y.L. (2017). A novel pathway for amyloids self-assembly in aggregates at nanomolar concentration mediated by the interaction with surfaces. Sci. Rep. 45592.

Barão, S., Moechars, D., Lichtenthaler, S.F., and De Strooper, B. (2016). BACE1 Physiological Functions May Limit Its Use as Therapeutic Target for Alzheimer's Disease. Trends Neurosci. 158–169.

Barthet, G., Dunys, J., Shao, Z., Xuan, Z., Ren, Y., Xu, J., et al. (2013). Presenilin mediates neuroprotective functions of ephrinB and brain-derived neurotrophic factor and regulates ligand-induced internalization and metabolism of EphB2 and TrkB receptors. Neurobiol. Aging 499–510.

Bartus, R., Dean, R., Beer, B., and Lippa, A. (1982). The cholinergic hypothesis of geriatric memory dysfunction. Science (80-.). *217*, 408–414.

Baruch-Suchodolsky, R., and Fischer, B. (2009). Ab40, either soluble or aggregated, is a remarkably potent antioxidant in cell-free oxidative systems. Biochemistry *48*, 4354–4370.

Le Bastard, N., Aerts, L., Sleegers, K., Martin, J.J., Van Broeckhoven, C., De Deyn, P.P., et al. (2013). Longitudinal stability of cerebrospinal fluid biomarker levels: Fulfilled requirement for pharmacodynamic markers in Alzheimer's disease. J. Alzheimer's Dis. *33*, 807–822.

Le Bastard, N., De Deyn, P.P., and Engelborghs, S. (2015). Importance and impact of preanalytical variables on Alzheimer disease biomarker concentrations in cerebrospinal fluid. Clin. Chem. *61*, 734–743.

Bateman, R.J., Wen, G., Morris, J.C., and Holtzman, D.M. (2007). Fluctuations of CSF amyloid-β levels: Implications for a diagnostic and therapeutic biomarker. Neurology *68*, 666–669.

Bayer, T.A., and Wirths, O. (2014). Focusing the amyloid cascade hypothesis on N-truncated Abeta peptides as drug targets against Alzheimer's disease. Acta Neuropathol. *127*, 787–801.

Beel, A.J., Sakakura, M., Barrett, P.J., and Sanders, C.R. (2010). Direct binding of cholesterol to the amyloid precursor protein: An important interaction in lipid-Alzheimer's disease relationships? Biochim. Biophys. Acta - Mol. Cell Biol. Lipids *1801*, 975–982.

Begum, A.N., Guoynes, C., Cho, J., Hao, J., Lutfy, K., and Hong, Y. (2015). Rapid generation of sub-type, region-specific neurons and neural networks from human pluripotent stem cell-derived neurospheres. Stem Cell Res. *15*, 731–741.

Bekris, L.M., Khrestian, M., Dyne, E., Shao, Y., Pillai, J., Rao, S., et al. (2018). Soluble TREM2 and biomarkers of central and peripheral inflammation in neurodegenerative disease. J.

Neuroimmunol. 19–27.

Bellingham, S.A., Ciccotosto, G.D., Needham, B.E., Fodero, L.R., White, A.R., Masters, C.L., et al. (2004). Gene knockout of amyloid precursor protein and amyloid precursor-like protein-2 increases cellular copper levels in primary mouse cortical neurons and embryonic fibroblasts. J. Neurochem. *91*, 423–428.

Belyaev, N.D., Nalivaeva, N.N., Makova, N.Z., and Turner, A.J. (2009). Neprilysin gene expression requires binding of the amyloid precursor protein intracellular domain to its promoter: Implications for Alzheimer disease. EMBO Rep. 94–100.

Bennett, B.D., Babu-Khan, S., Loeloff, R., Louis, J.C., Curran, E., Citron, M., et al. (2000). Expression analysis of BACE2 in brain and peripheral tissues. J. Biol. Chem. 20647–20651.

Benson, D., Davis, R., and Snyder, B. (1988). Posterior cortical atrophy. Arch. Neurol. *7*, 193–203.

Berge, G., Lauridsen, C., Sando, S.B., Holder, D.J., Moller, I., Aasly, J.O., et al. (2015). Effect of tween-20 on core biomarkers measured in cerebrospinal fluid from patients with Alzheimer's disease, mild cognitive impairment, or healthy control individuals. J. Alzheimer's Dis. 493–502.

Bergmans, B.A., Shariati, S.A.M., Habets, R.L.P., Verstreken, P., Schoonjans, L., Müller, U., et al. (2010). Neurons generated from APP/APLP1/APLP2 triple knockout embryonic stem cells behave normally in vitro and in vivo: Lack of evidence for a cell autonomous role of the amyloid precursor protein in neuronal differentiation. Stem Cells *28*, 399–406.

Bergstrom, P., Agholme, L., Nazir, F.H., Satir, T.M., Toombs, J., Wellington, H., et al. (2016). Amyloid precursor protein expression and processing are differentially regulated during cortical neuron differentiation. Sci. Rep. *6*, 29200.

Bero, Adam W; Cirrito, John; Holtzman, David; Lee, Jin-Moo; Raichle, Marvus; Roh, J. (2011). Neuronal activity regulates the regional vulnerability to amyloid-[beta] deposition. Nat. Neurosci. *14*, 750.

Berridge, M.J. (2010). Calcium hypothesis of Alzheimer's disease. Pflügers Arch. - Eur. J. Physiol. *459*, 441–449.

Berridge, M.J. (2011). Calcium signalling and Alzheimer's disease. Neurochem. Res. 1149–1156.

Berry, B.J., Smith, A.S.T., Young, J.E., and Mack, D.L. (2018). Advances and Current Challenges Associated with the Use of Human Induced Pluripotent Stem Cells in Modeling Neurodegenerative Disease. Cells. Tissues. Organs 1–19.

Bezprozvanny, I., and Mattson, M.P. (2008). Neuronal calcium mishandling and the pathogenesis of Alzheimer's disease. Trends Neurosci. 454–463.

Bibl, M., Esselmann, H., Otto, M., Lewczuk, P., Cepek, L., Rüther, E., et al. (2004). Cerebrospinal fluid amyloid β peptide patterns in Alzheimer's disease patients and nondemented controls

depend on sample pretreatment: Indication of carrier-mediated epitope masking of amyloid β peptides. Electrophoresis *25*, 2912–2918.

Birks, J.S., Chong, L.Y., and Grimley Evans, J. (2015). Rivastigmine for Alzheimer's disease. Cochrane Database Syst. Rev.

Bittner, T., Zetterberg, H., Teunissen, C.E., Ostlund, R.E., Militello, M., Andreasson, U., et al. (2016). Technical performance of a novel, fully automated electrochemiluminescence immunoassay for the quantitation of beta-amyloid (1-42) in human cerebrospinal fluid. Alzheimer's Dement. *12*, 517–526.

Bjerke, M., Portelius, E., Minthon, L., Wallin, A., Anckarsäter, H., Anckarsäter, R., et al. (2010). Confounding factors influencing amyloid Beta concentration in cerebrospinal fluid. Int. J. Alzheimers. Dis. *2010*, 1–12.

Blennow, K. (2017). A Review of Fluid Biomarkers for Alzheimer's Disease: Moving from CSF to Blood. Neurol. Ther. 15–24.

Blennow, K., and Zetterberg, H. (2009). Cerebrospinal fluid biomarkers for Alzheimer's disease. J. Alzheimers. Dis. *18*, 413–417.

Blennow, K., Hampel, H., Weiner, M., and Zetterberg, H. (2010). Cerebrospinal fluid and plasma biomarkers in Alzheimer disease. Nat. Rev. Neurol. *6*, 131–144.

Blennow, K., Zetterberg, H., and Fagan, A.M. (2012). Fluid biomarkers in Alzheimer disease. Cold Spring Harb. Perspect. Med. *2*, a006221.

Blurton-Jones, M., and LaFerla, F.M. (2006). Pathways by which Aβ facilitates tau pathology. Curr. Alzheimer Res. 437–448.

Boehm, J. (2013). A "danse macabre": Tau and Fyn in STEP with amyloid beta to facilitate induction of synaptic depression and excitotoxicity. Eur. J. Neurosci. *37*, 1925–1930.

Bohm, G., and Zech, G. (2010). Introduction to statistics and data analysis for physicists. Statsref.Com *37*, 452.

Boissart, C., Poulet, A., Georges, P., Darville, H., Julita, E., Delorme, R., et al. (2013). Differentiation from human pluripotent stem cells of cortical neurons of the superficial layers amenable to psychiatric disease modeling and high-throughput drug screening. Transl. Psychiatry *3*, e294–e294.

Bolduc, D.M., Montagna, D.R., Seghers, M.C., Wolfe, M.S., and Selkoe, D.J. (2016). The amyloid-beta forming tripeptide cleavage mechanism of γ-Secretase. Elife e17578.

Boteva, K., Vitek, M., Mitsuda, H., de Silva, H., Xu, P.-T., Small, G., et al. (1996). Mutation analysis of presenilin 1 gene in Alzheimer's disease. Lancet *347*, 130–131.

Braak, H., Alafuzoff, I., Arzberger, T., Kretzschmar, H., and Tredici, K. (2006). Staging of Alzheimer

disease-associated neurofibrillary pathology using paraffin sections and immunocytochemistry. Acta Neuropathol. *112*, 389–404.

Bratcher, P.E., and Gaggar, A. (2014). Factors influencing the measurement of plasma/serum surfactant protein D levels by ELISA. PLoS One e111466.

British Standards Institution (1994). Accuracy (trueness and precision) of measurement methods and results -- Part 2: Basic method for the determination of repeatability and reproducibility of a standard measurement method.

Brothers, H.M., Gosztyla, M.L., and Robinson, S.R. (2018). The physiological roles of amyloid-β peptide hint at new ways to treat Alzheimer's disease. Front. Aging Neurosci. 118.

Brownjohn, P.W., Smith, J., Portelius, E., Serneels, L., Kvartsberg, H., De Strooper, B., et al. (2017). Phenotypic Screening Identifies Modulators of Amyloid Precursor Protein Processing in Human Stem Cell Models of Alzheimer's Disease. Stem Cell Reports *8*, 870–882.

Brunholz, S., Sisodia, S., Lorenzo, A., Deyts, C., Kins, S., and Morfini, G. (2012). Axonal transport of APP and the spatial regulation of APP cleavage and function in neuronal cells. Exp. Brain Res. *217*, 353–364.

Buckner, R.L. (2005). Molecular, Structural, and Functional Characterization of Alzheimer's Disease: Evidence for a Relationship between Default Activity, Amyloid, and Memory. J. Neurosci. *25*, 7709–7717.

Burgos, P. V., Mardones, G.A., Rojas, A.L., daSilva, L.L.P., Prabhu, Y., Hurley, J.H., et al. (2010). Sorting of the Alzheimer's Disease Amyloid Precursor Protein Mediated by the AP-4 Complex. Dev. Cell *18*, 425–436.

Burns, A., and Iliffe, S. (2009). Alzheimer's disease. BMJ *338*, b158–b158.

Bush, A.I., and Tanzi, R.E. (2008). Therapeutics for Alzheimer's disease based on the metal hypothesis. Neurotherapeutics *5*, 421–432.

Bush, A.I., Pettingell, W.H., Paradis, M.D., and Tanzi, R.E. (1994). Modulation of Aβ adhesiveness and secretase site cleavage by zinc. J. Biol. Chem. 12152–12158.

Butterfield, D.A., and Pocernich, C.B. (2003). The glutamatergic system and Alzheimer's disease: Therapeutic implications. CNS Drugs 641–652.

Caglayan, S., Takagi-Niidome, S., Liao, F., Carlo, A.S., Schmidt, V., Burgert, T., et al. (2014). Lysosomal Sorting of Amyloid-beta by the SORLA Receptor Is Impaired by a Familial Alzheimer's Disease Mutation. Sci Transl Med *6*, 223ra20.

Cai, H., Wang, Y., McCarthy, D., Wen, H., Borchelt, D.R., Price, D.L., et al. (2001). BACE1 is the major β-secretase for generation of Aβ peptides by neurons. Nat. Neurosci. 233–234.

Cai, Y., An, S.S.A., and Kim, S. (2015). Mutations in presenilin 2 and its implications in Alzheimer's

disease and other dementia-associated disorders. Clin. Interv. Aging *10*, 1163–1172.

Camandola, S., and Mattson, M.P. (2011). Aberrant subcellular neuronal calcium regulation in aging and Alzheimer's disease. Biochim Biophys Acta *1813*, 965–973.

Campbell, a (2001). Beta-Amyloid: Friend or Foe. Med. Hypotheses *56*, 388–391.

Campion, D., Flaman, J.M., Brice, A., Hannequin, D., Dubois, B., Martin, C., et al. (1995). Mutations of the presenilin I gene in families with early-onset alzheimer's disease. Hum. Mol. Genet. *4*, 2373–2377.

Campion, D., Dumanchin, C., Hannequin, D., Dubois, B., Belliard, S., Puel, M., et al. (1999). Early-onset autosomal dominant Alzheimer disease: prevalence, genetic heterogeneity, and mutation spectrum. Am. J. Hum. Genet. *65*, 664–670.

del Campo, M., Mollenhauer, B., Bertolotto, A., Engelborghs, S., Hampel, H., Simonsen, A.H., et al. (2012). Recommendations to standardize preanalytical confounding factors in Alzheimer's and Parkinson's disease cerebrospinal fluid biomarkers: an update. Biomark. Med. *6*, 419–430.

Capell, A., Steiner, H., Willem, M., Kaiser, H., Meyer, C., Walter, J., et al. (2000). Maturation and pro-peptide cleavage of β-secretase. J. Biol. Chem. 30849–30854.

Capell, A., Kaether, C., Edbauer, D., Shirotani, K., Merkl, S., Steiner, H., et al. (2003). Nicastrin Interacts with γ-Secretase Complex Components via the N-terminal Part of Its Transmembrane Domain. J. Biol. Chem. 52519–52523.

Carrasquillo, M.M., Khan, Q.U.A., Murray, M.E., Krishnan, S., Aakre, J., Pankratz, V.S., et al. (2014). Late-onset Alzheimer disease genetic variants in posterior cortical atrophy and posterior AD. Neurology *82*, 1455–1462.

Carrillo, M.C., Blennow, K., Soares, H., Lewczuk, P., Mattsson, N., Oberoi, P., et al. (2013). Global standardization measurement of cerebral spinal fluid for Alzheimer's disease: An update from the Alzheimer's Association Global Biomarkers Consortium. Alzheimer's Dement. 137–140.

Carroll, C.M., and Li, Y.M. (2016). Physiological and pathological roles of the γ-secretase complex. Brain Res. Bull. 199–206.

Caspersen, C., Wang, N., Yao, J., Sosunov, A., Chen, X., Lustbader, J.W., et al. (2005). Mitochondrial Abeta: a potential focal point for neuronal metabolic dysfunction in Alzheimer's disease. FASEB J. *19*, 2040–2041.

Van Cauwenberghe, C., Van Broeckhoven, C., Sleegers, K., Cauwenberghe, C. Van, Van Broeckhoven, C., and Sleegers, K. (2016). The genetic landscape of Alzheimer disease: clinical implications and perspectives. Genet. Med. *18*, 421–430.

Cermakova, P., Johnell, K., Fastbom, J., Garcia-Ptacek, S., Winblad, B., Eriksdotter, M., et al. (2015). Cardiovascular comorbidities in dementia. Alzheimer's Dement. *1*, 448.

Chakraborty, S., and Das, P. (2017). Emergence of Alternative Structures in Amyloid Beta 1-42 Monomeric Landscape by N-terminal Hexapeptide Amyloid Inhibitors. Sci. Rep. 9941.

Chan, S.L., Mayne, M., Holden, C.P., Geiger, J.D., and Mattson, M.P. (2000). Presenilin-1 mutations increase levels of ryanodine receptors and calcium release in PC12 cells and cortical neurons. J. Biol. Chem. 18195–18200.

Chang, K.-A., Kim, H.-S., Ha, T.-Y., Ha, J.-W., Shin, K.Y., Jeong, Y.H., et al. (2006). Phosphorylation of Amyloid Precursor Protein (APP) at Thr668 Regulates the Nuclear Translocation of the APP Intracellular Domain and Induces Neurodegeneration. Mol. Cell. Biol. 4327–4338.

Charkhkar, H., Meyyappan, S., Matveeva, E., Moll, J.R., McHail, D.G., Peixoto, N., et al. (2015). Amyloid beta modulation of neuronal network activity in vitro. Brain Res. *1629*, 1–9.

Chavez-Gutierrez, L., Bammens, L., Benilova, I., Vandersteen, A., Benurwar, M., Borgers, M., et al. (2012). The mechanism of gamma-Secretase dysfunction in familial Alzheimer disease. EMBO J. *31*, 2261–2274.

Chávez-Gutiérrez, L., Bammens, L., Benilova, I., Vandersteen, A., Benurwar, M., Borgers, M., et al. (2012). The mechanism of γ-Secretase dysfunction in familial Alzheimer disease. EMBO J. *31*, 2261–2274.

Chen, J., Wang, M., and Turko, I. V. (2013). Quantification of amyloid precursor protein isoforms using quantification concatamer internal standard. Anal. Chem. *85*, 303–307.

Chen, K.G., Mallon, B.S., McKay, R.D.G., and Robey, P.G. (2014). Human pluripotent stem cell culture: Considerations for maintenance, expansion, and therapeutics. Cell Stem Cell 13–26.

Chen, M., Lee, H.K., Moo, L., Hanlon, E., Stein, T., and Xia, W. (2018). Common proteomic profiles of induced pluripotent stem cell-derived three-dimensional neurons and brain tissue from Alzheimer patients. J. Proteomics *182*, 21–33.

Cheung, K.H., Shineman, D., Müller, M., Cárdenas, C., Mei, L., Yang, J., et al. (2008). Mechanism of Ca2+ Disruption in Alzheimer's Disease by Presenilin Regulation of InsP3 Receptor Channel Gating. Neuron 871–883.

Chiang, P.M., Fortna, R.R., Price, D.L., Li, T., and Wong, P.C. (2012). Specific domains in anterior pharynx-defective 1 determine its intramembrane interactions with nicastrin and presenilin. Neurobiol. Aging 277–285.

Chin, M.H., Pellegrini, M., Plath, K., and Lowry, W.E. (2010). Molecular analyses of human induced pluripotent stem cells and embryonic stem cells. Cell Stem Cell *7*, 263–269.

Choi, S.H., Kim, Y.H., Hebisch, M., Sliwinski, C., Lee, S., D'Avanzo, C., et al. (2014). A three-dimensional human neural cell culture model of Alzheimer's disease. Nature *515*, 274–278.

Choi, S.H., Kim, Y.H., D'Avanzo, C., Aronson, J., Tanzi, R.E., and Kim, D.Y. (2015). Recapitulating

amyloid β and tau pathology in human neural cell culture models: clinical implications. US Neurol. *11*, 102–105.

Choi, Y.J., Park, J., and Lee, S.-H. (2013). Size-controllable networked neurospheres as a 3D neuronal tissue model for Alzheimer's disease studies. Biomaterials *34*, 2938–2946.

Chu, C.S., Tseng, P.T., Stubbs, B., Chen, T.Y., Tang, C.H., Li, D.J., et al. (2018). Use of statins and the risk of dementia and mild cognitive impairment: A systematic review and meta-analysis. Sci. Rep. 5804.

Chu, J., Li, J.G., Joshi, Y.B., Giannopoulos, P.F., Hoffman, N.E., Madesh, M., et al. (2015). Gamma secretase-activating protein is a substrate for caspase-3: Implications for Alzheimer's disease. Biol. Psychiatry 720–728.

Cicognola, C., Chiasserini, D., and Parnetti, L. (2015). Preanalytical Confounding Factors in the Analysis of Cerebrospinal Fluid Biomarkers for Alzheimer's Disease: The Issue of Diurnal Variation. Front. Neurol. *6*, 143.

Cirrito, J.R., Yamada, K. a., Finn, M.B., Sloviter, R.S., Bales, K.R., May, P.C., et al. (2005). Synaptic activity regulates interstitial fluid amyloid-beta levels in vivo. Neuron *48*, 913–922.

Cirrito, J.R., Kang, J.E., Lee, J., Stewart, F.R., Verges, D.K., Silverio, L.M., et al. (2008). Endocytosis Is Required for Synaptic Activity-Dependent Release of Amyloid-beta In Vivo. Neuron *58*, 42–51.

Clapham, D.E. (2007). Calcium Signaling. Cell *131*, 1047–1058.

Clark, R.F., Hutton, M., Fuldner, M., Froelich, S., Karran, E., Talbot, C., et al. (1995). The structure of the presenilin 1 (S182) gene and identification of six novel mutations in early onset AD families. Nat. Genet. *11*, 219–222.

Clodomiro, A., Gareri, P., Puccio, G., Frangipane, F., Lacava, R., Castagna, A., et al. (2013). Somatic comorbidities and Alzheimer's disease treatment. Neurol. Sci. *34*, 1581–1589.

Cloe, A.L., Orgel, J.P.R.O., Sachleben, J.R., Tycko, R., and Meredith, S.C. (2011). The Japanese mutant Aβ (ΔE22-Aβ 1-39) forms fibrils instantaneously, with low-thioflavin T fluorescence: Seeding of wild-type Aβ 1-40 into atypical fibrils by Δe22- Aβ 1-39. Biochemistry *50*, 2026–2039.

Colvin, M.T., Silvers, R., Ni, Q.Z., Can, T. V., Sergeyev, I., Rosay, M., et al. (2016). Atomic Resolution Structure of Monomorphic Ab42 Amyloid Fibrils. J. Am. Chem. Soc. *138*, 9663–9674.

Corder, E.H., Saunders, A.M., Strittmatter, W.J., Schmechel, D.E., Gaskell, P.C., Small, G.W., et al. (1993). Gene dose of apolipoprotein E type 4 allele and the risk of Alzheimer's disease in late onset families. Science (80-.). *261*, 921–923.

Counts, S.E., Ikonomovic, M.D., Mercado, N., Vega, I.E., and Mufson, E.J. (2017). Biomarkers for the Early Detection and Progression of Alzheimer's Disease. Neurotherapeutics *14*, 35–53.

Craddock, T.J.A., Tuszynski, J.A., Chopra, D., Casey, N., Goldstein, L.E., Hameroff, S.R., et al. (2012). The Zinc Dyshomeostasis Hypothesis of Alzheimer's Disease. PLoS One *7*, e33552.

Craig-Schapiro, R., Perrin, R.J., Roe, C.M., Xiong, C., Carter, D., Cairns, N.J., et al. (2010). YKL-40: A novel prognostic fluid biomarker for preclinical Alzheimer's disease. Biol. Psychiatry *68*, 903–912.

Craig, L.A., Hong, N.S., and McDonald, R.J. (2011). Revisiting the cholinergic hypothesis in the development of Alzheimer's disease. Neurosci. Biobehav. Rev. *35*, 1397–1409.

Crawford, F., Hardy, J., Mullan, M., Goate, A., Hughes, D., Fidani, L., et al. (1991). Sequencing of exons 16 and 17 of the beta-amyloid precursor protein gene in 14 families with early onset Alzheimer's disease fails to reveal mutations in the beta-amyloid sequence. Neurosci.Lett. *133*, 1–2.

Crean, S., Ward, A., Mercaldi, C.J., Collins, J.M., Cook, M.N., Baker, N.L., et al. (2011). Apolipoprotein E ε4 prevalence in Alzheimer's disease patients varies across global populations: A systematic literature review and meta-analysis. Dement. Geriatr. Cogn. Disord. 20–30.

Creemers, J.W.M., Dominguez, D.I., Plets, E., Serneels, L., Taylor, N.A., Multhaup, G., et al. (2001). Processing of β-Secretase by Furin and Other Members of the Proprotein Convertase Family. J. Biol. Chem. 4211–4217.

Crutch, S.J., Lehmann, M., Schott, J.M., Rabinovici, G.D., Rossor, M.N., and Fox, N.C. (2012). Posterior cortical atrophy. Lancet Neurol. *11*, 170–178.

Cullen, V.C., Fredenburg, R.A., Evans, C., Conliffe, P.R., and Solomon, M.E. (2012). Development and advanced validation of an optimized method for the quantitation of Aβ42 in human cerebrospinal fluid. AAPS J. *14*, 510–518.

Cunningham, E.L., McGuinness, B., McAuley, D.F., Toombs, J., Mawhinney, T., O'Brien, S., et al. (2018). CSF Beta-amyloid 1–42 Concentration Predicts Delirium Following Elective Arthroplasty Surgery in an Observational Cohort Study. Ann. Surg. 1.

D'Andrea, M.R., and Nagele, R.G. (2010). Morphologically distinct types of amyloid plaques point the way to a better understanding of Alzheimer's disease pathogenesis. Biotech. Histochem. *85*, 133–147.

D'Andrea, M.R., Nagele, R.G., Wang, H.Y., Peterson, P.A., and Lee, D.H.S. (2001). Evidence that neurones accumulating amyloid can undergo lysis to form amyloid plaques in Alzheimer's disease. Histopathology 120–134.

Den Daas, I., Wemer, J., Abou Farha, K., Tamminga, W., De Boer, T., Spanjersberg, R., et al. (2013). Serial CSF sampling over a period of 30 h via an indwelling spinal catheter in healthy

volunteers: Headache, back pain, tolerability and measured acetylcholine profile. Eur. J. Clin. Pharmacol. *69*, 1083–1090.

Das, U., Scott, D.A., Ganguly, A., Koo, E.H., Tang, Y., and Roy, S. (2013). Activity-induced convergence of app and bace-1 in acidic microdomains via an endocytosis-dependent pathway. Neuron *79*, 447–460.

Das, U., Wang, L., Ganguly, A., Saikia, J.M., Wagner, S.L., Koo, E.H., et al. (2015). Visualizing APP and BACE-1 approximation in neurons yields insight into the amyloidogenic pathway. Nat. Neurosci. *19*, 55–64.

Dawkins, E., and Small, D.H. (2014). Insights into the physiological function of the β-amyloid precursor protein: Beyond Alzheimer's disease. J. Neurochem. *129*, 756–769.

Deechongkit, S., Wen, J., Narhi, L.O., Jiang, Y., Park, S.S., Kim, J., et al. (2009). Physical and biophysical effects of polysorbate 20 and 80 on darbepoetin alfa. J. Pharm. Sci. 3200–3217.

DeKosky, S.T., and Scheff, S.W. (1990). Synapse loss in frontal cortex biopsies in Alzheimer's disease: Correlation with cognitive severity. Ann. Neurol. *27*, 457–464.

Demuro, A., Mina, E., Kayed, R., Milton, S.C., Parker, I., and Glabe, C.G. (2005). Calcium dysregulation and membrane disruption as a ubiquitous neurotoxic mechanism of soluble amyloid oligomers. J. Biol. Chem. *280*, 17294–17300.

Desrumaux, C., Labeur, C., Verhee, A., Tavernier, J., Vandekerckhove, J., Rosseneu, M., et al. (2001). A Hydrophobic Cluster at the Surface of the Human Plasma Phospholipid Transfer Protein Is Critical for Activity on High Density Lipoproteins. J. Biol. Chem. 5908–5915.

Deurveilher, S., and Semba, K. (2011). Basal forebrain regulation of cortical activity and sleep-wake states: Roles of cholinergic and non-cholinergic neurons. Sleep Biol. Rhythms *9*, 65–70.

Devi, L., and Anandatheerthavarada, H.K. (2010). Mitochondrial trafficking of APP and alpha synuclein: Relevance to mitochondrial dysfunction in Alzheimer's and Parkinson's diseases. Biochim. Biophys. Acta - Mol. Basis Dis. *1802*, 11–19.

Dieckmann, M., Dietrich, M.F., and Herz, J. (2010). Lipoprotein receptors-an evolutionarily ancient multifunctional receptor family. Biol. Chem. *391*, 1341–1363.

Dill, K.A. (1990). Dominant forces in protein folding. Biochemistry *29*, 7133–7155.

Dineley, K.T., Bell, K.A., Bui, D., and Sweatt, J.D. (2002). β-amyloid peptide activates α7 nicotinic acetylcholine receptors expressed in Xenopus oocytes. J. Biol. Chem. 25056–25061.

Domingues, a, Almeida, S., da Cruz e Silva, E.F., Oliveira, C.R., and Rego, a C. (2007). Toxicity of beta-amyloid in HEK293 cells expressing NR1/NR2A or NR1/NR2B N-methyl-D-aspartate receptor subunits. Neurochem. Int. *50*, 872–880.

Dooley, M., and Lamb, H.M. (2000). Donepezil. Drugs Aging *16*, 199–226.

Doran, E., Keator, D., Head, E., Phelan, M.J., Kim, R., Totoiu, M., et al. (2017). Down Syndrome, Partial Trisomy 21, and Absence of Alzheimer's Disease: The Role of APP. J. Alzheimer's Dis. 459–470.

Dougherty, J.J., Wu, J., and Nichols, R. a (2003). Beta-amyloid regulation of presynaptic nicotinic receptors in rat hippocampus and neocortex. J. Neurosci. *23*, 6740–6747.

Drolle, E., Negoda, A., Hammond, K., Pavlov, E., and Leonenko, Z. (2017). Changes in lipid membranes may trigger amyloid toxicity in Alzheimer's disease. PLoS One *12*, e0182194.

Dubois, B., Feldman, H.H., Jacova, C., Hampel, H., Molinuevo, J.L., Blennow, K., et al. (2014). Advancing research diagnostic criteria for Alzheimer's disease: The IWG-2 criteria. Lancet Neurol. *13*, 614–629.

Duthie, A., Chew, D., and Soiza, R.L. (2011). Non-psychiatric comorbidity associated with Alzheimer's disease. QJM *104*, 913–920.

Dzamba, D., Harantova, L., Butenko, O., and Anderova, M. (2016). Glial Cells - The Key Elements of Alzheimer´s Disease. Curr. Alzheimer Res. *13*, 894–911.

Eckert, G.P., Wood, W.G., and Müller, W.E. (2005). Membrane disordering effects of beta-amyloid peptides. Subcell. Biochem. *38*, 319–337.

Eckert, G.P., Wood, W.G., and Müller, W.E. (2010). Lipid membranes and beta-amyloid: a harmful connection. Curr. Protein Pept. Sci. *11*, 319–325.

Eckman, C.B., Mehta, N.D., Crook, R., Perez-tur, J., Prihar, G., Pfeiffer, E., et al. (1997). A new pathogenic mutation in the APP gene (1716V) increases the relative proportion of Aβ42(43). Hum. Mol. Genet. 2087–2089.

Eckman, E.A., Reed, D.K., and Eckman, C.B. (2001). Degradation of the Alzheimer's amyloid beta peptide by endothelin- converting enzyme. J Biol Chem *276*, 24540–8.

Ellis, T.A., Li, J., Leblond, D., and Waring, J.F. (2012). The relationship between different assays for detection and quantification of amyloid beta 42 in human cerebrospinal fluid. Int. J. Alzheimers. Dis. 984746.

Enache, T.A., Chiorcea-Paquim, A.M., and Oliveira-Brett, A.M. (2018). Amyloid Beta Peptide VHHQ, KLVFF, and IIGLMVGGVV Domains Involved in Fibrilization: AFM and Electrochemical Characterization. Anal. Chem. 2285–2292.

Endres, K., and Deller, T. (2017). Regulation of Alpha-Secretase ADAM10 In vitro and In vivo: Genetic, Epigenetic, and Protein-Based Mechanisms. Front. Mol. Neurosci. *10*, 56.

Esbjörner, E.K., Chan, F., Rees, E., Erdelyi, M., Luheshi, L.M., Bertoncini, C.W., et al. (2014). Direct observations of amyloid beta Self-assembly in live cells provide insights into differences in the kinetics of Abeta(1-40) and Abeta(1-42) aggregation. Chem. Biol. *21*, 732–742.

Esselens, G., Oorschot, V., Baert, V., Raemaekers, T., Spittaels, K., Serneels, L., et al. (2004). Presenilin 1 mediates the turnover of telencephalin in hippocampal neurons via an autophagic degradative pathway. J. Cell Biol. 1041–1054.

Esterházy, D., Stützer, I., Wang, H., Rechsteiner, M.P., Beauchamp, J., Döbeli, H., et al. (2011). Bace2 is a β cell-enriched protease that regulates pancreatic β cell function and mass. Cell Metab. 365–377.

Fagan, A.M., and Perrin, R.J. (2012). Upcoming candidate cerebrospinal fluid biomarkers of Alzheimer's disease. Biomark. Med. *6*, 455–476.

Fagan, A.M., Mintun, M.A., Mach, R.H., Lee, S.-Y., Dence, C.S., Shah, A.R., et al. (2006). Inverse relation between in vivo amyloid imaging load and cerebrospinal fluid Aβ 42 in humans. Ann. Neurol. *59*, 512–519.

Fagan, A.M., Shaw, L.M., Xiong, C., Vanderstichele, H., Mintun, M.A., Trojanowski, J.Q., et al. (2011). Comparison of analytical platforms for cerebrospinal fluid measures of beta-amyloid 1-42, total tau, and p-tau181 for identifying Alzheimer disease amyloid plaque pathology. Arch. Neurol. *68*, 1137–1144.

Faghihnejad, A., and Zeng, H. (2012). Hydrophobic interactions between polymer surfaces: Using polystyrene as a model system. Soft Matter 2746–2758.

Farzan, M., Schnitzler, C.E., Vasilieva, N., Leung, D., and Choe, H. (2000). BACE2, a beta-secretase homolog, cleaves at the beta site and within the amyloid-beta region of the amyloid-beta precursor protein. Proc. Natl. Acad. Sci. *97*, 9712–9717.

FDA (2001). Guidance for Industry Bioanalytical Method Validation. U.S. Dep. Heal. Hum. Serv. 1–27.

Felgenhauer, K. (1974). Protein size and cerebrospinal fluid composition. Klin. Wochenschr. 1158–1164.

De Felice, F.G., Velasco, P.T., Lambert, M.P., Viola, K., Fernandez, S.J., Ferreira, S.T., et al. (2007). Abeta oligomers induce neuronal oxidative stress through an N-methyl-D-aspartate receptor-dependent mechanism that is blocked by the Alzheimer drug memantine. J. Biol. Chem. *282*, 11590–11601.

Fernandez, M.A., Biette, K.M., Dolios, G., Seth, D., Wang, R., and Wolfe, M.S. (2016). Transmembrane Substrate Determinants for γ-Secretase Processing of APP CTFβ. Biochemistry 5675–5688.

Ferreira, D., Perestelo-Pérez, L., Westman, E., Wahlund, L.O., Sarrisa, A., and Serrano-Aguilar, P. (2014). Meta-review of CSF core biomarkers in Alzheimer's disease: The state-of-the-art after the new revised diagnostic criteria. Front. Aging Neurosci. 47.

Ferrer, I., and Gullotta, F. (1990). Down's syndrome and Alzheimer's disease: Dendritic spine counts

in the hippocampus. Acta Neuropathol. *79*, 680–685.

Fiala, M., Cribbs, D.H., Rosenthal, M., and Bernard, G. (2007). Phagocytosis of amyloid-beta and inflammation: two faces of innate immunity in Alzheimer's disease. J. Alzheimers. Dis. *11*, 457–463.

Finckh, U., Müller-Thomsen, T., Mann, U., Eggers, C., Marksteiner, J., Meins, W., et al. (2000). High prevalence of pathogenic mutations in patients with early-onset dementia detected by sequence analyses of four different genes. Am. J. Hum. Genet. *66*, 110–117.

Finckh, U., Kuschel, C., Anagnostouli, M., Patsouris, E., Pantes, G. V., Gatzonis, S., et al. (2005). Novel mutations and repeated findings of mutations in familial Alzheimer disease. Neurogenetics *6*, 85–89.

Finlay, B.L., and Darlington, R.B. (1995). Linked regularities in the development and evolution of mammalian brains. Science (80-.). 1578–1584.

Van der Flier, W.M. (2016). Clinical heterogeneity in familial Alzheimer's disease. Lancet. Neurol. *15*, 1296–1298.

Van Der Flier, W.M., Schoonenboom, S.N.M., Pijnenburg, Y.A.L., Fox, N.C., and Scheltens, P. (2006). The effect of APOE genotype on clinical phenotype in Alzheimer disease. Neurology *67*, 526–527.

Fourier, A., Portelius, E., Zetterberg, H., Blennow, K., Quadrio, I., and Perret-Liaudet, A. (2015). Pre-analytical and analytical factors influencing Alzheimer's disease cerebrospinal fluid biomarker variability. Clin. Chim. Acta *449*, 9–15.

Fox, N.C., Kennedy, A.M., Harvey, R.J., Lantos, P.L., Roques, P.K., Collinge, J., et al. (1997). Clinicopathological features of familial Alzheimer's disease associated with the M139V mutation in the presenilin 1 gene. Pedigree but not mutation specific age at onset provides evidence for a further genetic factor. Brain 491–501.

Fraering, P.C., Ye, W., Strub, J.M., Dolios, G., LaVoie, M.J., Ostaszewski, B.L., et al. (2004). Purification and characterization of the human γ-secretase complex. Biochemistry 9774–9789.

Francis, P.T., Palmer, A.M., Snape, M., and Wilcock, G.K. (1999). The cholinergic hypothesis of Alzheimer's disease: a review of progress. J. Neurol. Neurosurg. Psychiatry *66*, 137–147.

Fraser, P.E., Nguyen, J.T., Inouye, H., Kirschner, D.A., Surewicz, W.K., Selkoe, D.J., et al. (1992). Fibril Formation by Primate, Rodent, and Dutch-Hemorrhagic Analogues of Alzheimer Amyloid β-Protein. Biochemistry 10716–10723.

Fulop, T., Witkowski, J.M., Bourgade, K., Khalil, A., Zerif, E., Larbi, A., et al. (2018). Can an Infection Hypothesis Explain the Beta Amyloid Hypothesis of Alzheimer's Disease? Front. Aging Neurosci. *10*, 224.

Fusaki, N., Ban, H., Nishiyama, A., Saeki, K., and Hasegawa, M. (2009). Efficient induction of transgene-free human pluripotent stem cells using a vector based on Sendai virus, an RNA virus that does not integrate into the host genome. Proc. Jpn. Acad. Ser. B. Phys. Biol. Sci. *85*, 348–362.

Galtieri, D.J., Estep, C.M., Wokosin, D.L., Traynelis, S., and Surmeier, D.J. (2017). Pedunculopontine glutamatergic neurons control spike patterning in substantia nigra dopaminergic neurons. Elife *5*, e30352.

Games, D., Adams, D., Alessandrini, R., Barbour, R., Berthelette, P., Blackwell, C., et al. (1995). Alzheimer-type neuropathology in transgenic mice overexpressing V717F beta-amyloid precursor protein. Nature *373*, 523–527.

Garciá Barrado, L., Coart, E., Vanderstichele, H.M.J., and Burzykowski, T. (2015). Transferring Cut-off Values between Assays for Cerebrospinal Fluid Alzheimer's Disease Biomarkers. J. Alzheimer's Dis. 187–199.

Germain, P.L., and Testa, G. (2017). Taming Human Genetic Variability: Transcriptomic Meta-Analysis Guides the Experimental Design and Interpretation of iPSC-Based Disease Modeling. Stem Cell Reports 1784–1796.

Giacobini, E. (1998). Invited Review Cholinesterase inhibitors for Alzheimer's disease therapy: from tacrine to future applications. Neurochem. Int. *32*, 413–419.

Giorgetti, A., Montserrat, N., Rodriguez-Piza, I., Azqueta, C., Veiga, A., and Belmonte, J.C.I. (2010). Generation of induced pluripotent stem cells from human cord blood cells with only two factors: Oct4 and Sox2. Nat. Protoc. *5*, 811–820.

Glenner, G.G., and Wong, C.W. (1984a). Alzheimer's disease: initial report of the purification and characterization of a novel cerebrovascular amyloid protein. Biochem. Biophys. Res. Commun. *120*, 885–890.

Glenner, G.G., and Wong, C.W. (1984b). Alzheimer's disease and Down's syndrome: Sharing of a unique cerebrovascular amyloid fibril protein. Biochem. Biophys. Res. Commun. 1131–1135.

Goate, A., Chartier-Harlin, M.-C.C., Mullan, M., Brown, J., Crawford, F., Fidani, L., et al. (1991). Segregation of a missense mutation in the amyloid precursor protein gene with familial Alzheimer's disease. Nature *349*, 704–706.

Godbolt, a K., Beck, J. a, Collinge, J., Garrard, P., Warren, J.D., Fox, N.C., et al. (2004). A presenilin 1 R278I mutation presenting with language impairment. Neurology *63*, 1702–1704.

Golde, T.E., Estus, S., Usiak, M., Younkin, L.H., and Younkin, S.G. (1990). Expression of β amyloid protein precursor mRNAs: Recognition of a novel alternatively spliced form and quantitation in alzheimer's disease using PCR. Neuron *4*, 253–267.

Gómez-Isla, T., Growdon, W.B., McNamara, M.J., Nochlin, D., Bird, T.D., Arango, J.C., et al. (1999). The impact of different presenilin 1 and presenilin 2 mutations on amyloid deposition, neurofibrillary changes and neuronal loss in the familial Alzheimer's disease brain. Evidence for other phenotype-modifying factors. Brain 1709–1719.

Gorno-Tempini, M.L., Hillis, A.E., Weintraub, S., Kertesz, A., Mendez, M., Cappa, S.F., et al. (2011). Classification of primary progressive aphasia and its variants. Neurology *76*, 1006–1014.

Götz, J., Deters, N., Doldissen, A., Bokhari, L., Ke, Y., Wiesner, A., et al. (2007). A decade of tau transgenic animal models and beyond. In Brain Pathology, pp. 91–103.

Gouras, G.K., Relkin, N.R., Sweeney, D., Munoz, D.G., Mackenzie, I.R., and Gandy, S. (1997). Increased apolipoprotein E epsilon 4 in epilepsy with senile plaques. Ann. Neurol. *41*, 402–404.

Green, K.N., Demuro, A., Akbari, Y., Hitt, B.D., Smith, I.F., Parker, I., et al. (2008). SERCA pump activity is physiologically regulated by presenilin and regulates amyloid beta production. J. Cell Biol. 1107–1116.

Grimmer, T., Riemenschneider, M., Förstl, H., Henriksen, G., Klunk, W.E., Mathis, C.A., et al. (2009). Beta Amyloid in Alzheimer's Disease: Increased Deposition in Brain Is Reflected in Reduced Concentration in Cerebrospinal Fluid. Biol. Psychiatry 927–934.

Grösgen, S., Grimm, M.O.W., Frieß, P., and Hartmann, T. (2010). Role of amyloid beta in lipid homeostasis. Biochim. Biophys. Acta - Mol. Cell Biol. Lipids *1801*, 966–974.

Grothe, M.J., Barthel, H., Sepulcre, J., Dyrba, M., Sabri, O., and Teipel, S.J. (2017). In vivo staging of regional amyloid deposition. Neurology *89*, 2031–2038.

Group CW (1998). Consensus Report of the Working Group on: "Molecular and Biochemical Markers of Alzheimer's Disease". Neurobiol. Aging *19*, 109–116.

Guerreiro, R., Wojtas, A., Bras, J., Carrasquillo, M., Rogaeva, E., Majounie, E., et al. (2013). TREM2 variants in Alzheimer's disease. N. Engl. J. Med. *368*, 117–127.

Gunhanlar, N., Shpak, G., van der Kroeg, M., Gouty-Colomer, L.A., Munshi, S.T., Lendemeijer, B., et al. (2018). A simplified protocol for differentiation of electrophysiologically mature neuronal networks from human induced pluripotent stem cells. Mol. Psychiatry *23*, 1336–1344.

Guo, X., Qiu, W., Garcia-Milian, R., Lin, X., Zhang, Y., Cao, Y., et al. (2017). Genome-wide significant, replicated and functional risk variants for Alzheimer's disease. J. Neural Transm. *124*, 1455–1471.

Haass, C., Koo, E.H., Mellon, A., Hung, A.Y., and Selkoe, D.J. (1992). Targeting of cell-surface β-amyloid precursor protein to lysosomes: Alternative processing into amyloid-bearing fragments. Nature 500–503.

Haass, C., Kaether, C., Thinakaran, G., and Sisodia, S. (2012). Trafficking and proteolytic processing

of APP. Cold Spring Harb. Perspect. Med. *2*, a006270.

Haenseler, W., Sansom, S.N., Buchrieser, J., Newey, S.E., Moore, C.S., Nicholls, F.J., et al. (2017). A Highly Efficient Human Pluripotent Stem Cell Microglia Model Displays a Neuronal-Co-culture-Specific Expression Profile and Inflammatory Response. Stem Cell Reports *8*, 1727–1742.

Haggerty, L., Watson, B.A., Barteau, M.A., and Lenhoff, A.M. (1991). Ordered arrays of proteins on graphite observed by scanning tunneling microscopy. J. Vac. Sci. Technol. B Microelectron. Nanom. Struct. *9*, 1219.

Halle, A., Hornung, V., Petzold, G.C., Stewart, C.R., Monks, B.G., Reinheckel, T., et al. (2008). The NALP3 inflammasome is involved in the innate immune response to amyloid-beta. Nat Immunol *9*, 857–865.

Hamid, R., Kilger, E., Willem, M., Vassallo, N., Kostka, M., Bornhövd, C., et al. (2007). Amyloid precursor protein intracellular domain modulates cellular calcium homeostasis and ATP content. J. Neurochem. 1264–1275.

Han, S., Kollmer, M., Markx, D., Claus, S., Walther, P., and Fändrich, M. (2017). Amyloid plaque structure and cell surface interactions of β-amyloid fibrils revealed by electron tomography. Sci. Rep. 43577.

Handel, A.E., Chintawar, S., Lalic, T., Whiteley, E., Vowles, J., Giustacchini, A., et al. (2016). Assessing similarity to primary tissue and cortical layer identity in induced pluripotent stem cell-derived cortical neurons through single-cell transcriptomics. Hum. Mol. Genet. *25*, 989–1000.

Hanisch, F., and Kolmel, H.W. (2004). Genotype-phenotype analysis in early-onset Alzheimer's disease due to presenilin-1 mutations at codon 139. Eur.J.Med.Res. 361–364.

Hansson, O., Zetterberg, H., Buchhave, P., Londos, E., Blennow, K., and Minthon, L. (2006). Association between CSF biomarkers and incipient Alzheimer's disease in patients with mild cognitive impairment: a follow-up study. Lancet. Neurol. *5*, 228–234.

Hansson, O., Mikulskis, A., Fagan, A.M., Teunissen, C., Zetterberg, H., Vanderstichele, H., et al. (2018). The impact of preanalytical variables on measuring cerebrospinal fluid biomarkers for Alzheimer's disease diagnosis: A review. Alzheimer's Dement. 1313–1333.

Härd, T. (2014). Amyloid fibrils: Formation, polymorphism, and inhibition. J. Phys. Chem. Lett. 607–614.

Hardy, J. (2006). Alzheimer's disease: the amyloid cascade hypothesis: an update and reappraisal. J. Alzheimers. Dis. *9*, 151–153.

Hardy, J. (2009). The amyloid hypothesis for Alzheimer's disease: A critical reappraisal. J. Neurochem. *110*, 1129–1134.

Hardy, J., and Allsop, D. (1991). Amyloid deposition as the central event in the aetiology of Alzheimer's disease. Trends Pharmacol. Sci. *12*, 383–388.

Hardy, J.A., and Higgins, G.A. (1992). Alzheimer's disease: the amyloid cascade hypothesis. Science *256*, 184–185.

Hartmann, T. (2006). Role of amyloid precursor protein, amyloid-beta and gamma-secretase in cholesterol maintenance. Neurodegener. Dis. *3*, 305–311.

Hatami, A., Monjazeb, S., Milton, S., and Glabe, C.G. (2017). Familial Alzheimer's disease mutations within the amyloid precursor protein alter the aggregation and conformation of the amyloid beta peptide. J. Biol. Chem. jbc.M116.755264.

Haynes, C.A., and Norde, W. (1994). Globular proteins at solid/liquid interfaces. Colloids Surfaces B Biointerfaces *2*, 517–566.

Hayrapetyan, V., Rybalchenko, V., Rybalchenko, N., and Koulen, P. (2008). The N-terminus of presenilin-2 increases single channel activity of brain ryanodine receptors through direct protein-protein interaction. Cell Calcium 507–518.

Heber, S., Herms, J., Gajic, V., Hainfellner, J., Aguzzi, A., Rülicke, T., et al. (2000). Mice with combined gene knock-outs reveal essential and partially redundant functions of amyloid precursor protein family members. J. Neurosci. *20*, 7951–7963.

Herl, L., Thomas, A. V, Lill, C.M., Banks, M., Deng, A., Jones, P.B., et al. (2009). Mutations in amyloid precursor protein affect its interactions with presenilin/gamma-secretase. Mol. Cell. Neurosci. *41*, 166–174.

Hill, R.S., and Walsh, C.A. (2005). Molecular insights into human brain evolution. Nature 64–67.

Hippius, H., and Neundörfer, G. (2003). The discovery of Alzheimer's disease. Dialogues Clin. Neurosci. *5*, 101–108.

Hjelm, B.E., Salhia, B., Kurdoglu, A., Szelinger, S., Reiman, R.A., Sue, L.I., et al. (2013). In vitro-differentiated neural cell cultures progress towards donor-identical brain tissue. Hum. Mol. Genet. *22*, 3534–3546.

Hlady, V., Buijs, J., and Jennissen, H.P. (1999). Methods for studying protein adsorption. Methods Enzymol. 402–429.

Holmes, C. (2002). Genotype and phenotype in Alzheimer's disease. Br J Psychiatry *180*, 131–134.

Hou, L., Shao, H., Zhang, Y., Li, H., Menon, N.K., Neuhaus, E.B., et al. (2004). Solution NMR Studies of the Aβ(1-40) and Aβ(1-42) Peptides Establish that the Met35 Oxidation State Affects the Mechanism of Amyloid Formation. J. Am. Chem. Soc. 1992–2005.

Houlden, H., Baker, M., McGowan, E., Lewis, P., Hutton, M., Crook, R., et al. (2000). Variant Alzheimer's disease with spastic paraparesis and cotton wool plaques is caused by PS-1

mutations that lead to exceptionally high amyloid-β concentrations. Ann. Neurol. *48*, 806–808.

Hsieh, H., Boehm, J., Sato, C., Iwatsubo, T., Tomita, T., Sisodia, S., et al. (2006). AMPAR Removal Underlies Aβ-Induced Synaptic Depression and Dendritic Spine Loss. Neuron 831–843.

Hüll, M., Fiebich, B.L., Dykierek, P., Schmidtke, K., Nitzsche, E., Orszagh, M., et al. (1998). Early-onset Alzheimer's disease due to mutations of the presenilin-1 gene on chromosome 14: A 7-year follow-up of a patient with a mutation at codon 139. Eur. Arch. Psychiatry Clin. Neurosci. 123–129.

Humpel, C. (2011). Identifying and validating biomarkers for Alzheimer's disease. Trends Biotechnol. *29*, 26–32.

Hung, C.O.Y., and Livesey, F.J. (2018). Altered γ-Secretase Processing of APP Disrupts Lysosome and Autophagosome Function in Monogenic Alzheimer's Disease. Cell Rep. *25*, 3647–3660.e2.

Hutton, M., Busfield, F., Wragg, M., Crook, R., Perez-Tur, J., Clark, R.F., et al. (1996). Complete analysis of the presenilin 1 gene in early onset Alzheimer's disease. Neuroreport 801–805.

Iljina, M., Garcia, G.A., Dear, A.J., Flint, J., Narayan, P., Michaels, T.C.T., et al. (2016). Quantitative analysis of co-oligomer formation by amyloid-beta peptide isoforms. Sci. Rep. 28658.

Iovino, M., Agathou, S., González-Rueda, A., Del Castillo Velasco-Herrera, M., Borroni, B., Alberici, A., et al. (2015). Early maturation and distinct tau pathology in induced pluripotent stem cell-derived neurons from patients with MAPT mutations. Brain *138*, 3345–3359.

Irizarry, M.C., Locascio, J.J., and Hyman, B.T. (2001). β-site APP cleaving enzyme mRNA expression in APP transgenic mice: Anatomical overlap with transgene expression and static levels with aging. Am. J. Pathol. 173–177.

Israel, M.A., Yuan, S.H., Bardy, C., Reyna, S.M., Mu, Y., Herrera, C., et al. (2012). Probing sporadic and familial Alzheimer's disease using induced pluripotent stem cells. Nature *482*, 216–220.

Itkin, A., Salnikov, E.S., Aisenbrey, C., Raya, J., Glattard, E., Raussens, V., et al. (2017). Structural Characterization of the Amyloid Precursor Protein Transmembrane Domain and Its γ-Cleavage Site. ACS Omega *2*, 6525–6534.

Itzhaki, R.F., Lathe, R., Balin, B.J., Ball, M.J., Bearer, E.L., Braak, H., et al. (2016). Microbes and Alzheimer's Disease. J. Alzheimers. Dis. *51*, 979–984.

Jack, C.R., Knopman, D.S., Jagust, W.J., Petersen, R.C., Weiner, M.W., Aisen, P.S., et al. (2013). Update on hypothetical model of Alzheimer's disease biomarkers. Lancet Neurol. *12*, 207–216.

Jacobsen, J.S., Muenkel, H.A., Blume, A.J., and Vitek, M.P. (1991). A novel species-specific RNA related to alternatively spliced amyloid precursor protein mRNAs. Neurobiol. Aging *12*, 575–583.

Jahn, R., and Fasshauer, D. (2012). Molecular machines governing exocytosis of synaptic vesicles.

Nature 201–207.

Janelidze, S., Hertze, J., Zetterberg, H., Landqvist Waldo, M., Santillo, A., Blennow, K., et al. (2015). Cerebrospinal fluid neurogranin and YKL-40 as biomarkers of Alzheimer's disease. Ann. Clin. Transl. Neurol. *3*, 12–20.

Janelidze, S., Zetterberg, H., Mattsson, N., Palmqvist, S., Vanderstichele, H., Lindberg, O., et al. (2016). CSF Aβ42/Aβ40 and Aβ42/Aβ38 ratios: better diagnostic markers of Alzheimer disease. Ann. Clin. Transl. Neurol. *3*, 154–165.

Jang, S.Y., and Kim, D.S. (2016). Physical properties of polypropylene composites with hydrophobized cellulose powder by soybean oil. J. Appl. Polym. Sci. *133*.

Janssen, J.C., Beck, J.A., Campbell, T.A., Dickinson, A., Fox, N.C., Harvey, R.J., et al. (2003). Early onset familial Alzheimer's disease: Mutation frequency in 31 families. Neurology *60*, 235–239.

Jarosz-Griffiths, H.H., Corbett, N.J., Rowland, H.A., Fisher, K., Jones, A.C., Baron, J., et al. (2019). Proteolytic shedding of the prion protein via activation of metallopeptidase ADAM10 reduces cellular binding and toxicity of amyloid-β oligomers. J. Biol. Chem. *294*, 7085–7097.

Jaunmuktane, Z., Mead, S., Ellis, M., Wadsworth, J.D.F., Nicoll, A.J., Kenny, J., et al. (2015). Evidence for human transmission of amyloid-β pathology and cerebral amyloid angiopathy. Nature *525*, 247–250.

Ji, S.-R., Wu, Y., and Sui, S.-F. (2002). Study of beta-amyloid peptide (Abeta40) insertion into phospholipid membranes using monolayer technique. Biochem. Biokhimiia *67*, 1283–1288.

De Jong, D., Jansen, R.W.M.M., Kremer, B.P.H., and Verbeek, M.M. (2006). Cerebrospinal fluid amyloid β42/phosphorylated tau ratio discriminates between Alzheimer's disease and vascular dementia. Journals Gerontol. - Ser. A Biol. Sci. Med. Sci. *7*, 755–758.

De Jonghe, C., Cruts, M., Rogaeva, E.A., Tysoe, C., Singleton, A., Vanderstichele, H., et al. (1999). Aberrant splicing in the presenilin-1 intron 4 mutation causes presenile Alzheimer's disease by increased Aβ42 secretion. Hum. Mol. Genet. *8*, 1529–1540.

De Jonghe, C., Esselens, C., Kumar-Singh, S., Craessaerts, K., Serneels, S., Checler, F., et al. (2001). Pathogenic APP mutations near the gamma-secretase cleavage site differentially affect Abeta secretion and APP C-terminal fragment stability. Hum. Mol. Genet. *10*, 1665–1671.

Joo, Y., Ha, S., Hong, B.H., Kim, J.A., Chang, K.A., Liew, H., et al. (2010). Amyloid precursor protein binding protein-1 modulates cell cycle progression in fetal neural stem cells. PLoS One e14203.

Jørgensen, P., Bus, C., Pallisgaard, N., Bryder, M., and Jørgensen, A.L. (2008). Familial Alzheimer's disease co-segregates with a Met 146 Ile substitution in presenilin-1. Clin. Genet. *50*, 281–286.

Jorissen, E., Prox, J., Bernreuther, C., Weber, S., Schwanbeck, R., Serneels, L., et al. (2010). The disintegrin/metalloproteinase ADAM10 is essential for the establishment of the brain cortex. J.

Neurosci. *30*, 4833–4844.

Josephy, P.D., Eling, T., and Mason, R.P. (1982). The horseradish peroxidase-catalyzed oxidation of 3,5,3',5'-tetramethylbenzidine. Free radical and charge-transfer complex intermediates. J. Biol. Chem. *257*, 3669–3675.

Julia, T.C.W., and Goate, A.M. (2017). Genetics of beta-Amyloid Precursor Protein in Alzheimer's Disease. COLD SPRING Harb. Perspect. Med. *7*, a024539.

Jung, C.K.E., and Herms, J. (2012). Role of APP for dendritic spine formation and stability. Exp. Brain Res. 463–470.

Kadavil, J. (2013). Guidance for Industry Bioanalytical Method Validation Guidance for Industry Bioanalytical Method Validation Center for Veterinary Medicine (CVM) Contains Nonbinding Recommendations. Commun. Staff *20855*, 240–276.

Kaether, C., Skehel, P., and Dotti, C.G. (2000). Axonal Membrane Proteins Are Transported in Distinct Carriers: A Two-Color Video Microscopy Study in Cultured Hippocampal Neurons. Mol. Biol. Cell *11*, 1213–1224.

Kaether, C., Capell, A., Edbauer, D., Winkler, E., Novak, B., Steiner, H., et al. (2004). The presenilin C-terminus is required for ER-retention, nicastrin-binding and γ-secretase activity. EMBO J. 4738–4748.

Kaiser, E., Schönknecht, P., Thomann, P.A., Hunt, A., and Schröder, J. (2007). Influence of delayed CSF storage on concentrations of phospho-tau protein (181), total tau protein and beta-amyloid (1-42). Neurosci. Lett. *417*, 193–195.

Kakio, A., Yano, Y., Takai, D., Kuroda, Y., Matsumoto, O., Kozutsumi, Y., et al. (2004). Interaction between amyloid beta-protein aggregates and membranes. J. Pept. Sci. *10*, 612–621.

Kamenetz, F., Tomita, T., Hsieh, H., Seabrook, G., Borchelt, D., Iwatsubo, T., et al. (2003). APP processing and synaptic function. Neuron *37*, 925–937.

Kametani, F., and Hasegawa, M. (2018). Reconsideration of Amyloid Hypothesis and Tau Hypothesis in Alzheimer's Disease. Front. Neurosci. *12*, 25.

Kammoun, S., Gold, G., Bouras, C., Giannakopoulos, P., McGee, W., Herrmann, F., et al. (2000). Immediate causes of death of demented and non-demented elderly. Acta Neurol. Scand. Suppl. *176*, 96–99.

Kang, J., Lemaire, H.G., Unterbeck, A., Salbaum, J.M., Masters, C.L., Grzeschik, K.H., et al. (1987). The precursor of Alzheimer's disease amyloid A4 protein resembles a cell-surface receptor. Nature *325*, 733–736.

Kastantin, M., Langdon, B.B., and Schwartz, D.K. (2014). A bottom-up approach to understanding protein layer formation at solid-liquid interfaces. Adv. Colloid Interface Sci. *207*, 240–252.

Katzman, R. (1976). The prevalence and malignancy of alzheimer disease: A major killer. Arch. Neurol. *33*, 217–218.

Kay, K.R., Smith, C., Wright, A.K., Serrano-Pozo, A., Pooler, A.M., Koffie, R., et al. (2013). Studying synapses in human brain with array tomography and electron microscopy. Nat. Protoc. *8*, 1366–1380.

Kelleher, R.J., and Shen, J. (2017). Presenilin-1 mutations and Alzheimer's disease. Proc. Natl. Acad. Sci. *114*, 629–631.

Kelly, B.L., and Ferreira, A. (2006). beta-amyloid-induced dynamin 1 degradation is mediated by N-methyl-D-aspartate receptors in hippocampal neurons. J. Biol. Chem. *281*, 28079–28089.

Kennedy, A.M., Newman, S.K., Frackowiak, R.S.J., Cunningham, V.J., Roques, P., Stevens, J., et al. (1995). Chromosome 14 linked familial alzheimer's disease: A clinico-pathological study of a single pedigree. Brain 185–205.

Kester, M.I., Teunissen, C.E., Crimmins, D.L., Herries, E.M., Ladenson, J.H., Scheltens, P., et al. (2015a). Neurogranin as a Cerebrospinal Fluid Biomarker for Synaptic Loss in Symptomatic Alzheimer Disease. JAMA Neurol. *72*, 1275–1280.

Kester, M.I., Teunissen, C.E., Sutphen, C., Herries, E.M., Ladenson, J.H., Xiong, C.J., et al. (2015b). Cerebrospinal fluid VILIP-1 and YKL-40, candidate biomarkers to diagnose, predict and monitor Alzheimer's disease in a memory clinic cohort. Alzheimers Res. Ther. *7*, 9.

Khachaturian, Z.S. (1989). Calcium, membranes, aging and Alzheimer's disease: Introduction and overview. Ann. N. Y. Acad. Sci. 1–4.

Ben Khalifa, N., Tyteca, D., Marinangeli, C., Depuydt, M., Collet, J.-F., Courtoy, P.J., et al. (2012). Structural features of the KPI domain control APP dimerization, trafficking, and processing. FASEB J. *26*, 855–867.

Kieburtz, K., and Olanow, C.W. (2007). Translational experimental therapeutics: The translation of laboratory-based discovery into disease-related therapy. Mt. Sinai J. Med. 7–14.

Kim, K., Doi, A., Wen, B., Ng, K., Zhao, R., Cahan, P., et al. (2010). Epigenetic memory in induced pluripotent stem cells. Nature *467*, 285–290.

Kins, S., Lauther, N., Szodorai, A., and Beyreuther, K. (2006). Subcellular trafficking of the amyloid precursor protein gene family and its pathogenic role in Alzheimer's disease. Neurodegener Dis *3*, 218–226.

Kirazov, E., Kirazov, L., Bigl, V., and Schliebs, R. (2001). Ontogenetic changes in protein level of amyloid precursor protein (APP) in growth cones and synaptosomes from rat brain and prenatal expression pattern of APP mRNA isoforms in developing rat embryo. In International Journal of Developmental Neuroscience, pp. 287–296.

Kirwan, P., Turner-Bridger, B., Peter, M., Momoh, A., Arambepola, D., Robinson, H.P.C., et al. (2015). Development and function of human cerebral cortex neural networks from pluripotent stem cells in vitro. Development *142*, 3178–3187.

Klunk, W.E., Engler, H., Nordberg, A., Wang, Y., Blomqvist, G., Holt, D.P., et al. (2004). Imaging Brain Amyloid in Alzheimer's Disease with Pittsburgh Compound-B. Ann. Neurol. *55*, 306–319.

Knappenberger, K.S., Tian, G., Ye, X., Sobotka-Briner, C., Ghanekar, S. V., Greenberg, B.D., et al. (2004). Mechanism of γ-secretase cleavage activation: Is γ-secretase regulated through autoinhibition involving the presenilin-1 exon 9 loop? Biochemistry 6208–6218.

Von Koch, C.S., Zheng, H., Chen, H., Trumbauer, M., Thinakaran, G., Van Der Ploeg, L.H.T., et al. (1997). Generation of APLP2 KO mice and early postnatal lethality in APLP2/APP double KO mice. Neurobiol. Aging *18*, 661–669.

Koedam, E.L.G.E., Lauffer, V., Van Der Vlies, A.E., Van Der Flier, W.M., Scheltens, P., and Pijnenburg, Y.A.L. (2010). Early-versus late-onset Alzheimer's disease: More than age alone. J. Alzheimer's Dis. *19*, 1401–1408.

Kofanova, O. a., Mommaerts, K., and Betsou, F. (2015). Tube Polypropylene: A Neglected Critical Parameter for Protein Adsorption During Biospecimen Storage. Biopreserv. Biobank. *00*, 150717092401003.

Koffie, R.M., Meyer-Luehmann, M., Hashimoto, T., Adams, K.W., Mielke, M.L., Garcia-Alloza, M., et al. (2009). Oligomeric amyloid beta associates with postsynaptic densities and correlates with excitatory synapse loss near senile plaques. Proc. Natl. Acad. Sci. U. S. A. *106*, 4012–4017.

Kohli, B.M., Pflieger, D., Mueller, L.N., Carbonetti, G., Aebersold, R., Nitsch, R.M., et al. (2012). Interactome of the amyloid precursor protein APP in brain reveals a protein network involved in synaptic vesicle turnover and a close association with synaptotagmin-1. J. Proteome Res. 4075–4090.

Kokiko-Cochran, O.N., and Godbout, J.P. (2018). The Inflammatory Continuum of Traumatic Brain Injury and Alzheimer's Disease. Front. Immunol. *9*, 672.

Komarova, N.L., and Thalhauser, C.J. (2011). High degree of heterogeneity in Alzheimer's disease progression patterns. PLoS Comput. Biol. *7*, e1002251.

Koppaka, V., and Axelsen, P.H. (2000). Accelerated accumulation of amyloid beta proteins on oxidatively damaged lipid membranes. Biochemistry *39*, 10011–10016.

Korff, A., Liu, C., Ginghina, C., Shi, M., and Zhang, J. (2013). α-Synuclein in cerebrospinal fluid of Alzheimer's disease and mild cognitive impairment. *36*, 679–688.

Krantic, S., Isorce, N., Mechawar, N., Davoli, M.A., Vignault, E., Albuquerque, M., et al. (2012). Hippocampal GABAergic neurons are susceptible to amyloid-β toxicity in vitro and are

decreased in number in the alzheimer's disease TgCRND8 mouse model. J. Alzheimer's Dis. 293–308.

Kuhn, P.-H., Wang, H., Dislich, B., Colombo, A., Zeitschel, U., Ellwart, J.W., et al. (2010). ADAM10 is the physiologically relevant, constitutive α-secretase of the amyloid precursor protein in primary neurons. EMBO J. *29*, 3020–3032.

Kukar, T.L., Ladd, T.B., Robertson, P., Pintchovski, S.A., Moore, B., Bann, M.A., et al. (2011). Lysine 624 of the amyloid precursor protein (APP) is a critical determinant of amyloid β peptide length: Support for a sequential model of γ-secretase intramembrane proteolysis and regulation by the amyloid β precursor protein (APP) juxtamembrane region. J. Biol. Chem. *286*, 39804–39812.

Kukull, W.A., Brenner, D.E., Speck, C.E., Nochlin, D., Bowen, J., McCormick, W., et al. (1994). Causes of Death Associated with Alzheimer Disease: Variation by Level of Cognitive Impairment Before Death. J. Am. Geriatr. Soc. *42*, 723–726.

Kummer, M.P., and Heneka, M.T. (2014). Truncated and modified amyloid-beta species. Alzheimers. Res. Ther. *6*, 28.

Kunkle, B.W., Grenier-Boley, B., Sims, R., Bis, J.C., Damotte, V., Naj, A.C., et al. (2019). Genetic meta-analysis of diagnosed Alzheimer's disease identifies new risk loci and implicates Aβ, tau, immunity and lipid processing. Nat. Genet. *51*, 414–430.

de la Torre, J.C. (2010). The vascular hypothesis of Alzheimer's disease: bench to bedside and beyond. Neurodegener. Dis. *7*, 116–121.

De la Torre, J.C., and Mussivand, T. (1993). Can disturbed brain microcirculation cause Alzheimer's disease? Neurol. Res. 146–153.

LaFerla, F.M. (2002). Calcium dyshomeostasis and intracellular signalling in alzheimer's disease. Nat. Rev. Neurosci. *3*, 862–872.

LaFerla, F.M., and Green, K.N. (2012). Animal models of Alzheimer disease. Cold Spring Harb. Perspect. Med. *2*, a006320.

LaFerla, F.M., Green, K.N., and Oddo, S. (2007). Intracellular amyloid-β in Alzheimer's disease. Nat. Rev. Neurosci. *8*, 499–509.

Lam, B., Masellis, M., Freedman, M., Stuss, D.T., and Black, S.E. (2013). Clinical, imaging, and pathological heterogeneity of the Alzheimer's disease syndrome. Alzheimer's Res. Ther. 1.

Lancaster, M.A., and Knoblich, J. (2014). Generation of Cerebral Organoids from Human Pluripotent Stem. Nat. Protoc. 2329–2340.

Lancaster, M.A., Renner, M., Martin, C.-A., Wenzel, D., Bicknell, L.S., Hurles, M.E., et al. (2013). Cerebral organoids model human brain development and microcephaly. Nature *501*, 373–379.

Larner, A.J., and Du Plessis, D.G. (2003). Early-onset Alzheimer's disease with presenilin-1 M139V mutation: Clinical, neuropsychological and neuropathological study. Eur. J. Neurol. 319–323.

Laudon, H., Hansson, E.M., Melén, K., Bergman, A., Farmery, M.R., Winblad, B., et al. (2005). A nine-transmembrane domain topology for presenilin 1. J. Biol. Chem. 35352–35360.

Lauren, J., Gimbel, D. a, Nygaard, H.B., Gilbert, J.W., and Strittmatter, S.M. (2009). Cellular prion protein mediates impairment of synaptic plasticity by amyloid-β oligomers. Nature *457*, 1128.

Lauridsen, C., Sando, S.B., Møller, I., Berge, G., Pomary, P.K., Grøntvedt, G.R., et al. (2017). Cerebrospinal fluid Aβ43 is reduced in early-onset compared to late-onset Alzheimer's disease, but has similar diagnostic accuracy to Aβ42. Front. Aging Neurosci. 210.

LaVoie, M.J., Fraering, P.C., Ostaszewski, B.L., Ye, W., Kimberly, W.T., Wolfe, M.S., et al. (2003). Assembly of the γ-secretase complex involves early formation of an intermediate subcomplex of Aph-1 and nicastrin. J. Biol. Chem. 37213–37222.

Lazarevic, V., Fieńko, S., Andres-Alonso, M., Anni, D., Ivanova, D., Montenegro-Venegas, C., et al. (2017). Physiological Concentrations of Amyloid Beta Regulate Recycling of Synaptic Vesicles via Alpha7 Acetylcholine Receptor and CDK5/Calcineurin Signaling. Front. Mol. Neurosci. 221.

Lazarov, O. (2005). Axonal Transport, Amyloid Precursor Protein, Kinesin-1, and the Processing Apparatus: Revisited. J. Neurosci. *25*, 2386–2395.

Lee, S.C.M., and Lueck, C.J. (2014). Cerebrospinal fluid pressure in adults. J. Neuro-Ophthalmology *34*, 278–283.

Lee, S.H., and Ruckenstein, E. (1988). Adsorption of proteins onto polymeric surfaces of different hydrophilicities-a case study with bovine serum albumin. J. Colloid Interface Sci. *125*, 365–379.

Lee, M.S., Kao, S.C., Lemere, C.A., Xia, W., Tseng, H.C., Zhou, Y., et al. (2003). APP processing is regulated by cytoplasmic phosphorylation. J. Cell Biol. 83–95.

Lewczuk, P., Beck, G., Esselmann, H., Bruckmoser, R., Zimmermann, R., Fiszer, M., et al. (2006a). Effect of Sample Collection Tubes on Cerebrospinal Fluid Concentrations of Tau Proteins and Amyloid β Peptides. Clin. Chem. *52*, 331–334.

Lewczuk, P., Beck, G., Ganslandt, O., Esselmann, H., Deisenhammer, F., Regeniter, A., et al. (2006b). International quality control survey of neurochemical dementia diagnostics. Neurosci. Lett. 1–4.

Lewczuk, P., Kornhuber, J., Vanderstichele, H., Vanmechelen, E., Esselmann, H., Bibl, M., et al. (2008). Multiplexed quantification of dementia biomarkers in the CSF of patients with early dementias and MCI: A multicenter study. Neurobiol. Aging *29*, 812–818.

Li, T., Pires, C., Nielsen, T.T., Waldemar, G., Hjermind, L.E., Nielsen, J.E., et al. (2016). Generation of induced pluripotent stem cells (iPSCs) from an Alzheimer's disease patient carrying a M146I

mutation in PSEN1. Stem Cell Res. *16*, 334–337.

Li, Z.W., Stark, G., Götz, J., Rülicke, T., Gschwind, M., Huber, G., et al. (1996). Generation of mice with a 200-kb amyloid precursor protein gene deletion by Cre recombinase-mediated site-specific recombination in embryonic stem cells. Proc. Natl. Acad. Sci. U. S. A. *93*, 6158–6162.

Liao, L., Cheng, D., Wang, J., Duong, D.M., Losik, T.G., Gearing, M., et al. (2004). Proteomic characterization of postmortem amyloid plaques isolated by laser capture microdissection. J. Biol. Chem. *279*, 37061–37068.

Lindquist, S., Schwartz, M., Batbayli, M., Waldemar, G., and Nielsen, J. (2009). Genetic testing in familial AD and FTD: Mutation and phenotype spectrum in a Danish cohort. Clin. Genet. *76*, 205–209.

Liu, L., and Caselli, R.J. (2018). Age stratification corrects bias in estimated hazard of APOE genotype for Alzheimer's disease. 602–608.

Liu, Q., and Zhang, J. (2014). Lipid metabolism in Alzheimer's disease. Neurosci. Bull. *30*, 331–345.

Liu, D., Cao, B., Zhao, Y., Huang, H., McIntyre, R.S., Rosenblat, J.D., et al. (2018). Soluble TREM2 changes during the clinical course of Alzheimer's disease: A meta-analysis. Neurosci. Lett. 10–16.

Liu, K., Doms, R.W., and Lee, V.M.Y. (2002). Glu11 site cleavage and N-terminally truncated Aβ production upon BACE overexpression. Biochemistry 3128–3136.

Logovinsky, V., Satlin, A., Lai, R., Swanson, C., Kaplow, J., Osswald, G., et al. (2016). Safety and tolerability of BAN2401 - a clinical study in Alzheimer's disease with a protofibril selective Aβ antibody. Alzheimers. Res. Ther. *8*, 14.

Lorenzen, A., Samosh, J., Vandewark, K., Anborgh, P.H., Seah, C., Magalhaes, A.C., et al. (2010). Rapid and Direct Transport of Cell Surface APP to the Lysosome defines a novel selective pathway. Mol. Brain *3*, 11.

Lucey, B.P., Gonzales, C., Das, U., Li, J., Siemers, E.R., Slemmon, J.R., et al. (2015). An integrated multi-study analysis of intra-subject variability in cerebrospinal fluid amyloid-β concentrations collected by lumbar puncture and indwelling lumbar catheter. Alzheimers. Res. Ther. *7*, 53.

Luo, Y., Bolon, B., Damore, M.A., Fitzpatrick, D., Liu, H., Zhang, J., et al. (2003). BACE1 (beta-secretase) knockout mice do not acquire compensatory gene expression changes or develop neural lesions over time. Neurobiol. Dis. *14*, 81–88.

Mahairaki, V., Ryu, J., Peters, A., Chang, Q., Li, T., Park, T.S., et al. (2014). Induced pluripotent stem cells from familial Alzheimer's disease patients differentiate into mature neurons with amyloidogenic properties. Stem Cells Dev. *23*, 2996–3010.

Mallon, B.S., Hamilton, R.S., Kozhich, O.A., Johnson, K.R., Fann, Y.C., Rao, M.S., et al. (2014).

Comparison of the molecular profiles of human embryonic and induced pluripotent stem cells of isogenic origin. Stem Cell Res. *12*, 376–386.

Markesbery, W.R. (1997). Oxidative Stress Hypothesis in Alzheimer's Disease. Free Radic. Biol. Med. *23*, 134–147.

Martin, U. (2017). Therapeutic Application of Pluripotent Stem Cells: Challenges and Risks. Front. Med. *4*, 229.

Martin Prince, A., Wimo, A., Guerchet, M., Gemma-Claire Ali, M., Wu, Y.-T., Prina, M., et al. (2015). World Alzheimer Report 2015: The Global Impact of Dementia - An analysis of prevalence, incidence, cost and trends. Alzheimer's Dis. Int. 1–84.

Marzesco, A.M., Flötenmeyer, M., Bühler, A., Obermüller, U., Staufenbiel, M., Jucker, M., et al. (2016). Highly potent intracellular membrane-associated Aβ seeds. Sci. Rep. 28125.

Masters, C.L., Simms, G., Weinman, N.A., Multhaup, G., McDonald, B.L., and Beyreuther, K. (1985). Amyloid plaque core protein in Alzheimer disease and Down syndrome. Proc. Natl. Acad. Sci. U. S. A. *82*, 4245–4249.

Masters, M.C., Morris, J.C., and Roe, C.M. (2015). "Noncognitive" symptoms of early Alzheimer disease : A longitudinal analysis. Neurology *84*, 617–622.

Mathews, P.M., Cataldo, A.M., Kao, B.H., Rudnicki, A.G., Qin, X., Yang, J.L., et al. (2000). Brain expression of presenilins in sporadic and early-onset, familial Alzheimer's disease. Mol Med *6*, 878–891.

Matsui, T., Ingelsson, M., Fukumoto, H., Ramasamy, K., Kowa, H., Frosch, M.P., et al. (2007). Expression of APP pathway mRNAs and proteins in Alzheimer's disease. Brain Res. *1161*, 116–123.

Matsumura, N., Takami, M., Okochi, M., Wada-Kakuda, S., Fujiwara, H., Tagami, S., et al. (2014). γ-secretase associated with lipid rafts: Multiple interactive pathways in the stepwise processing of β-carboxylterminal fragment. J. Biol. Chem. *289*, 5109–5121.

Matthews, F.E., Arthur, A., Barnes, L.E., Bond, J., Jagger, C., Robinson, L., et al. (2013). A two-decade comparison of prevalence of dementia in individuals aged 65 years and older from three geographical areas of England: Results of the cognitive function and ageing study i and II. Lancet 1405–1412.

Mattson, M.P., Cheng, B., Culwell, A.R., Esch, F.S., Lieberburg, I., and Rydel, R.E. (1993). Evidence for excitoprotective and intraneuronal calcium-regulating roles for secreted forms of the β-amyloid precursor protein. Neuron 243–254.

Mattsson, N., Zetterberg, H., and Blennow, K. (2010). Lessons from Multicenter Studies on CSF Biomarkers for Alzheimer's Disease. Int. J. Alzheimers. Dis. *2010*, 610613.

Mattsson, N., Andreasson, U., Persson, S., Arai, H., Batish, S.D., Bernardini, S., et al. (2011). The Alzheimer's Association external quality control program for cerebrospinal fluid biomarkers. Alzheimer's Dement. *7*, 386–395.e6.

Mattsson, N., Zegers, I., Andreasson, U., Bjerke, M., Blankenstein, M.A., Bowser, R., et al. (2012a). Reference measurement procedures for Alzheimer's disease cerebrospinal fluid biomarkers: definitions and approaches with focus on amyloid beta42. Biomark.Med. *6*, 409–417.

Mattsson, N., Andreasson, U., Carrillo, M.C., Persson, S., Shaw, L.M., Zegers, I., et al. (2012b). Proficiency testing programs for Alzheimer's disease cerebrospinal fluid biomarkers. Biomark. Med. *6*, 401–407.

Mattsson, N., Andreasson, U., Persson, S., Carrillo, M.C., Collins, S., Chalbot, S., et al. (2013). CSF biomarker variability in the Alzheimer's Association quality control program. Alzheimer's Dement. *9*, 251–261.

McGeer, P.L., and McGeer, E.G. (2013). The amyloid cascade-inflammatory hypothesis of Alzheimer disease: implications for therapy. Acta Neuropathol. *126*, 479–497.

McKhann, G.M., Knopman, D.S., Chertkow, H., Hyman, B.T., Jack, C.R., Kawas, C.H., et al. (2011). The diagnosis of dementia due to Alzheimer's disease: Recommendations from the National Institute on Aging-Alzheimer's Association workgroups on diagnostic guidelines for Alzheimer's disease. Alzheimer's Dement. *7*, 263–269.

McLaurin, J., and Chakrabartty, a (1997). Characterization of the interactions of Alzheimer beta-amyloid peptides with phospholipid membranes. Eur. J. Biochem. *245*, 355–363.

Medina, M. (2018). An overview on the clinical development of tau-based therapeutics. Int. J. Mol. Sci. 1160.

Mehta, D., Jackson, R., Paul, G., Shi, J., and Sabbagh, M. (2017). Why do trials for Alzheimer's disease drugs keep failing? A discontinued drug perspective for 2010-2015. Expert Opin. Investig. Drugs 735–739.

Mehta, S.R., Tom, C.M., Wang, Y., Mathkar, P.P., Tang, J., Mattis Correspondence, V.B., et al. (2018). Human Huntington's Disease iPSC-Derived Cortical Neurons Display Altered Transcriptomics, Morphology, and Maturation. Cell Rep. *25*, 1081–1096.e6.

Meisl, G., Yang, X., Hellstrand, E., Frohm, B., Kirkegaard, J.B., Cohen, S.I.A., et al. (2014). Differences in nucleation behavior underlie the contrasting aggregation kinetics of the Aβ40 and Aβ42 peptides. Proc. Natl. Acad. Sci. *111*, 9384–9389.

Miguel-Avarez, M., Santos-Lozano, A., Sanchis-Gomar, F., Fiuza-Luces, C., Pareja-Galeano, H., Garatachea, N., et al. (2015). Non-steroidal anti-inflammatory drugs as a treatment for Alzheimer's disease: a systematic review and meta-analysis of treatment effect. Drugs Aging

139–147.

Miklossy, J., Qing, H., Radenovic, A., Kis, A., Vileno, B., Làszló, F., et al. (2010). Beta amyloid and hyperphosphorylated tau deposits in the pancreas in type 2 diabetes. Neurobiol. Aging 1503–1515.

Milanesi, L., Sheynis, T., Xue, W.-F., Orlova, E. V, Hellewell, A.L., Jelinek, R., et al. (2012). Direct three-dimensional visualization of membrane disruption by amyloid fibrils. PNAS *109*, 20455–20460.

Mo, J.-A., Lim, J.-H., Sul, A.-R., Lee, M., Youn, Y.C., and Kim, H.-J. (2015). Cerebrospinal Fluid β-Amyloid1–42 Levels in the Differential Diagnosis of Alzheimer's Disease—Systematic Review and Meta-Analysis. PLoS One *10*, 1–16.

Mo, Y., Stromswold, J., Wilson, K., Holder, D., Sur, C., Laterza, O., et al. (2017). A multinational study distinguishing Alzheimer's and healthy patients using cerebrospinal fluid tau/Aβ42 cutoff with concordance to amyloid positron emission tomography imaging. Alzheimer's Dement. Diagnosis, Assess. Dis. Monit. 201–209.

Modrego, P.J. (2010). Depression in Alzheimer's disease. Pathophysiology, diagnosis, and treatment. J. Alzheimers. Dis. *21*, 1077–1087.

Moolman, D.L., Vitolo, O. V., Vonsattel, J.P.G., and Shelanski, M.L. (2004). Dendrite and dendritic spine alterations in Alzheimer models. J. Neurocytol. *33*, 377–387.

Moore, B.D., Chakrabarty, P., Levites, Y., Kukar, T.L., Baine, A.-M., Moroni, T., et al. (2012). Overlapping profiles of Abeta peptides in the Alzheimer's disease and pathological aging brains. Alzheimers. Res. Ther. *4*, 18.

Moore, B.D., Martin, J., de Mena, L., Sanchez, J., Cruz, P.E., Ceballos-Diaz, C., et al. (2018). Short Aβ peptides attenuate Aβ42 toxicity in vivo. J. Exp. Med. *215*, 283–301.

Moore, S., Evans, L.D.B., Andersson, T., Portelius, E., Smith, J., Dias, T.B., et al. (2015). APP Metabolism Regulates Tau Proteostasis in Human Cerebral Cortex Neurons. Cell Rep. *11*, 689–696.

Moores, B., Drolle, E., Attwood, S.J., Simons, J., and Leonenko, Z. (2011). Effect of Surfaces on Amyloid Fibril Formation. PLoS One *6*, e25954.

Mortimer, J.A., French, L.R., Hutton, J.T., and Schuman, L.M. (1985). Head injury as a risk factor for Alzheimer's disease. Neurology *35*, 264–267.

Mudher, A., and Lovestone, S. (2002). Alzheimer's disease – do tauists and baptists finally shake hands? Trends Neurosci. *25*, 22–26.

Mufson, E.J., Counts, S.E., Perez, S.E., and Ginsberg, S.D. (2008). Cholinergic system during the progression of Alzheimer's disease: Therapeutic implications. Expert Rev. Neurother. 1703–

1718.

Muizelaar, J.P., Marmarou, a, Ward, J.D., Kontos, H. a, Choi, S.C., Becker, D.P., et al. (1991). Adverse effects of prolonged hyperventilation in patients with severe head injury: a randomized clinical trial. J. Neurosurg. *75*, 731–739.

Müller, U., Cristina, N., Li, Z.W., Wolfer, D.P., Lipp, H.P., Rülicke, T., et al. (1994). Behavioral and anatomical deficits in mice homozygous for a modified β-amyloid precursor protein gene. Cell *79*, 755–765.

Muratore, C.R., Rice, H.C., Srikanth, P., Callahan, D.G., Shin, T., Benjamin, L.N.P., et al. (2014). The familial alzheimer's disease APPV717I mutation alters APP processing and Tau expression in iPSC-derived neurons. Hum. Mol. Genet. *23*, 3523–3536.

Murayama, O., Tomita, T., Nihonmatsu, N., Murayama, M., Sun, X., Honda, T., et al. (1999). Enhancement of amyloid beta 42 secretion by 28 different presenilin 1 mutations of familial Alzheimer's disease. Neurosci. Lett. *265*, 61–63.

Murphy, B.M., Swarts, S., Mueller, B.M., van der Geer, P., Manning, M.C., and Fitchmun, M.I. (2013). Protein instability following transport or storage on dry ice. Nat. Methods *10*, 278–279.

Murray, A.N., Palhano, F.L., Bieschke, J., and Kelly, J.W. (2013). Surface adsorption considerations when working with amyloid fibrils in multiwell plates and Eppendorf tubes. Protein Sci. *22*, 1531–1541.

Nadadhur, A.G., Emperador Melero, J., Meijer, M., Schut, D., Jacobs, G., Li, K.W., et al. (2017). Multi-level characterization of balanced inhibitory-excitatory cortical neuron network derived from human pluripotent stem cells. PLoS One *12*, e0178533.

Naj, A.C., and Schellenberg, G.D. (2017). Genomic variants, genes, and pathways of Alzheimer's disease: An overview. Am. J. Med. Genet. Part B Neuropsychiatr. Genet. *174*, 5–26.

Nakanishi, K., Sakiyama, T., and Imamura, K. (2001). On the adsorption of proteins on solid surfaces, a common but very complicated phenomenon. J. Biosci. Bioeng. *91*, 233–244.

Nakaya, Y., Yamane, T., Shiraishi, H., Wang, H.-Q.Q., Matsubara, E., Sato, T., et al. (2005). Random mutagenesis of presenilin-1 identifies novel mutants exclusively generating long amyloid β-peptides. J. Biol. Chem. *280*, 19070–19077.

Nalivaeva, N.N., and Turner, A.J. (2013). The amyloid precursor protein: A biochemical enigma in brain development, function and disease. FEBS Lett. *587*, 2046–2054.

Natascha Weiß, W.W. and P.M. (2010). Application Note 180 – Eppendorf LoBind®: Evaluation of protein recovery in Eppendorf Protein LoBind Tubes and Plates.

National Institute of Health (2018). https://clinicaltrials.gov/.

Nelson, T.J., and Alkon, D.L. (2005). Oxidation of cholesterol by amyloid precursor protein and beta-

amyloid peptide. J. Biol. Chem. *280*, 7377–7387.

Nerelius, C., Sandegren, A., Sargsyan, H., Raunak, R., Leijonmarck, H., Chatterjee, U., et al. (2009). Alpha-helix targeting reduces amyloid-beta peptide toxicity. Proc. Natl. Acad. Sci. U. S. A. *106*, 9191–9196.

Niederst, E.D., Reyna, S.M., and Goldstein, L.S.B. (2015). Axonal amyloid precursor protein and its fragments undergo somatodendritic endocytosis and processing. Mol. Biol. Cell *26*, 205–217.

Nikolic, A., Baud, S., Rauscher, S., and Pomès, R. (2011). Molecular mechanism of β-sheet self-organization at water-hydrophobic interfaces. Proteins Struct. Funct. Bioinforma. 1–22.

Novo, M., Freire, S., and Al-Soufi, W. (2018). Critical aggregation concentration for the formation of early Amyloid-β (1-42) oligomers. Sci. Rep. 1783.

Nunomura, A., Perry, G., Aliev, G., Hirai, K., Takeda, A., Balraj, E.K., et al. (2001). Oxidative Damage Is the Earliest Event in Alzheimer Disease. J. Neuropathol. Exp. Neurol. *60*, 759–767.

Nussbaum, J.M., Schilling, S., Cynis, H., Silva, A., Swanson, E., Wangsanut, T., et al. (2012). Prion-like behaviour and tau-dependent cytotoxicity of pyroglutamylated amyloid-β. Nature *485*, 651–655.

O'Brien, R.J., and Wong, P.C. (2012). Amyloid Precursor Protein Processing and Alzheimer's Disease. Annu. Rev. Neurosci. *12*, 173–189.

Ochalek, A., Mihalik, B., Avci, H.X., Chandrasekaran, A., Téglási, A., Bock, I., et al. (2017). Neurons derived from sporadic Alzheimer's disease iPSCs reveal elevated TAU hyperphosphorylation, increased amyloid levels, and GSK3B activation. Alzheimers. Res. Ther. *9*, 90.

Octave, J.N., Pierrot, N., Ferrao Santos, S., Nalivaeva, N.N., and Turner, A.J. (2013). From synaptic spines to nuclear signaling: Nuclear and synaptic actions of the amyloid precursor protein. J. Neurochem. 183–190.

Odawara, A., Katoh, H., Matsuda, N., and Suzuki, I. (2016). Physiological maturation and drug responses of human induced pluripotent stem cell-derived cortical neuronal networks in long-term culture. Sci. Rep. *6*, 26181.

Oddo, S., Caccamo, A., Shepherd, J.D., Murphy, M.P., Golde, T.E., Kayed, R., et al. (2003). Triple-transgenic model of Alzheimer's Disease with plaques and tangles: Intracellular Aβ and synaptic dysfunction. Neuron *39*, 409–421.

Oddo, S., Billings, L., Kesslak, J.P., Cribbs, D.H., and LaFerla, F.M. (2004). Aβ immunotherapy leads to clearance of early, but not late, hyperphosphorylated tau aggregates via the proteasome. Neuron *43*, 321–332.

Oddo, S., Caccamo, A., Smith, I.F., Green, K.N., and LaFerla, F.M. (2006). A dynamic relationship between intracellular and extracellular pools of Aβ. Am. J. Pathol. *168*, 184–194.

Office for National Statistics (2016). Leading causes of death in England and Wales (revised 2016) - Office for National Statistics.

Ohkawara, T., Nagase, H., Koh, C.S., and Nakayama, K. (2011). The amyloid precursor protein intracellular domain alters gene expression and induces neuron-specific apoptosis. Gene 1–9.

Olsson, B., Lautner, R., Andreasson, U., Öhrfelt, A., Portelius, E., Bjerke, M., et al. (2016). CSF and blood biomarkers for the diagnosis of Alzheimer's disease: a systematic review and meta-analysis. Lancet Neurol. *15*, 673–684.

Olsson, T.T., Klementieva, O., and Gouras, G.K. (2018). Prion-like seeding and nucleation of intracellular amyloid-β. Neurobiol. Dis. 1–10.

Ooms, S., Overeem, S., Besse, K., Rikkert, M.O., Verbeek, M., and Claassen, J. a H.R. (2014). Effect of 1 Night of Total Sleep Deprivation on Cerebrospinal Fluid β-Amyloid 42 in Healthy Middle-Aged Men: A Randomized Clinical Trial. JAMA Neurol. *71*, 971–977.

Ossenkoppele, R., Pijnenburg, Y.A.L., Perry, D.C., Cohn-Sheehy, B.I., Scheltens, N.M.E., Vogel, J.W., et al. (2015). The behavioural/dysexecutive variant of Alzheimer's disease: clinical, neuroimaging and pathological features. Brain *138*, 2732–2749.

Ovsepian, S. V., and O'Leary, V.B. (2015). Neuronal Activity and Amyloid Plaque Pathology: An Update. J. Alzheimer's Dis. *49*, 13–19.

Pakaski, M., Farkas, Z., Kasa, P., Forgon, M., Papp, H., Zarandi, M., et al. (1998). Vulnerability of small GABAergic neurons to human β-amyloid pentapeptide. Brain Res. 239–246.

Palmer, M.S., Beck, J.A., Campbell, T.A., Humphries, C.B., Roques, P.K., Fox, N.C., et al. (1999). Pathogenic presenilin 1 mutations (P436S & I143F) in early-onset Alzheimer's disease in the UK. Mutations in brief no. 223. Online. Hum. Mutat. 256.

Pardossi-Piquard, R., and Checler, F. (2012). The physiology of the β-amyloid precursor protein intracellular domain AICD. J. Neurochem. 109–124.

Pardossi-Piquard, R., Petit, A., Kawarai, T., Sunyach, C., Da Costa, C.A., Vincent, B., et al. (2005). Presenilin-dependent transcriptional control of the Aβ-degrading enzyme neprilysin by intracellular domains of βAPP and APLP. Neuron *46*, 541–554.

Pardossi-Piquard, R., Dunys, J., Yu, G., St. George-Hyslop, P., Alves Da Costa, C., and Checler, F. (2006). Neprilysin activity and expression are controlled by nicastrin. J. Neurochem. 1052–1056.

Pardossi-Piquard, R., Yang, S.P., Kanemoto, S., Gu, Y., Chen, F., Böhm, C., et al. (2009). APH1 polar transmembrane residues regulate the assembly and activity of presenilin complexes. J. Biol. Chem. 16298–16307.

Parihar, M.S., and Brewer, G.J. (2011). Amyloid Beta as a Modulator of Synaptic Plasticity. J.

Alzheimer's Dis. *22*, 741–763.

Paşca, A.M., Sloan, S.A., Clarke, L.E., Tian, Y., Makinson, C.D., Huber, N., et al. (2015). Functional cortical neurons and astrocytes from human pluripotent stem cells in 3D culture. Nat Methods. *12*, 671–678.

Passier, R., Orlova, V., and Mummery, C. (2016). Complex Tissue and Disease Modeling using hiPSCs. Cell Stem Cell 309–321.

Patani, R., Lewis, P.A., Trabzuni, D., Puddifoot, C.A., Wyllie, D.J.A., Walker, R., et al. (2012). Investigating the utility of human embryonic stem cell-derived neurons to model ageing and neurodegenerative disease using whole-genome gene expression and splicing analysis. J. Neurochem. *122*, 738–751.

Paterson, R.W.R.W., Toombs, J., Slattery, C.F.C.F., Schott, J.M.J.M., and Zetterberg, H. (2014). Biomarker modelling of early molecular changes in Alzheimer's disease. Mol. Diagnosis Ther. *18*, 213–227.

Paterson, R.W.W., Toombs, J., Slattery, C.F.F., Nicholas, J.M.M., Andreasson, U., Magdalinou, N.K.K., et al. (2015). Dissecting IWG-2 typical and atypical Alzheimer's disease: insights from cerebrospinal fluid analysis. J. Neurol. *262*, 2722–2730.

Pearson, H.A., and Peers, C. (2006). Physiological roles for amyloid β peptides. J. Physiol. *575*, 5–10.

Penn, Y., Segal, M., and Moses, E. (2016). Network synchronization in hippocampal neurons. Proc. Natl. Acad. Sci. *113*, 3341–3346.

Perl, D.P. (2010). Neuropathology of Alzheimer's disease. Mt. Sinai J. Med. *77*, 32–42.

Perret-Liaudet, A., Pelpel, M., Tholance, Y., Dumont, B., Vanderstichele, H., Zorzi, W., et al. (2012a). Risk of alzheimer's disease biological misdiagnosis linked to cerebrospinal collection tubes. J. Alzheimer's Dis. *31*, 13–20.

Perret-Liaudet, A., Pelpel, M., Tholance, Y., Dumont, B., Vanderstichele, H., Zorzi, W., et al. (2012b). Cerebrospinal fluid collection tubes: A critical issue for alzheimer disease diagnosis. Clin. Chem. 0000–0000.

Perry, G., Lipphardt, S., Mulvihill, P., Kancherla, M., Autilio-Gambetti, L., Gambetti, P., et al. (1988). Amyloid Precursor Protein. Alzheimer Dis. Assoc. Disord. *2*, 411.

Peters, I., Igbavboa, U., Schütt, T., Haidari, S., Hartig, U., Rosello, X., et al. (2009). The interaction of beta-amyloid protein with cellular membranes stimulates its own production. Biochim. Biophys. Acta - Biomembr. *1788*, 964–972.

Petersen, R.C., Smith, G.E., Waring, S.C., Ivnik, R.J., Tangalos, E.G., and Kokmen, E. (1999). Mild cognitive impairment: Clinical characterization and outcome. Arch. Neurol. 760.

Pica-Mendez, A.M., Tanen, M., Dallob, A., Tanaka, W., and Laterza, O.F. (2010). Nonspecific binding

of Aβ42 to polypropylene tubes and the effect of Tween-20. Clin. Chim. Acta 1833.

Plácido, a I., Pereira, C.M.F., Duarte, a I., Candeias, E., Correia, S.C., Santos, R.X., et al. (2014). The role of endoplasmic reticulum in amyloid precursor protein processing and trafficking: Implications for Alzheimer's disease. Biochim. Biophys. Acta *1842*, 1444–1453.

Portelius, E., Tran, A.J., Andreasson, U., Persson, R., Brinkmann, G., Zetterberg, H., et al. (2007). Characterization of amyloid β peptides in cerebrospinal fluid by an automated immunoprecipitation procedure followed by mass spectrometry. J. Proteome Res. *6*, 4433–4439.

Portelius, E., Price, E., Brinkmalm, G., Stiteler, M., Olsson, M., Persson, R., et al. (2011). A novel pathway for amyloid precursor protein processing. Neurobiol. Aging *32*, 1090–1098.

Portelius, E., Zetterberg, H., Dean, R.A., Marcil, A., Bourgeois, P., Nutu, M., et al. (2012). Amyloid-β1-15/16as a marker for γ-secretase inhibition in Alzheimer's disease. J. Alzheimer's Dis. *31*, 335–341.

Portelius, E., Dean, R.A., Andreasson, U., Mattsson, N., Westerlund, A., Olsson, M., et al. (2014). β-site amyloid precursor protein-cleaving enzyme 1(BACE1) inhibitor treatment induces Aβ5-X peptides through alternative amyloid precursor protein cleavage. Alzheimers. Res. Ther. *6*, 75.

Del Prete, D., Suski, J.M., Oulès, B., Debayle, D., Gay, A.S., Lacas-Gervais, S., et al. (2017). Localization and Processing of the Amyloid-β Protein Precursor in Mitochondria-Associated Membranes. J. Alzheimer's Dis. *55*, 1549–1570.

Prince, M., Knapp, M., Guerchet, M., McCrone, P., Prina, M., Comas-Herrera, A., et al. (2014). Dementia UK: Second Edition. Ann. Surg. 1–62.

Prince, M., Ali, G.-C., Guerchet, M., Prina, A.M., Albanese, E., and Wu, Y.-T. (2016). Recent global trends in the prevalence and incidence of dementia, and survival with dementia. Alzheimers Res. Ther. *8*.

Puig, K.L., and Combs, C.K. (2013). Expression and function of APP and its metabolites outside the central nervous system. Exp. Gerontol. *48*, 608–611.

Puzzo, D., Privitera, L., Leznik, E., Fà, M., Staniszewski, A., Palmeri, A., et al. (2008). Picomolar amyloid-beta positively modulates synaptic plasticity and memory in hippocampus. J. Neurosci. 14537–14545.

Qi-Takahara, Y. (2005). Longer Forms of Amyloid Protein: Implications for the Mechanism of Intramembrane Cleavage by -Secretase. J. Neurosci. 436–445.

Qin, W., Jia, L., Zhou, A., Zuo, X., Cheng, Z., Wang, F., et al. (2011). The -980C/G polymorphism in APH-1A promoter confers risk of Alzheimer's disease. Aging Cell 711–719.

Quinn, J.P., Corbett, N.J., Kellett, K.A.B., and Hooper, N.M. (2018). Tau Proteolysis in the

Pathogenesis of Tauopathies: Neurotoxic Fragments and Novel Biomarkers. J. Alzheimers. Dis. *63*, 13–33.

Rabe, M., Verdes, D., and Seeger, S. (2011). Understanding protein adsorption phenomena at solid surfaces. Adv. Colloid Interface Sci. *162*, 87–106.

Raja, W.K., Mungenast, A.E., Lin, Y.-T., Ko, T., Abdurrob, F., Seo, J., et al. (2016). Self-Organizing 3D Human Neural Tissue Derived from Induced Pluripotent Stem Cells Recapitulate Alzheimer's Disease Phenotypes. PLoS One *11*, e0161969.

Rajendran, L., Honsho, M., Zahn, T.R., Keller, P., Geiger, K.D., Verkade, P., et al. (2006). Alzheimer's disease beta-amyloid peptides are released in association with exosomes. Proc. Natl. Acad. Sci. 11172–11177.

Rakic, P. (2009). Evolution of the neocortex: A perspective from developmental biology. Nat. Rev. Neurosci. 724–735.

Rammes, G., Hasenjäger, A., Sroka-Saidi, K., Deussing, J.M., and Parsons, C.G. (2011). Therapeutic significance of NR2B-containing NMDA receptors and mGluR5 metabotropic glutamate receptors in mediating the synaptotoxic effects of β-amyloid oligomers on long-term potentiation (LTP) in murine hippocampal slices. Neuropharmacology 982–990.

Rammes, G., Mattusch, C., Wulff, M., Seeser, F., Kreuzer, M., Zhu, K., et al. (2017). Involvement of GluN2B subunit containing N-methyl-D-aspartate (NMDA) receptors in mediating the acute and chronic synaptotoxic effects of oligomeric amyloid-beta (Aβ) in murine models of Alzheimer's disease (AD). Neuropharmacology 100–115.

Rammes, G., Seeser, F., Mattusch, K., Zhu, K., Haas, L., Kummer, M., et al. (2018). The NMDA receptor antagonist Radiprodil reverses the synaptotoxic effects of different amyloid-beta (Aβ) species on long-term potentiation (LTP). Neuropharmacology 184–192.

Ranganathan, S., Polshyna, A., Nicholl, G., Lyons-Weiler, J., and Bowser, R. (2006). Assessment of Protein Stability in Cerebrospinal Fluid Using Surface-Enhanced Laser Desorption/Ionization Time-of-Flight Mass Spectrometry Protein Profiling. Clin. Proteomics *2*, 91–101.

Ranjan, V.D., Qiu, L., Tan, E.K., Zeng, L., and Zhang, Y. (2018). Modelling Alzheimer's disease: Insights from *in vivo* to *in vitro* three-dimensional culture platforms. J. Tissue Eng. Regen. Med. *12*, 1944–1958.

Rasmussen, J., Mahler, J., Beschorner, N., Kaeser, S.A., Häsler, L.M., Baumann, F., et al. (2017). Amyloid polymorphisms constitute distinct clouds of conformational variants in different etiological subtypes of Alzheimer's disease. Proc. Natl. Acad. Sci. *114*, 13018–13023.

Reijn, T.S.M., Rikkert, M.O., Van Geel, W.J.A., De Jong, D., and Verbeek, M.M. (2007). Diagnostic accuracy of ELISA and xMAP technology for analysis of amyloid beta42 and tau proteins. Clin.

Chem. *53*, 859–865.

Rembach, A., Evered, L.A., Li, Q.-X., Nash, T., Vidaurre, L., Fowler, C.J., et al. (2015). Alzheimer's disease cerebrospinal fluid biomarkers are not influenced by gravity drip or aspiration extraction methodology. Alzheimers. Res. Ther. *7*, 71.

Rice, H.C., Townsend, M., Bai, J., Suth, S., Cavanaugh, W., Selkoe, D.J., et al. (2012). Pancortins interact with amyloid precursor protein and modulate cortical cell migration. Development 3986–3996.

Riek, R., Güntert, P., Döbeli, H., Wipf, B., and Wüthrich, K. (2001). NMR studies in aqueous solution fail to identify significant conformational differences between the monomeric forms of two Alzheimer peptides with widely different plaque-competence, Aβ(1-40)ox and Aβ(1-42)ox. Eur. J. Biochem. 5930–5936.

Rippon, G.A., Crook, R., Baker, M., Halvorsen, E., Chin, S., Hutton, M., et al. (2003). Presenilin 1 Mutation in an African American Family Presenting With Atypical Alzheimer Dementia. Arch. Neurol. *60*, 884.

Robinson, D.M., and Keating, G.M. (2006). Memantine. Drugs *66*, 1515–1534.

Rocca, W.A., Hofman, A., Brayne, C., Breteler, M.M.B., Clarke, M., Copeland, J.R.M., et al. (1991). Frequency and distribution of Alzheimer's disease in Europe: A collaborative study of 1980–1990 prevalence findings. Ann. Neurol. *30*, 381–390.

Rocha, S., Krastev, R., Thünemann, A., Pereira, M., Möhwald, H., and Brezesinski, G. (2005). Adsorption of amyloid beta-peptide at polymer surfaces: a neutron reflectivity study. Chemphyschem *6*, 2527–2534.

Roche, J., Shen, Y., Lee, J.H., Ying, J., and Bax, A. (2016). Monomeric Aβ1-40and Aβ1-42Peptides in Solution Adopt Very Similar Ramachandran Map Distributions That Closely Resemble Random Coil. Biochemistry 762–775.

Rochin, L., Hurbain, I., Serneels, L., Fort, C., Watt, B., Leblanc, P., et al. (2013). BACE2 processes PMEL to form the melanosome amyloid matrix in pigment cells. Proc. Natl. Acad. Sci. 10658–10663.

Roessler, R., Goldmann, J., Shivalila, C., and Jaenisch, R. (2018). JIP2 haploinsufficiency contributes to neurodevelopmental abnormalities in human pluripotent stem cell–derived neural progenitors and cortical neurons. Life Sci. Alliance *1*, e201800094.

Rogaeva, E.A., Fafel, K.C.C., Song, Y.Q.Q., Medeiros, H., Sato, C., Liang, Y., et al. (2001). Screening for PS1 mutations in a referral-based series of AD cases: 21 Novel mutations. Neurology *57*, 621–625.

Rogers, J., Cooper, N.R., Webster, S., Schultz, J., McGeer, P.L., Styren, S.D., et al. (1992).

Complement activation by beta-amyloid in Alzheimer disease. Proc. Natl. Acad. Sci. U. S. A. *89*, 10016–10020.

Rossor, M.N., Garrett, N.J., Johnson, A.L., Mountjoy, C.Q., Roth, M., and Iversen, L.L. (1982). A post-mortem study of the cholinergic and gaba systems in senile dementia. Brain 313–330.

Rulifson, I.C., Cao, P., Miao, L., Kopecky, D., Huang, L., White, R.D., et al. (2016). Identification of Human Islet Amyloid Polypeptide as a BACE2 Substrate. PLoS One e0147254.

Ryan, J., Fransquet, P., Wrigglesworth, J., and Lacaze, P. (2018). Phenotypic Heterogeneity in Dementia: A Challenge for Epidemiology and Biomarker Studies. Front. Public Heal. 181.

Ryan, N.S., Nicholas, J.M., Weston, P.S.J., Liang, Y., Lashley, T., Guerreiro, R., et al. (2016). Clinical phenotype and genetic associations in autosomal dominant familial Alzheimer's disease: a case series. Lancet Neurol. *15*, 1326–1335.

Sabo, S.L., Ikin, A.F., Buxbaum, J.D., and Greengard, P. (2001). The Alzheimer amyloid precursor protein (APP) and FE65, an APP-binding protein, regulate cell movement. J. Cell Biol. 7952–7957.

Sadigh-Eteghad, S., Talebi, M., Farhoudi, M., Golzari, S.E.J., Sabermarouf, B., and Mahmoudi, J. (2014). Beta-amyloid exhibits antagonistic effects on alpha 7 nicotinic acetylcholine receptors in orchestrated manner. J. Med. Hypotheses Ideas *8*, 849–852.

Saftig, P., and Reiss, K. (2011). The "A Disintegrin And Metalloproteases" ADAM10 and ADAM17: Novel drug targets with therapeutic potential? Eur. J. Cell Biol. *90*, 527–535.

Saha, K., Mei, Y., Reisterer, C.M., Pyzocha, N.K., Yang, J., Muffat, J., et al. (2011). Surface-engineered substrates for improved human pluripotent stem cell culture under fully defined conditions. Proc. Natl. Acad. Sci. *108*, 18714–18719.

Sahara, S., Yanagawa, Y., O'Leary, D.D.M., and Stevens, C.F. (2012). The Fraction of Cortical GABAergic Neurons Is Constant from Near the Start of Cortical Neurogenesis to Adulthood. J. Neurosci. 4755–4761.

Saido, T., and Leissring, M.A. (2012). Proteolytic Degradation of Amyloid β-Protein. Cold Spring Harb. Perspect. Med. *2*, a006379–a006379.

Saito, T., Suemoto, T., Brouwers, N., Sleegers, K., Funamoto, S., Mihira, N., et al. (2011). Potent amyloidogenicity and pathogenicity of Aβ43. Nat. Neurosci. *14*, 1023–1032.

Sanabria-Castro, A., Alvarado-Echeverría, I., and Monge-Bonilla, C. (2017). Molecular Pathogenesis of Alzheimer's Disease: An Update. Ann. Neurosci. *24*, 46–54.

Sancesario, G.M.G., Esposito, Z., Nuccetelli, M., Bernardini, S., Sorge, R., Martorana, A., et al. (2010). Aβ1-42 Detection in CSF of Alzheimer's disease is influenced by temperature: Indication of reversible Aβ1-42 aggregation? Exp. Neurol. *223*, 371–376.

Sandbrink, R., Masters, C.L., and Beyreuther, K. (1994). βA4-Amyloid protein precursor mRNA isoforms without exon 15 are ubiquitously expressed in rat tissues including brain, but not in neurons. J. Biol. Chem. *269*, 1510–1517.

Sandbrink, R., Masters, C.L., and Beyreuther, K. (1996a). APP gene family: Alternative splicing generates functionally related isoforms. Ann. N. Y. Acad. Sci. *777*, 281–287.

Sandbrink, R., Zhang, D., Beyreuther, K., Schaeffer, S., Bauer, J., Masters, C.L., et al. (1996b). Missense mutations of the *PS-1/S182* gene in german early-onset Alzheimer's disease patients. Ann. Neurol. *40*, 265–266.

Van Der Sanden, B., Dhobb, M., Berger, F., and Wion, D. (2010). Optimizing stem cell culture. J. Cell. Biochem. *111*, 801–807.

Sannerud, R., Esselens, C., Ejsmont, P., Mattera, R., Rochin, L., Tharkeshwar, A.K., et al. (2016). Restricted Location of PSEN2/γ-Secretase Determines Substrate Specificity and Generates an Intracellular Aβ Pool. Cell *166*, 193–208.

Sano, Y., Nakaya, T., Pedrini, S., Takeda, S., Iijima-Ando, K., Iijima, K., et al. (2006). Physiological mouse brain Aβ levels are not related to the phosphorylation state of threonine-668 of Alzheimer's APP. PLoS One e51.

Sassi, C., Guerreiro, R., Gibbs, R., Ding, J., Lupton, M.K., Troakes, C., et al. (2014). Exome sequencing identifies 2 novel presenilin 1 mutations (p.L166V and p.S230R) in British early-onset Alzheimer's disease. Neurobiol. Aging *35*, 2422.e13-6.

Satizabal, C.L., Beiser, A.S., Chouraki, V., Chêne, G., Dufouil, C., and Seshadri, S. (2016). Incidence of Dementia over Three Decades in the Framingham Heart Study. N. Engl. J. Med. 93.

Saunders, A., Strittmatter, W., D, S., George-Hyslop, P., Pericak-Vance, M., Joo, S., et al. (1993). Association of apolipoprotein E allele epsilon 4 with late-onset familial and sporadic Alzheimer's disease. Neurology *43*, 1467–1472.

Scheff, S.W., Price, D.A., Schmitt, F.A., Dekosky, S.T., and Mufson, E.J. (2007). Synaptic alterations in CA1 in mild Alzheimer disease and mild cognitive impairment. Neurology *68*, 1501–1508.

Scheltens, P., and Rockwood, K. (2011). How golden is the gold standard of neuropathology in dementia? Alzheimer's Dement. *7*, 486–489.

Schladitz, C., Vieira, E.P., Hermel, H., and Möhwald, H. (1999). Amyloid-beta-sheet formation at the air-water interface. Biophys. J. *77*, 3305–3310.

Schmidt, V., Subkhangulova, A., and Willnow, T.E. (2017). Sorting receptor SORLA: cellular mechanisms and implications for disease. Cell. Mol. Life Sci. *74*, 1475–1483.

Schoonenboom, N.S.M., Mulder, C., Vanderstichele, H., Van Elk, E.-J., Kok, A., Van Kamp, G.J., et al. (2005). Effects of processing and storage conditions on amyloid beta (1-42) and tau

concentrations in cerebrospinal fluid: implications for use in clinical practice. Clin. Chem. *51*, 189–195.

Schott, J.M., Ridha, B.H., Crutch, S.J., Healy, D.G., Uphill, J.B., Warrington, E.K., et al. (2006). Apolipoprotein E genotype modifies the phenotype of Alzheimer disease [2]. Arch. Neurol. *63*, 155–156.

Schrijvers, E.M.C., Verhaaren, B.F.J., Koudstaal, P.J., Hofman, A., Ikram, M.A., and Breteler, M.M.B. (2012). Is dementia incidence declining? Trends in dementia incidence since 1990 in the Rotterdam Study. Neurology 1456–1463.

Scott, L.J., and Goa, K.L. (2000). Galantamine. Drugs *60*, 1095–1122.

Seals, D.F., and Courtneidge, S.A. (2003). The ADAMs family of metalloproteases: Multidomain proteins with multiple functions. Genes Dev. *17*, 7–30.

Seegar, T.C.M., Killingsworth, L.B., Saha, N., Meyer, P.A., Patra, D., Zimmerman, B., et al. (2017). Structural Basis for Regulated Proteolysis by the α-Secretase ADAM10. Cell *171*, 1638–1648.e7.

Selkoe, D.J., and Hardy, J. (2016). The amyloid hypothesis of Alzheimer's disease at 25 years. EMBO Mol. Med. *8*, 595–608.

Senechal, Y., Kelly, P.H., and Dev, K.K. (2008). Amyloid precursor protein knockout mice show age-dependent deficits in passive avoidance learning. Behav. Brain Res. *186*, 126–132.

Serpell, L.C. (2000). Alzheimer's amyloid fibrils: structure and assembly. Biochim. Biophys. Acta - Mol. Basis Dis. *1502*, 16–30.

Serrano-Pozo, A., Frosch, M.P., Masliah, E., and Hyman, B.T. (2011). Neuropathological alterations in Alzheimer disease. Cold Spring Harb. Perspect. Med. *1*, a006189.

Shankar, G.M., Bloodgood, B.L., Townsend, M., Walsh, D.M., Selkoe, D.J., and Sabatini, B.L. (2007). Natural Oligomers of the Alzheimer Amyloid- Protein Induce Reversible Synapse Loss by Modulating an NMDA-Type Glutamate Receptor-Dependent Signaling Pathway. J. Neurosci. 2866–2875.

Shariati, S.A., and De Strooper, B. (2013). Redundancy and divergence in the amyloid precursor protein family. FEBS Lett *587*, 2036–2045.

Shaw, L.M., Korecka, M., Clark, C.M., Lee, V.M.-Y.M.Y., and Trojanowski, J.Q. (2007). Biomarkers of neurodegeneration for diagnosis and monitoring therapeutics. Nat. Rev. Drug Discov. *6*, 295–303.

Shen, J., and Kelleher, R.J. (2007). The presenilin hypothesis of Alzheimer's disease: Evidence for a loss-of-function pathogenic mechanism. Proc. Natl. Acad. Sci. *104*, 403–409.

Shen, L., and Jia, J. (2016). An Overview of Genome-Wide Association Studies in Alzheimer's Disease. Neurosci. Bull. *32*, 183–190.

Sherrington, R., Rogaev, E.I., Liang, Y., Rogaeva, E.A., Levesque, G., Ikeda, M., et al. (1995). Cloning of a gene bearing missense mutations in early-onset familial Alzheimer's disease. Nature *375*, 754–760.

Shi, M., Tang, L., Toledo, J.B., Ginghina, C., Wang, H., Aro, P., et al. (2018). Cerebrospinal fluid α-synuclein contributes to the differential diagnosis of Alzheimer's disease. Alzheimer's Dement. *14*, 1052–1062.

Shi, X.P., Tugusheva, K., Bruce, J.E., Lucka, A., Wu, G.X., Chen-Dodson, E., et al. (2003). β-secretase cleavage at amino acid residue 34 in the amyloid β peptide is dependent upon γ-secretase activity. J. Biol. Chem. *278*, 21286–21294.

Shi, Y., Kirwan, P., Smith, J., Robinson, H.P.C., and Livesey, F.J. (2012a). Human cerebral cortex development from pluripotent stem cells to functional excitatory synapses. Nat. Neurosci. *15*, 477–486, S1.

Shi, Y., Kirwan, P., and Livesey, F.J. (2012b). Directed differentiation of human pluripotent stem cells to cerebral cortex neurons and neural networks. Nat. Protoc. *7*, 1836–1846.

Shi, Y., Kirwan, P., Smith, J., MacLean, G., Orkin, S.H., and Livesey, F.J. (2012c). A Human Stem Cell Model of Early Alzheimer's Disease Pathology in Down Syndrome. Sci. Transl. Med. *4*, 124ra29-124ra29.

Shioi, J., Georgakopoulos, A., Mehta, P., Kouchi, Z., Litterst, C.M., Baki, L., et al. (2007). FAD mutants unable to increase neurotoxic Abeta 42 suggest that mutation effects on eurodegeneration may be independent of effects on A?? J. Neurochem. *101*, 674–681.

Shum, C., Macedo, S.C., Warre-Cornish, K., Cocks, G., Price, J., and Srivastava, D.P. (2015). Utilizing induced pluripotent stem cells (iPSCs) to understand the actions of estrogens in human neurons. Horm. Behav. *74*, 228–242.

Siegel, G., Gerber, H., Koch, P., Bruestle, O., Fraering, P.C., and Rajendran, L. (2017). The Alzheimer's Disease γ-Secretase Generates Higher 42:40 Ratios for β-Amyloid Than for p3 Peptides. Cell Rep. 1967–1976.

De Silva, H.A.R., Jen, A., Wickenden, C., Jen, L.S., Wilkinson, S.L., and Patel, A.J. (1997). Cell-specific expression of β-amyloid precursor protein isoform mRNAs and proteins in neurons and astrocytes. Mol. Brain Res. *47*, 147–156.

Simons, T.J.B.B. (1988). Calcium and neuronal function. Neurosurg. Rev. *11*, 119–129.

Simons, M., de Strooper, B., Multhaup, G., Tienari, P.J., Dotti, C.G., and Beyreuther, K. (1996). Amyloidogenic processing of the human amyloid precursor protein in primary cultures of rat hippocampal neurons. J Neurosci 899–908.

Simonsen, A.H., Bahl, J.M.C., Danborg, P.B., Lindstrom, V., Larsen, S.O., Grubb, A., et al. (2013).

Pre-analytical factors influencing the stability of cerebrospinal fluid proteins. J. Neurosci. Methods 234–240.

Skillbäck, T., Delsing, L., Synnergren, J., Mattsson, N., Janelidze, S., Nägga, K., et al. (2017). CSF/serum albumin ratio in dementias: a cross-sectional study on 1861 patients. Neurobiol. Aging *59*, 1–9.

Slats, D., Claassen, J.A., Spies, P.E., Borm, G., Besse, K.T., van Aalst, W., et al. (2012). Hourly variability of cerebrospinal fluid biomarkers in Alzheimer's disease subjects and healthy older volunteers. Neurobiol Aging *33*, 831 e1-9.

Slemmon, J.R., Meredith, J., Guss, V., Andreasson, U., Andreasen, N., Zetterberg, H., et al. (2012). Measurement of Abeta1-42 in cerebrospinal fluid is influenced by matrix effects. J. Neurochem. *120*, 325–333.

Slemmon, J.R., Shapiro, A., Mercken, M., Streffer, J., Romano, G., Andreasen, N., et al. (2015). Impact of cerebrospinal fluid matrix on the detection of Alzheimer's disease with Abeta42 and influence of disease on the total-Abeta42/Abeta40 ratio. J. Neurochem. *135*, 1049–1058.

Smith, E.E., and Greenberg, S.M. (2009). Beta-amyloid, blood vessels, and brain function. Stroke. *40*, 2601–2606.

Snyder, E.M., Nong, Y., Almeida, C.G., Paul, S., Moran, T., Choi, E.Y., et al. (2005). Regulation of NMDA receptor trafficking by amyloid-beta. Nat. Neurosci. *8*, 1051–1058.

Somavarapu, A.K., and Kepp, K.P. (2016). The dynamic mechanism of presenilin-function: Sensitive gate dynamics and loop unplugging control protein access. Neurobiol. Dis. *89*, 147–156.

Sosa, L.J., Cáceres, A., Dupraz, S., Oksdath, M., Quiroga, S., and Lorenzo, A. (2017). The physiological role of the amyloid precursor protein as an adhesion molecule in the developing nervous system. J. Neurochem. 11–29.

Soto, C., Branes, M.C., Alvarez, J., and Inestrosa, N.C. (1994). Structural determinants of the Alzheimer's amyloid beta-peptide. J Neurochem 1191–1198.

Spasic, D., Tolia, A., Dillen, K., Baert, V., Strooper, B. De, Vrijens, S., et al. (2006). Presenilin-1 maintains a nine-transmembrane topology throughout the secretory pathway. J. Biol. Chem. 26569–26577.

Sperling, R.A., LaViolette, P.S., O'Keefe, K., O'Brien, J., Rentz, D.M., Pihlajamaki, M., et al. (2009). Amyloid Deposition Is Associated with Impaired Default Network Function in Older Persons without Dementia. Neuron *63*, 178–188.

Spires, T.L. (2005). Dendritic Spine Abnormalities in Amyloid Precursor Protein Transgenic Mice Demonstrated by Gene Transfer and Intravital Multiphoton Microscopy. J. Neurosci. *25*, 7278–7287.

Sposito, T., Preza, E., Mahoney, C.J., Setó-Salvia, N., Ryan, N.S., Morris, H.R., et al. (2015). Developmental regulation of tau splicing is disrupted in stem cell-derived neurons from frontotemporal dementia patients with the 10 + 16 splice-site mutation in MAPT. Hum. Mol. Genet. *24*, 5260–5269.

Sproul, A.A., Jacob, S., Pre, D., Kim, S.H., Nestor, M.W., Navarro-Sobrino, M., et al. (2014). Characterization and molecular profiling of PSEN1 familial alzheimer's disease iPSC-Derived neural progenitors. PLoS One *9*, e84547.

Stampfer, M.J. (2006). Cardiovascular disease and Alzheimer's disease: common links. J. Intern. Med. *260*, 211–223.

Steinbach, J.P., Müller, U., Leist, M., Li, Z.W., Nicotera, P., and Aguzzi, A. (1998). Hypersensitivity to seizures in β-amyloid precursor protein deficient mice. Cell Death Differ. *5*, 858–866.

Steiner, H., Winkler, E., and Haass, C. (2008). Chemical cross-linking provides a model of the γ-secretase complex subunit architecture and evidence for close proximity of the C-terminal fragment of presenilin with APH-1. J. Biol. Chem. 34677–34686.

Stelzmann, R.A., Schnitzlein, H.N., Murtagh, F.R., Norman Schnitzlein, H., and Reed Murtagh, F. (1995). An english translation of alzheimer's 1907 paper, uber eine eigenartige erkankung der hirnrinde. Clin. Anat. *8*, 429–431.

Stern, Y. (2012). Cognitive reserve in ageing and Alzheimer's disease. Lancet. Neurol. *11*, 1006–1012.

Strittmatter, W.J., Saunders, A.M., Schmechel, D., Pericak-Vance, M., Enghild, J., Salvesen, G.S., et al. (1993). Apolipoprotein E: high-avidity binding to beta-amyloid and increased frequency of type 4 allele in late-onset familial Alzheimer disease. Proc. Natl. Acad. Sci. *90*, 1977–1981.

Strominger, N.L., Demarest, R.J., and Laemle, L.B. (2012). Neurons and Associated Cells. In Noback's Human Nervous System, Seventh Edition: Structure and Function, (Totowa, NJ: Humana Press), pp. 11–38.

De Strooper, B. (2003). Aph-1, Pen-2, and Nicastrin with Presenilin generate an active γ-Secretase complex. Neuron 9–12.

De Strooper, B., Vassar, R., and Golde, T. (2010). The secretases: Enzymes with therapeutic potential in Alzheimer disease. Nat. Rev. Neurol. *6*, 99–107.

Struyfs, H., Van Broeck, B., Timmers, M., Fransen, E., Sleegers, K., Van Broeckhoven, C., et al. (2015). Diagnostic Accuracy of Cerebrospinal Fluid Amyloid-beta Isoforms for Early and Differential Dementia Diagnosis. J. Alzheimer's Dis. *45*, 813–822.

Sun, L., Zhou, R., Yang, G., and Shi, Y. (2017). Analysis of 138 pathogenic mutations in presenilin-1 on the in vitro production of Aβ42 and Aβ40 peptides by γ-secretase. Proc. Natl. Acad. Sci. *114*, E476–E485.

Sun, X., He, G., and Song, W. (2006). BACE2, as a novel APP θ-secretase, is not responsible for the pathogenesis of Alzheimer's disease in Down syndrome. FASEB J. *20*, 1369–1376.

Swistowski, A., Zhang, Q., Orcholski, M.E., Crippen, D., Vitelli, C., Kurakin, A., et al. (2009). Novel mediators of amyloid precursor protein signaling. J. Neurosci. 15703–15712.

Szaruga, M., Veugelen, S., Benurwar, M., Lismont, S., Sepulveda-Falla, D., Lleo, A., et al. (2015). Qualitative changes in human γ-secretase underlie familial Alzheimer's disease. J. Exp. Med. *212*, 2003–2013.

Szaruga, M., Munteanu, B., Lismont, S., Veugelen, S., Horré, K., Mercken, M., et al. (2017). Alzheimer's-Causing Mutations Shift Aβ Length by Destabilizing γ-Secretase-Aβn Interactions. Cell *170*, 443–456.e14.

Szodorai, A., Kuan, Y.-H., Hunzelmann, S., Engel, U., Sakane, A., Sasaki, T., et al. (2009). APP Anterograde Transport Requires Rab3A GTPase Activity for Assembly of the Transport Vesicle. J. Neurosci. *29*, 14534–14544.

Tabaton, M., Zhu, X., Perry, G., Smith, M.A., and Giliberto, L. (2010). Signaling effect of amyloid-beta(42) on the processing of AbetaPP. Exp. Neurol. *221*, 18–25.

Takagi-Niidome, S., Sasaki, T., Osawa, S., Sato, T., Morishima, K., Cai, T., et al. (2015). Cooperative Roles of Hydrophilic Loop 1 and the C-Terminus of Presenilin 1 in the Substrate-Gating Mechanism of Gamma-Secretase. J. Neurosci. *35*, 2646–2656.

Takahashi, K., and Yamanaka, S. (2006). Induction of Pluripotent Stem Cells from Mouse Embryonic and Adult Fibroblast Cultures by Defined Factors. Cell *126*, 663–676.

Takahashi, K., Tanabe, K., Ohnuki, M., Narita, M., Ichisaka, T., Tomoda, K., et al. (2007). Induction of Pluripotent Stem Cells from Adult Human Fibroblasts by Defined Factors. Cell *107*, 861–872.

Takahashi, R.H., Almeida, C.G., Kearney, P.F., Yu, F., Lin, M.T., Milner, T. a, et al. (2004). Oligomerization of Alzheimer's beta-amyloid within processes and synapses of cultured neurons and brain. J. Neurosci. *24*, 3592–3599.

Takami, M., Nagashima, Y., Sano, Y., Ishihara, S., Morishima-Kawashima, M., Funamoto, S., et al. (2009). Gamma-Secretase: Successive Tripeptide and Tetrapeptide Release from the Transmembrane Domain of -Carboxyl Terminal Fragment. J. Neurosci. *29*, 13042–13052.

Takasugi, N., Tomita, T., Hayashi, I., Tsuruoka, M., Niimura, M., Takahashi, Y., et al. (2003). The role of presenilin cofactors in the gamma-secretase complex. Nature 438–441.

Tampellini, D., Rahman, N., Gallo, E.F., Huang, Z., Dumont, M., Capetillo-Zarate, E., et al. (2009). Synaptic Activity Reduces Intraneuronal A , Promotes APP Transport to Synapses, and Protects against A -Related Synaptic Alterations. J. Neurosci. *29*, 9704–9713.

Tanaka, S., Nakamura, S., Ueda, K., Kameyama, M., Shiojiri, S., Takahashi, Y., et al. (1988). Three

types of amyloid protein precursor mRNA in human brain: their differential expression in Alzheimer's disease. Biochem. Biophys. Res. Commun. *157*, 472–479.

Tang, K., Wang, C., Shen, C.Y., Sheng, S.L., Ravid, R., and Jing, N.H. (2003). Identification of a novel alternative splicing isoform of human amyloid precursor protein gene, APP639. Eur. J. Neurosci. *18*, 102–108.

Tanzi, R.E., Gusella, J.F., Watkins, P.C., Bruns, G.A., St George-Hyslop, P., Van Keuren, M.L., et al. (1987). Amyloid beta protein gene: cDNA, mRNA distribution, and genetic linkage near the Alzheimer locus. Science *235*, 880–884.

Tellechea, P., Pujol, N., Esteve-Belloch, P., Echeveste, B., García-Eulate, M.R., Arbizu, J., et al. (2018). Early- and late-onset Alzheimer disease: Are they the same entity? Neurol. (English Ed. *33*, 244–253.

Terrill-Usery, S.E., Colvin, B.A., Davenport, R.E., and Nichols, M.R. (2016). Ab40 has a subtle effect on Ab42 protofibril formation, but to a lesser degree than Ab42 concentration, in Ab42/Ab40 mixtures. Arch. Biochem. Biophys. *597*, 1–11.

Terry, R.D., Masliah, E., Salmon, D.P., Butters, N., DeTeresa, R., Hill, R., et al. (1991). Physical basis of cognitive alterations in alzheimer's disease: Synapse loss is the major correlate of cognitive impairment. Ann. Neurol. *30*, 572–580.

Teunissen, C.E., Petzold, A., Bennett, J.L., Berven, F.S., Brundin, L., Comabella, M., et al. (2009). A consensus protocol for the standardization of cerebrospinal fluid collection and biobanking. Neurology 1914–1922.

Texidó, L., Martín-Satué, M., Alberdi, E., Solsona, C., and Matute, C. (2011). Amyloid beta peptide oligomers directly activate NMDA receptors. Cell Calcium *49*, 184–190.

Thal, D.R., Rub, U., Orantes, M., and Braak, H. (2002). Phases of Aβ-deposition in the human brain and its relevance for the development of AD. Neurology *58*, 1791–1800.

The Human Protein Atlas (2019). Tissue expression of APP - Summary - The Human Protein Atlas.

Theuns, J., Marjaux, E., Vandenbulcke, M., Van Laere, K., Kumar-Singh, S., Bormans, G., et al. (2006). Alzheimer dementia caused by a novel mutation located in the APP C-terminal intracytosolic fragment. Hum. Mutat. *27*, 888–896.

Thinakaran, G., Borchelt, D.R., Lee, M.K., Slunt, H.H., Spitzer, L., Kim, G., et al. (1996). Endoproteolysis of presenilin 1 and accumulation of processed derivatives in vivo. Neuron 181–190.

Thorsell, A., Bjerke, M., Gobom, J., Brunhage, E., Vanmechelen, E., Andreasen, N., et al. (2010). Neurogranin in cerebrospinal fluid as a marker of synaptic degeneration in Alzheimer's disease. Brain Res. *1362*, 13–22.

Tolia, A., Chávez-Gutiérrez, L., and De Strooper, B. (2006). Contribution of presenilin transmembrane domains 6 and 7 to a water-containing cavity in the γ-secretase complex. J. Biol. Chem. 27633–27642.

Toombs, J., Paterson, R.W., Lunn, M.P., Nicholas, J.M., Fox, N.C., Chapman, M.D., et al. (2013). Identification of an important potential confound in CSF AD studies: Aliquot volume. Clin. Chem. Lab. Med. *51*, 2311–2317.

Törnquist, M., Michaels, T.C.T., Sanagavarapu, K., Yang, X., Meisl, G., Cohen, S.I.A., et al. (2018). Secondary nucleation in amyloid formation. Chem. Commun. 8667–8684.

Tran, J., Chang, D., Hsu, F., Wang, H., and Guo, Z. (2017). Cross-seeding between Aβ40 and Aβ42 in Alzheimer's disease. FEBS Lett. 177–185.

Tu, H., Nelson, O., Bezprozvanny, A., Wang, Z., Lee, S.F., Hao, Y.H., et al. (2006). Presenilins Form ER Ca2+Leak Channels, a Function Disrupted by Familial Alzheimer's Disease-Linked Mutations. Cell 981–993.

Tyan, S.-H., Shih, A.Y.-J., Walsh, J.J., Maruyama, H., Sarsoza, F., Ku, L., et al. (2012). Amyloid Precursor Protein (APP) Regulates Synaptic Structure and Function. Mol. Cell. Neurosci. *51*, 43–52.

Vandersteen, A., Hubin, E., Sarroukh, R., De Baets, G., Schymkowitz, J., Rousseau, F., et al. (2012). A comparative analysis of the aggregation behavior of amyloid-β peptide variants. FEBS Lett. *586*, 4088–4093.

Vanderstichele, H., Van Kerschaver, E., Hesse, C., Davidsson, P., Buyse, M.A., Andreasen, N., et al. (2000). Standardization of measurement of β-amyloid((1-42)) in cerebrospinal fluid and plasma. Amyloid 245–258.

Vanderstichele, H., Demeyer, L., Janelidze, S., Coart, E., Stoops, E., Mauroo, K., et al. (2017). Recommendations for cerebrospinal fluid collection for the analysis by ELISA of neurogranin trunc P75, α-synuclein, and total tau in combination with Aβ(1-42)/Aβ(1-40). Alzheimer's Res. Ther. 40.

Vanderstichele, H.M.J., Janelidze, S., Demeyer, L., Coart, E., Stoops, E., Herbst, V., et al. (2016). Optimized Standard Operating Procedures for the Analysis of Cerebrospinal Fluid Ab42 and the Ratios of Ab Isoforms Using Low Protein Binding Tubes. J. Alzheimer's Dis. *53*, 1121–1132.

Vassar, R., Bennett, B.D., Babu-Khan, S., Kahn, S., Mendiaz, E.A., Denis, P., et al. (1999). β-Secretase cleavage of Alzheimer's amyloid precursor protein by the transmembrane aspartic protease BACE. Science (80-.). *286*, 735–741.

Vassar, R., Kovacs, D.M., Yan, R., and Wong, P.C. (2009). The Beta-Secretase Enzyme BACE in Health and Alzheimer's Disease: Regulation, Cell Biology, Function, and Therapeutic Potential. J.

Neurosci. 12787–12794.

Vazin, T., Ball, K.A., Lu, H., Park, H., Ataeijannati, Y., Head-Gordon, T., et al. (2014). Efficient derivation of cortical glutamatergic neurons from human pluripotent stem cells: A model system to study neurotoxicity in Alzheimer's disease. Neurobiol. Dis. *62*, 62–72.

Verdile, G., Gnjec, A., Miklossy, J., Fonte, J., Veurink, G., Bates, K., et al. (2004). Protein markers for Alzheimer in the frontal cortex and cerebellum. Neurology *63*, 1385–1392.

Verwey, N.A., van der Flier, W.M., Blennow, K., Clark, C., Sokolow, S., De Deyn, P.P., et al. (2009). A worldwide multicentre comparison of assays for cerebrospinal fluid biomarkers in Alzheimer's disease. Ann. Clin. Biochem. *46*, 235–240.

Vetrivel, K.S., and Thinakaran, G. (2010). Membrane rafts in Alzheimer's disease beta-amyloid production. Biochim. Biophys. Acta - Mol. Cell Biol. Lipids *1801*, 860–867.

Veugelen, S., Saito, T., Saido, T.C., Chávez-Gutiérrez, L., and De Strooper, B. (2016). Familial Alzheimer's Disease Mutations in Presenilin Generate Amyloidogenic Aβ Peptide Seeds. Neuron *90*, 410–416.

Villa, J.C., Chiu, D., Brandes, A.H., Escorcia, F.E., Villa, C.H., Maguire, W.F., et al. (2014). Nontranscriptional role of hif-1α in activation of γ-secretase and notch signaling in breast cancer. Cell Rep. 1077–1092.

Viola, K.L., Velasco, P.T., and Klein, W.L. (2008). Why Alzheimer's is a disease of memory: The attack on synapses by Aß oligomers (ADDLs). J. Nutr. Heal. Aging 51s–57s.

Vivekanandan, S., Brender, J.R., Lee, S.Y., and Ramamoorthy, A. (2011). A partially folded structure of amyloid-beta(1-40) in an aqueous environment. Biochem. Biophys. Res. Commun. 312–316.

Vos, S.J.B., Visser, P.J., Verhey, F., Aalten, P., Knol, D., Ramakers, I., et al. (2014). Variability of CSF alzheimer's disease biomarkers: Implications for clinical practice. PLoS One *9*, e100784.

Voytyuk, I., Mueller, S.A., Herber, J., Snellinx, A., Moechars, D., van Loo, G., et al. (2018). BACE2 distribution in major brain cell types and identification of novel substrates. Life Sci. Alliance e201800026.

Walter, J., Fluhrer, R., Hartung, B., Willem, M., Kaether, C., Capell, A., et al. (2001). Phosphorylation Regulates Intracellular Trafficking of β-Secretase. J. Biol. Chem. 15634–14641.

Wälti, M.A., Ravotti, F., Arai, H., Glabe, C.G., Wall, J.S., Böckmann, A., et al. (2016). Atomic-resolution structure of a disease-relevant Aβ(1-42) amyloid fibril. Proc. Natl. Acad. Sci. U. S. A. *113*, E4976-84.

Wang, B., Yang, W., Wen, W., Sun, J., Su, B., Liu, B., et al. (2010). γ-secretase gene mutations in familial acne inversa. Science (80-.). 1065.

Wang, H., Sang, N., Zhang, C., Raghupathi, R., Tanzi, R.E., and Saunders, A. (2015). Cathepsin L

mediates the degradation of novel APP C-terminal fragments. Biochemistry 2806–2816.

Wang, H.Y., Lee, D.H., Davis, C.B., and Shank, R.P. (2000b). Amyloid peptide Abeta(1-42) binds selectively and with picomolar affinity to alpha7 nicotinic acetylcholine receptors. J. Neurochem. *75*, 1155–1161.

Wang, H.Y., Lee, D.H., D'Andrea, M.R., Peterson, P.A., Shank, R.P., and Reitz, A.B. (2000a). beta-Amyloid(1-42) binds to alpha7 nicotinic acetylcholine receptor with high affinity. Implications for Alzheimer's disease pathology. J. Biol. Chem. *275*, 5626–5632.

Wang, L.S., Leung, Y.Y., Chang, S.K., Leight, S., Knapik-Czajka, M., Baek, Y., et al. (2012). Comparison of xMAP and ELISA assays for detecting cerebrospinal fluid biomarkers of Alzheimer's disease. J. Alzheimer's Dis. *31*, 439–445.

Wang, Z., Jackson, R.J., Hong, W., Taylor, W.M., Corbett, G.T., Moreno, A., et al. (2017). Human Brain-Derived Aβ Oligomers Bind to Synapses and Disrupt Synaptic Activity in a Manner That Requires APP. J. Neurosci. *37*, 11947–11966.

Wanngren, J., Lara, P., Öjemalm, K., Maioli, S., Moradi, N., Chen, L., et al. (2014). Changed membrane integration and catalytic site conformation are two mechanisms behind the increased Aβ42/Aβ40 ratio by presenilin 1 familial Alzheimer-linked mutations. FEBS Open Bio *4*, 393–406.

Ward, J., Wang, H., Saunders, A.J., Tanzi, R.E., Zhang, C., Author, C., et al. (2017). Mechanisms that Synergistically Regulate η-Secretase Processing of APP and Aη-α Protein Levels: Relevance to Pathogenesis and Treatment of Alzheimer's Disease HHS Public Access Author manuscript. Discov Med *23*, 121–128.

Ward, M.W., Concannon, C.G., Whyte, J., Walsh, C.M., Corley, B., and Prehn, J.H.M. (2010). The amyloid precursor protein intracellular domain (AICD) disrupts actin dynamics and mitochondrial bioenergetics. J. Neurochem. 275–284.

Warren, L., Manos, P.D., Ahfeldt, T., Loh, Y.-H., Li, H., Lau, F., et al. (2010). Highly efficient reprogramming to pluripotency and directed differentiation of human cells with synthetic modified mRNA. Cell Stem Cell *7*, 618–630.

Watanabe, N., Tomita, T., Sato, C., Kitamura, T., Morohashi, Y., and Iwatsubo, T. (2005). Pen-2 is incorporated into the γ-secretase complex through binding to transmembrane domain 4 of presenilin 1. J. Biol. Chem. 41967–41975.

Waters, J. (2010). The Concentration of Soluble Extracellular Amyloid-β Protein in Acute Brain Slices from CRND8 Mice. PLoS One e15709.

Wei, G., and Shea, J.-E. (2006). Effects of solvent on the structure of the Alzheimer amyloid-beta(25-35) peptide. Biophys. J. 1638–1647.

Weisner, B., and Bernhardt, W. (1978). Protein fractions of lumbar, cisternal, and ventricular cerebrospinal fluid. Separate areas of reference. J. Neurol. Sci. *37*, 205–214.

Wellington, H., Törnqvist, U., Portelius, E., Paterson, R.W., Magdalinou, N.K., Fox, N.C., et al. (2015). Quantification of the synaptic protein neurogranin in cerebrospinal fluid across different neurodegenerative diseases: A selective Alzheimer's disease biomarker? Alzheimer's Dement. *11*, 340.

Wernig, M. (2016). Overcoming iPSC Obstacles. Cell Stem Cell *19*, 291–292.

Wilcock, D.M., and Griffin, W.S.T. (2013). Down's syndrome, neuroinflammation, and Alzheimer neuropathogenesis. J. Neuroinflammation *10*, 84.

Willem, M., Tahirovic, S., Busche, M.A., Ovsepian, S. V., Chafai, M., Kootar, S., et al. (2015). η-Secretase processing of APP inhibits neuronal activity in the hippocampus. Nature *526*, 443–447.

Willemse, E., van Uffelen, K., Brix, B., Engelborghs, S., Vanderstichele, H., and Teunissen, C. (2017). How to handle adsorption of cerebrospinal fluid amyloid-beta (1-42) in laboratory practice? Identifying problematic handlings and resolving the issue by use of the Aβ42/Aβ40 ratio. Alzheimer's Dement. 885–892.

Wilson, S.W., and Rubenstein, J.L.R. (2000). Induction and dorsoventral patterning of the telencephalon. Neuron 641–651.

Winkler, E.A., Sagare, A.P., and Zlokovic, B. V. (2014). The pericyte: A forgotten cell type with important implications for alzheimer's disease? In Brain Pathology, pp. 371–386.

Wise-Scira, O., Xu, L., Kitahara, T., Perry, G., and Coskuner, O. (2011). Amyloid-β peptide structure in aqueous solution varies with fragment size. J. Chem. Phys. 205101.

Wiseman, F.K., Al-Janabi, T., Hardy, J., Karmiloff-Smith, A., Nizetic, D., Tybulewicz, V.L.J., et al. (2015). A genetic cause of Alzheimer disease: Mechanistic insights from Down syndrome. Nat. Rev. Neurosci. *16*, 564–574.

Wiseman, F.K., Pulford, L.J., Barkus, C., Liao, F., Portelius, E., Webb, R., et al. (2018). Trisomy of human chromosome 21 enhances amyloid-b deposition independently of an extra copy of APP. Brain *141*, 2457–2474.

Wolfe, M.S. (2013). Toward the structure of presenilin/γ-secretase and presenilin homologs. Biochim. Biophys. Acta - Biomembr. 2886–2897.

Wonders, C.P., and Anderson, S.A. (2006). The origin and specification of cortical interneurons. Nat. Rev. Neurosci. 687–696.

Wood, J.G., Mirra, S.S., Pollock, N.L., and Binder, L.I. (1986). Neurofibrillary tangles of Alzheimer's disease share antigenic determinants with the axonal microtubule-associated protein tau. Proc.

Natl. Acad. Sci. USA *83*, 4040–4043.

Wood, S.J., Maleeff, B., Hart, T., and Wetzel, R. (1996). Physical, morphological and functional differences between pH 5.8 and 7.4 aggregates of the Alzheimer's amyloid peptide Aβ. J. Mol. Biol. 870–877.

Wood, W.G., Eckert, G.P., Igbavboa, U., and M??ller, W.E. (2003). Amyloid beta-protein interactions with membranes and cholesterol: Causes or casualties of Alzheimer's disease. Biochim. Biophys. Acta - Biomembr. *1610*, 281–290.

Woodhouse, A., West, A.K., Chuckowree, J.A., Vickers, J.C., and Dickson, T.C. (2005). Does β-amyloid plaque formation cause structural injury to neuronal processes? Neurotox. Res. *7*, 5–15.

Woodruff-Pak, D.S. (2008). Animal Models of Alzheimer's Disease: Therapeutic Implications. J. Alzheimer's Dis. *15*, 507–521.

Woodruff, G., Young, J.E., Martinez, F.J., Buen, F., Gore, A., Kinaga, J., et al. (2013). The presenilin-1 ΔE9 mutation results in reduced γ-secretase activity, but not total loss of PS1 function, in isogenic human stem cells. Cell Rep. *5*, 974–985.

World Health Organisation (2016). https://www.who.int/news-room/fact-sheets/detail/the-top-10-causes-of-death.

Wright, B.L.C., Lai, J.T.F., and Sinclair, A.J. (2012). Cerebrospinal fluid and lumbar puncture: A practical review. J. Neurol. *259*, 1530–1545.

Wu, H.-Y., Hudry, E., Hashimoto, T., Kuchibhotla, K., Rozkalne, A., Fan, Z., et al. (2010). Amyloid {beta} Induces the Morphological Neurodegenerative Triad of Spine Loss, Dendritic Simplification, and Neuritic Dystrophies through Calcineurin Activation. J. Neurosci. *30*, 2636–2649.

Wu, J.W., Hussaini, S.A., Bastille, I.M., Rodriguez, G.A., Mrejeru, A., Rilett, K., et al. (2016). Neuronal activity enhances tau propagation and tau pathology in vivo. Nat. Neurosci. *19*, 1085–1092.

Yagi, T., Ito, D., Okada, Y., Akamatsu, W., Nihei, Y., Yoshizaki, T., et al. (2011). Modeling familial Alzheimer's disease with induced pluripotent stem cells. Hum. Mol. Genet. *20*, 4530–4539.

Yan, R., Han, P., Miao, H., Greengard, P., and Xu, H. (2001a). The Transmembrane Domain of the Alzheimer's β-Secretase (BACE1) Determines its Late Golgi Localization and Access to β-Amyloid Precursor Protein (APP) Substrate. J. Biol. Chem. *276*, 36788–36796.

Yan, R., Munzner, J.B., Shuck, M.E., and Bienkowski, M.J. (2001b). BACE2 Functions as an Alternative α-Secretase in Cells. J. Biol. Chem. 34019–34027.

Yan, R., Munzner, J.B., Shuck, M.E., and Bienkowski, M.J. (2001c). BACE2 Functions as an

Alternative β-Secretase in Cells. J. Biol. Chem. *276*, 34019–34027.

Yanagisawa, K. (2015). GM1 ganglioside and Alzheimer's disease. Glycoconj. J. *32*, 87–91.

Yanagisawa, K., Odaka, A., Suzuki, N., and Ihara, Y. (1995). GM1 ganglioside–bound amyloid β–protein (Aβ): A possible form of preamyloid in Alzheimer's disease. Nat. Med. 1062–1066.

Yang, T., Li, S., Xu, H., Walsh, D.M., and Selkoe, D.J. (2017). Large Soluble Oligomers of Amyloid β-Protein from Alzheimer Brain Are Far Less Neuroactive Than the Smaller Oligomers to Which They Dissociate. J. Neurosci. 152–163.

Yoshikai, S., Sasaki, H., Doh-ura, K., Furuya, H., and Sakaki, Y. (1990). Genomic organization of the human amyloid beta-protein precursor gene. Gene *87*, 257–263.

Young-Pearse, T.L., Chen, A.C., Chang, R., Marquez, C., and Selkoe, D.J. (2008). Secreted APP regulates the function of full-length APP in neurite outgrowth through interaction with integrin beta1. Neural Dev. *3*, 15.

Yu, J., Vodyanik, M.A., Smuga-Otto, K., Antosiewicz-Bourget, J., Frane, J.L., Tian, S., et al. (2007). Induced pluripotent stem cell lines derived from human somatic cells. Sci. (New York, NY) *318*, 1917–1920.

Yu, J., Hu, K., Smuga-Otto, K., Tian, S., Stewart, R., Slukvin, I.I., et al. (2009). Human Induced Pluripotent Stem Cells Free of Vector and Transgene Sequences. Science *324*, 797–801.

Żekanowski, C., Styczyńska, M., Pepłońska, B., Gabryelewicz, T., Religa, D., Ilkowski, J., et al. (2003). Mutations in presenilin 1, presenilin 2 and amyloid precursor protein genes in patients with early-onset Alzheimer's disease in Poland. Exp. Neurol. *184*, 991–996.

Zempel, H., Thies, E., Mandelkow, E., and Mandelkow, E.-M. (2010). Abeta oligomers cause localized Ca(2+) elevation, missorting of endogenous Tau into dendrites, Tau phosphorylation, and destruction of microtubules and spines. J. Neurosci. *30*, 11938–11950.

Żenkiewicz, M. (2001). Wettability and surface free energy of corona-treated biaxially-oriented polypropylene film. J. Adhes. Sci. Technol. *15*, 1769–1785.

Zetterberg, H., Wilson, D., Andreasson, U., Minthon, L., Blennow, K., Randall, J., et al. (2013). Plasma tau levels in Alzheimer's disease. Alzheimer's Res. Ther. *5*, 9.

Zhao, Y., and Zhao, B. (2013). Oxidative stress and the pathogenesis of Alzheimer's disease. Oxid. Med. Cell. Longev. *2013*, 316523.

Zheng, H., Jiang, M., Trumbauer, M.E., Sirinathsinghji, D.J.S., Hopkins, R., Smith, D.W., et al. (1995). β-amyloid precursor protein-deficient mice show reactive gliosis and decreased locomotor activity. Cell *81*, 525–531.

Zhou, W., and Freed, C.R. (2009). Adenoviral gene delivery can reprogram human fibroblasts to induced pluripotent stem cells. Stem Cells *27*, 2667–2674.

Zhou, F., Gong, K., Song, B., Ma, T., van Laar, T., Gong, Y., et al. (2012). The APP intracellular domain (AICD) inhibits Wnt signalling and promotes neurite outgrowth. Biochim. Biophys. Acta - Mol. Cell Res. 1233–1241.

Zoltowska, K.M., and Maesako, M. (2016). Interrelationship between Changes in the Amyloid β 42/40 Ratio and Presenilin 1 Conformation. Mol. Med. 329–337.

Zou, K., Gong, J., Yanagisawa, K., and Michikawa, M. (2002). A novel function of monomeric amyloid β-protein serving as an antioxidant molecule against metal-induced oxidative damage. J. Neurosci. *22*, 4833–4841.

Zuo, L., van Dyck, C.H., Luo, X., Kranzler, H.R., Yang, B.Z., and Gelernter, J. (2006). Variation at APOE and STH loci and Alzheimer's disease. Behav. Brain Funct. 13.